Synthesis and Behavior of Amphiphilic pH-Responsive Binary Heterografted Molecular Bottlebrush Polymers at Interfaces

A Dissertation Presented for the

Doctor of Philosophy

Degree

The University of Tennessee, Knoxville

Michael T. Kelly

August 2023

Dedication

This dissertation is dedicated to my parents George and Mary Kelly.

"To the moon and back."

Acknowledgements

First, I would like to express my sincere thanks to my research advisor Professor Bin Zhao for his guidance, support, and insight during my time in graduate school. Prof. Zhao's expertise and commitment to excellence have been instrumental in shaping this dissertation and in my development as a scientist. I am grateful for your mentorship and helping me to reach my full potential.

In addition, I would like to thank my committee members Prof. Michael Kilbey, Prof. Fred Heberle, and Prof. Qixin Zhong. I have greatly appreciated your time and your constructive feedback throughout this process.

Thank you to the National Science Foundation and the University of Tennessee for providing financial support which has allowed me to pursue my graduate studies.

I thank Dr. Carlos Steren for sharing his expertise on NMR and his willingness to help with new experiments. Thanks also to Jaydeep Kolape for his advice and help with microscopy. I would like to thank Mr. Zhan Chen of UMass Amherst for training me on the use of the pendant drop tensiometry instrument and Prof. Thomas Russell for the collaboration.

I thank the members of the Zhao research group, both past and present, for their advice and friendship over the years: Dr. Bryan Seymour, Dr. Ethan Kent, Dr. Evan Lewoczko, Dr. Caleb Bohannon, Andrew Chancellor, Blake Day, Sakunthala Wijesundera, Sachini Dayarathne, Kingsley Ojima. I owe a special thanks to Ethan, Evan, Caleb, and Andrew who shared their expertise and were patient in answering all of my questions during my formative years of graduate school. I wish you all the best in life and your future careers.

I would like to thank my undergraduate chemistry professors at Georgia Southern, especially my undergraduate research advisor Prof. Sarah Zingales, for helping me establish a solid academic foundation, introducing me to scientific research, and encouraging me to apply for graduate school.

I would also like to acknowledge the individuals I had the opportunity to work with at Kraton especially: Dr. Tim Costner, Amanda Quaranta, Don Scott, Abbie Jones, and Frank Mikula. I am thankful for the opportunities I had to learn from them and their contributions to my professional development.

A heartfelt thanks to my girlfriend, Marieli Valencia. Her unwavering love, constant encouragement and understanding have been invaluable sources of strength and motivation. Being far from my family while in graduate school was difficult at times, and I feel lucky to have gotten the opportunity to be part of yours. I look forward to starting the next chapter together.

I thank my entire family for their support; I feel very blessed to have them. Most importantly, I want to express my sincere gratitude to my parents. Their love, guidance and sacrifices throughout my life are immeasurable. I will always be eternally grateful to them.

Abstract

Molecular bottlebrush (MBB) polymers are a class of architecturally complex polymers characterized by a backbone polymer densely grafted with relatively shorter polymeric side chains. Due to the dense grafting nature and the large molecular size, MBBs exhibit many unique characteristics and have attracted considerable interest. This dissertation research primarily explored the synthesis of novel amphiphilic pH-responsive heterografted bicomponent MBBs with tertiary amine-containing side chains and their behavior at interfaces.

A series of linear MBBs composed of heterografted poly(*n*-butyl acrylate) (P*n*BA) and pH-responsive poly(2-(*N,N*-diethylamino)ethyl methacrylate) (PDEAEMA) side chains with various molar ratios was synthesized by a click "grafting to" method, along with two homografted MBBs. At pH 4.0, below the PDEAEMA's pK_a of 7.4, MBBs with appropriate side chain compositions were effective and efficient emulsion stabilizers, producing water-in-toluene emulsions with excellent long-term stability after vortexing. Upon adjusting the pH to 10.0, the emulsions were broken. The formation and breaking of emulsions can be repeated ≥ 10 times, and atomic force microscopy showed that the MBBs remained intact. Pendant drop tensiometry revealed that the lowest toluene-water interfacial tension decreased with increasing molar content of PDEAEMA in the bottlebrushes, but no clear correlation was found between the interfacial tension reduction and the MBB's emulsion stabilization ability. Interfacial jamming of MBBs with certain side chain compositions, manifested in wrinkled interfaces, was observed at pH 4.0 upon reducing the interfacial area of droplets, which correlated well with their abilities to stabilize emulsions. This was attributed to the strong adsorption of MBBs to the interface with P*n*BA and protonated PDEAEMA side chains extending only into the toluene and aqueous phase, respectively. Using a Langmuir-Blodgett trough, heterografted P*n*BA/PDEAEMA MBBs exhibited wormlike-to-

globular shape transitions upon lateral compression on the acidic water surface when P*n*BA was the major component of side chains. Additionally, stepwise conformational changes of linear MBBs from wormlike to partially collapsed, and stable globular were achieved in aqueous solutions using two distinct stimuli-responsive polymers and poly(ethylene oxide) as the side chains. The insights obtained from this dissertation research will provide guidelines for design of stimuli-responsive MBBs for potential applications, e.g., in emulsion and substance delivery.

Table of Contents

Chapter 1. Introduction 1

1.1. Introduction 2

1.1.1. Introduction to Molecular Bottlebrush Polymers 2

1.1.2. Molecular Bottlebrushes as Emulsion Stabilizers 7

1.1.3. Conformational Transitions of Molecular Bottlebrushes at Flat Interfaces 12

1.1.4. Conformational Transitions of Stimuli-Responsive Molecular Bottlebrush Polymers in Solution 14

1.2. Dissertation Overview 22

References 23

Chapter 2. Amphiphilic Heterografted Bottlebrush Polymers with Tertiary Amine-Containing Side Chains as Effective and Efficient pH-Responsive Emulsion Stabilizers 32

Abstract 33

2.1. Introduction 34

2.2. Experimental Section 38

2.2.1. Materials 38

2.2.2. General Characterization 39

2.2.3. Synthesis of Azide-Functionalized Backbone Polymer (PHEMA-N_3) 39

2.2.4. Synthesis of Alkyne End-Functionalized Side Chain Polymer P*n*BA 42

2.2.6. Synthesis of MBBs 43

2.2.7. Control of pH Values of the Aqueous Phases in 1.0 mM Aqueous Phosphate Buffer-Toluene Mixtures 46

2.2.8. Emulsion Formation and Breaking 47

2.2.9. Repeated Formation and Breaking of Emulsions 49

2.2.10. Long-Term Stability of Water-in-Toluene Emulsions Stabilized by MBB-$B_{0.51}E_{0.49}$ 49

2.2.11. Optical Microscopy and Confocal Microscopy 50

2.2.12. Atomic Force Microscopy (AFM) 50

2.3. Results and Discussion 51

2.3.1. Synthesis and Characterization of MBBs Comprising P*n*BA and PDEAEMA Side Chains with Different Molar Ratios 51

2.3.2. Heterografted P*n*BA/PDEAEMA MBBs as pH-Responsive Emulsion Stabilizers: Effect of Side Chain Composition 56

2.3.3. Long-Term Stability of MBB-$B_{0.51}E_{0.49}$-Stabilized Emulsions 66

2.3.4. Repeatability of pH-Induced Formation and Breaking of Water-Toluene Emulsion with MBB-$B_{0.51}E_{0.49}$ as Stabilizer 68

2.3.5. Further Discussion on pH-Induced Formation and Breaking of Emulsion with Heterografted P*n*BA/PDEAEMA MBBs as a pH-Responsive Stabilizer 72

2.4. Conclusions 77

References 78

Appendix A 84

Chapter 3. Effects of Side Chain Composition and pH on Reduction of Toluene-Water Interfacial Tension by Amphiphilic pH-Responsive Binary Heterografted Bottlebrush Polymers 100

Abstract 101

3.1. Introduction 102

3.2. Experimental Section 104

3.2.1. Materials 104

3.2.2. Toluene-Water Interfacial Tension Measurements by Pendant Drop Tensiometry 105

3.2.3. Optical Micrographs of Emulsion Drops 105

3.3. Results and Discussion 106

3.3.1. Interfacial Tensions Between Toluene Solutions of MBBs and Aqueous Solutions with pH of 4.0 and 10.0 Measured by Pendant Drop Tensiometry 106

3.3.2. Assembly Dynamics of MBBs at the Interfaces Between Toluene and Aqueous Solutions with pH of 4.0 and 10.0 112

3.3.3. Jamming Test Experiments by Reducing Interfacial Area of Droplets 115

3.4. Conclusions 120

References 122

Appendix B 124

Chapter 4. Conformational Behavior of Tertiary Amine-Containing Binary Heterografted Molecular Bottlebrushes at Planar Air-Water Interfaces In Response to Lateral Compression and pH Changes 130

Abstract 131

4.1. Introduction 133

4.2. Experimental Section 136

4.2.1. Materials 136

4.2.2. Langmuir-Blodgett Lateral Compression and Sample Transfer 136

4.2.2. Atomic Force Microscopy (AFM) 139

4.3. Results and Discussion 139

4.3.1. Amphiphilic pH-Responsive Heterografted MBBs at Interfaces between Air and Aqueous Solutions in a LB Trough at a Surface Pressure of 0.5 mN/m: pH Effect 139

4.3.2. Lateral Compression-Induced Reversible Worm-Sphere Conformational Transitions of Homografted P*n*BA Bottlebrushes, MBB-$B_{1.00}E_{0.00}$, at the Air-Water Interface in a Langmuir-Blodgett Trough 144

4.3.3. Conformational Behavior of Amphiphilic pH-Responsive Binary Heterografted MBBs at Interface between Air and a 1.0 mM Aqueous Phosphate Buffer Solution with pH of 4.0 in Response to Lateral Compression and Decompression 148

4.3.4. Conformational Behavior of Amphiphilic pH-Responsive Heterografted P*n*BA/PDEAEMA MBBs at the Interface Between Air and a 1.0 mM Aqueous Phosphate Buffer Solution with a pH of 10.0 in Response to Lateral Compression and Expansion 155

4.3.5. Conformational Behavior of MBB-$B_{0.00}E_{1.00}$ at Interface between Air and a 1.0 mM Phosphate Aqueous Buffer Solution with pH = 10.0 in Response to Lateral Compression and Decompression in a Langmuir-Blodgett Trough 162

4.3.6. Further Discussion on Different Conformational Behavior of MBB-$B_{1.00}E_{0.00}$ and MBB-$B_{0.00}E_{1.00}$ at Air-Aqueous Solution Interfaces in Response to Lateral Compression 162

4.3.7. Further Discussion on Conformational Behaviors of Four Heterografted P*n*BA/PDEAEMA MBBs at Air-Aqueous Solution Interfaces with Subphase pH of 4.0 and 10.0 in Response to Lateral Mechanical Compression 164

4.4. Conclusions 169

References 171

Appendix C 177

Chapter 5. Stepwise Conformational Transitions of Stimuli-Responsive Linear Ternary Heterografted Bottlebrush Polymers in Aqueous Solution 179

Abstract 180

5.1. Introduction 182

5.2. Experimental Section 186

5.3. Results and Discussion 186

5.3.1. Synthesis and Characterization of Dually Responsive Ternary MBBs 186

5.3.2. pH-Induced Stepwise Conformational Transitions of MBB-PP in Aqueous Solution 189

5.3.3. Temperature-Induced Stepwise Conformational Transitions of MBB-TT in Aqueous Solution 195

5.3.4. pH- and Temperature-Induced Stepwise Conformational Changes of MBB-TP in Aqueous Solution 199

5.3.5. Stepwise Release of Hydrophobic Model Drug, Nile Red, from Collapsed Globular MBB-PP 209

5.4. Conclusions 211

References 213

Appendix D 222

Chapter 6. Synthesis of Homografted and Heterografted Molecular Bottlebrushes with Semi-Crystalline Polymer Side Chains 255

Abstract 256

6.1. Introduction 257

6.2. Experimental Section 258

6.2.1. Materials 258

6.2.2. General Characterization 259

6.2.3. Synthesis of 2-(2-Hydroxyethoxy)ethyl Pent-4-ynoate (Alkyne-DEG-OH) 260

6.2.4. Synthesis of Alkyne End-Functionalized PCL 261

6.2.5. Synthesis of Homografted MBBs 262

6.2.6. Synthesis of Heterografted PEO/PCL MBBs 263

6.3. Results and Discussion 264

6.3.1. Synthesis of Alkyne End-Functionalized Side Chain Polymers 264

6.3.2. Synthesis of Homografted Linear and Three-Arm Star PEO MBBs with Various Grafting Densities 267

6.4. Conclusions 275

References 282

Chapter 7. Conclusions and Future Work 284

References 289

Vita 291

List of Tables

Table 2.1. Characterization data for the backbone polymer, PHEMA-N_3, and the alkyne-end-functionalized side chain polymers, P*n*BA and PDEAEMA, used in this work. 53

Table 2.2. Characterization Data for Six Bottlebrush Polymers Used in This Work..... 57

Table 5.1. Characterization Data for Side Chain Polymers Used for Synthesizing MBBs..... 187

Table 5.2. Characterization Data and Calculated Values for MBBs 190

Table 6.1. Characterization Data for Azide-Functionalized Backbone and Alkyne End-Functionalized Side Chain Polymers. 268

Table 6.2. Summary of synthetic conditions and characterization data for homografted PEO MBBs 271

Table 6.3. Summary of MBBs with PEO and/or PCL side chains..... 277

List of Figures

Figure 1.1. (A) Atomic force microscopy height image of molecular bottlebrushes spin cast on a mica substrate in which the backbone and side chain polymers are clearly visible. (B) A flower from a bottlebrush plant. 3

Figure 1.2. (A) The proposed arrangement of amphiphilic molecular bottlebrushes with PEO and PnBA grafts. (B) and (C) digital photos of water-in-xylene emulsions stabilized by amphiphilic MBBs. 9

Figure 1.3. (a) Time dependence of interfacial tension at the water-toluene interface for MBBs with different backbone lengths at a concentration of 0.001 mg/mL. (b) Semi log plot of interfacial tension (linear) vs time (log). (c) Equilibrium interfacial tension and the corresponding induction time. (d) Characteristic relaxation times of MBBs fitted with an exponential relaxation function. 11

Figure 1.4. Sequential AFM images demonstrating the collapse and uncoiling of MBBs with PnBA side chains on a mica substrate in vapors saturated with humidified ethanol. 15

Figure 1.5. Hydrodynamic diameter (D_h) of (A) a homografted brush polymer with PDEAEMA homopolymer side chains and (B) a homografted brush polymer with diblock copolymer side chains composed of pH-responsive PDEAEMA as the inner block and thermoresponsive PTEGMA as the outer block as a function of pH. The D_h values were measured by dynamic light scattering. 20

Figure 1.6. AFM height images showing that a three-arm star brush polymer with heterografted pH-responsive PDEAEMA and thermoresponsive PDEGEA side chains collapsed into two distinct globular states under different conditions. 21

Figure 2.1. SEC traces of (A) the final reaction mixture for the synthesis of MBB-$B_{0.80}E_{0.20}$ and (B) after removal of unreacted side chain polymers, (C) ^{1}H NMR spectrum of the purified MBB-$B_{0.80}E_{0.20}$ in $CDCl_3$, and (D) AFM height image of MBB-$B_{0.80}E_{0.20}$. The average length of 250 measured bottlebrush molecules was 100.6 ± 28.2 nm. 55

Figure 2.2. Digital optical photos of the mixtures of toluene with a brush polymer and a 1.0 mM phosphate buffer at pH = 4.0 after vortexing for 60 sec and sitting still for 24 h, at pH 10.0 after addition of NaOH and gentle shaking for 30 sec, and at pH = 4.0 after the addition of HCl and vortexing for 60 sec again for MBB-$B_{1.00}E_{0.00}$ (A), MBB-$B_{0.80}E_{0.20}$ (B), MBB-$B_{0.64}E_{0.36}$ (C), MBB-$B_{0.51}E_{0.49}$ (D), MBB-$B_{0.24}E_{0.76}$ (E), and MBB-$B_{0.00}E_{1.00}$ (F) at concentrations of 0.02 wt% (i), 0.01 wt% (ii), and 0.005 wt% (iii). For MBB-$B_{0.80}E_{0.20}$ and MBB-$B_{0.64}E_{0.36}$, the mixtures at pH = 10.0 were stirred with a magnetic stir bar at 60 rpm for a few hours to facilitate the emulsion breaking. 59

Figure 2.3. Laser confocal image (A) and optical micrograph (B) of the same portion of the emulsion of toluene and the 1.0 mM phosphate buffer formed with the use of 0.02 wt% MBB-$B_{0.51}E_{0.49}$ as the stabilizer at pH = 4.0. Nile Red was added into the toluene phase as a fluorescent dye. 61

Figure 2.4. Representative optical micrographs of emulsions droplets from the MBB-$B_{0.80}E_{0.20}$ (A), MBB-$B_{0.64}E_{0.36}$ (B), and MBB-$B_{0.51}E_{0.49}$ (C)-stabilized emulsions at a brush polymer concentration of 0.02 wt% (left), 0.01 wt% (middle), and 0.005 wt% (right). Scale bars: 200 μm. 62

Figure 2.5. Side chain composition range of MBBs to function as effective stabilizers for the emulsions of toluene and the 1.0 mM phosphate buffer solution with a pH of 4.0. 64

Figure 2.6. AFM height images of (A) the original brush polymer MBB-$B_{0.51}E_{0.49}$ and (B) the MBB-$B_{0.51}E_{0.49}$ from the water-in-toluene emulsion at pH = 4.0 formed in the second cycle. 67

Figure 2.7. Long-term stability study of the emulsions stabilized by 0.02 wt% and 0.01 wt% MBB-$B_{0.51}E_{0.49}$ under the acidic conditions (pH = 4.0 for the aqueous phases). Optical micrograph of emulsion droplets from the 0.02 wt% emulsion (left), photo of two emulsions (middle), and optical micrograph of emulsion droplets from the 0.01 wt% emulsion after 1 day (top row), one week (2nd row), two weeks (3rd row), three weeks (4th row), and six weeks (5th row). Scale bars: 200 μm. 69

Figure 2.8. Digital optical photos (top two rows) of the mixtures of toluene, a 1.0 mM aqueous phosphate buffer solution, and MBB-$B_{0.51}E_{0.49}$ at concentrations of 0.03 wt%, 0.02 wt%, 0.01 wt%, and 0.005 wt% for the formation and breaking of emulsions from 1st cycle, 3rd cycle, 6th cycle, and 10th cycle, showing the repeatability of pH-induced formation and breaking of water-toluene emulsion. Note that starting in the 9th cycle, 0.005% brush polymer was unable to produce stable emulsions. The bottom two rows are optical micrographs of emulsion droplets from the 1st cycle and 10th cycle for different concentrations of the brush polymer. Scale bars in bottom two rows: 200 μm. 71

Figure 2.9. AFM height image (left) and corresponding phase image (right) of MBB-$B_{0.51}E_{0.49}$ after 10 cycles of emulsion formation and breaking. 73

Figure 2.10. Optical micrograph of partially dried emulsion droplets from a 0.03 wt% MBB-$B_{0.51}E_{0.49}$-stabilized emulsion at pH = 4.0. As the toluene and water were evaporating, the droplets began to crumple on themselves, leaving behind a thin polymer film. 76

Figure A1. Size exclusion chromatography (SEC) curves of PHEMA-TMS, PHEMA-Br, and PHEMA-N_3. SEC analysis was performed using PL-GPC 50 plus equipped with GRAM columns and an RI detector using 50 mM LiBr as eluent. 85

Figure A2. ^{1}H NMR spectra of purified PHEMA-TMS (A), PHEMA-Br (B), and PHEMA-N_3 (C) in $CDCl_3$. 86

Figure A3. (A) ^{1}H NMR spectrum of the alkyne-end-functionalized P*n*BA side chain polymer in $CDCl_3$ and (B) size exclusion chromatography (SEC) trace of P*n*BA from SEC analysis using GRAM columns and DMF with 50 mM LiBr as eluent. 87

Figure A4. (A) ^{1}H NMR spectrum of the alkyne-end-functionalized PDEAEMA side chain polymer in $CDCl_3$ and (B) size exclusion chromatography (SEC) trace of PDEAEMA from SEC analysis using GRAM columns and DMF with 50 mM LiBr as eluent. 87

Figure A5. Additional AFM height images of MBB-$B_{0.80}E_{0.20}$. The AFM sample was prepared using a Langmuir-Blodgett trough with a pH of 4.0 for the aqueous subphase. The average length of 250 brush molecules was 100.6 ± 28.2 nm....88

Figure A6. SEC traces of (A) the final reaction mixture for the synthesis of binary heterografted molecular bottlebrushes MBB-$B_{0.64}E_{0.36}$ and (B) after removal of residual side chain polymers, and (C) ^{1}H NMR spectrum of the purified MBB-$B_{0.64}E_{0.36}$ in $CDCl_3$. 89

Figure A7. AFM height images of MBB-$B_{0.64}E_{0.36}$. The AFM sample was prepared using a Langmuir-Blodgett trough with a pH of 4.0 for the aqueous subphase. The average length of 217 measured brush molecules was 102.4 ± 26.4 nm....90

Figure A8. SEC traces of (A) the final reaction mixture for the synthesis of binary heterografted molecular bottlebrushes MBB-$B_{0.51}E_{0.49}$ and (B) after removal of residual side chain polymers, and (C) ^{1}H NMR spectrum of the purified MBB-$B_{0.51}E_{0.49}$ in $CDCl_3$. 91

Figure A9. AFM height images of MBB-$B_{0.51}E_{0.49}$. The AFM sample was prepared using a Langmuir-Blodgett trough with a pH of 4.0 for the aqueous subphase. The average length of 287 brush molecules was 99.8 ± 26.9 nm. 92

Figure A10. ^{1}H NMR spectra of (A) the initial reaction mixture and (B) the final reaction mixture for the synthesis of MBB-$B_{0.24}E_{0.76}$ for estimating the grafting density of MBB-$B_{0.24}E_{0.76}$. The initial feed molar ratio of the alkyne-end-functionalized side chains to the azide groups is 1.38. Therefore, the grafting density is estimated to be 1.38 × [1 – (4.06/10.9)] = 86.7%.....92

Figure A11. SEC analysis of (A) a mixture of MBB-$B_{0.24}E_{0.76}$ (3 mg) and a 100 kDa PMMA standard (3 mg) dissolved in THF (2 mL), (B) a mixture of MBB-$B_{0.00}E_{1.00}$ (3 mg) and a 100 kDa PMMA standard (3 mg) dissolved in THF (2 mL), (C) alkyne end-functionalized side chain polymer P*n*BA, and (D) alkyne end-functionalized side chain polymer PDEAEMA using the THF GPC system. MBB-$B_{0.24}E_{0.76}$ and MBB-$B_{0.00}E_{1.00}$ cannot be eluted out from our THF GPC system, but P*n*BA and PDEAEMA can be analyzed by this GPC system. To confirm the removal of unreacted side chain polymers, a 100 kDa PMMA standard was added into the purified brush polymer with similar amounts. As can be seen from (A) and (B), the PMMA standard can be seen but not any side chain polymers, proving that they were completely removed.....93

Figure A12. ^{1}H NMR spectrum of the purified MBB-$B_{0.24}E_{0.76}$ in $CDCl_3$.....94

Figure A13. AFM height images of MBB-$B_{0.24}E_{0.76}$. The AFM sample was prepared using a Langmuir-Blodgett trough with a pH of 4.0 for the aqueous subphase. The average length of 234 measured brush molecules was 99.2 ± 30.2 nm.....94

Figure A14. ^{1}H NMR spectra of (A) the initial reaction mixture and (B) the final reaction mixture for the synthesis of MBB-$B_{0.00}E_{1.00}$ for estimating the grafting density of MBB-$B_{0.00}E_{1.00}$. The initial feed molar ratio of the alkyne-end-functionalized side chains to the azide groups is 1.29. Therefore, the grafting density is estimated to be 1.29 × [1 – (3.47/11.13)] = 88.8%.....95

Figure A15. ^{1}H NMR spectrum of the purified homografted molecular bottlebrushes MBB-$B_{0.00}E_{1.00}$ in $CDCl_3$. 95

Figure A16. AFM height images of MBB-$B_{0.00}E_{1.00}$. The AFM sample was prepared using a Langmuir-Blodgett trough with a pH of 10.0 for the aqueous subphase. The average length of 211 measured brush molecules was 109.2 ± 26.5 nm.....96

Figure A17. SEC traces of (A) the final reaction mixture for the synthesis of homografted P*n*BA molecular bottlebrushes MBB-$B_{1.00}E_{0.00}$ and (B) after removal of residual side chain polymers, and (C) ^{1}H NMR spectrum of the purified MBB-$B_{1.00}E_{0.00}$ in $CDCl_3$. 97

Figure A18. AFM height images of homografted P*n*BA molecular bottlebrushes MBB-$B_{1.00}E_{0.00}$. The AFM sample was prepared using a Langmuir-Blodgett trough using Milli-Q water as the subphase. The average length of 251 measured brush molecules was 100.1 ± 23.6 nm. 98

Figure A19. Additional AFM height images of the brush polymer MBB-$B_{0.51}E_{0.49}$ on a glass disc from the water-in-toluene emulsion at pH = 4.00 formed in the second cycle with 0.02 wt% of MBB-$B_{0.51}E_{0.49}$ as stabilizer. The AFM sample was prepared by depositing 25 μL of the emulsion layer onto the surface of the subphase of 1.0 mM phosphate buffer with pH of 4.0 in a Langmuir-Blodgett trough. After 20 min, the barriers were compressed at a rate of 10 mm/min until a surface pressure of 0.5 mN/m was reached. Once the pressure stabilized the monolayer was transferred on a glass coverslip at a rate of 2 mm/min.....98

Figure A20. Additional AFM height images of the brush polymer MBB-$B_{0.51}E_{0.49}$ on a glass disc from the water-in-toluene emulsion at pH = 4.00 formed in the tenth cycle with 0.02 wt% of MBB-$B_{0.51}E_{0.49}$ as stabilizer. The AFM sample was prepared by depositing 25 μL of the emulsion layer onto the surface of the subphase of 1.0 mM phosphate buffer with pH of 4.0 in a Langmuir-Blodgett trough. After 20 min, the barriers were compressed at a rate of 10 mm/min until a surface pressure of 0.5 mN/m was reached. Once the pressure stabilized the monolayer was transferred on a glass coverslip at a rate of 5 mm/min as described in the experimental section.....99

Figure 3.1. Time dependence of interfacial tension a toluene solution of a brush polymer with a concentration of 0.2 mg/g and an aqueous solution with a pH value of 4.0 (A) and 10.0 (B) measured by pendant drop tensiometry for six brush polymers (MBB-$B_{1.00}E_{0.00}$, and MBB-$B_{0.80}E_{0.20}$, MBB-$B_{0.64}E_{0.36}$, MBB-$B_{0.51}E_{0.49}$, MBB-$B_{0.24}E_{0.76}$, and MBB-$B_{0.00}E_{1.00}$). A 7 μL drop of a 0.2 mg/g solution of a brush polymer toluene was injected into the aqueous solution (10 mL). 108

Figure 3.2. Plot of the lowest interfacial tension, obtained from Figure 3.1, versus the mole fraction of PDEAEMA in the side chains of MBBs. 111

Figure 3.3. Interfacial tension between a toluene solution of a brush polymer with a concentration of 0.2 mg/g and an aqueous solution with a pH value of 4.0 (A) and 10.0 (B) versus time (log) for six brush polymers. 113

Figure 3.4. Photos of a toluene droplet containing 0.2 mg/g MBBs injected into a pH 4.0 aqueous solution and then gradually withdrawn for MBB-$B_{1.00}E_{0.00}$ (A), MBB-$B_{0.80}E_{0.20}$ (B) (withdrawn at γ = 23 mN/m), MBB-$B_{0.64}E_{0.36}$ (C) (withdrawn at γ = 20 mN/m), MBB-$B_{0.51}E_{0.49}$ (D) (withdrawn at γ = 18 mN/m), MBB-$B_{0.24}E_{0.76}$ (E), and MBB-$B_{0.00}E_{1.00}$ (F). For each sample, the left photo shows the initial state and the right photo shows the droplet before being fully withdrawn into the syringe..... 116

Figure 3.5. Photos of a toluene droplet containing 0.2 mg/g MBBs injected into a pH 10.0 aqueous solution and then gradually withdrawn for MBB-$B_{1.00}E_{0.00}$ (A), MBB-$B_{0.80}E_{0.20}$ (B), MBB-$B_{0.64}E_{0.36}$ (C), MBB-$B_{0.51}E_{0.49}$ (D), MBB-$B_{0.24}E_{0.76}$ (E), and MBB-$B_{0.00}E_{1.00}$ (F). For each sample, the left photo shows the initial state and the right photo shows the droplet before being fully withdrawn into the syringe..... 117

Figure 3.6. The images show screenshots of videos recorded using an optical microscope to study emulsion droplet morphology at different timepoints. (A) Emulsion droplet, stabilized by MBB-$B_{0.51}E_{0.49}$ at a concentration of 0.03 wt% with a pH of 4.0 for the aqueous phase. (B) Unstable emulsion droplet, formed with the use of 0.03 wt% MBB-$B_{0.51}E_{0.49}$ at a pH of 10.0 for the aqueous phase. (C) Emulsion droplet, stabilized by sodium dodecyl sulfonate (SDS) at a concentration of 0.03 wt% and a pH of 4.0 for an aqueous phase. 119

Figure B1. H NMR spectrum Plot of interfacial tension (γ) between a toluene solution of 0.2 mg/g $MBB_{0.80}E_{0.20}$ and a pH 4.0 aqueous solution on a linear scale versus time on a semi-log scale for two repeated measurements. 125

Figure B2. Plot of interfacial tension (γ) between a toluene solution of 0.2 mg/g $MBB_{0.64}E_{0.36}$ and a pH 4.0 aqueous solution on a linear scale versus time on a semi-log scale for three repeated measurements. 125

Figure B3. Plot of interfacial tension (γ) between a toluene solution of 0.2 mg/g $MBB_{0.51}E_{0.49}$ and a pH 4.0 aqueous solution on a linear scale versus time on a semi-log scale for three repeated measurements 126

Figure B4. Plot of interfacial tension (γ) between a toluene solution of 0.2 mg/g $MBB_{0.24}E_{0.76}$ and a pH 4.0 aqueous solution on a linear scale versus time on a semi-log scale for three repeated measurements. 126

Figure B5. Plot of interfacial tension (γ) between a toluene solution of 0.2 mg/g $MBB_{0.00}E_{1.00}$ and a pH 4.0 aqueous solution on a linear scale versus time on a semi-log scale for three repeated measurements. 127

Figure B6. Plot of interfacial tension (γ) between a toluene solution of 0.2 mg/g $MBB_{0.80}E_{0.20}$ and a pH 10.0 aqueous solution on a linear scale versus time on a semi-log scale for three repeated measurements. 127

Figure B7. Plot of interfacial tension (γ) between a toluene solution of 0.2 mg/g $MBB_{0.64}E_{0.36}$ and a pH 10.0 aqueous solution on a linear scale versus time on a semi-log scale for three repeated measurements 128

Figure B8. Plot of interfacial tension (γ) between a toluene solution of 0.2 mg/g $MBB_{0.51}E_{0.49}$ and a pH 10.0 aqueous solution on a linear scale versus time on a semi-log scale for two repeated measurements. 128

Figure B9. Plot of interfacial tension (γ) between a toluene solution of 0.2 mg/g $MBB_{0.24}E_{0.76}$ and a pH 10.0 aqueous solution on a linear scale versus time on a semi-log scale for three repeated measurements. 129

Figure B10. Plot of interfacial tension (γ) between a toluene solution of 0.2 mg/g $MBB_{0.00}E_{1.00}$ and a pH 10.0 aqueous solution on a linear scale versus time on a semi-log scale for two repeated measurements. 129

Figure 4.1. AFM height images of MBB-$B_{0.80}E_{0.20}$ (A,B), MBB-$B_{0.64}E_{0.36}$ (C,D), MBB-$B_{0.51}E_{0.49}$ (E,F), MBB-$B_{0.24}E_{0.76}$ (G,I) transferred onto "Piranha" solution-cleaned glass disks from the interface between air and a 1.0 mM aqueous phosphate buffer solution with a pH of 4.0 (A,C,E,G) or 10.0 (B,D,F,I) at a surface pressure of 0.5 mN/m using a Langmuir-Blodgett trough..... 141

Figure 4.2. AFM height image of homografted MBB-$B_{0.00}E_{1.00}$ transferred to a "Piranha" solution-cleaned glass disk from the interface between air and a 1.0 mM phosphate aqueous buffer solution with a pH of 10.0 at a surface pressure of 0.5 mM/m using a Langmuir-Blodgett trough..... 143

Figure 4.3. (A) Isotherm plots of surface pressure (π) vs mean area per brush (A) from two cycles of lateral compression and expansion for MBB-$B_{1.00}E_{0.00}$ on Milli-Q water and AFM images at different compression-expansion stages: (B) π = 0.5 mN/m, (C) π = 18 mN/m, (D) π = 19 mN/m, (E) π = 20 mN/m, and (E) π = 0.5 mN/m again..... 146

Figure 4.4. (A) Isotherm plots of surface pressure (π) vs mean area per brush (A) from two cycles of compression and expansion for MBB-$B_{0.80}E_{0.20}$ on the surface of a 1.0 mM phosphate buffer aqueous solution with a pH of 4.0 and AFM height images of MBB-$B_{0.80}E_{0.20}$ at different surface pressures: (B) π = 0.5 mN/m, (C) π = 19 mN/m, (D) π = 22 mN/m, and (E) π = 3 mN/m..... 149

Figure 4.5. (A) Isotherm plots of surface pressure (π) vs mean area per brush (A) from two cycles of compression and expansion for MBB-$B_{0.64}E_{0.36}$ on the surface of a 1.0 mM phosphate buffer aqueous solution with a pH of 4.0 and AFM height images of MBB-$B_{0.64}E_{0.36}$ at different surface pressures: (B) π = 0.5 mN/m, (C) π = 20 mN/m, (D) π = 23 mN/m, and (E) π = 3.0 mN/m..... 151

Figure 4.6. (A) Isotherm plots of surface pressure (π) vs mean area per brush (A) from two cycles of compression and expansion for MBB-$B_{0.51}E_{0.49}$ on the surface of a 1.0 mM phosphate buffer aqueous solution with a pH of 4.0 and AFM height images of MBB-$B_{0.51}E_{0.49}$ bottlebrush molecules at different surface pressures: (B) π = 0.5 mN/m, (C) π = 21 mN/m, (D) π = 24 mN/m, and (E) π = 3.5 mN/m. 152

Figure 4.7. (A) Isotherm plots of surface pressure (π) vs mean area per brush (A) from two cycles of compression and expansion for MBB-$B_{0.24}E_{0.76}$ on the surface of a 1.0 mM phosphate buffer aqueous solution with a pH of 4.0 and AFM height images of MBB-$B_{0.24}E_{0.76}$ bottlebrush molecules at different surface pressures: (B) π = 0.5 mN/m, (C) π = 20 mN/m, (D) π = 30 mN/m, and (E) π = 3.5 mN/m. 154

Figure 4.8. (A) LB isotherm plots of surface pressure (π) vs mean area per brush (A) from two cycles of compression and expansion for MBB-$B_{0.80}E_{0.20}$ on the surface of a 1.0 mM phosphate buffer aqueous solution with a pH of 10.0 and AFM height images of MBB-$B_{0.80}E_{0.20}$ bottlebrush molecules at different surface pressures: (B) π = 0.5 mN/m, (C) π = 19 mN/m, (D) π = 22 mN/m, and (E) π = 1.0 mN/m. 156

Figure 4.9. (A) Isotherm plots of surface pressure (π) vs mean area per brush (A) from two cycles of compression and expansion for MBB-$B_{0.64}E_{0.36}$ on the surface of a 1.0 mM phosphate buffer aqueous solution with a pH of 10.0 and AFM height images of MBB-$B_{0.64}E_{0.36}$ bottlebrush molecules at different surface pressures: (B) π = 0.5 mN/m, (C) π = 20 mN/m, (D) π = 23 mN/m, and (E) π = 2.5 mN/m. 158

Figure 4.10. (A) Isotherm plots of surface pressure (π) vs mean area per brush (A) from two cycles of compression and expansion for MBB-$B_{0.51}E_{0.49}$ on the surface of a 1.0 mM phosphate buffer aqueous solution with a pH of 10.0 and AFM height images of MBB-$B_{0.51}E_{0.49}$ bottlebrush molecules at different surface pressures: (B) π = 0.5 mN/m, (C) π = 21 mN/m, (D) π = 24 mN/m, and (E) π = 2.5 mN/m. 160

Figure 4.11. (A) Isotherm plots of surface pressure (π) vs mean area per brush (A) from two cycles of compression and expansion for MBB-$B_{0.24}E_{0.76}$ on the surface of a 1.0 mM phosphate buffer aqueous solution with a pH of 10.0 and AFM height images of MBB-$B_{0.24}E_{0.76}$ bottlebrush molecules at different surface pressures: (B) π = 1.0 mN/m, (C) π = 20 mN/m, (D) π = 30 mN/m, and (E) π = 6.5 mN/m. 161

Figure 4.12. (A) Isotherm plots of surface pressure (π) vs mean area per brush (A) from two cycles of compression and expansion for MBB-$B_{0.00}E_{1.00}$ on the surface of a 1.0 mM phosphate buffer aqueous solution with a pH of 10.0 and AFM height images of MBB-$B_{0.00}E_{1.00}$ bottlebrush

molecules at different surface pressures: (B) π = 0.5 mN/m, (C) π = 20 mN/m, (D) π = 25 mN/m, and (E) π = 6.0 mN/m after expansion. 163

Figure 4.13. Plot of A_0 (nm^2/brush) versus mole fraction of PDEAEMA side chains in the brush polymer. 165

Figure C1. Additional AFM height images of MBB-$B_{0.80}E_{0.20}$ (A,B), MBB-$B_{0.64}E_{0.36}$ (C,D), MBB-$B_{0.51}E_{0.49}$ (E,F), MBB-$B_{0.24}E_{0.76}$ (G,I) transferred onto "Piranha" solution-cleaned glass disks from the interface between air and a 1.0 mM aqueous phosphate buffer solution with a pH of 4.0 (A,C,E,G) or 10.0 (B,D,F,I) at a surface pressure of 0.5 mN/m using a Langmuir-Blodgett trough. 177

Figure C2. Additional AFM height images of homografted MBB-$B_{0.00}E_{1.00}$ transferred to a "Piranha" solution-cleaned glass disk from the interface between air and a 1.0 mM phosphate aqueous buffer solution with a pH of 10.0 at a surface pressure of 0.5 mM/m using a Langmuir-Blodgett trough. 177

Figure 5.1. (A) Apparent hydrodynamic diameter (D_h) of 0.2 mg/g MBB-PP in a 25 mM phosphate buffer at 25 °C upon increasing pH. The three red diamond data points were collected from the process of decreasing pH from pH = 9.50. The inset shows hydrodynamic size distributions of MBB-PP at pH values of 3.50, 6.00, and 9.50. (B) ^{1}H NMR spectra of 4.0 mg/g MBB-PP in a 10 mM phosphate buffer prepared using D_2O at various pH values. The ^{1}H NMR spectra were normalized against the HDO peak at 4.79 ppm. 192

Figure 5.2. AFM height images of MBB-PP spin cast on PMMA-coated mica from a 0.050 mg/g solution of MBB-PP in a 10 mM phosphate buffer with a pH of 4.00 (A), 6.00 (B), and 9.50 (C). The plot in the bottom of each image shows the cross-sectional profile along the dashed line. 194

Figure 5.3. (A) Plot of D_h of 1.0 mg/g MBB-TT in Milli-Q water versus temperature in a heating process from a DLS study. The inset shows hydrodynamic size distributions at 1, 25, and 65 °C, and variable temperature ^{1}H NMR spectra of MBB-TT in D_2O with a concentration of 4.0 mg/g in the temperature ranges of 5 to 20 °C (B) and of 35 to 50 °C (C). The ^{1}H NMR spectra were normalized again the HDO peak at 4.79 ppm. 196

Figure 5.4. AFM height images of MBB-TT spin cast on PMMA-coated mica from a 0.050 mg/g solution of MBB-PP in Milli-Q water at T = 0 °C (A), 30 °C (B), and 65 °C (C). The plot in the bottom of each image shows the cross-sectional profile along the dashed line..... 198

Figure 5.5. (A) Plot of D_h of 1.0 mg/g MBB-TP in a 10 mM phosphate buffer at 1 °C versus pH from DLS measurements. The inset shows the hydrodynamic size distributions of MBB-TP at T = 1 °C and two pH values (5.00 and 9.50). (B) Plot of D_h of 1.0 mg/g MBB-TP in a 10 mM phosphate buffer at pH = 9.50 versus temperature. The inset shows the hydrodynamic size distributions of MBB-TP at pH = 9.50 and two different temperatures (1 and 30 °C). 200

Figure 5.6. (A) Plot of D_h of 1.0 mg/g MBB-TP in a 10 mM phosphate buffer at pH = 5.00 versus temperature from DLS measurements upon heating. The inset shows the hydrodynamic size distributions of MBB-TP at pH = 5.00 and two temperatures (T = 1 and 19 °C). (B) Plot of D_h of 1.0 mg/g MBB-TP in a 10 mM phosphate buffer at T = 19 °C versus pH. The inset shows the hydrodynamic size distributions of MBB-TP at T = 19 °C and two pH values (5.00 and 9.50).203

Figure 5.7. ^{1}H NMR spectra of a 4.0 mg/g solution of MBB-TP in a 10 mM phosphate buffer made with D_2O at 4 °C with increasing pH value from 5.00 to 9.50 (A), at pH = 9.50 with increasing temperature from 4 to 16 °C (B), at pH = 5.00 and various temperatures upon heating (C), and at 25 °C with increasing pH value from 5.00 to 9.50 (D). The ^{1}H NMR spectra were normalized against the HDO peak at 4.79 ppm. 205

Figure 5.8. AFM height images of MBB-TP spin cast on PMMA-coated mica from a 0.050 mg/g solution of MBB-TP in a 5 mM phosphate buffer at T = 0 °C and pH = 5.00 (A), T = 0 °C and pH = 9.50 (C), T = 20 °C and pH = 9.50 (C), T = 20 °C and pH = 5.00 (D), and T = 20 °C and pH = 9.50 (E). The plot in the bottom of each AFM micrograph shows the cross-sectional profile along the dashed line in the height image. 207

Figure 5.9. (A) Fluorescence emission spectra of Nile Red in a 4.0 mL solution of 0.2 mg/g MBB-PP in a 25 mM phosphate buffer with decreasing pH from 9.50 to 3.50. The nominal concentration of Nile Red was 6.7×10^{-7} M. The pH of the solution was decreased at a step of 0.50 pH unit, and at each pH the sample was equilibrated for 10 min before the fluorescence emission spectrum was taken. The excitation wavelength is 540 nm, and the spectra were recorded from 550 to 720 nm. (B) Plot of fluorescent emission intensity at the maximum peak versus pH. (C) Plot of λ_{max} versus pH. 210

Figure D1. H (A) and ^{13}C (B) NMR spectra of CTA-Alkyne in $CDCl_3$. 236

Figure D2. (A) SEC chromatogram of alkyne-end-functionalized PDEGEA with a DP of 57 from SEC analysis using a PL-GPC 20 with mixed-C columns and THF as the eluent and (B) ^1H NMR spectrum of PDEGEA in $CDCl_3$. 236

Figure D3. (A) SEC chromatogram of alkyne-end-functionalized PDEGMA with a DP of 55 from SEC analysis using a PL-GPC 20 with mixed-C columns and THF as the eluent and (B) ^1H NMR spectrum of PDEGMA in $CDCl_3$. 237

Figure D4. (A) SEC chromatogram of alkyne-end-functionalized PDEAEMA-56 from SEC analysis using a PL-GPC 20 with mixed-C columns and THF as the eluent and (B) ^1H NMR spectrum of PDEAEMA-56 in $CDCl_3$. 237

Figure D5. (A) SEC chromatogram of alkyne-end-functionalized PDEAEMA-45 obtained from a PL-GPC 20 with mixed-C columns and THF as the eluent and (B) ^{1}H NMR spectrum of PDEAEMA-45 in $CDCl_3$. 238

Figure D6. (A) SEC chromatogram of alkyne-end-functionalized PDBAEMA from SEC analysis using a PL-GPC 20 with mixed-C columns and THF as the eluent and (B) ^{1}H NMR spectrum of PDBAEMA in $CDCl_3$. 238

Figure D7. (A) ^{1}H NMR spectrum of MBB-TT in $CDCl_3$. (B) SEC chromatograms of the final reaction mixture for the synthesis of MBB-TT and the purified MBB-TT from SEC analysis using a PL-GPC 50 Plus system equipped with GRAL columns and DMF containing 50 mM LiBr as the eluent. (C) SEC chromatogram of MBB-TT from SEC analysis using a SEC-MALS system comprising PSS GRAM columns and a Varian 390 LC detector system consisting of an RI detector and a two-angle light scattering detector (15° and 90°) at 50 °C. The mobile phase was DMF with 100 mM LiBr. 239

Figure D8. (A) ^{1}H NMR spectrum of purified MBB-TP in $CDCl_3$ and (B) SEC chromatograms of the final reaction mixture and purified MBB-TP from SEC analysis using the PL-GPC 50 Plus system equipped with GRAL columns and DMF containing 50 mM LiBr as the mobile phase. (C) SEC chromatogram of MBB-TP obtained from a SEC-MALS system comprising PSS GRAM columns and a Varian 390 LC detector system consisting of an RI detector and a two-angle light scattering detector (15° and 90°) at 50 °C. The mobile phase was DMF with 100 mM LiBr. 240

Figure D9. (A) ^{1}H NMR spectrum of purified MBB-PP in $CDCl_3$. (B) SEC chromatograms of the final reaction mixture and the purified MBB-PP from SEC analysis using a PL-GPC-50 equipped with GRAL columns and DMF containing 50 mM LiBr as the eluent. Note that PDBAEMA could not be eluted from this SEC system. The absence of the peaks in the retention time range of 16 –

21 min indicated the complete removal of PDEAEMA-45 and PEO side chain polymers. (C) SEC chromatograms of the final reaction mixture for the synthesis of MBB-PP and a mixture of purified MBB-PP and PMMA from SEC analysis using a PL-GPC 20 system with mixed-C columns and THF as the eluent. MBB-PP was not always eluted out from this PL-GPC 20 system, but the absence of the peak in the retention time range of 15 to 18 min in (C) indicated the removal of PDBAEMA. (D) SEC chromatogram of a mixture of a 100 kDa PMMA standard and PDBAEMA from SEC analysis using the PL-GPC 20 system with mixed-C columns and THF as the eluent. 241

Figure D10. SEC chromatogram of MBB-PP from SEC analysis using a SEC-MALS system comprising PSS GRAM columns and a Varian 390 LC detector system consisting of an RI detector and a two-angle light scattering detector (15° and 90°) at 50 °C. The mobile phase was DMF with 100 mM LiBr. The sample for SEC-MALS analysis was prepared by gradually adding DMF (10 mL) into a solution of MBB-PP in THF (10 mL, conc = 0.10 mg/g) and then evaporating THF under a stream of nitrogen. The final concentration of MBB-PP in DMF was 0.43 mg/g. DLS measurements showed that the apparent hydrodynamic diameter (D_h) was 67.9 nm with a polydispersity index (PDI) of 0.16. 242

Figure D11. Additional AFM height images of MBB-PP spin cast onto PMMA-coated mica at room temperature (~ 20 °C) from a 0.05 mg/g MBB-PP solution in a 10 mM phosphate buffer with a pH of 4.00. The average length of 131 MBB molecules from the upper left image was 171.1 ± 42.6 nm. 243

Figure D12. Additional AFM height images of MBB-PP spin cast onto PMMA-coated mica at room temperature (~ 20 °C) from a 0.05 mg/g MBB-PP solution in a 10 mM phosphate buffer with

a pH of 6.00. The average length of 144 MBB-PP molecules from the upper left image was 110.9 ± 44.3 nm. 244

Figure D13. Additional AFM height images of MBB-PP spin cast onto PMMA-coated mica at room temperature (~ 20 °C) from a 0.05 mg/g MBB-PP solution in a 10 mM phosphate buffer with a pH of 9.50. The average diameter of 75 MBB molecules (two measurements for each in perpendicular directions) from the upper left image was 48.9 ± 9.3 nm. 245

Figure D14. Comparison of hydrodynamic size distributions of MBB-TT in Milli-Q water with concentrations of 1.0 and 0.2 mg/g at 1 °C (A) and 65 °C (B), respectively. 246

Figure D15. Additional AFM height images of MBB-TT spin cast onto PMMA-coated mica at 0 °C from a 0.05 mg/g MBB-PP solution in Milli-Q water. The average length of 106 MBB molecules from the upper left image was 169.2 ± 37.5 nm. 247

Figure D16. Additional AFM height images of MBB-TT spin cast onto PMMA-coated mica at 30 °C from a 0.05 mg/g MBB-PP solution in Milli-Q water. The average length of 152 MBB molecules from the upper left image: 124.8 ± 42.4 nm. 248

Figure D17. Additional AFM height images of MBB-TT spin cast onto PMMA-coated mica at 65 °C from a 0.05 mg/g MBB-PP solution in Milli-Q water. The average diameter of 66 globular MBB-TT molecules (two measurements for each in perpendicular directions) from the upper left image: 52.1 ± 15.2 nm. 249

Figure D18. Additional AFM height images of MBB-TP spin cast onto PMMA-coated mica at 0 °C from a 0.05 mg/g MBB-TP solution in a 5 mM phosphate buffer with a pH of 5.00. The average length of 142 MBB molecules from the upper left image was 179.5 ± 41.7 nm. 250

Figure D19. AFM height images of MBB-TP spin cast onto PMMA-coated mica at 0 °C from a 0.05 mg/g MBB-TP solution in a 5 mM phosphate buffer with a pH of 9.50. The average length of 246 MBB-TP molecules from the upper left image: 160.8 ± 40.7 nm. 251

Figure D20. AFM height images of MBB-TP spin cast onto PMMA-coated mica at 20 °C from a 0.05 mg/g MBB-TP solution in a 5 mM phosphate buffer with a pH of 9.50. The solution was prepared by first adjusting the pH from 5.00 to 9.50 and then increasing the temperature from 0 °C to 20 °C. The average length of 100 MBB globular molecules (two measurements for each in perpendicular directions) from the upper left image was 54.5 ± 9.7 nm. 252

Figure D21. Additional AFM height images of MBB-TP spin cast onto PMMA-coated mica at 20 °C from a 0.05 mg/g MBB-TP solution in a 5 mM phosphate buffer with a pH of 5.00. The average length of 211 MBB-TP molecules from the upper left image was 167.1 ± 36.4 nm. 253

Figure D22. Additional AFM height images of MBB-TP spin cast onto PMMA-coated mica at 20 °C from a 0.05 mg/g MBB-TP solution in a 5 mM phosphate buffer with a pH of 9.50. The solution was prepared by first increasing the temperature from 0 to 20 °C and then the pH from 5.00 to 9.50. The average length of 93 MBB-TP globular molecules (two measurements for each in perpendicular directions) from the upper right image was 51.8 ± 9.9 nm. 254

Figure 6.1. (A) ^{1}H and (B) ^{13}C NMR spectra of purified Alkyne DEG-OH in $CDCl_3$. (C) ^{1}H NMR spectrum of PCL in $CDCl_3$. Integrals and peak assignments are shown, which were used to calculate the DP in end-group analysis. (D) SEC analysis of PCL using a GPC system equipped with Mixed-C columns and THF as eluent. 266

Figure 6.2. (A) ^{1}H NMR spectrum of PHEMA-N_3 in $CDCl_3$. (B) SEC analysis of PHEMA-N_3 using a GPC system equipped with Mixed-B columns and DMF with 50 mM LiBr as eluent. 270

Figure 6.3. SEC analysis of PEO MBBs before and after purification for (A) PEO-MBB-0.19, (B) PEO-MBB-0.47, (C) PEO-MBB-0.73, (D) PEO-MBB-0.94, and (E) PEO-MBB-0.96. SEC was performed with a GPC system equipped with Mixed-B columns and DMF with 50 mM LiBr as eluent. 272

Figure 6.4. SEC analysis of PEO MBBs before and after purification for (A) PEO-MBB-0.61 and (B) PEO-MBB-078. SEC analysis was performed using a GPC system equipped with GRAL columns and DMF with 50 mM LiBr as eluent. 273

Figure 6.5. SEC analysis of three-arm star PEO brushes (SBBs) before and after purification for (A) PEO-SBB-0.18, (B) PEO-SBB-0.44, (C) PEO-SBB-0.66, and (D) PEO-SBB-0.88. SEC analysis was performed using a GPC system equipped with Mixed-B columns and DMF with 50 mM LiBr as eluent. 274

Figure 6.6. SEC (A,C,E) of crude and purified MBBs and ^{1}H NMR spectra of purified brushes in $CDCl_3$ (B,D,F) for MBB-$E_{1.00}C_{0.00}$ (A,B), MBB-$E_{0.91}C_{0.09}$ (C,D), and MBB-$E_{0.81}C_{0.19}$ (E,F). .. 278

Figure 6.7. SEC (A,C,E) of crude and purified MBBs and ^{1}H NMR spectra of purified brushes in $CDCl_3$ (B,D,F) for MBB-$E_{0.71}C_{0.29}$ (A,B), MBB-$E_{0.61}C_{0.39}$ (C,D), and MBB-$E_{0.49}C_{0.51}$ (E,F). .. 279

Figure 6.8. SEC (A,C,E) of crude and purified MBBs and ^{1}H NMR spectra of purified brushes in $CDCl_3$ (B,D,F) for MBB-$E_{0.40}C_{0.60}$ (A,B), MBB-$E_{0.30}C_{0.70}$ (C,D), and MBB-$E_{0.21}C_{0.79}$ (E,F). .. 280

Figure 6.9. SEC (A,C) of crude and purified MBBs and ^{1}H NMR spectra of purified brushes in $CDCl_3$ (B,D) for MBB-$E_{0.10}C_{0.90}$ (A,B), and MBB-$E_{0.00}C_{1.00}$ (C,D). 281

List of Schemes

Scheme 1.1. An Overview of Common Synthetic Routes to Prepare Linear Molecular Bottlebrushes with Corresponding Examples Including: Grafting from (a, d), Grafting to (b, e), and Grafting through (c, f) 5

Scheme 1.2. Synthesis of Binary Heterografted Bottlebrush Polymers by a Grafting-to Method Using the Copper(I)-Catalyzed Azide-Alkyne Cycloaddition Reaction. 18

Scheme 2.1. Synthesis of Amphiphilic Heterografted MBBs with Hydrophobic Poly(*n*-butyl acrylate) (P*n*BA) and pH-Responsive Poly(2-(*N*,*N*-diethylamino)ethyl methacrylate) (PDEAEMA) Side Chains by a Click Grafting-to Method 37

Scheme 2.2. Schematic Illustration of Formation and Breaking of Water-in-Oil Emulsion with pH-Responsive Amphiphilic Molecular Bottlebrushes as Emulsifier 75

Scheme A1. Synthesis of PHEMA-TMS, PHEMA-Br, and PHEMA-N_3 85

Scheme 4.1. Conformational Behavior of Amphiphilic Linear Heterografted P*n*BA/PDEAEMA Molecular Bottlebrushes at Planar Air-Water Interfaces in Response to pH Changes and Lateral Compression and Expansion 137

Scheme 5.1. Synthesis of Dually Responsive Linear Ternary Heterografted Molecular Bottlebrushes, MBB-PP, -TT, and -TP, and Stimuli-Induced Stepwise Collapse in Aqueous Solution 185

Scheme 6.1. Synthesis of Alkyne-DEG-OH and Alkyne-End-Functionalized PCL 265

Scheme 6.2. Synthesis of MBBs with PEO Side Chains with Varying Grafting Density 269

Scheme 6.3. Synthesis of MBBs with Semi-Crystalline Polymer Side Chains 276

Chapter 1. Introduction

1.1. Introduction

This dissertation primarily focuses on the synthesis and behavior of responsive heterografted molecular bottlebrush (MBB) polymers at interfaces. Section 1.1.1. gives a basic introduction to MBBs and an overview of the synthetic approaches used to prepare them. Section 1.1.2. summarizes previous research on the use of MBBs as emulsion stabilizers and their interfacial activities. Section 1.1.3. covers the conformational changes of molecular brushes at the planar interfaces. Since a portion of this dissertation work deals with the conformational transitions of responsive multicomponent MBBs in solution, Section 1.1.4. introduces stimuli-responsive shape-changing MBBs in solution and our research group's contributions to this area. An overview of the dissertation work is presented in Section 1.2 at the end of this Chapter.

1.1.1. Introduction to Molecular Bottlebrush Polymers

In recent years, there has been a remarkable surge in the development of novel and complex macromolecular architectures driven by the need to tailor polymeric materials for a wide variety of applications. Among these architectures, MBBs are a special class of macromolecules that has unique structural characteristics and adaptable properties.[1-5] MBBs are composed of a polymer backbone that has densely and covalently grafted side chain polymers extending radially from the backbone as shown in Figure 1A.[1-5] Their molecular structures resemble the flowers of plants in the genus Callistemon, which are also commonly referred to as bottlebrushes (Figure 1B).[7] For MBBs, if the backbone length is significantly larger than the length of the side chains, the brush molecules exhibit a characteristic cylindrical conformation that can be readily seen using molecular imaging techniques such as atomic force microscopy (AFM).[1-6] The distinctive molecular architecture of MBBs imparts many unique properties, including, but not limited to, large persistence length, minimal entanglement along the backbone, and adaptable conformations.

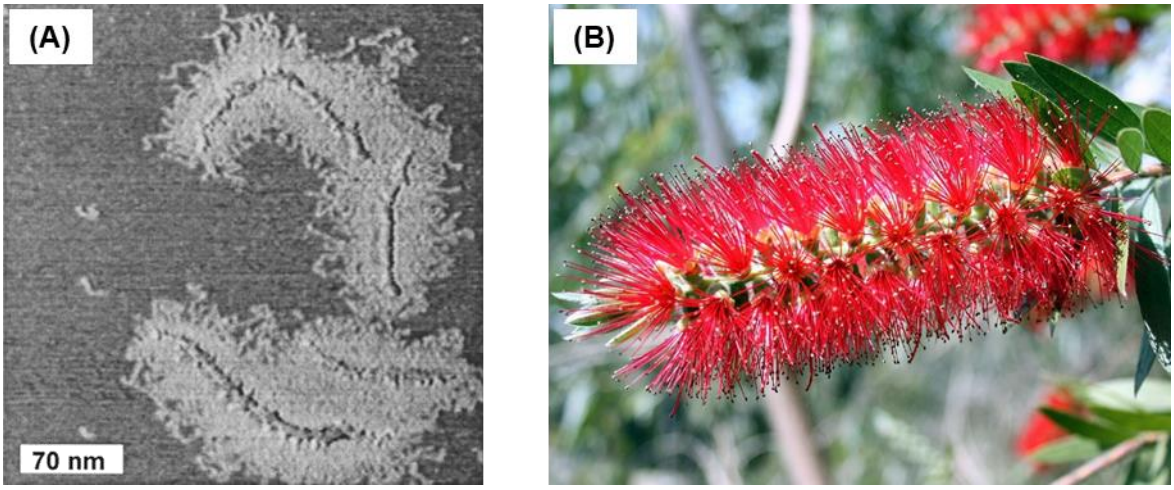

Figure 1.1. (A) Atomic force microscopy height image of molecular bottlebrushes spin cast on a mica substrate in which the backbone and side chain polymers are clearly visible.[8] Reproduced from Ref. 8 with permission from ACS. (B) A flower from a bottlebrush plant.

The side chains of MBBs can be a combination of hydrophilic and hydrophobic polymers, and the unique architecture could lead to enhanced interfacial activity especially for the design of amphiphilic systems. A noteworthy property of MBBs is that they can undergo large and abrupt conformational changes from an extended wormlike state to a unimolecular globular shape in response to external stimuli, which has been shown to occur at liquid-air interfaces, on solid substrates, and in solution.[5,6] This can be accomplished by lateral mechanical compression or by the incorporation of pH or temperature-responsive polymers as side chains. These distinctive characteristics and tunable properties have made MBBs attractive candidates for many potential applications, such as drug delivery, emulsion stabilizers, lubrication, photonic crystals, and nanomaterial fabrication.[9-18]

Historically, there were synthetic challenges in preparing MBBs, especially those with uniform sizes and well-defined structures. Early examples in the literature utilized free radical polymerization of (meth)acrylate based macromonomers, but this approach lacked the ability to produce MBBs with good control.[19,20] In the past thirty years, with the development of "living"/controlled polymerization techniques such as atom transfer radical polymerization (ATRP), reversible addition-fragmentation chain transfer (RAFT) polymerization, and ring-opening metathesis polymerization (ROMP), researchers have a larger toolbox to prepare brush materials and as a result many different subsets of MBBs have emerged, including MBB block copolymers, core shell MBBs, Janus MBBs, and brush on brush architectures.[1-4]

As shown in Scheme 1.1, there are three primary avenues to synthesize MBBs, which include "grafting from", "grafting through", and "grafting to". Grafting-from is a process of synthesizing polymeric side chains from initiating sites along a polymer backbone, also known as a macroinitiator.[1-4,20] This method has primarily been used to prepare homografted MBBs consisting

Scheme 1.1. An Overview of Common Synthetic Routes to Prepare Linear Molecular Bottlebrushes with Corresponding Examples Including: Grafting from (a, d), Grafting to (b, e), and Grafting through (c, f).[5] Reproduced from Ref. 5 with permission from ACS.

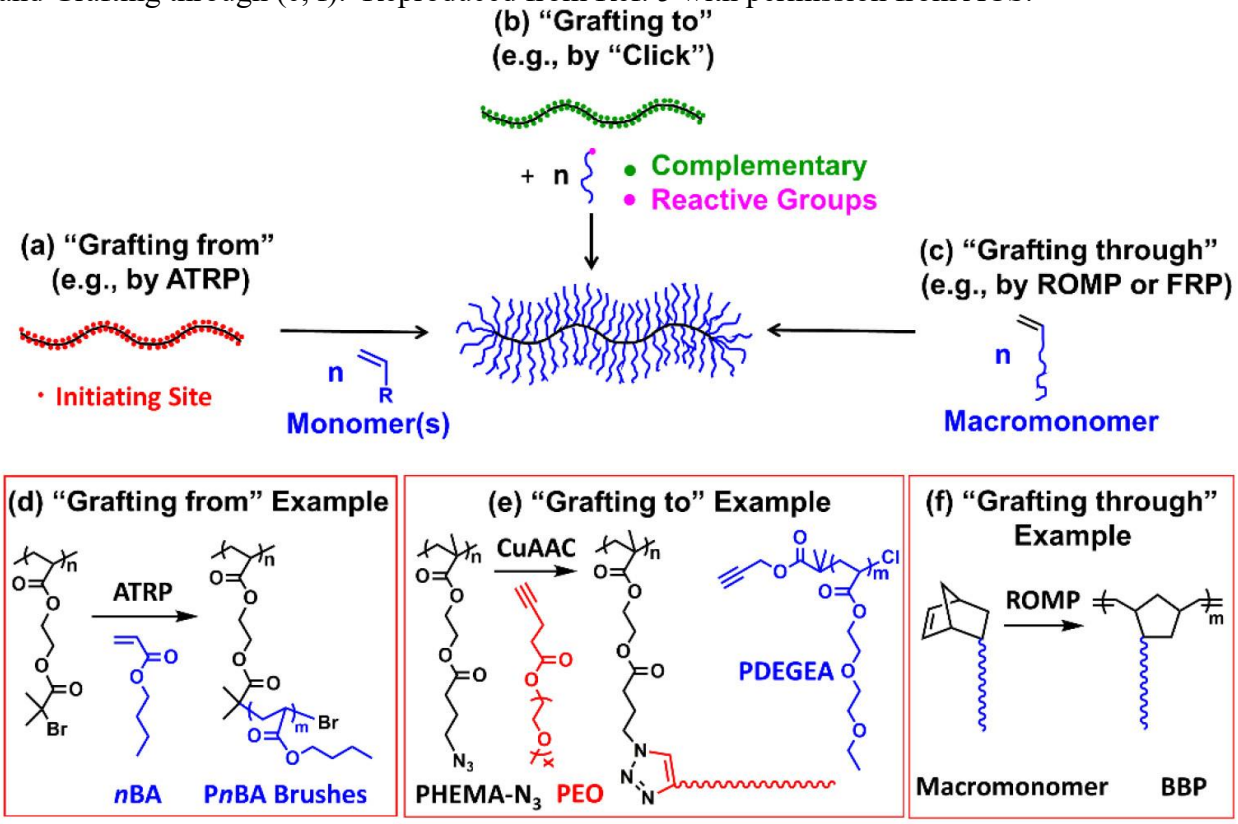

of only one type of polymer side chain. It is possible to prepare brush polymers with additional functionality by growing block copolymer side chains and to achieve MBBs with heterografted side chains by utilizing two distinct polymer initiating groups.[21-23] If the initiation efficiency is sufficiently, MBBs with densely grafted side chains can be made, and unreacted monomer molecules can be readily removed from the brush polymers by precipitation. However, there are some challenges in the grafting from approach. For example, it is possible and likely that termination occurs by coupling of different brush molecules during the side chain synthesis, which could lead to the crosslinking of bottlebrush polymers. Also, in this method, it is difficult to accurately determine the side chain length and composition without cleaving them from the backbone.

The grafting through technique involves the polymerization of macromonomers, which are the polymers with a polymerizable end group, and has been used more commonly in recent years. As mentioned previously, early examples of this approach using (meth)acrylate-end-functionalized macromonomers were unable to produce MBBs with a large backbone length and a uniform composition,[19,20] which was attributed to the bulky nature of the macromonomers. With the advent and utilization of ROMP and norbornene macromonomers, researchers have been able to achieve greater and more uniform backbone lengths.[1-4,24-26] However, there are some drawbacks with this method, including the rigidity of polynorbornene backbones compared with poly(meth)acrylate counterparts. In addition, if we assume one side chain per backbone repeat unit, the theoretical grafting density of polynorbornene-based MBBs from ROMP is lower that of poly(methy)acrylate-based MBBs as there are five carbon atoms per repeat unit rather than two.

In the grafting-to method, the backbone polymer and side chain polymers are prepared separately. The polymer backbone is composed of numerous pendant functional sites, often at

every repeat unit, and the side chain polymers have a functional end group that can react with the complementary pendant groups on the backbone polymer.[1-4] By using highly efficient click chemistries, such as the copper(I)-catalyzed azide-alkyne cycloaddition (CuAAC) reaction, it is possible to achieve high grafting densities.[27-39] Our group has primarily used this approach by preparing backbone polymers with azide functional groups in each repeat unit and alkyne end-functionalized side chain polymers using controlled radical polymerization or post polymerization modification.[28-36] This offers advantages as both backbone and side chain polymers are synthesized separately and can be fully characterized prior to the synthesis of MBBs, which allows for a better control of the molecular architecture. In addition, the grafting-to method is a modular approach, and it is relatively easy to prepare heterografted MBBs with different types of side chains and vary the side chain composition of MBBs by modifying the type and amounts of side chain polymers used in the synthesis. The multicomponent heterografted MBBs described in this dissertation work were prepared using the grafting-to approach.

1.1.2. Molecular Bottlebrushes as Emulsion Stabilizers

One potential application of MBBs is to act as macromolecular surfactants for stabilizing emulsions. Due to the large molecular size, MBBs could offer some of the advantageous properties of Pickering emulsions. Pickering emulsions are the emulsions stabilized by particles and are noted for their stability and the particle tunability for certain applications, such as stimuli responsive emulsions.[40] In a similar fashion, judiciously designed MBBs could also have a strong affinity for water/oil interfaces by using a combination of hydrophilic and hydrophilic grafts. However, to date, there is not a significant amount of literature reporting their use for as emulsion stabilizers or emulsifiers. One of the earliest examples was reported by Cheng et al., in which they prepared polynorbornene-based bottlebrush polymers with a combination of hydrophilic poly(ethylene

oxide) (PEO) and hydrophobic poly(lactic acid) (PLA) side chains on each backbone repeat unit.[12] By ultrasonication, they prepared MBB-stabilized oil-in-water miniemulsions that showed enhanced stability compared with the use of corresponding macromonomer, which was attributed to the large size of the brush polymer. Dynamic light scattering (DLS) measurements showed little fluctuation in the diameter of the emulsion droplets, demonstrating the superior performance of the MBB-stabilized emulsion systems. Matyjaszewski et al. reported heterografted bottlebrush polymers with a combination of poly(*n*-butyl acrylate) (P*n*BA) and PEO as the side chains, which were synthesized in a combination of grafting from and through approach.[13] They observed that heterografted MBBs were able to stabilize water-in-oil type emulsions at concentrations as low as 0.005 wt% and that MBBs performed better than diblock copolymer analogs as emulsifiers. The better performances of MBBs were attributed to several factors, including the combination of hydrophilic and hydrophobic grafts that had preferential attachment to the aqueous and organic phase, respectively, acting in a similar fashion to Janus particles (Figure 1.2). They performed pendant drop experiments to measure the interfacial tension as a function of time and found that all MBBs lowered the interfacial tension. However, they noted that the decrease did not always correlate with the emulsifying efficiencies of brush polymer samples. A more recent study by Qi et al. used a relatively small polyurethane-based backbone with poly(*N,N*-dimethyl acrylamide) and poly(methyl methacrylate) side chains that could stabilize ionic liquid-in-benzene emulsions.[41] Shi et al. reported that stable emulsions were generated by exploiting strong electrostatic interactions between homografted MBBs with poly(acrylic acid) (PAA) side chains from the water phase and amine-functionalized polyhedral oligomeric silesequioxane (POSS-NH_2) from the toluene phase to form robust assemblies at the interface.[42] The emulsion type could be tailored by altering the amount of each component. Interestingly, PAA MBBs and POSS-NH_2 alone could not

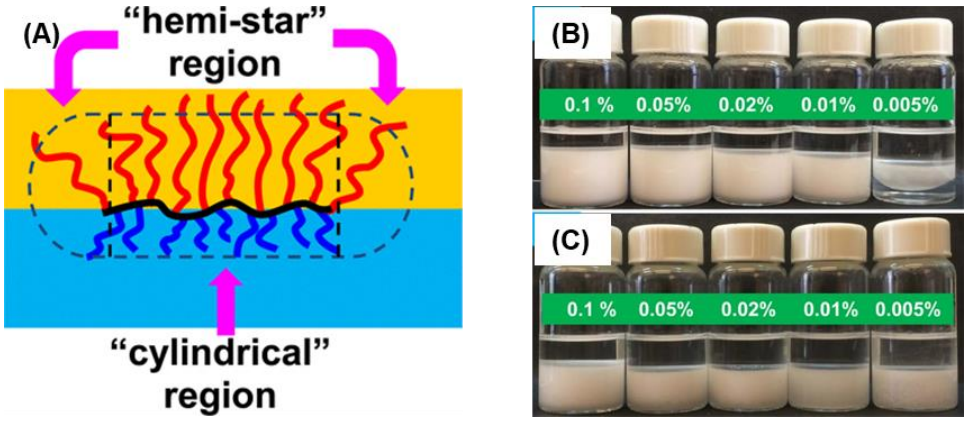

Figure 1.2. (A) The proposed arrangement of amphiphilic molecular bottlebrushes with PEO and PnBA grafts.[13] (B) and (C) digital photos of water-in-xylene emulsions stabilized by amphiphilic MBBs.[13] Reproduced from Ref. 13 with permission from ACS.

produce stable emulsions. Pendant drop tensiometry experiments showed that the interfacial tension decreased significantly when PAA MBBs in water and POSS-NH_2 formed assemblies at the interface. When the water droplet containing PAA bottlebrushes was withdrawn from a toluene solution of POSS-NH_2, wrinkling was observed at the interface, indicating the solid like nature of the interfacial assembly. They exploited this phenomenon to print stable 3D liquid structures. A subsequent work used the same system to form emulsions of *N*,*N*-dimethylformamide and octane, and the interfacial tension reduction was demonstrated similarly.[43]

Russell and Emrick et al. recently reported amphiphilic polynorbornene-based MBBs with PEO and polydimethylsiloxane side chains synthesized using a grafting through approach via the use of ROMP.[44] This work focused on the mechanism of MBBs' dynamic assembly at water-toluene interfaces; the roles of molecular weight and grafting density were systematically studied through interfacial tension measurements and fluorescence recovery after photobleaching experiments. They found that the interfacial assembly of amphiphilic PEO/PDMS MBBs occurs in three major steps: diffusion to the water-oil interface, adsorption and reconfiguration into a Janus-like conformation, and then reorganization at the interface. As shown in Figure 1.3a, they found that the lowest molecular weight MBB (P1, backbone DP = 20) lowered the interfacial tension (γ) more rapidly. MBBs with progressively longer backbone DPs (DP_{P2} = 50, DP_{P3} = 100, DP_{P4} = 200) exhibited increasingly slower diffusion rates (Figure 1.3a). It was found that the ability of these MBBs to lower γ decreased with increasing molecular weight (Figure 1.3a and c). Plotting the interfacial tension on a linear scale with time on a log scale showed three distinct regimes: induction, adsorption/reconfiguration, and reorganization (Figure 1.3b). Exponential relaxation functions were used to extract the relaxation times for adsorption and reorganization for each brush polymer, and interestingly, larger MBBs underwent reorganization more rapidly once absorbed at

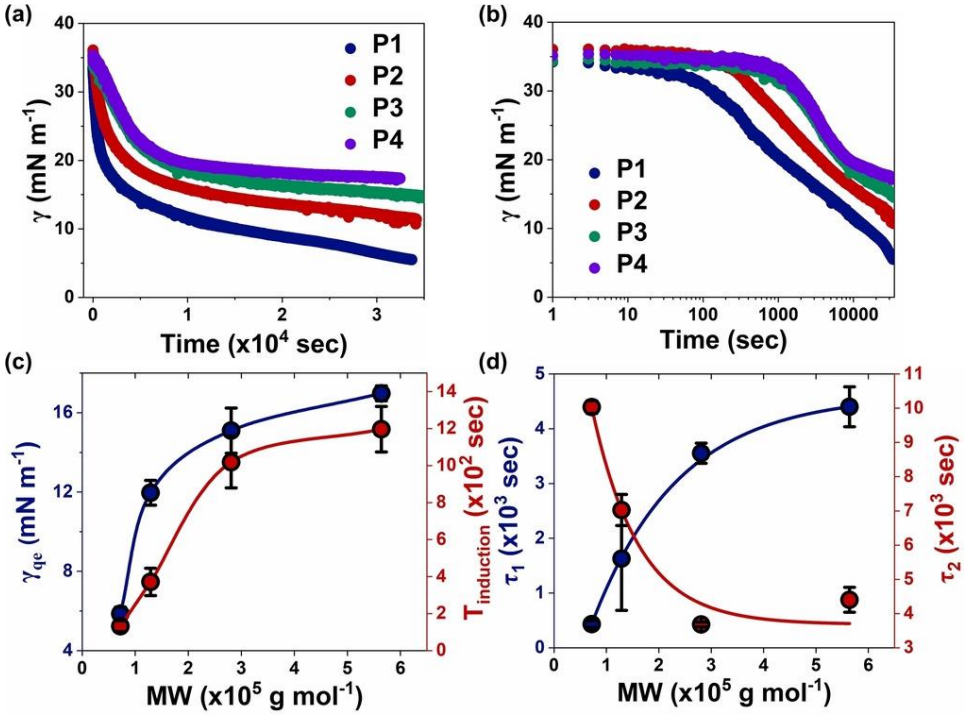

Figure 1.3. (a) Time dependence of interfacial tension at the water-toluene interface for MBBs with different backbone lengths at a concentration of 0.001 mg/mL. (b) Semi log plot of interfacial tension (linear) vs time (log). (c) Equilibrium interfacial tension and the corresponding induction time. (d) Characteristic relaxation times of MBBs fitted with an exponential relaxation function.[44] Reproduced from Ref. 44 with permission from Wiley.

the interface (Figure 1.3d). They also found that MBBs with higher grafting densities showed a reduced interfacial activity, which was attributed to the increased steric hindrance of side chains, limiting their ability to effectively reconfigure at the interface.

There is a great interest in developing emulsion stabilizers using advanced polymer architectures for stimuli-responsive and reversible emulsion breaking.[45] In the oil and gas industry, one challenge is that it is energy intensive to break water/oil emulsions.[40,46] Being able to introduce a simple stimulus such as a change in temperature or pH could provide a means of saving time and reducing energy consumption. There are many examples in the literature reporting on responsive Pickering emulsion systems. However, there are few examples utilizing MBBs for emulsions, and up to this point, we are not aware of any report describing the use of amphiphilic stimuli responsive MBBs as emulsion stabilizers.

1.1.3. Conformational Transitions of Molecular Bottlebrushes at Flat Interfaces

Sheiko et al. published a series of articles on the behavior of MBBs at flat air-water interfaces using a Langmuir-Blodgett (LB) trough. Although flat air-water surfaces are not analogous to the liquid-liquid interfaces in emulsion droplets, the study of the behavior of MBBs at flat interfaces can provide insight into the general ways that MBBs respond to external stimuli. When an LB trough is used, a dilute polymer solution is added onto the surface of a liquid subphase, commonly water, and a monolayer is formed after the organic solvent is evaporated. The monolayer can be laterally compressed and decompressed, and the surface pressure is monitored using a Wilhelmy plate as a function of mean surface area per molecule. This compression-decompression LB isotherm can provide insight into the molecular arrangement and the area that the analyte occupies at the interface. Another useful aspect of the LB trough is that uniform monolayers can be

transferred to a solid substrate for various purposes, e.g., study of surface morphology by molecular imaging techniques such as AFM.

Sheiko et. al demonstrated that it was possible to use lateral mechanical compression to induce the rod-globule shape transitions of MBBs at the air-water interface using a LB trough.[8] They synthesized MBBs with homografted P*n*BA side chains and spread the brushes on the water surface in a LB trough. By compressing the P*n*BA bottlebrushes to a certain point, they found that the surface pressure initially increased rapidly, followed by the appearance of a distinct plateau region where there was minimal change in surface pressure. Upon decompression, only a slight hysteresis was observed, and the surface pressure returned approximately to its initial value. AFM samples at different levels of compression were prepared for studying the morphology of the brush molecules. They found that if the side chains were sufficiently long, the brush molecules exhibited a "pseudo"-first-order phase transition from extended wormlike molecules to uniform spheres. In a subsequent work, four-armed star MBBs with P*n*BA side chains were studied.[47] Like their linear counterparts, lateral compression of P*n*BA star brushes at the air/water interface resulted in a conformation transition from an extended starlike to a compact disklike shape. One additional interesting observation from AFM was that disklike brush molecules exhibited well-defined hexagonal packing, which was not seen for linear P*n*BA brushes in the globular state. This was attributed to the lower dispersity of the four-armed star brush polymers. Similar conformational changes of linear P*n*BA MBBs were also achieved by adjusting the subphase via the addition of methanol to alter the surface free energy of the subphase and the interfacial free energy between P*n*BA MBBs and the subphase.[48] There are some other reports of bottlebrush-type polymers at the air/water interface,[49-51] but none showed large changes in molecular conformation.

In addition to air/liquid interfaces, Sheiko et. al studied the behavior of P*n*BA MBBs on solid substrates in response to different solvent vapors.[52-54] The brush molecules exhibited a cylindrical conformation on mica after spin casting and underwent swelling upon exposure to ethanol vapor. Intriguingly, when water vapor was introduced into the sample chamber, the bottlebrushes began to transform to a globular shape, which was monitored in real time by AFM (Figure 1.4).[54] The ethanol content of the vapor was important, and they found that at lower ethanol content the brush molecules expanded. When the ethanol content in the vapor was sufficiently high, the P*n*BA MBBs contracted into a globular shape. This was attributed to the lower surface tension of ethanol relative to water, which was confirmed by a subsequent study using different solvents with varying surface tension values.[54] These observations are analogous to the LB trough studies utilizing a methanol/water subphase.[48]

1.1.4. Conformational Transitions of Stimuli-Responsive Molecular Bottlebrush Polymers in Solution

By using stimuli-responsive polymers as the side chains, MBBs have been shown to undergo unimolecular shape transitions or assemble into other morphologies in solution.[5,6] Many stimuli have been studied for this purpose, including temperature, pH, light, and ion effects.[28-36,55-66] An early example was presented by Schmidt et al. who synthesized a bottlebrush polymer with poly(*N*-isopropylacrylamide) (PNIPAM) side chains and investigated its behavior in water.[55] PNIPAM is a thermoresponsive polymer exhibiting lower critical solution temperature (LCST) behavior and is only fully water soluble at temperatures below its LCST of 32 °C. Using dynamic light scattering (DLS), they observed that the hydrodynamic size of the brush polymer decreased drastically in a narrow temperature range upon heating to above the LCST. When the temperature was increased further to 38 °C, the brushes aggregated and precipitated, which was seen from AFM images.

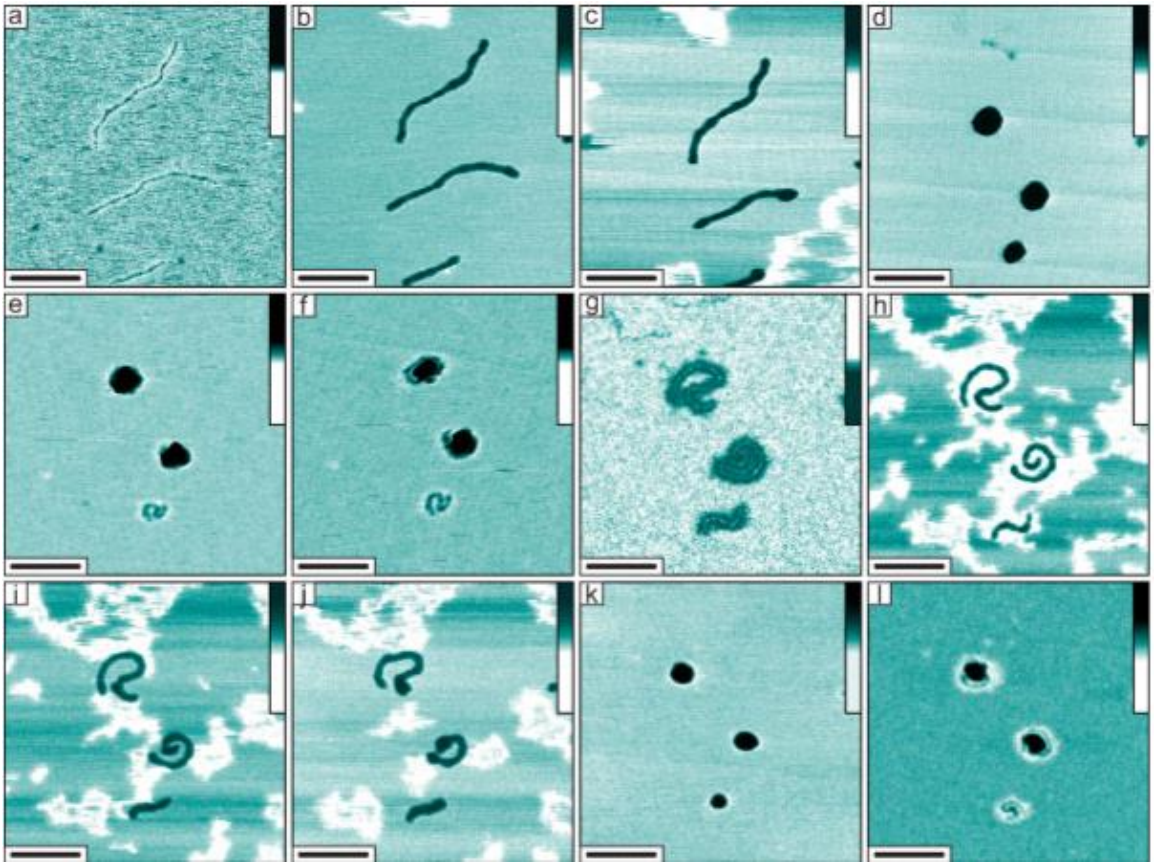

Figure 1.4. Sequential AFM images demonstrating the collapse and uncoiling of MBBs with PnBA side chains on a mica substrate in vapors saturated with humidified ethanol.[53] Reproduced from Ref. 53 with permission from Wiley.

Subsequent studies investigated MBBs with various stimuli-responsive polymers as side chains. Matyjaszewski and coworkers reported on several examples of responsive bottlebrush polymers and their conformation behavior in response to pH or temperature changes.[56-61] They synthesized MBBs with homografted copolymer side chains composed of poly(*N*,*N*-dimethylacrylamide-*co*-*n*-butyl acrylate) and observed from DLS studies that the brush molecules showed a decrease in hydrodynamic size as temperature increased when the polymer concentration in the aqueous solution was only 0.1 wt%.[57] However, at a concentration of 1.0 wt%, the measured hydrodynamic size of MBBs increased upon increasing temperature, which was attributed to the aggregation of brush molecules. A subsequent paper reported the synthesis of bottlebrush polymers composed of random copolymers of di(ethylene glycol) methyl ether methacrylate (DEGMMA) and tri(ethylene glycol) methyl ether methacrylate (TEGMMA) as well as block copolymers of these two monomers as side chains by grafting from a macroinitiator backbone via ATRP.[58] For MBBs with copolymer side chains, they showed that the cloud point of the brush polymers in water was proportional to the amount of TEGMMA, which was more hydrophilic. For the core-shell bottlebrushes with diblock copolymer side chains, they found that if the inner block had a lower LCST, the measured hydrodynamic size decreased initially upon heating and increased when the temperature was raised to above the LCST of poly(TEGMMA), suggesting that PTEGMMA formed a water-soluble corona around the aggregated PDEGMMA inner blocks at temperatures below its LCST. In another example, the same group studied the pH-responsive conformational behavior of MBBs with PAA side chains as a function of pH by AFM.[59] PAA was insoluble in water under acidic conditions but became soluble at basic conditions when the -COOH groups were deprotonated. At low grafting densities, the brushes were found to undergo a transition from

a compact to an extended conformation, correlating with the increase of the solubility of PAA side chains in water.

Reversible shape-changing bottlebrushes have many potential applications, for instance, encapsulation and delivery of substances. To make them viable materials, it is important to be able to stabilize the collapsed state in order to avoid aggregation of the brush molecules. In the above examples, it is important to note that those responsive MBBs tended to aggregate in the collapsed state unless under very dilute conditions. In recent years, our research group has developed robust approaches to achieve stabilization of collapsed globular MBBs by introducing hydrophilic polymers into the side chains of stimuli-responsive MBBs, either as a second set of side chains in heterografted brushes or as the out block of block copolymer side chains in homografted MBBs.[28-36] Using these strategies, we have demonstrated unimolecular shape changes of MBBs in water in response to several types of stimuli: temperature, pH, light, and chaotropic anions. Henn et al. prepared binary heterografted MBBs with poly(diethylene glycol ethyl ether acrylate) (PDEGEA, LCST 9 °C) and poly(ethylene oxide) (PEO) as side chains (BMB) by a click grafting to method (Scheme 1.2) and compared their solution behavior with homografted PDEGEA brushes (HMB).[28] Aqueous solutions of HMB turned from clear to cloudy at temperatures above the LCST of PDEGEA, while solutions of BMB remained clear. DLS studies of BMB showed the decrease in hydrodynamic size as the temperature of the solution was increased to above the LCST of the PDEGEA side chains; the size distributions overlapped for 0.2 and 1.0 mg/g solutions, which indicated that the shape change of the MBBs was unimolecular. Further studies by AFM provided direct evidence of the wormlike-to-globular shape transition of the brush molecules, demonstrating the role of PEO as a hydrophilic stabilizer. A subsequent study demonstrated that longer PEO side chains were more effective in stabilizing the collapsed state of thermoresponsive MBBs in

Scheme 1.2. Synthesis of Binary Heterografted Bottlebrush Polymers by a Grafting-to Method Using the Copper(I)-Catalyzed Azide-Alkyne Cycloaddition Reaction.[28] Reproduced from Ref. 28 with permission from ACS.

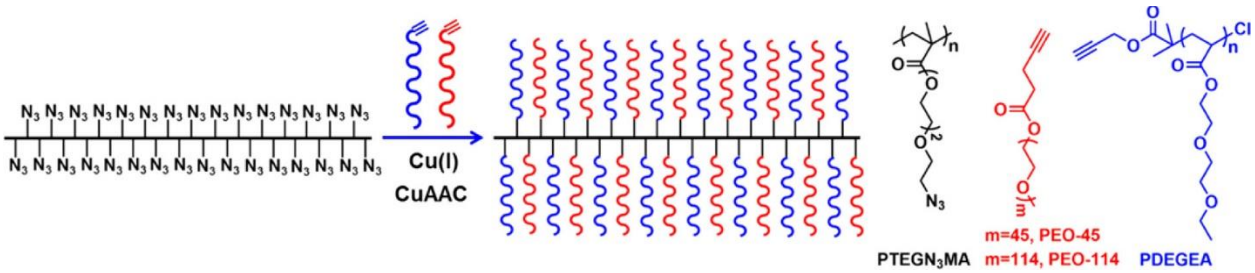

moderately concentrated aqueous solutions.[30] They also provided evidence that the MBBs could undergo reversible unimolecular shape transitions at concentrations as high as 100 mg/g by incorporating a photocrosslinkable moiety into the thermoresponsive side chains of the MBBs and crosslinking the collapsed brushes by UV irradiation prior to dilution for DLS and AFM studies.

Later, Kent et al. synthesized a bottlebrush polymer with homografted diblock side chains composed of pH-responsive poly(2-(*N*,*N*-diethylamino)ethyl methacrylate (PDEAEMA, pK_a = 7.4) as the inner block and temperature-responsive poly(methoxytri(ethylene glycol) acrylate) (PTEGMA) as the outer block.[31] For comparison, a brush polymer with only PDEAEMA side chains was also prepared. DLS measurements of the homografted PDEAEMA brushes in an aqueous solution showed an initial decrease in hydrodynamic size (D_h) as the pH was increased from acidic conditions, but large increases in D_h were observed when the pH was further increased to above the pK_a of PDEAEMA, indicating intermolecular aggregation (Figure 1.5). In contrast, the brush polymer with diblock copolymer side chains underwent a unimolecular shape change in response to pH changes; DLS measurements showed a significant decrease in D_h as the pH was increased to above the pK_a of PDEAEMA and the D_h remained stable even at a pH of 10.0. AFM provided further evidence of the unimolecular collapse. By heating to above the LCST of the PTEGMA outer block, the brushes aggregated, and much larger species were observed from AFM images. In a subsequent work, Kent synthesized a three-arm star brush polymer that was heterografted with a combination of PDEAEMA and PDEGEA side chains to impart both pH- and temperature-responsive properties.[32] This work demonstrated that two distinct collapsed states of star brushes could be achieved by keeping one side chain polymer soluble in water, either at low temperatures or at acidic pH values, while decreasing the solubility of the other polymer (Figure 1.6). If both side chain polymers were insoluble, the star MBB would precipitate from water.

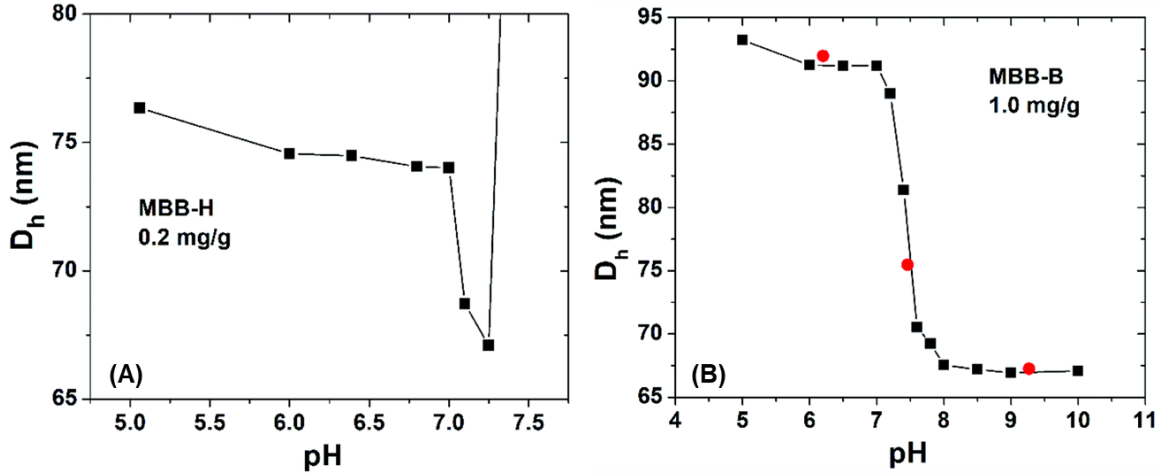

Figure 1.5. Hydrodynamic diameter (D_h) of (A) a homografted brush polymer with PDEAEMA homopolymer side chains and (B) a homografted brush polymer with diblock copolymer side chains composed of pH-responsive PDEAEMA as the inner block and thermoresponsive PTEGMA as the outer block as a function of pH. The D_h values were measured by dynamic light scattering.[31] Reproduced from Ref. 31 with permission from RCS.

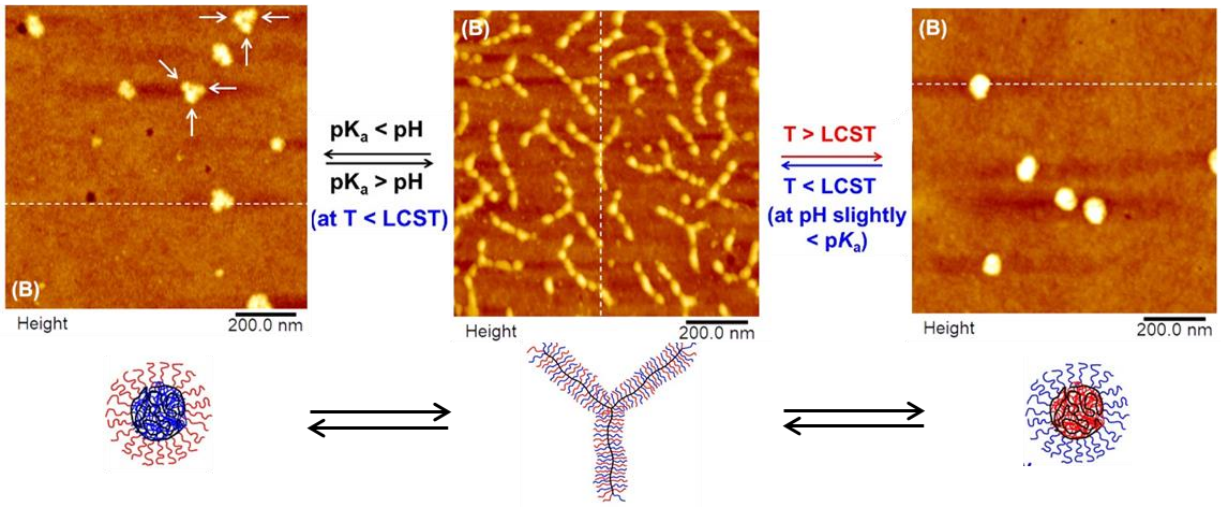

Figure 1.6. AFM height images showing that a three-arm star brush polymer with heterografted pH-responsive PDEAEMA and thermoresponsive PDEGEA side chains collapsed into two distinct globular states under different conditions.[32] Reproduced from Ref. 32 with permission from ACS.

1.2. Dissertation Overview

This dissertation research investigates the behavior of amphiphilic pH-responsive binary heterografted bottlebrush polymers at liquid/liquid and air/water interfaces and the shape transitions of dually responsive ternary heterografted MBBs in aqueous solutions. Chapter 2 presents a detailed study of amphiphilic heterografted bicomponent MBBs with hydrophobic P*n*BA and PDEAEMA side chains as pH-responsive emulsifiers. We show that MBBs with appropriate side chain compositions are effective and efficient emulsifiers for forming stable water-in-oil type emulsions that can be broken by adjusting the pH of the aqueous phase. In chapter 3, we take a closer look at the effects of side chain composition and pH on the reduction of the interfacial tension between toluene and water by amphiphilic pH-responsive MBBs using pendant drop tensiometry. Chapter 4 studies the conformational behavior of these amphiphilic bottlebrush polymers at the planar air/water interface in a Langmuir-Blodgett trough in response to pH changes and lateral mechanical compression. Chapter 5 presents three ternary bottlebrush polymers with a combination of a hydrophilic polymer and two stimuli-responsive polymers as the side chains, all of which show stepwise shape changing behavior. A potential application for drug delivery is demonstrated using a fluorescent probe. Chapter 6 presents the synthesis of two series of MBBs with semicrystalline polymer side chains. The first series is linear and three-arm star MBBs with homografted PEO arms and the second series is linear heterografted MBBs composed of PEO and poly(ε-caprolactone) (PCL) side chains. Chapter 7 offers a summary of my graduate research and a perspective for future study. This dissertation work reveals the interesting behavior of stimuli-responsive multicomponent heterografted bottlebrush polymers at interfaces and in solution, providing insights about this class of architecturally complex polymers for potential applications in diverse areas.

References

1. Zhang, M.; Müller, A. H. E., Cylindrical polymer brushes. *Journal of Polymer Science Part A: Polymer Chemistry* **2005,** *43* (16), 3461-3481.
2. Sheiko, S. S.; Sumerlin, B. S.; Matyjaszewski, K., Cylindrical molecular brushes: Synthesis, characterization, and properties. *Progress in Polymer Science* **2008,** *33* (7), 759-785.
3. Yuan, J.; Müller, A. H. E.; Matyjaszewski, K.; Sheiko, S. S., 6.06 - Molecular Brushes. In *Polymer Science: A Comprehensive Reference*, Matyjaszewski, K.; Möller, M., Eds. Elsevier: Amsterdam, 2012; pp 199-264.
4. Li, Z.; Tang, M.; Liang, S.; Zhang, M.; Biesold, G. M.; He, Y.; Hao, S.-M.; Choi, W.; Liu, Y.; Peng, J.; Lin, Z., Bottlebrush polymers: From controlled synthesis, self-assembly, properties to applications. *Progress in Polymer Science* **2021,** *116*, 101387.
5. Zhao, B., Shape-Changing Bottlebrush Polymers. *J. Phys. Chem. B* **2021**, *125(24)*, 6373-6389.
6. Lee, H.-i.; Pietrasik, J.; Sheiko, S. S.; Matyjaszewski, K. Stimuli-responsive molecular brushes. *Progress in Polymer Science* **2010**, *35(1)*, 24-44.
7. Mitchem, C., Callistemon-the beautiful bottlebrushes. *Plantsman* **1993**.
8. Sheiko, S. S.; Prokhorova, S. A.; Beers, K. L.; Matyjaszewski, K.; Potemkin, I. I.; Khokhlov, A. R.; Möller, M., Single Molecule Rod−Globule Phase Transition for Brush Molecules at a Flat Interface. *Macromolecules* **2001,** *34* (23), 8354-8360.
9. Johnson, J. A.; Lu, Y. Y.; Burts, A. O.; Xia, Y.; Durrell, A. C.; Tirrell, D. A.; Grubbs, R. H., Drug-Loaded, Bivalent-Bottle-Brush Polymers by Graft-through ROMP. *Macromolecules* **2010,** *43* (24), 10326-10335.

10. Liao, L.; Liu, J.; Dreaden, E. C.; Morton, S. W.; Shopsowitz, K. E.; Hammond, P. T.; Johnson, J. A., A Convergent Synthetic Platform for Single-Nanoparticle Combination Cancer Therapy: Ratiometric Loading and Controlled Release of Cisplatin, Doxorubicin, and Camptothecin. *Journal of the American Chemical Society* **2014,** *136* (16), 5896-5899.
11. Müllner, M., Molecular polymer bottlebrushes in nanomedicine: therapeutic and diagnostic applications. *Chemical Communications* **2022**.
12. Li, Y.; Zou, J.; Das, B. P.; Tsianou, M.; Cheng, C., Well-Defined Amphiphilic Double-Brush Copolymers and Their Performance as Emulsion Surfactants. *Macromolecules* **2012,** *45* (11), 4623-4629.
13. Xie, G.; Krys, P.; Tilton, R. D.; Matyjaszewski, K., Heterografted Molecular Brushes as Stabilizers for Water-in-Oil Emulsions. *Macromolecules* **2017,** *50* (7), 2942-2950.
14. Banquy, X.; Burdyńska, J.; Lee, D. W.; Matyjaszewski, K.; Israelachvili, J., Bioinspired Bottle-Brush Polymer Exhibits Low Friction and Amontons-like Behavior. *Journal of the American Chemical Society* **2014,** *136* (17), 6199-6202.
15. Adibnia, V.; Olszewski, M.; De Crescenzo, G.; Matyjaszewski, K.; Banquy, X., Superlubricity of Zwitterionic Bottlebrush Polymers in the Presence of Multivalent Ions. *Journal of the American Chemical Society* **2020,** *142* (35), 14843-14847.
16. Liberman-Martin, A. L.; Chu, C. K.; Grubbs, R. H., Application of Bottlebrush Block Copolymers as Photonic Crystals. *Macromolecular Rapid Communications* **2017,** *38* (13), 1700058.
17. Rzayev, J., Molecular Bottlebrushes: New Opportunities in Nanomaterials Fabrication. *ACS Macro Letters* **2012,** *1* (9), 1146-1149.

18. Pelras, T.; Mahon, C. S.; Nonappa; Ikkala, O.; Gröschel, A. H.; Müllner, M., Polymer Nanowires with Highly Precise Internal Morphology and Topography. *Journal of the American Chemical Society* **2018,** *140* (40), 12736-12740.

19. Dziezok, P.; Fischer, K.; Schmidt, M.; Sheiko, S. S.; Möller, M., Cylindrical Molecular Brushes. *Angewandte Chemie International Edition in English* **1997,** *36* (24), 2812-2815.

20. Beers, K. L.; Gaynor, S. G.; Matyjaszewski, K.; Sheiko, S. S.; Möller, M., The Synthesis of Densely Grafted Copolymers by Atom Transfer Radical Polymerization. *Macromolecules* **1998,** *31* (26), 9413-9415.

21. Börner, H. G.; Beers, K.; Matyjaszewski, K.; Sheiko, S. S.; Möller, M., Synthesis of Molecular Brushes with Block Copolymer Side Chains Using Atom Transfer Radical Polymerization. *Macromolecules* **2001,** *34* (13), 4375-4383.

22. Cheng, G.; Böker, A.; Zhang, M.; Krausch, G.; Müller, A. H. E., Amphiphilic Cylindrical Core−Shell Brushes via a "Grafting From" Process Using ATRP. *Macromolecules* **2001,** *34* (20), 6883-6888.

23. Lee, H.-i.; Matyjaszewski, K.; Yu-Su, S.; Sheiko, S. S., Hetero-Grafted Block Brushes with PCL and PBA Side Chains. *Macromolecules* **2008,** *41* (16), 6073-6080.

24 Jha, S.; Dutta, S.; Bowden, N. B., Synthesis of Ultralarge Molecular Weight Bottlebrush Polymers Using Grubbs' Catalysts. *Macromolecules* **2004,** *37* (12), 4365-4374.

25. Xia, Y.; Kornfield, J. A.; Grubbs, R. H., Efficient Synthesis of Narrowly Dispersed Brush Polymers via Living Ring-Opening Metathesis Polymerization of Macromonomers. *Macromolecules* **2009,** *42* (11), 3761-3766.

26. Li, Z.; Ma, J.; Cheng, C.; Zhang, K.; Wooley, K. L., Synthesis of Hetero-Grafted Amphiphilic Diblock Molecular Brushes and Their Self-Assembly in Aqueous Medium. *Macromolecules* **2010,** *43* (3), 1182-1184.

27. Fournier, D.; Hoogenboom, R.; Schubert, U. S., Clicking polymers: a straightforward approach to novel macromolecular architectures. *Chemical Society Reviews* **2007,** *36* (8), 1369-1380.

28. Henn, D. M.; Fu, W.; Mei, S.; Li, C. Y.; Zhao, B., Temperature-Induced Shape Changing of Thermosensitive Binary Heterografted Linear Molecular Brushes between Extended Wormlike and Stable Globular Conformations. *Macromolecules* **2017**, 50 (4), 1645-1656.

29. Henn, D. M.; Lau, C. M.; Li, C. Y.; Zhao, B., Light-triggered unfolding of single linear molecular bottlebrushes from compact globular to wormlike nano-objects in water. *Polymer Chemistry* **2017**, 8 (17), 2702-2712.

30. Henn, D. M.; Holmes, J. A.; Kent, E. W.; Zhao, B., Worm-to-Sphere Shape Transition of Thermoresponsive Linear Molecular Bottlebrushes in Moderately Concentrated Aqueous Solution. *The Journal of Physical Chemistry B* **2018**, 122 (27), 7015-7025.

31. Kent, E. W.; Henn, D. M.; Zhao, B., Shape-changing linear molecular bottlebrushes with dually pH- and thermo-responsive diblock copolymer side chains. *Polymer Chemistry* **2018**, 9 (41), 5133-5144.

32. Kent, E. W.; Zhao, B., Stimuli-Induced Star-Globule Shape Transitions of Dually Responsive Binary Heterografted Three-Arm Star Molecular Brushes in Aqueous Solution. *Macromolecules* **2019**, 52 (17), 6714-6724.

33. Kent, E. W.; Lewoczko, E. M.; Zhao, B., Effect of Buffer Anions on Pearl-Necklace Morphology of Tertiary Amine-Containing Binary Heterografted Linear Molecular Bottlebrushes in Acidic Aqueous Buffers. *Langmuir* **2020**, 36 (44), 13320-13330.

34. Kent, E. W.; Lewoczko, E. M.; Zhao, B., pH- and chaotropic anion-induced conformational changes of tertiary amine-containing binary heterografted star molecular bottlebrushes in aqueous solution. *Polymer Chemistry* **2021**, 12 (2), 265-276.

35. Lewoczko, E. M.; Kelly, M. T.; Kent, E. W.; Zhao, B., Effects of temperature on chaotropic anion-induced shape transitions of star molecular bottlebrushes with heterografted poly(ethylene oxide) and poly(N,N-dialkylaminoethyl methacrylate) side chains in acidic water. *Soft Matter* **2021**, 17 (27), 6566-6579.

36. Kelly, M. T.; Kent, E. W.; Zhao, B., Stepwise Conformational Transitions of Stimuli-Responsive Linear Ternary Heterografted Bottlebrush Polymers in Aqueous Solution. *Macromolecules* **2022,** *55* (5), 1629-1641.

37. Gan, W.; Shi, Y.; Jing, B.; Cao, X.; Zhu, Y.; Gao, H., Produce Molecular Brushes with Ultrahigh Grafting Density Using Accelerated CuAAC Grafting-Onto Strategy. *Macromolecules* **2017,** *50* (1), 215-222.

38. Yan, Y.; Shi, Y.; Zhu, W.; Chen, Y., Highly efficient synthesis of cylindrical polymer brushes with various side chains via click grafting-onto approach. *Polymer* **2013,** *54* (21), 5634-5642.

39. Engler, A. C.; Lee, H.-i.; Hammond, P. T., Highly Efficient "Grafting onto" a Polypeptide Backbone Using Click Chemistry. *Angewandte Chemie International Edition* **2009,** *48* (49), 9334-9338.

40. Tang, J.; Quinlan, P. J.; Tam, K. C., Stimuli-responsive Pickering emulsions: recent advances and potential applications. *Soft Matter* **2015,** *11* (18), 3512-3529.

41. Gao, Y.; Wu, X.; Xiang, Z.; Qi, C., Amphiphilic Double-Brush Copolymers with a Polyurethane Backbone: A Bespoke Macromolecular Emulsifier for Ionic Liquid-in-Oil Emulsion. *Langmuir* **2021,** *37* (7), 2376-2385.

42. Wang, B.; Liu, T.; Chen, H.; Yin, B.; Zhang, Z.; Russell, T. P.; Shi, S., Molecular Brush Surfactants: Versatile Emulsifiers for Stabilizing and Structuring Liquids. *Angewandte Chemie International Edition* **2021,** *60* (36), 19626-19630.

43. Wang, B.; Zhang, Z.; Feng, W.; Luo, J.; Shi, S., Stabilizing and structuring oil–oil interfaces by molecular brush surfactants. *Aggregate* **2022,** *3* (6), e292.

44. Seong, H.-G.; Chen, Z.; Emrick, T.; Russell, T. P., Reconfiguration and Reorganization of Bottlebrush Polymer Surfactants. *Angewandte Chemie International Edition* **2022,** *61* (19), e202200530.

45. Hu, M.; Russell, T. P., Polymers with advanced architectures as emulsifiers for multi-functional emulsions. *Materials Chemistry Frontiers* **2021,** *5* (3), 1205-1220.

46. Umar, A. A.; Saaid, I. B. M.; Sulaimon, A. A.; Pilus, R. B. M., A Review of Petroleum Emulsions and Recent Progress on Water-in-Crude Oil Emulsions Stabilized by Natural Surfactants and Solids. *Journal of Petroleum Science and Engineering* **2018,** *165*, 673-690.

47. Boyce, J. R.; Shirvanyants, D.; Sheiko, S. S.; Ivanov, D. A.; Qin, S.; Börner, H.; Matyjaszewski, K., Multiarm Molecular Brushes: Effect of the Number of Arms on the Molecular Weight Polydispersity and Surface Ordering. *Langmuir* **2004,** *20* (14), 6005-6011.

48. Sun, F.; Sheiko, S. S.; Möller, M.; Beers, K.; Matyjaszewski, K., Conformational Switching of Molecular Brushes in Response to the Energy of Interaction with the Substrate. *The Journal of Physical Chemistry A* **2004,** *108* (45), 9682-9686.

49. Zhao, L.; Byun, M.; Rzayev, J.; Lin, Z., Polystyrene−Polylactide Bottlebrush Block Copolymer at the Air/Water Interface. *Macromolecules* **2009,** *42* (22), 9027-9033.

50. Ogbonna, N. D.; Dearman, M.; Bharti, B.; Peters, A. J.; Lawrence, J., Elucidating the impact of side chain dispersity on the assembly of bottlebrush polymers at the air-water interface. *Journal of Polymer Science* **2021,** *59* (21), 2458-2467.

51. Ogbonna, N. D.; Dearman, M.; Cho, C.-T.; Bharti, B.; Peters, A. J.; Lawrence, J., Topologically Precise and Discrete Bottlebrush Polymers: Synthesis, Characterization, and Structure–Property Relationships. *JACS Au* **2022**.

52. Gallyamov, M. O.; Tartsch, B.; Khokhlov, A. R.; Sheiko, S. S.; Börner, H. G.; Matyjaszewski, K.; Möller, M., Reversible Collapse of Brushlike Macromolecules in Ethanol and Water Vapours as Revealed by Real-Time Scanning Force Microscopy. *Chemistry – A European Journal* **2004,** *10* (18), 4599-4605.

53. Gallyamov, M. O.; Tartsch, B.; Khokhlov, A. R.; Sheiko, S. S.; Börner, H. G.; Matyjaszewski, K.; Möller, M., Real-Time Scanning Force Microscopy of Macromolecular Conformational Transitions. *Macromolecular Rapid Communications* **2004,** *25* (19), 1703-1707.

54. Gallyamov, M. O.; Tartsch, B.; Khokhlov, A. R.; Sheiko, S. S.; Borner, H. G.; Matyjaszewski, K.; Moller, M., Conformational dynamics of single molecules visualized in real time by scanning force microscopy: macromolecular mobility on a substrate surface in different vapours. *J Microsc* **2004,** *215* (Pt 3), 245-56.

55. Li, C.; Gunari, N.; Fischer, K.; Janshoff, A.; Schmidt, M., New Perspectives for the Design of Molecular Actuators: Thermally Induced Collapse of Single Macromolecules from Cylindrical Brushes to Spheres. *Angewandte Chemie International Edition* **2004,** *43* (9), 1101-1104.

56. Lee, H.-i.; Pietrasik, J.; Matyjaszewski, K., Phototunable Temperature-Responsive Molecular Brushes Prepared by ATRP. *Macromolecules* **2006,** *39* (11), 3914-3920.

57. Pietrasik, J.; Sumerlin, B. S.; Lee, R. Y.; Matyjaszewski, K., Solution Behavior of Temperature-Responsive Molecular Brushes Prepared by ATRP. *Macromolecular Chemistry and Physics* **2007,** *208* (1), 30-36.

58. Yamamoto, S.-i.; Pietrasik, J.; Matyjaszewski, K., ATRP Synthesis of Thermally Responsive Molecular Brushes from Oligo(ethylene oxide) Methacrylates. *Macromolecules* **2007,** *40* (26), 9348-9353.

59. Lee, H.-i.; Boyce, J. R.; Nese, A.; Sheiko, S. S.; Matyjaszewski, K., pH-induced conformational changes of loosely grafted molecular brushes containing poly(acrylic acid) side chains. *Polymer* **2008,** *49* (25), 5490-5496.

60. Nese, A.; Lebedeva, N. V.; Sherwood, G.; Averick, S.; Li, Y.; Gao, H.; Peteanu, L.; Sheiko, S. S.; Matyjaszewski, K., pH-Responsive Fluorescent Molecular Bottlebrushes Prepared by Atom Transfer Radical Polymerization. *Macromolecules* **2011,** *44* (15), 5905-5910.

61. Zhang, Y.; Fu, L.; Martinez, M. R.; Sun, H.; Nava, V.; Yan, J.; Ristroph, K.; Averick, S. E.; Marelli, B.; Giraldo, J. P.; Matyjaszewski, K.; Tilton, R. D.; Lowry, G. V., Temperature-Responsive Bottlebrush Polymers Deliver a Stress-Regulating Agent In Vivo for Prolonged

Plant Heat Stress Mitigation. *ACS Sustainable Chemistry & Engineering* **2023,** *11* (8), 3346-3358.

62. Gunari, N.; Cong, Y.; Zhang, B.; Fischer, K.; Janshoff, A.; Schmidt, M., Surfactant-Induced Helix Formation of Cylindrical Brush Polymers with Poly(L-lysine) Side Chains. *Macromolecular Rapid Communications* **2008,** *29* (10), 821-825.
63. Xu, Y.; Bolisetty, S.; Ballauff, M.; Müller, A. H. E., Switching the Morphologies of Cylindrical Polycation Brushes by Ionic and Supramolecular Inclusion Complexes. *Journal of the American Chemical Society* **2009,** *131* (5), 1640-1641.
64. Xu, Y.; Bolisetty, S.; Drechsler, M.; Fang, B.; Yuan, J.; Harnau, L.; Ballauff, M.; Müller, A. H. E., Manipulating cylindrical polyelectrolyte brushes on the nanoscale by counterions: collapse transition to helical structures. *Soft Matter* **2009,** *5* (2), 379-384.
65. Xu, Y.; Borisov, O. V.; Ballauff, M.; Müller, A. H. E., Manipulating the Morphologies of Cylindrical Polyelectrolyte Brushes by Forming Interpolyelectrolyte Complexes with Oppositely Charged Linear Polyelectrolytes: An AFM Study. *Langmuir* **2010,** *26* (10), 6919-6926.
66. Luo, H.; Szymusiak, M.; Garcia, E. A.; Lock, L. L.; Cui, H.; Liu, Y.; Herrera-Alonso, M., Solute-Triggered Morphological Transitions of an Amphiphilic Heterografted Brush Copolymer as a Single-Molecule Drug Carrier. *Macromolecules* **2017,** *50* (5), 2201-2206.

Chapter 2. Amphiphilic Heterografted Bottlebrush Polymers with Tertiary Amine-Containing Side Chains as Effective and Efficient pH-Responsive Emulsion Stabilizers

Abstract

This Chapter presents the synthesis of a series of linear amphiphilic tertiary amine-containing molecular bottlebrush (MBB) polymers with heterografted bicomponent side chains and the study of their abilities to function as pH-responsive emulsion stabilizers. The linear brush polymers were prepared by grafting alkyne end-functionalized pH-responsive poly(2-(*N*,*N*-diethylamino)ethyl methacrylate) (PDEAEMA) with a pK_a of 7.4 and poly(*n*-butyl acrylate) (P*n*BA) onto an azide-functionalized backbone polymer using the copper(I)-catalyzed alkyne-azide cycloaddition click reaction. At a pH of 4.0, MBBs with appropriate side chain compositions were able to form water-in-toluene emulsions after vortexing of a mixture of toluene, a 1.0 mM aqueous phosphate buffer solution, and a brush polymer with a concentration as low as 0.005 wt%. When the pH was changed from 4.0 to 10.0, the emulsions were broken. With the use of a brush polymer with a symmetric side chain composition at concentrations of ≥ 0.01 wt%, the generation and breaking of emulsions can be repeated at least 10 times by cycling the pH of the aqueous phase between 4.0 and 10.0. Atomic force microscopy showed that there was no noticeable change to the brush polymer even after ten rounds of generating, via vortexing, and breaking emulsions. The emulsions formed at pH = 4.0 exhibited excellent long-term stability, and no noticeable changes were observed over a course of six weeks. The exceptional stability and the pH-responsiveness of the MBB-stabilized water-toluene emulsions were attributed to the large molecular size of the bottlebrushes, the strong adsorption to the interface with protonated PDEAEMA side chains stretching into the acidic aqueous phase and P*n*BA side chains extending into the toluene phase, and the pH-responsive property of PDEAEMA side chains. This was further corroborated by the observation of a crumpled interfacial polymer film formed on the emulsion droplets stabilized by a brush polymer at pH = 4.0 during the evaporation of toluene and water under an optical microscope.

2.1. Introduction

Molecular bottlebrushes (MBBs) are a class of graft copolymer that are typically characterized by a linear polymer backbone with densely grafted polymeric side chains protruding radially, resembling the bristles of a bottlebrush.[1-5] Due to their unique molecular structures, MBBs exhibit many intriguing characteristics and properties, including minimal chain entanglement, high and tunable persistence length, large and abrupt conformational changes in response to external stimuli, and unusual crystallization behavior.[1-7] There has been a growing interest in MBBs in recent years, from development of new synthetic methods to elucidation of their structures and conformations, and potential applications in diverse areas.[8-16] MBBs are commonly synthesized by one of the following three main methods: (i) grafting to, where end-functionalized polymers are grafting onto a polymer backbone, (ii) grafting from, where side chains are grown from an initiator-functionalized polymer, typically, by a controlled/"living" polymerization, and (iii) grafting through, where a macromonomer is polymerized directly into the brush polymer.[1-4] Although historically, the "grafting to" method does not yield MBBs with high grafting densities due to the steric hindrance, with the use of click chemistry such as copper(I)-catalyzed alkyne-azide cycloaddition (CuAAC) reaction, high grafting density MBBs with well-defined backbone and side chain lengths and precisely controlled side chain compositions can be routinely synthesized.[7,17-31] Our research group has been using the click grafting to approach to prepare well-defined multicomponent linear and star brush polymers.[7,18-26]

Amphiphilic MBBs with side chains composed of a hydrophilic polymer and a hydrophobic polymer have been investigated for application as emulsion stabilizers.[32-35] Many factors can affect their ability to function as surfactants such as lengths of backbone and side chain polymers, molar/weight ratio of the hydrophilic to the hydrophobic polymer in the side chains, grafting

density, and distribution of different types of side chain polymers. In general, compared with diblock copolymers, amphiphilic brush polymers exhibit several advantages. (i) Upon adsorption onto the water-oil (organic) interface, the brush molecules spontaneously re-configure into a Janus structure, with the hydrophilic and hydrophobic side chains extending into the aqueous and the organic phase, respectively. The contrasting attractions of the two types of side chains for different phases result in a strong affinity for the MBBs to the interface and consequently a high stability of the emulsions. (ii) The giant size of the MBBs in the Janus conformation means a considerably higher energy required for brush molecules to desorb from the interface than that for small molecule and block copolymer surfactants, and thus amphiphilic MBBs resemble Janus particle surfactants. The strong adsorption of MBBs to the water-oil interface and the resultant high stability of emulsions have been demonstrated, for example, by Matyjaszewski et al. using MBBs with heterografted poly(*n*-butyl acrylate) (P*n*BA) and poly(ethylene oxide) (PEO) side chains, Cheng et al. using double brush copolymers with PEO and polylactide grafts, and Russell and Emrick et al. using brush polymers with PEO and polydimethylsiloxane side chains.[32-34] A recent study showed that a brush polymer with poly(acrylic acid) side chains was able to bind strongly to the water/toluene interface from the aqueous phase when combined with amine-functionalized oligomeric silsesquioxane (POSS-NH_2) from the toluene phase, producing stable emulsions.[36] (iii) Amphiphilic MBBs have been shown to exhibit lower tendency to form micelles or other types of self-assemblies in bulk liquid phases than small molecule and block copolymer surfactants, which could potentially result in a higher efficiency as there is a higher probability for the MBBs to be located at the interface. For example, Matyjaszewski et al. showed that a stable emulsion could be achieved at a lower concentration of MBBs than the analogous diblock copolymer.[33] (iv) The densely grafted brush architecture can reduce the thinning of thin films in the coalescence process,

thus decreasing the coalescence of droplets and enhancing the stability of emulsions. By optimizing various parameters, efficient and effective emulsion surfactants could be crafted from MBBs by combining the advantages of particle stabilizers and polymer emulsifiers for generating robust emulsions.

For many applications such as crude oil recovery and drug delivery, it is highly desired to generate stimuli-responsive emulsions that are highly stable under certain conditions but can be broken upon application of external stimuli such as pH change, temperature variation, and light.[37-41] Such systems could, for example, greatly enhance the efficiency of the separation process and reduce energy consumption. There are many examples of stimuli-responsive Pickering emulsions in the literature but few reports on brush-type polymers.[41]

It is highly desired to design amphiphilic heterografted MBBs that can act as stimuli-responsive emulsion stabilizers. In this Chapter, we present the synthesis of a series of MBBs with side chains composed of heterografted hydrophobic P*n*BA and pH-responsive poly(2-(*N*,*N*-diethylamino)ethyl methacrylate) (PDEAEMA) with various molar ratios along with two homografted brush polymers and the study of their abilities to function as pH-responsive emulsion stabilizers (Scheme 2.1). The reported pK_a value of protonated PDEAEMA is 7.4, above which PDEAEMA is insoluble in water. A click grafting to approach was employed to synthesize MBBs by grafting alkyne end-functionalized P*n*BA and/or PDEAEMA onto a linear azide-carrying backbone polymer. This grafting to approach makes it possible to readily tune the side chain composition while maintaining chain lengths of the backbone and side chain polymers, allowing us to better understand how varying the side chain composition affects the abilities of the brush polymers to function as emulsion stabilizers. Under acidic conditions, PDEAEMA side chains are protonated and soluble in water, and we found that the heterografted P*n*BA/PDEAEMA brush

Scheme 2.1. Synthesis of Amphiphilic Heterografted MBBs with Hydrophobic Poly(*n*-butyl acrylate) (P*n*BA) and pH-Responsive Poly(2-(*N*,*N*-diethylamino)ethyl methacrylate) (PDEAEMA) Side Chains by a Click Grafting-to Method

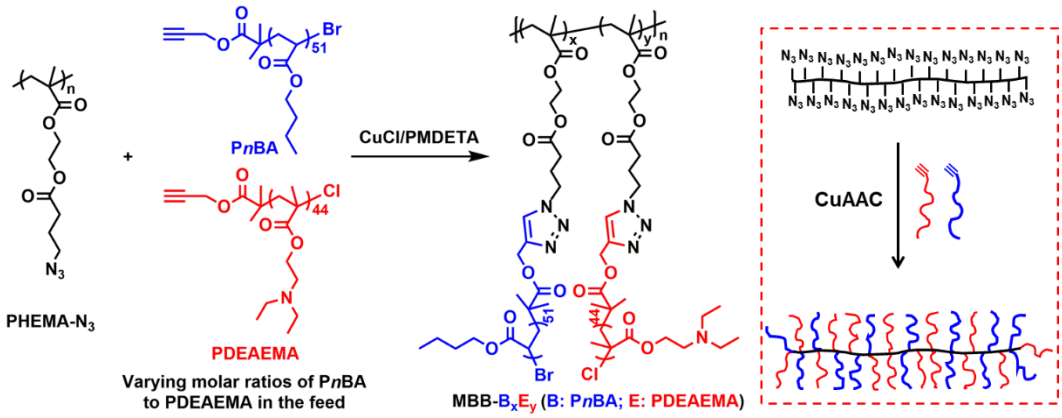

polymers at certain side chain compositions formed stable water-in-toluene emulsions after vortexing. When the pH of the aqueous phase was adjusted to a basic value, the emulsions broke as the MBBs were deprotonated and retreated to the toluene phase from the water-toluene interface. The formation and breaking of emulsions can be repeated at least 10 times with the use of a symmetric brush polymer at a concentration of 0.01 wt% or above. The emulsions exhibited a high stability even at a concentration of MBBs as low as 0.005 wt%.

2.2. Experimental Section

2.2.1. Materials

CuCl (97%, Alfa Aesar) and CuBr (99%, Thermo Scientific) were purified by stirring in glacial acetic acid at ambient temperature overnight. The solid was then filtered, washed extensively with absolute ethanol and diethyl ether, transferred into a 4-dram vial, and dried under high vacuum. The vial was subsequently filled with argon and stored in a desiccator. Butyl acrylate (*n*BA, 99%, Acros Organics) and 2-(*N*,*N*-diethylamino)ethyl methacrylate (DEAEMA, 98.5%, TCI) were passed through a basic alumina (top)/silica gel (bottom) column to remove inhibitor immediately before polymerization. Propargyl 2-bromoisobutyrate (PBiB) was prepared by a reaction of propargyl alcohol with 2-bromo-2-methylpropionyl bromide as described previously.[18] 2-Bromoisobutyryl bromide (EBiB, 98%, TCI) and *N*,*N*,*N*′,*N*″,*N*″-pentamethyldiethylenetriamine (PMDETA, 99%, TCI) were stirred over calcium hydride and purified by vacuum distillation before use. 2-((Trimethylsilyl)oxy)ethyl methacrylate (HEMA-TMS) was synthesized following a procedure in the literature. 1,1,4,7,10,10-Hexamethyltriethylenetetramine (HMTETA, 97%, Alfa Aesar), 4-bromobutyryl chloride (95%, Oakwood Chemical), potassium fluoride (KF, 99%, Oakwood Chemical), tetrabutylammonium fluoride (TBAF, 1 M solution in THF, Thermo

Scientific), sodium azide (99%, Acros), anisole (99%, Acros), and dimethylformamide (DMF, 99.8%, Fisher) were all used directly without further purification. Dry tetrahydrofuran (THF, 99%, Fisher) was distilled from sodium benzophenone ketyl. All other chemicals described in this work were purchased from Fisher Scientific or Sigma-Aldrich and used as received.

2.2.2. General Characterization

^{1}H NMR spectra were recorded on a Varian VNMRS 500 NMR spectrometer. Size exclusion chromatography (SEC) analysis of linear and bottlebrush polymers was performed using a PL-GPC 50 (integrated GPC/SEC system from Polymer Laboratories, Inc.) equipped with one PSS GRAM 10 μm precolumn (8 × 50 mm, Polymer Standards Service-USA, Inc.), two PSS GRAM 10 μm column (8 × 300 mm, PSS-USA, Inc.), and a differential refractive index (RI) detector. The SEC system was operated using *N*,*N*-dimethylformamide (DMF) with 50 mM LiBr as eluent and was calibrated using a series of narrow disperse linear polystyrene standards (Scientific Polymer Products, Inc.). Note that DMF was passed through a 0.45 μm filter prior to the addition of solid LiBr for the preparation of the eluent. A PL-GPC 20 (integrated GPC/SEC system from Polymer Laboratories, Inc.) was used to confirm the purity of MBBs insoluble in DMF. It was equipped with one PLgel 5 μm guard column (50 × 7.5 mm, Agilent), two PLgel 5μm Mixed-C columns (each 300 × 7.5 mm, linear range from 200 to 2 000 000 Da, Agilent), and a RI detector, and THF was used as eluent. For pH measurements, an Accument AB-15 pH meter was used and was calibrated using a series of standard buffer solutions (pH = 4.01, 7.00, and 10.01) at ambient temperature.

2.2.3. Synthesis of Azide-Functionalized Backbone Polymer (PHEMA-N_3)

A linear azide-functionalized backbone polymethacrylate with a degree of polymerization (DP) of 406, PHEMA-N_3 (see the molecular structure in Scheme 2.1), was synthesized following

a previously reported procedure with slight modifications to the atom transfer radical polymerization (ATRP) step (Scheme A2.1).[23] EBiB (5.51 mg, 0.0283 mmol, added from 0.289 g of a 19.11 mg/g stock solution of EBiB in anisole), HEMA-TMS (4.524 g, 22.36 mmol), HMTETA (21 µL, 77 mmol), and anisole (2.800 g total) were weighed into a two-necked, 25 mL flask. After copper(I) chloride (7.41 mg, 74.8 mmol) was added, the flask was promptly sealed with a gas flow control adapter. The reaction mixture was degassed by four cycles of freeze-pump-thaw and was backfilled with argon. The flask was placed in an oil bath preheated to 75 °C, and the monomer conversion was monitored by ^{1}H NMR spectroscopy. After 2.75 h, the flask was removed from the oil bath and opened to air, and the reaction mixture was diluted with THF. The diluted mixture, with a lower viscosity, was passed through a neutral alumina/silica column to remove the catalyst. The unreacted monomer was evaporated at 60 °C under a high vacuum, yielding a light green, tacky polymer (2.447 g, >96% pure); ^{1}H NMR spectroscopy showed that a small amount of the HEMA-TMS monomer remained (< 4%), which was removed in the subsequent post-polymerization modifications and purification. The monomer conversion at the end of the polymerization was determined to be 51.3% by ^{1}H NMR analysis using the integral ratio of the peaks corresponding to the -COOC*H*$_2$- groups of the monomer and the polymer (4.22 and 3.99 ppm, respectively). Considering the initial monomer-to-initiator molar ratio (792 : 1) and monomer conversion, the calculated degree of polymerization (DP) of the obtained polymer was 406. SEC analysis using GRAM columns and DMF with 50 mM LiBr as eluent yielded a $M_{n,SEC}$ = 60.2 kDa and $Đ$ = 1.10 relative to polystyrene standards.

PHEMA-TMS (0.867 g, 4.28 mmol of -$CH_2CH_2OSi(CH_3)_3$ groups) dissolved in THF (4 mL) was added to a 50 mL two-necked round bottom flask with a magnetic stir bar. The THF was evaporated under a gentle nitrogen gas stream, and the polymer was dried under high vacuum for

15 min. After the flask was backfilled with N_2, KF (0.393 g, 6.77 mmol) was added. The flask was sealed immediately with a rubber septum and dried under vacuum for 15 min. After the flask was backfilled with N_2, dry THF (10 mL) was injected via a syringe with a gauge 22 stainless steel needle. Once the polymer had fully dissolved in THF, the flask was placed in an ice/water bath. 4-Bromobutyryl chloride (1.00 mL, 8.63 mmol) was added, followed directly by TBAF (200 µL of a 1 *M* solution of TBAF in THF, 0.20 mmol). After 5 h, additional 4-bromobutyryl chloride (0.50 mL, 4.31 mmol) and TBAF (200 µL of a 1 *M* solution of TBAF in THF, 0.20 mmol) were injected into the flask. After 10 h, the polymer was precipitated into MeOH/H_2O (4/1, v/v) two times, MeOH once, and hexanes once. The product was dried under vacuum, yielding a white tacky polymer (0.805 g, 67.3% yield). The polymer obtained is abbreviated as PHEMA-Br. SEC analysis was performed using GRAM columns and DMF with 50 mM LiBr as eluent, yielding $M_{n,SEC}$ = 73.5 kDa and $Đ$ = 1.10. Based on ^{1}H NMR analysis, the deprotection of trimethylsilyl groups was quantitative, and 98.2% of repeat units were substituted with bromine-containing pendant groups (3.52 ppm, -OOCCH$_2$CH$_2$C*H*$_2$Br). The remaining 1.8% was attributed to the presence of -OOCCH$_2$CH$_2$C*H*$_2$Cl (3.65 ppm, -OOCCH$_2$CH$_2$C*H*$_2$Cl) due to the halogen exchange in the starting material 4-bromobutyryl chloride to form 4-chlorobutanoyl bromide.

PHEMA-Br (0.745 g, 2.67 mmol of monomer units) was dissolved in DMF (12 mL) and transferred to a 50 mL two-necked round bottom flask. Sodium azide (0.944 g, 14.5 mmol) was added, and the reaction mixture was stirred under nitrogen. After 18 h, the polymer was precipitated into MeOH/H_2O (80/20, v/v) twice, then MeOH once, and lastly hexanes. The purified polymer was dried under high vacuum yielding a tacky white solid (0.542 g, 84% yield). SEC analysis of PHEMA-N_3 using a GPC/SEC system with GRAM columns and DMF containing 50 mM LiBr as eluent yielded $M_{n,SEC}$ = 75.2 kDa and $Đ$ = 1.12. From ^{1}H NMR spectroscopy analysis,

PHEMA-N_3 was calculated to have an azide functionalization of 97.5%. There were two characteristic unreacted pendant group peaks in the ^{1}H NMR spectrum that accounted for the remaining 2.5%: 1.5% chloride-containing group (3.65 ppm, -OOCCH$_2$CH$_2$C*H*$_2$Cl from ClCH$_2$CH$_2$CH$_2$COBr, formed by halogen exchange in the starting material BrCH$_2$CH$_2$CH$_2$COCl) and 1.0% unreacted bromide-containing repeat units (3.52 ppm, -OOCCH$_2$CH$_2$C*H*$_2$Br).

2.2.4. Synthesis of Alkyne End-Functionalized Side Chain Polymer P*n*BA

PBiB (81.5 mg, 0.398 mmol), *n*BA (6.184 g, 48.25 mmol), PMDETA (74.3 mg, 0.429 mmol), CuBr (55.7 mg, 0.388 mmol), and anisole (4.905 g total) were added to a 50 mL two-necked round bottom flask. The flask was sealed with a rubber septum and a gas flow control adapter. After the reaction mixture was degassed via three cycles of freeze pump thaw, the reaction flask was backfilled with nitrogen gas. The flask was then placed into a preheated oil bath set to 80 °C to initiate the polymerization, and the monomer conversion was monitored using ^{1}H NMR spectroscopy. After 8 h, the flask was taken out of the oil bath and opened to air, and the reaction mixture was diluted with THF. The copper catalyst was removed by passing the reaction mixture through a neutral alumina/silica gel column, and the polymer was purified by multiple precipitations from THF into a mixture of methanol and water (6/1, v/v) at room temperature. The polymer was dried under high vacuum, yielding a light yellow, viscous polymer (1.780 g, 28.8% yield). The monomer conversion was calculated to be 42.2% based on the ^{1}H NMR analysis of the final reaction mixture by comparing the integrals of the characteristic -COOC*H*$_2$- peaks corresponding to the monomer (4.20-4.14 ppm) and the polymer (4.12-3.96 ppm). The calculated DP was 51 based on the monomer conversion and the initial monomer-to-initiator feed ratio. SEC analysis was performed on a GPC/SEC system with PSS GRAM columns using 50 mM LiBr DMF as eluent, and the $M_{n,SEC}$ was 7.9 kDa and the $Đ$ was 1.07, relative to polystyrene standards.

2.2.5. Synthesis of Alkyne End-Functionalized Side Chain Polymer PDEAEMA

PBiB (69.7 mg, 0.340 mmol), DEAEMA (5.002 g, 27.00 mmol), HMTETA (81.4 mg, 0.353 mmol), CuCl (33.8 mg, 0.341 mmol), and anisole (5.264 g total) were all added to a 50 mL two-necked round bottom flask. The reaction mixture was degassed by three cycles of freeze pump thaw; the reaction flask was then backfilled with nitrogen gas and placed in a preheated oil bath set to 50 °C. After 1.5 h, the flask was removed from the oil bath and opened to air, and the reaction mixture was diluted with THF before passing the reaction mixture through an alumina/silica gel column to remove the copper catalyst. The polymer was purified by precipitation from THF into hexanes using a dry ice/acetone bath. The polymer was then dried under high vacuum, yielding a yellow amorphous solid (2.234 g, 44.7% yield). The monomer conversion was calculated to be 55.3% by analyzing the integrals of the peaks at 4.25-4.19 ppm (-COOCH_2- of the monomer) and 4.10-3.93 ppm (-COOCH_2- of the polymer) in the ^{1}H NMR spectrum of the final reaction mixture. Based on the feed molar ratio of the monomer to the initiator and the monomer conversion, the DP of the obtained polymer, PDEAEMA, was calculated as 44. SEC analysis using PSS GRAM columns and DMF with 50 mM LiBr as eluent yielded a M_n of 9.7 kDa and a $Đ$ of 1.10, with respect to the polystyrene calibration curve.

2.2.6. Synthesis of MBBs

A total of six bottlebrush polymers, including two homografted and four heterografted MBBs, were prepared in a similar manner by a click grafting to method. The following is an example procedure detailing the synthesis of MBB-$B_{0.64}E_{0.36}$, where MBB stands for molecular bottlebrushes, B and E denote P*n*BA and PDEAEMA, respectively, and the subscripts represent the molar fractions of the two side chain polymers in the brushes. PHEMA-N_3 (6.52 mg, 2.70×10^{-2} mmol of -N_3 groups (assuming 100% azide functionalization) delivered from 0.205 g of a

31.83 mg/g stock solution in THF), alkyne-end-functionalized P*n*BA (142.6 mg, 2.12×10^{-2} mmol of P*n*BA chains), and alkyne-end-functionalized PDEAEMA (112.3 mg, 1.35×10^{-2} mmol) were added to a 2-dram vial and were dissolved in THF (5 mL total). CuCl (4.5 mg, 4.55×10^{-2} mmol) was then added into the vial, which was subsequently sealed with a rubber septum. The reaction mixture was bubbled with nitrogen gas for 15 min to remove O_2, at which point PMDETA (10 μL, 4.79×10^{-2} mmol) was injected using a microsyringe. After the reaction proceeded at room temperature for 20 h, benzyl propargyl ether (20 μL) was injected to attempt to cap unreacted azide functional groups. After an additional 2 h, the reaction mixture was diluted with THF and passed through a neutral alumina (top)/silica gel (bottom) column to remove the copper catalyst. The solution was then concentrated down to a volume of about 2 mL and transferred to a 4-dram vial. Three rounds of fractionation were performed at ambient temperature to remove unreacted alkyne end-functionalized polymers using THF (2 mL) as a good solvent and a mixture of methanol and water (1/1, v/v, 10 mL) as a poor solvent. SEC analysis showed that there were still residual unreacted side chain polymers. The polymer solution was transferred to a round bottom flask, and volatiles were removed using a rotary evaporator, leaving behind a thin polymer layer on the wall of the flask. Hexane (10 mL) was then added, and the flask was rotated for 15 s on the rotary evaporator. The hexane in the flask was decanted, and THF was added to the flask to re-dissolve the polymer residue. This process was repeated four times to remove the residual unreacted side chain polymers, and the bottlebrush polymer was determined to be pure from SEC analysis as the peaks corresponding to the side chain polymers were absent. The molar composition of the side chains in the obtained brush polymer was determined via ^{1}H NMR spectroscopy analysis by comparing the peak area integrals corresponding to the -COOCH_2- groups of P*n*BA and PDEAEMA (4.19-3.90 ppm) and the -COOCH$_2$CH_2N(CH_2CH$_3$)$_2$ of PDEAEMA (2.85–2.47 ppm)

along with the DPs of the two polymers. The mole fractions of P*n*BA and PDEAEMA were calculated to be 0.64 and 0.36, respectively, and thus this brush polymer was named as MBB-$B_{0.64}E_{0.36}$.

The grafting density of MBB-$B_{0.64}E_{0.36}$ was estimated to be 88.6% using SEC analysis by comparing the peak area percentages of the brush polymer (69.5%) and the remaining unreacted side chain polymers (30.5%) in the final reaction mixture as well as the feed ratio of the backbone and the side chain polymers in the initial reaction mixture. This calculation assumes that the refractive index changes with concentration are the same for the side chain polymers. The total mass of the side chain polymers that had reacted was 175.1 mg, which was calculated by multiplying the brush peak area percentage by the starting feed masses of the backbone PHEMA-N_3 and the two side chain polymers and subtracting the mass of the backbone polymer. Using the mole contents of the two polymers in the side chains from ^{1}H NMR analysis, the masses of P*n*BA and PDEAEMA that had reacted were 103.1 and 72.1 mg, respectively. On the basis of the molecular weights of the side chain polymers calculated from their DPs, the calculated moles of the side chains that reacted was 2.40×10^{-2} mmol. The number of moles of the repeat units in the backbone polymer PHEMA-N_3 was calculated to be 2.70×10^{-2} mmol. Therefore, the overall grafting density was determined to be 88.6%.

On the basis of the grafting density of MBB-$B_{0.64}E_{0.36}$ and the DP of PHEMA-N_3 (DP = 406), the numbers of P*n*BA and PDEAEMA side chains per brush molecule were 230 and 130, respectively. The calculated number-average molecular weight of MBB-$B_{0.64}E_{0.36}$ was 2,728 kDa (2.73×10^6 Da), which was obtained by multiplying the number of each side chain polymer by the respective molecular weight of the polymer determined from the DP (P*n*BA: 6742 Da; PDEAEMA: 8312 Da) and adding the molecular weight of the backbone polymer (98.1 kDa).

The other MBB samples were synthesized following a similar procedure with the only differences in the purification step for MBB-$B_{0.24}E_{0.76}$, MBB-$B_{1.00}E_{0.00}$, and MBB-$B_{0.00}E_{1.00}$. MBB-$B_{0.24}E_{0.76}$ was fractionated using THF and DI water prior to performing the trituration with hexane. MBB-$B_{1.00}E_{0.00}$ was purified solely by performing multiple fractionations with THF as a good solvent and a mixture of MeOH/H_2O (5 : 1, v : v) as a poor solvent. MBB-$B_{0.00}E_{1.00}$ was purified by fractionation in a dry ice/acetone bath using THF as a good solvent and pentanes as a poor solvent. MBB-$B_{0.51}E_{0.49}$ and MBB-$B_{0.80}E_{0.20}$ were purified in a similar manner to MBB-$B_{0.64}E_{0.36}$.

2.2.7. Control of pH Values of the Aqueous Phases in 1.0 mM Aqueous Phosphate Buffer-Toluene Mixtures

Due to the amphiphilic nature of the bottlebrush polymer and the continuous phase of the emulsions being toluene, it was not possible to directly measure the pH of the 1.0 mM aqueous phosphate buffer phase by a pH meter. To determine the amount of an acid or a base that would be needed to adjust the initial pH to 4.0 and then adjust the pH value from 4.0 to 10.0, multiple tests were performed using PDEAEMA side chain polymer as a control. For each concentration of each brush polymer used to evaluate the toluene-water emulsion formation, the amount of PDEAEMA side chains was calculated. We assumed that all PDEAEMA side chains in the brush polymer would be exposed to the aqueous phase during the vortexing of the mixture and protonated at low pH values. The alkyne-end-functionalized PDEAEMA side chain polymer with a DP of 44 was dissolved in 1.0 mM aqueous phosphate buffer with a pH of 4.0. The pH was adjusted back to 4.0 using a 1.0 or 0.1 *M* HCl aqueous solution and monitored by a pH meter, and the amount of the acid needed to bring the pH back to 4.0 was noted. The pH was then adjusted from 4.0 to 10.0 and then back to 4.0 using 1.0 M or 0.1 M NaOH and HCl, respectively, and the amounts of the base and the acid were recorded.

An example is shown in the following. For a 0.02 wt% emulsion from 1.0 g of toluene and 1.0 g of a 1.0 mM aqueous phosphate buffer with $MBB_{0.51}E_{0.49}$ as stabilizer, 0.40 mg of the brush polymer would be needed. Based on the ^1H NMR analysis, MBB-$B_{0.51}E_{0.49}$ was calculated to contain 52.3% PDEAEMA by mass, and thus for the 0.02 wt% emulsion, there was 0.209 mg of PDEAEMA side chains present. For more reliable measurements, the testing was performed using approximately 10.0 g of the 1.0 mM phosphate buffer, which was ten times the amount used in the emulsion testing and the amounts of acid/base needed would be scaled down accordingly when testing the pH-responsive nature of the emulsions. PDEAEMA (2.20 mg, delivered from a stock solution in THF) was added to a vial and dried under high vacuum. Subsequently, the 1.0 mM phosphate buffer with a pH of 4.0 (10.53 g) was added to give a concentration of 0.0209 wt% or 0.209 mg/g. 1.0 M HCl was gradually added using a micropipette, and a total of 11.0 µL was used to adjust the pH of the solution to 4.0. Note that PDEAEMA was thoroughly dissolved. Once the pH was stable, 1.0 M NaOH (27.0 µL) was added using a micropipette to adjust the pH of the solution to 10.0. The same volume (27.0 µL of a 1.0 M HCl solution was then added, and the pH was observed to come back to 4.0. Scaling this down to the scale of the 1.0 g aqueous phosphate buffer used for generating emulsions with toluene means 11.0 µL of 0.1 M HCl would be needed to adjust the initial pH to 4.0 and 27.0 µL of 0.1 M NaOH would be necessary to increase the pH to 10.0. To adjust the pH back to 4.0, 27.0 µL of 0.1 M HCl would be required. Similar experiments were performed using the PDEAEMA side chain polymer with a DP of 44 to model other brush polymers at the concentrations used in this study.

2.2.8. Emulsion Formation and Breaking

The weight percentage of the brush polymer used in this work is relative to the combined aqueous and organic phases. Prior to vortexing to generate emulsions, a solution of a bottlebrush

polymer in toluene with a concentration of 1.00 mg/g and a 1.0 mM phosphate buffer with a pH of 4.00 were prepared. A calculated amount of 0.1 M HCl, which would be required to adjust the pH of the 1.0 mM phosphate buffer back to 4.0 for the same concentration of the side chain PDEAEMA in the 1.0 mM phosphate buffer, was added into a 1-dram vial using a micropipette, followed by 1.00 g of the 1 mM phosphate buffer with pH = 4.0. After gentle shaking of the vial, a calculated amount of the solution of the MBB in toluene was placed on top of the aqueous solution, followed by additional toluene (1.00 g total) to achieve the desired concentration of the MBB in the mixture.

The following is a description for the preparation of the sample using MBB-$B_{0.51}E_{0.49}$ at a concentration of 0.02 wt%. To a 1-dram vial, the following was added in order: 10.48 μL of 0.1 M HCl, 1.00 g of the 1 mM phosphate buffer with a pH of 4.0, 0.401 g of MBB-$B_{0.51}E_{0.49}$ stock solution (1.00 mg/g in toluene), and lastly 0.602 g of toluene. The vial was capped, labeled, and vortexed using a vortex mixer (Fisherbrand Analog Vortex Mixer, max 3200 rpm) at the setting 8 out of 10 for a total of 60 s, divided into two 30 s intervals with 5-10 min in between.

The vial was then kept still on a bench or in a desiccator saturated with water vapor and toluene vapor, where one open vial containing water and another open vial containing toluene were placed to minimize evaporation. Digital photos were acquired using a Nikon camera COOLPIX B500 at defined time points. After 24 h, a calculated amount of 1.0 or 0.10 M NaOH, based on the control experiment of the PDEAEMA side chain polymer, was injected into the mixture using a mechanical micropipette (Gilson) to increase the pH from 4.0 to 10.0. The vial was gently shaken and kept still on a bench unless otherwise stated. After 24 h, photos were taken, and a calculated amount of 1.0 or 0.10 M HCl was added to bring the pH back to 4.0. The vial was capped tightly and vortexed for a total of 60 seconds as in the first time. The vial was then allowed to stand still

on the bench for 24 h, at which photos were taken. Similar procedures were used for other three bicomponent heterografted MBBs (MBB-$B_{0.80}E_{0.20}$, MBB-$B_{0.64}E_{0.36}$, and MBB-$B_{0.76}E_{0.24}$) and two homografted MBBs (MBB-$B_{1.00}E_{0.00}$ and MBB-$B_{0.00}E_{1.00}$). For some samples at pH = 10.0, a stir bar was used to expedite the breaking of the emulsion.

2.2.9. Repeated Formation and Breaking of Emulsions

MBB-$B_{0.51}E_{0.49}$ was selected to continue the cycles of formation and breaking of emulsions. The pH value of the aqueous phase was switched back and forth (presumably) between 4.0 and 10.0 by adding the calculated amount of 1.0 or 0.1 M HCl and 1.0 or 0.1 M NaOH, respectively, as stated in the preceding section. After the addition of the base, the vial was gently shaken and allowed to sit still on the bench for at least 6 h. After the pH was brought back to 4.0 by the injection of the acid, the vial was vortexed for a total of 60 seconds (divided into two and each 30 s). A total of 10 cycles of formation and breaking of emulsions were performed. At the 6th and 10th cycles, optical micrographs were collected on an Olympus BX51 optical microscope by using a mechanical micropipette to remove 10 μL of the emulsion layer and transferred to a microscope slide with toluene. The pipette tips used were cut to minimize any manipulation of the emulsion droplet morphology.

2.2.10. Long-Term Stability of Water-in-Toluene Emulsions Stabilized by MBB-$B_{0.51}E_{0.49}$

The stability of the emulsions over time was studied using MBB-$B_{0.51}E_{0.49}$ as the stabilizer at concentrations of 0.02 wt% and 0.01 wt%. Emulsions were prepared and then stored in a desiccator containing open vials of toluene and water liquids to form an environment with saturated toluene and water vapor for preventing solvent evaporation from emulsions. Digital photos of the vials and optical micrographs of emulsion droplets were acquired after one day and then at one-week intervals in order to assess the stability of the emulsions.

2.2.11. Optical Microscopy and Confocal Microscopy

An Olympus BX51 optical microscope was used to obtain microscopic images of the emulsions for different samples and concentrations to compare the size and uniformity of the emulsion droplets. A small portion of an emulsion layer was added onto a microscope slide via a micropipette and diluted with a small amount of toluene. The pipette tip was cut off to have a large mouth to minimize manipulation of the droplets when transferring them to the microscope slide. Several optical microscopic images were acquired under each condition to ensure that the micrographs were representative of the sample using a digital camera (Amscope, MU1603) mounted on the Olympus BX51 optical microscope.

The type of emulsion was further determined using a confocal microscope (Leica SP8). An emulsion was prepared using 0.02 wt% of MBB-$B_{0.51}E_{0.49}$ as the stabilizer at the pH of 4.0 for the aqueous phase in the same manner as described previously except that 40 μL of a 1.88×10^{-4} M stock solution of Nile Red in toluene was added to the toluene phase (1.0 g) prior to vortexing. The emulsion droplets were transferred to a microscope slide with toluene and then promptly imaged using an excitation wavelength of 514 nm and emission wavelength range of 520-640 nm.

2.2.12. Atomic Force Microscopy (AFM)

The bottlebrush molecules were visualized using a Digital Instruments Multimode IIIa Scanning Probe Microscope in the Tapping Mode under ambient conditions. Al-coated silicon cantilevers were used (Tap300Al-G, Budget Sensors) with a resonance frequency of 300 kHz and force constant of 40 N/m. The AFM samples of MBBs were prepared on cover glasses (Fisherbrand, 12 mm diameter disc) using a Langmuir-Blodgett trough (KSV Nima). The cover glasses were cleaned using a “Piranha” solution (98% H_2SO_4 and 30% H_2O_2, 70/30, v/v. Caution: it reacts violently with organics and must be handled with great care!), washed extensively with

Milli-Q water, and stored in isopropanol until used. The subphase (1.0 mM phosphate buffer) was adjusted to the desired pH value, measured by a pH meter, and then added to the Langmuir-Blodgett Teflon trough. For MBB-$B_{0.51}E_{0.49}$ from the water-in-toluene emulsion with a polymer concentration of 0.02 wt% formed in the first step of the second cycle and the tenth cycle, 25 µL of the emulsion layer was transferred to the surface of the subphase (1.0 mM phosphate buffer with a pH of 4.0) using a micropipette. A cover glass was immersed in the subphase before the addition of the polymer solution. After 15 min, the barriers were compressed at a rate of 10 mm/min until the surface pressure reached 0.5 mN/m. Once the surface pressure was stabilized, the dipping sequence was initiated, and the cover glass was pulled out of the subphase at a rate of 5 mm/min.

2.3. Results and Discussion

2.3.1. Synthesis and Characterization of MBBs Comprising P*n*BA and PDEAEMA Side Chains with Different Molar Ratios

Six molecular bottlebrush (MBB) polymers, including four binary heterografted MBBs and two different homografted brush polymers, were synthesized by a grafting-to-approach using the efficient copper(I)-catalyzed azide-alkyne cycloaddition (CuAAC) reaction to graft an alkyne-end-functionalized hydrophobic P*n*BA and/or an alkyne-end-functionalized pH-responsive PDEAEMA (pK_a = 7.4) onto a linear azide-bearing polymer backbone. Prior to preparing the bottlebrush polymers, an azide-functionalized backbone polymer (PHEMA-N_3, Scheme 2.1) with a degree of polymerization (DP) of 406 was synthesized by atom transfer radical polymerization (ATRP) of HEMA-TMS and subsequent functionalization reactions (Scheme A1). The post-polymerization modifications of poly(HEMA-TMS) were performed in two steps to convert the

trimethylsilyl ether groups to azide functional groups on the repeat units, yielding PHEMA-N_3 with a narrow dispersity ($Đ$ = 1.12) and a high degree of azide functionalization (97.5%) (Figures A1 and A2). Alkyne-end-functionalized side chain polymers, P*n*BA and PDEAEMA, were prepared by ATRP of respective monomers using an alkyne-functionalized ATRP initiator, propargyl 2-bromoisobutyrate, and their DPs were 51 and 44, respectively, calculated from the monomer conversions from ^{1}H NMR analysis and the initial monomer-to-initiator molar ratios. SEC analysis of these polymers showed low dispersities ($Đ \leq 1.10$) (Figures A3 and A4, demonstrating that the polymerizations were well controlled. The full characterization data for these polymers are summarized in Table 2.1. Note that the narrow chain length distributions of the azide-functionalized backbone polymer and the alkyne-end-capped side chain polymers are important for achieving uniform bottlebrush molecules.

Four amphiphilic binary heterografted pH-responsive bottlebrush polymers were prepared by grafting the alkyne end-functionalized P*n*BA and PDEAEMA with various feed molar ratios onto the azide functionalized backbone polymer using CuAAC, yielded MBBs with two types of side chains randomly grafted on the backbone polymer. Note that this click grafting to method is particularly suitable for the synthesis of multicomponent MBBs with varying side chain compositions and exhibits a number of advantages compared with more popular methods such as "grafting from" by ATRP and ring-opening metathesis polymerization of macromonomers. (i) The high efficiency of CuAAC allows for the preparation of MBBs with high and similar grafting densities; (ii) the molar ratio of different types of side chain polymers in MBBs can be easily tuned through the change of the feed ratios; (iii) the same backbone polymer and the same side chain polymers with very similar grafting densities allow for better comparison of the emulsification

Table 2.1. Characterization data for the backbone polymer, PHEMA-N_3, and the alkyne-end-functionalized side chain polymers, P*n*BA and PDEAEMA, used in this work.

Polymer Sample	DP [a]	$M_{n,SEC}$ (kDa) [b]	$Đ$ [b]
PHEMA-N_3	406	75.2	1.12
P*n*BA	51	7.9	1.07
PDEAEMA	44	9.7	1.10

[a] DP = degree of polymerization. The DP of PHEMA-N_3 was same as the DP of the precursor polymer poly(HEMA-TMS) that was calculated from the monomer conversion, determined by ^{1}H NMR spectroscopy analysis, and the initial monomer-to-initiator feed ratio.
[b] Number average molecular weight ($M_{n,SEC}$) and dispersity ($Đ$) were determined by size exclusion chromatography analysis using polystyrene standards as calibration.

behavior and abilities of bicomponent heterografted MBBs with different side chain compositions.[1-4]

The synthesis of bicomponent heterografted MBBs was conducted at ambient conditions using CuCl/PMDETA as the catalyst and THF as solvent. An excess of side chains relative to backbone repeat units, ~ 1.3 – 1.4 : 1, was used to achieve higher grafting densities. After the CuAAC click reaction proceeded overnight, a calculated amount of benzyl propargyl ether was injected into the reaction mixtures using a microsyringe to attempt to cap unreacted azide groups. To purify the brush polymers, the copper catalyst was first removed by passing the reaction mixtures through a silica gel/neutral alumina column and then several rounds of fractional precipitation were performed to remove unreacted side chain polymers. Some of the brush polymers were further purified by trituration to remove the unreacted alkyne-end-functionalized polymer(s) that remained after fractionation. Further details on the purification methods can be found in the Experimental Section. SEC analysis confirmed the removal of lower molecular weight side chain polymers from MBBs (Figures 2.1, A6, A8, and A11). AFM height images also confirmed the formation of the bottlebrush polymers, which exhibited a typical wormlike morphology with a relatively uniform size (Figures 2.1, A5, A7, A9, and A13). The molar composition of side chains in each heterografted brush polymer was determined by ^{1}H NMR spectroscopy using the integrals of the characteristic peaks at 4.15-3.90 ppm (-COOCH_2- from both P*n*BA and PDEAEMA) and 2.75-2.50 ppm (-CH_2N(CH_2CH$_3$)$_2$ from PDEAEMA); for each brush polymer, the molar ratio of the two polymers in the side chains was found to be similar to the initial feed ratio. In addition, a homografted P*n*BA brush polymer and a homografted PDEAEMA MBB were prepared and purified using similar conditions (Figures A11, A14-A18). The grafting densities for the brush polymers that can be eluted from the SEC system equipped with GRAM columns using DMF

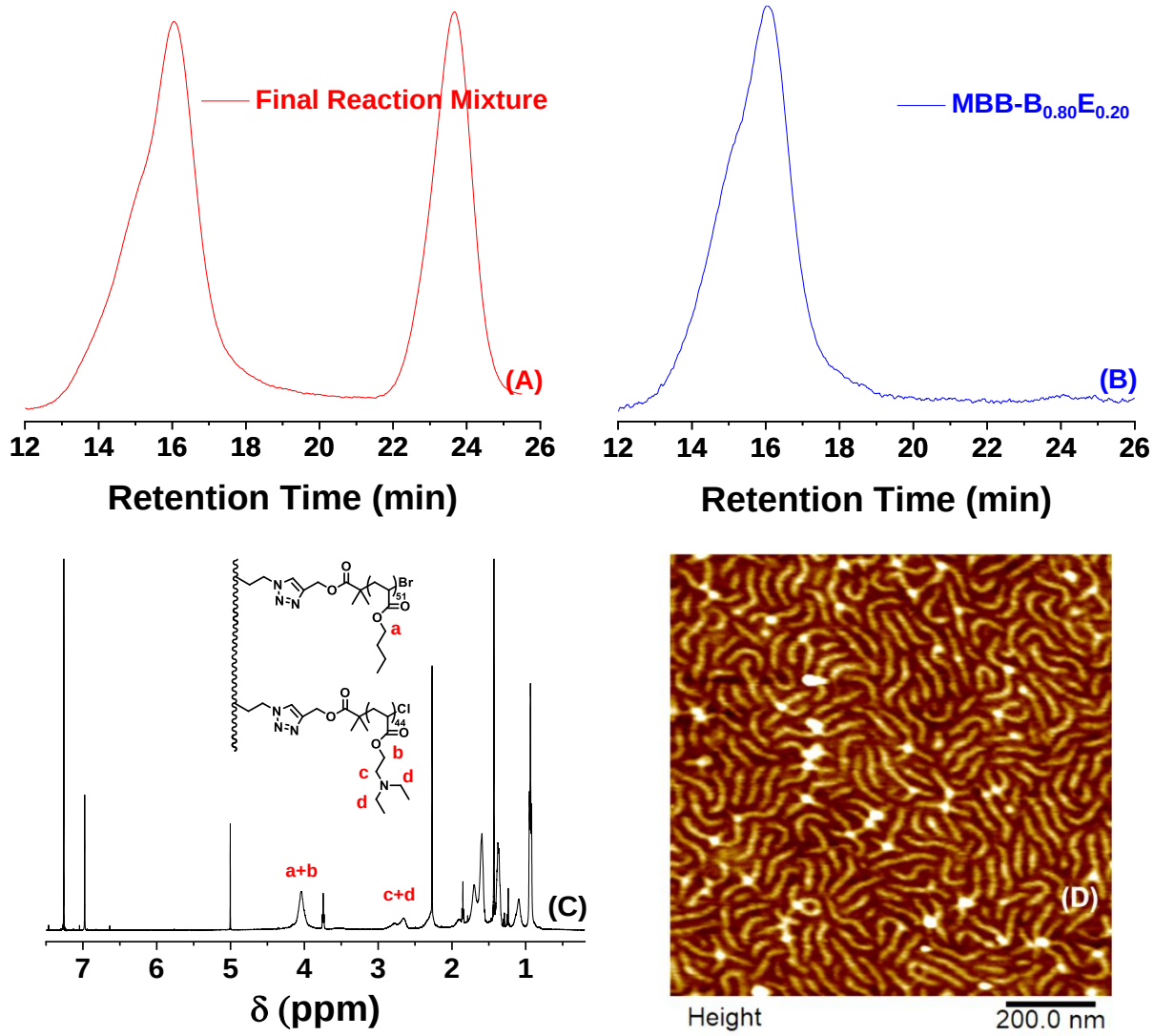

Figure 2.1. SEC traces of (A) the final reaction mixture for the synthesis of MBB-$B_{0.80}E_{0.20}$ and (B) after removal of unreacted side chain polymers, (C) ^{1}H NMR spectrum of the purified MBB-$B_{0.80}E_{0.20}$ in $CDCl_3$, and (D) AFM height image of MBB-$B_{0.80}E_{0.20}$. The average length of 250 measured bottlebrush molecules was 100.6 ± 28.2 nm.

containing 50 mM LiBr as the mobile phase were estimated from the SEC analysis of the final reaction mixtures. The brush polymer with the highest PDEAEMA content heterografted MBB and the homografted PDEAEMA brush polymer were found to be insoluble in DMF, and so ^{1}H NMR analysis of the initial and final reaction mixture was performed to estimate the grafting densities by comparing the peak integrals of the alkyne functional group before and after the reaction using the peak at 4.00 ppm (-COOC*H*$_2$- from both P*n*BA and PDEAEMA) as the internal reference (Figures A10 and A14). The calculated grafting densities for all samples were high, in the range of 86.7% – 94.5%. The characterization data are summarized in Table 2.2, and additional data can be found in Appendix A (Figures A5-A18). The brush polymer samples in this work are denoted as MBB-B$_x$E$_y$, where MBB stands for molecular bottlebrushes, B and E represent P*n*BA and PDEAEMA side chains, respectively, and x and y correspond to the mole fraction of P*n*BA and PDEAEMA side chains in the brushes, respectively.

2.3.2. Heterografted P*n*BA/PDEAEMA MBBs as pH-Responsive Emulsion Stabilizers: Effect of Side Chain Composition

Since the reported pK_a of protonated PDEAEMA is 7.4, we first examined the abilities of the four heterografted P*n*BA/PDEAEMA brush polymers to function as stabilizers for the emulsions of toluene and a 1.0 mM phosphate buffer solution at pH = 4.0, at which the PDEAEMA side chains would be fully protonated. The 1.0 mM aqueous phosphate buffer was employed to minimize the long-range charge-charge interactions and help ensure accurate pH values. Three concentrations of MBBs, 0.02 wt%, 0.01 wt%, and 0.005 wt%, were tested with respect to the total mass of toluene and the buffer. Because the addition of a tertiary-amine-containing brush polymer into the mixture will change the pH of the aqueous phase and there exists a difficulty in measuring the pH of the aqueous phase after the emulsion formation, an indirect method is adopted to achieve

Table 2.2. Characterization Data for Six Bottlebrush Polymers Used in This Work*

Bottlebrush Polymer	Grafting Density	Mole Ratio of P*n*BA to PDEAEMA Side Chains in MBB	Calculated M_n
MBB-$B_{1.00}E_{0.00}$	94.5%	1.00 : 0.00	2.69×10^6 Da
MBB-$B_{0.80}E_{0.20}$	87.3%	0.80 : 0.20	2.60×10^6 Da
MBB-$B_{0.64}E_{0.36}$	88.6%	0.64 : 0.36	2.73×10^6 Da
MBB-$B_{0.51}E_{0.49}$	86.8%	0.51 : 0.49	2.75×10^6 Da
MBB-$B_{0.24}E_{0.76}$	86.7%	0.24 : 0.76	2.89×10^6 Da
MBB-$B_{0.00}E_{1.00}$	88.8%	0.00 : 1.00	3.09×10^6 Da

* The degree of polymerization (DP) of the backbone is 406. The degree of azide functionalization for PHEMA-N_3 is 97.5%. The DP is 51 for P*n*BA and 44 for PDEAEMA side chains.

the desired pH values and is detailed below. For each concentration of each brush polymer in the mixture of toluene and the 1.0 mM buffer, we calculated the mass of the PDEAEMA side chains in the mixture on the basis of the characterization data of the brush polymer (DPs of backbone and side chain polymers, grafting density, and molar ratio of two polymers in the side chains) and assumed that the tertiary amine-containing side chains can be fully exposed to the aqueous phase. To determine the amount of a HCl or a NaOH solution that is needed to bring the pH to a desired value, an aqueous solution of the alkyne-end-functionalized PDEAEMA with the same concentration as in the aqueous phase of the PDEAEMA side chains of the brush polymer was prepared using the 1.0 mM phosphate buffer. The pH of the PDEAEMA solution was adjusted back to 4.0 by gradually adding either a 1.0 or 0.1 M HCl solution, and then to pH = 10.0 using an aqueous NaOH solution with a concentration of 0.10 M or 1.0 M, and back to pH = 4.0 again. The same amounts of HCl and NaOH solutions were applied to the mixture of toluene containing the brush polymer and the 1.0 mM phosphate buffer with an initial pH value of 4.0 to achieve the desired pH values of 4.0 and 10.0.

Each mixture of toluene, containing a certain amount of a brush polymer, and the 1.0 mM phosphate buffer, with a presumed pH value of 4.0 for the aqueous phase after the PDEAEMA side chains of the brush polymer were fully exposed to the aqueous phase, was vortexed for a total of 60 sec, divided into two 30 sec intervals with 5-10 min in between. Stable emulsions were formed with the use of MBB-$B_{0.80}E_{0.20}$, MBB-$B_{0.64}E_{0.36}$, and MBB-$B_{0.51}E_{0.49}$ as stabilizers, and no changes were observed after 24 h, as shown in Figure 2.2. Note that even with the use of only 0.005 wt% of the brush polymers, the emulsions were stable over a long period of time for these three brush polymers, similar to the observations of Xie et al. for the emulsions stabilized by MBBs

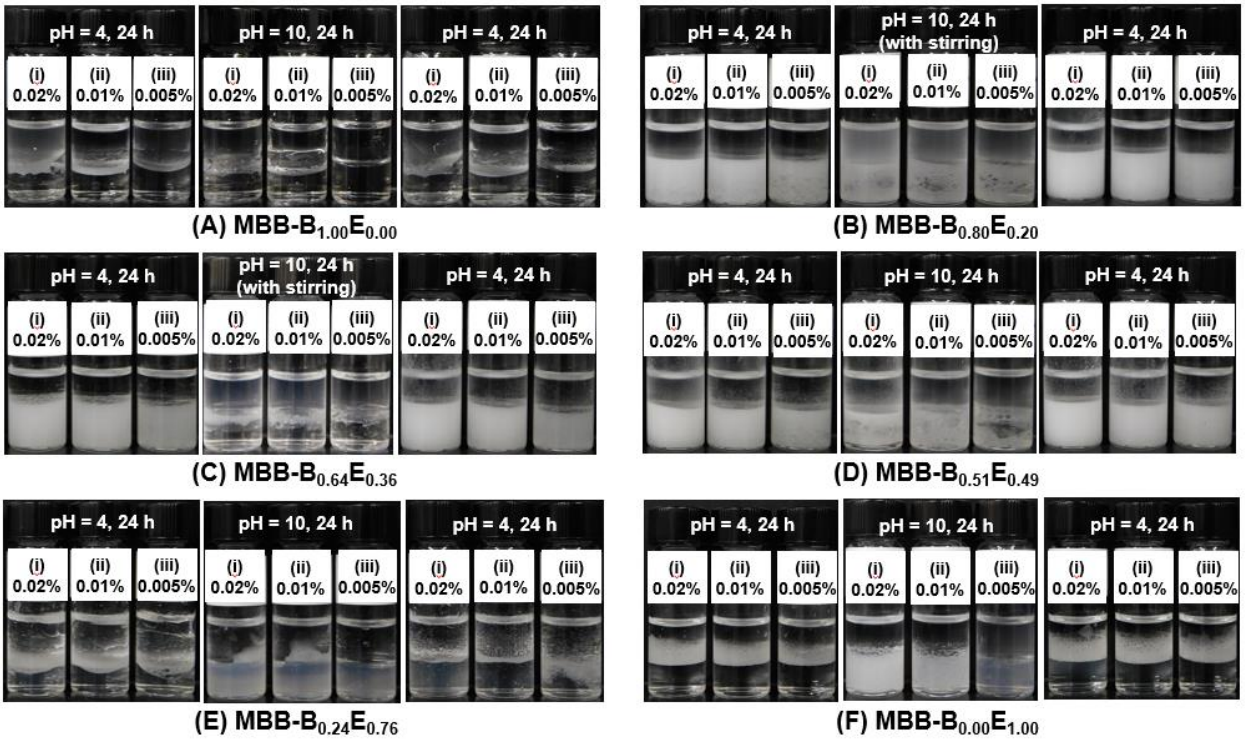

Figure 2.2. Digital optical photos of the mixtures of toluene with a brush polymer and a 1.0 mM phosphate buffer at pH = 4.0 after vortexing for 60 sec and sitting still for 24 h, at pH 10.0 after addition of NaOH and gentle shaking for 30 sec, and at pH = 4.0 after the addition of HCl and vortexing for 60 sec again for MBB-$B_{1.00}E_{0.00}$ (A), MBB-$B_{0.80}E_{0.20}$ (B), MBB-$B_{0.64}E_{0.36}$ (C), MBB-$B_{0.51}E_{0.49}$ (D), MBB-$B_{0.24}E_{0.76}$ (E), and MBB-$B_{0.00}E_{1.00}$ (F) at concentrations of 0.02 wt% (i), 0.01 wt% (ii), and 0.005 wt% (iii). For MBB-$B_{0.80}E_{0.20}$ and MBB-$B_{0.64}E_{0.36}$, the mixtures at pH = 10.0 were stirred with a magnetic stir bar at 60 rpm for a few hours to facilitate the emulsion breaking.

with P*n*BA and PEO side chains.[33] For MBB-$B_{0.24}E_{0.76}$, emulsions were formed initially after vortexing under the same conditions, however, they were not stable but broke after a few hours. For comparison, we also tested the two homografted brush polymers, MBB-$B_{1.00}E_{0.00}$ and MBB-$B_{0.00}E_{1.00}$, as emulsifiers for the mixtures of toluene and the 1.0 mM phosphate buffer under the same conditions (pH = 4.0), and no stable emulsions formed.

The type of the stable emulsions formed was determined to be water-in-oil emulsions for all three brush polymers, MBB-$B_{0.80}E_{0.20}$, MBB-$B_{0.64}E_{0.36}$, and MBB-$B_{0.51}E_{0.49}$, by adding the emulsion droplets into toluene and water as the emulsion droplets were dispersed in toluene but not in water. This was further supported by confocal microscopy using Nile Red, which is soluble in toluene but not in water, as a fluorescent probe. As shown in Figure 2.3, the continuous phase was red, while the dispersed phase was dark under the confocal microscope, indicating that the continuous phase was toluene and the droplets were the aqueous solution.

As shown in Figure 2.2, MBB-$B_{0.80}E_{0.20}$, MBB-$B_{0.64}E_{0.36}$, and MBB-$B_{0.51}E_{0.49}$ can produce stable water-in-toluene emulsions at all three concentrations (0.02 wt%, 0.01 wt%, and 0.005 wt%) under acidic conditions. To further study if there were differences in their abilities in stabilizing emulsions, we used an optical microscope to examine the emulsion droplets. Figure 2.4 shows representative optical micrographs of emulsion droplets at concentrations of 0.02, 0.01, and 0.005 wt% for all three MBBs at pH 4.0. For each sample, a small portion of the emulsion layer was transferred to toluene on a microscope glass slide and bright field optical images were taken. Although the droplet sizes and distributions appeared to be similar at the concentration of 0.02 wt% for all brush polymers, the droplets in the samples with 0.01% and 0.005% MBB-$B_{0.80}E_{0.20}$ appeared to be larger than those stabilized by the other two brush polymers at the same concentrations. The differences between the emulsions formed with MBB-$B_{0.64}E_{0.36}$ and MBB-

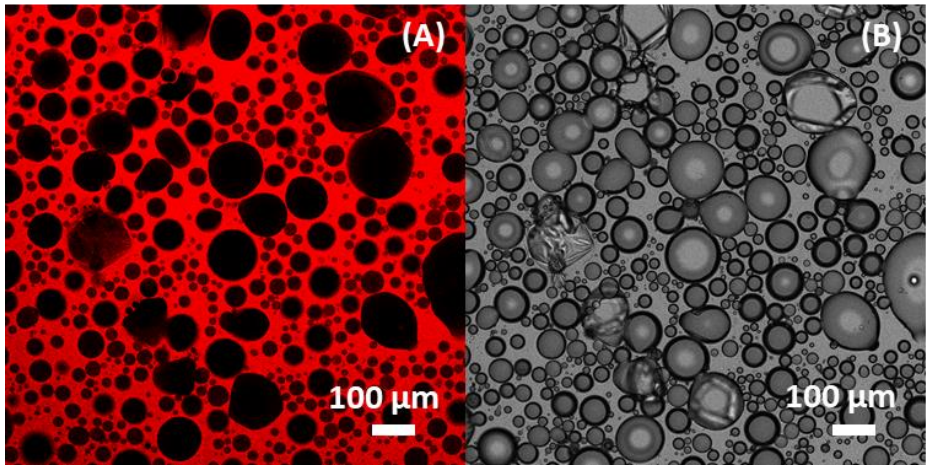

Figure 2.3. Laser confocal image (A) and optical micrograph (B) of the same portion of the emulsion of toluene and the 1.0 mM phosphate buffer formed with the use of 0.02 wt% MBB-$B_{0.51}E_{0.49}$ as the stabilizer at pH = 4.0. Nile Red was added into the toluene phase as a fluorescent dye.

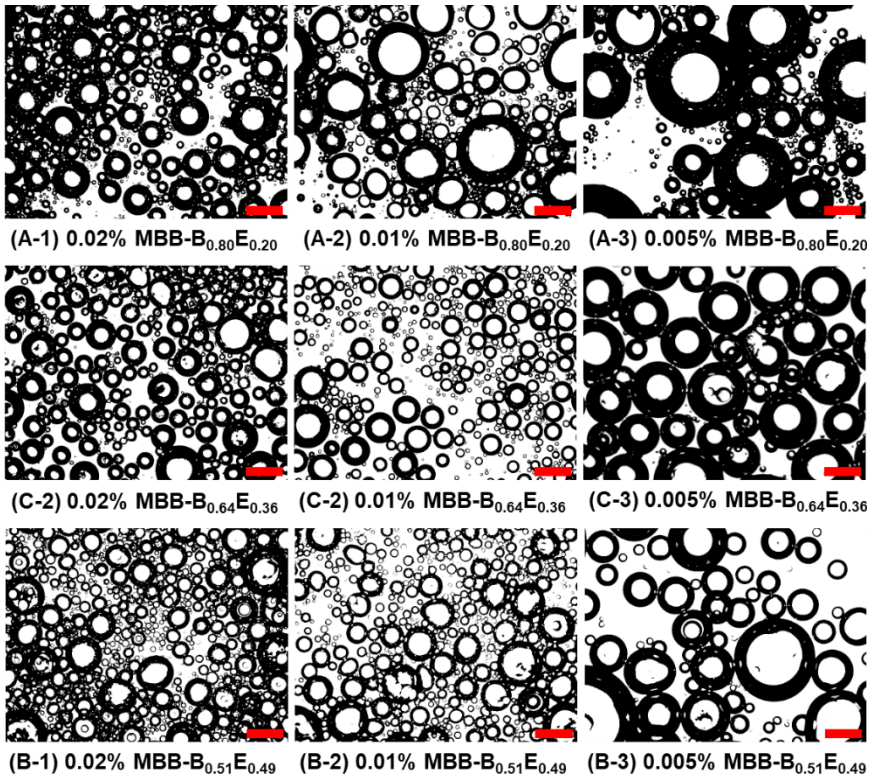

Figure 2.4. Representative optical micrographs of emulsions droplets from the MBB-$B_{0.80}E_{0.20}$ (A), MBB-$B_{0.64}E_{0.36}$ (B), and MBB-$B_{0.51}E_{0.49}$ (C)-stabilized emulsions at a brush polymer concentration of 0.02 wt% (left), 0.01 wt% (middle), and 0.005 wt% (right). Scale bars: 200 μm.

$B_{0.51}E_{0.49}$ as stabilizers were subtler, however, MBB-$B_{0.51}E_{0.49}$ appeared to be the best performer among the three MBBs. The better performance of MBB-$B_{0.51}E_{0.49}$ in stabilizing emulsions is likely a result of its more symmetric side chain composition (i.e., similar mole fractions of P*n*BA and PDEAEMA side chains in this brush polymer).

Based on the macroscopic observations of the emulsification behavior of the six brush polymers and the comparison of emulsion droplets for MBB-$B_{0.80}E_{0.20}$, MBB-$B_{0.64}E_{0.36}$, and MBB-$B_{0.51}E_{0.49}$, there is a side chain composition range for MBBs to function as stabilizers for water-toluene emulsions as represented in Figure 2.5. Outside of this range, the emulsions are not stable or cannot be formed. Note that the side chain composition range was not symmetric with respect to the mole fraction of 0.50. Although the underlying reason is unclear at this point, it is possibly related to the fact that one fully protonated PDEAEMA side chain at pH = 4.0 occupies a larger volume in water compared with one P*n*BA side chain in toluene. Thus, the brush molecules would exhibit an intrinsic curvature at the water-toluene interface when in the most stable or the lowest energy state. Presumably, if this intrinsic curvature is similar to that of the droplets, the emulsions would be more stable. However, it is known that many factors can affect the formation of emulsions.[37,41]

At pH = 4.0, the PDEAEMA side chains of the brush polymers are protonated and only soluble in the aqueous solution, while P*n*BA side chains are only soluble in toluene. As a result, the brush molecules with appropriate side chain compositions are reconfigured into a Janus structure and strongly adsorbed at the toluene-water interface, and consequently the emulsions are stabilized. When the pH is above the pK_a, PDEAEMA becomes insoluble in water; the brush polymers would retreat to the toluene phase and become only weakly associated with the interface. Consequently, the toluene-water interface would become unstable, and the emulsions would break. To investigate

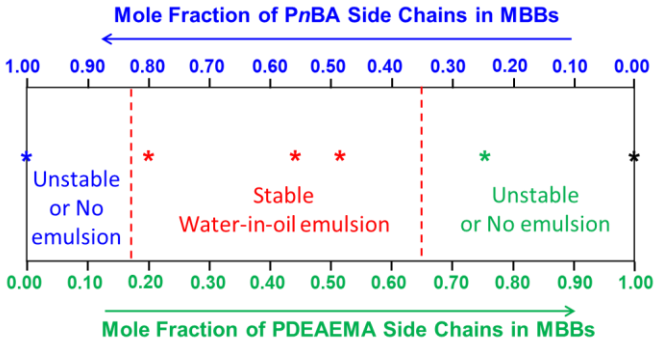

Figure 2.5. Side chain composition range of MBBs to function as effective stabilizers for the emulsions of toluene and the 1.0 mM phosphate buffer solution with a pH of 4.0.

the pH responsive behavior of the emulsions stabilized by those three brush polymers, for each sample, a calculated amount of a NaOH solution, based on the control experiment using a solution of the alkyne-end-functionalized PDEAEMA in the 1.0 mM phosphate buffer as discussed earlier, was introduced using a micropipette to change the pH from 4.0 to 10.0. Note that at pH = 10.0, the PDEAEMA side chains were nearly fully deprotonated, and thus the brush molecules would exhibit a rather low affinity to the toluene-water interface. Shortly after the addition of the aqueous NaOH solution into the emulsions, we observed that the droplets in the emulsion layer began to coalesce and eventually the emulsions were broken (Figure 2.2B,C,D). With gentle stirring by a small magnetic stir bar at a speed of 60 rpm, the breaking of emulsions was slightly faster. For the samples that did not generate a stable emulsion under acidic conditions (pH = 4.0), we vortexed the mixtures under the basic condition for a total of 60 sec, divided into two 30 sec intervals with 5-10 min in between as at pH = 4.0. For the homografted P*n*BA bottlebrushes, no emulsions were produced at all three concentrations as expected (Figure 2.2A). For MBB-$B_{0.24}E_{0.76}$ (Figure 2.2E), the bottom aqueous layers were cloudy aqueous solutions after sitting still on a bench for 24 h. Interestingly, the homografted PDEAEMA sample, MBB-$B_{0.00}E_{1.00}$, formed an emulsion layer with rather large droplets, visible to naked eye, after vortexing at concentrations of 0.01 wt% and above under the basic conditions. With gentle stirring for 2 h by a magnetic stir bar, the bottom aqueous layer of the 0.01 wt% sample became a mainly cloudy solution, though some large droplets can still be seen at the bottom of the vial. It was believed that the 0.02 wt% sample would need a longer time for the droplets to coalesce.

The pH values of the aqueous phase for all the samples in Figure 2.2 were then adjusted back to 4.0 by adding a calculated amount of a HCl solution in a similar manner, and the vials were gently shaken to allow for HCl to diffuse into the aqueous phase for protonation of the tertiary

amine groups of the PDEAEMA side chains in the brush polymers. Subsequently, the vials were vortexed for a total of 60 sec as in the first time. Stable water-in-oil emulsions were re-generated for MBB-$B_{0.80}E_{0.20}$, MBB-$B_{0.64}E_{0.36}$, and MBB-$B_{0.51}E_{0.49}$ as in the first time, demonstrating the reproducibility of the formation of emulsions. There were no noticeable differences between the first and the second vortexing after 24 h for the same brush polymer at the same concentration. Similar to the first round of vortexing at pH = 4.0, no stable emulsions were observed for the other three brush polymers, namely, MBB-$B_{1.00}E_{0.00}$, MBB-$B_{0.24}E_{0.76}$, and MBB-$B_{0.00}E_{1.00}$.

Atomic force microscopy (AFM) was used to visualize the brush molecules to examine if there were changes to the brush polymer after the formation, breaking, and re-formation of the emulsion. A small portion of the emulsion layer formed with 0.02 wt% MBB-$B_{0.51}E_{0.49}$ at pH = 4.0 in the second time was applied directly on the surface of a 1.0 mM phosphate buffer with a pH of 4.0 in a Langmuir-Blodgett trough. The brush molecules were compressed slightly to a surface pressure of 0.5 mN/m, and the monolayer of MBB-$B_{0.51}E_{0.49}$ was transferred to a cleaned glass disk for AFM imaging. Figure 2.6 shows a representative height image of the brushes (additional images can be found in Appendix A, Figure A19) along with an AFM micrograph of the original brush polymer. Analysis revealed that the average length of 230 brush molecules from the emulsion in Figure 2.6B was 98.2 ± 25.5 nm. For the original brush polymer MBB-$B_{0.51}E_{0.49}$ (Figure 2.6A), the average length and height of 270 measured brush molecules were 100.6 ± 25.7 nm. Given the two very close values of the brush length, this experiment suggested that the brush polymer was able to maintain the structure after the formation, breaking, and reformation of the emulsion.

2.3.3. Long-Term Stability of MBB-$B_{0.51}E_{0.49}$-Stabilized Emulsions

One advantage of Pickering emulsions compared to systems with lower molecular weight surfactants is their high stability. This is attributed to the high binding energy of particles to the

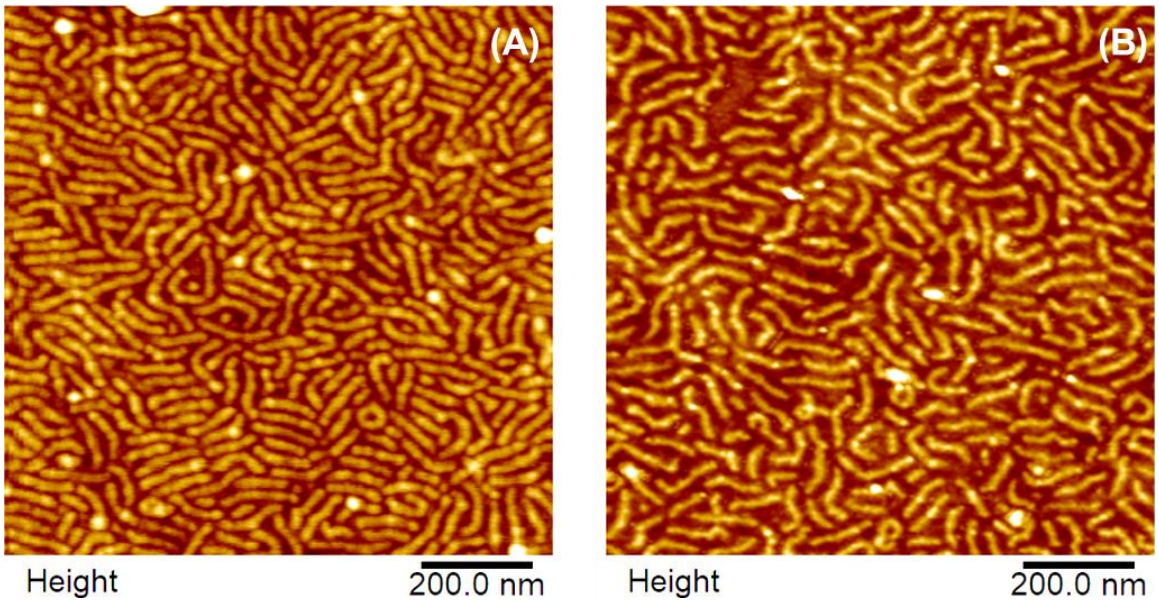

Figure 2.6. AFM height images of (A) the original brush polymer MBB-$B_{0.51}E_{0.49}$ and (B) the MBB-$B_{0.51}E_{0.49}$ from the water-in-toluene emulsion at pH = 4.0 formed in the second cycle.

interface as the energy required to remove the particles from the interface is proportional to the square of the particle size. Considering the length and width of our amphiphilic binary heterografted brush polymers, we can envisage that such giant molecules would exhibit similar behavior to particles with a suitable surface wettability in stabilizing emulsions. For example, Matyjaszewski and coworkers reported that the water-in-oil emulsions stabilized by heterografted PEO/P*n*BA brush polymers exhibited high stability. To study the emulsion stability with MBB-$B_{0.51}E_{0.49}$ as the emulsifier at pH = 4.0, we prepared two emulsions of toluene and the 1.0 mM phosphate buffer with 0.02 and 0.01 wt% of the brush polymer, respectively, under the acidic conditions by vortexing as for the emulsions in Figure 2.2. The vials that contained the emulsions were stored in a desiccator saturated with water and toluene vapors (achieved with the use of open vials of water and toluene). The macroscopic appearance and the droplets of the emulsions were examined by visual inspection and optical microscope, respectively, at different time points over a period of 6 weeks, and the results are presented in Figure 2.7. There were not any perceivable changes for the optical micrographs of emulsions droplets over the course of 6 weeks, demonstrating the high stability of both emulsions stabilized by MBB-$B_{0.51}E_{0.49}$ under the acidic conditions. Note that the changes of the heights of the top clear layer and the bottom emulsion layer for both emulsion systems were caused by multiple rounds of the removal of a portion of the sample for optical microscopy study of emulsion droplets.

2.3.4. Repeatability of pH-Induced Formation and Breaking of Water-Toluene Emulsion with MBB-$B_{0.51}E_{0.49}$ as Stabilizer

As shown in Figure 2.2, stable emulsions were formed, broken, and re-formed with the use of either MBB-$B_{0.80}E_{0.20}$, MBB-$B_{0.64}E_{0.36}$, or MBB-$B_{0.51}E_{0.49}$ as emulsifiers by changing the pH from 4.0 to 10.0, and 4.0 again, respectively. From a practical point of view, it would be advantageous

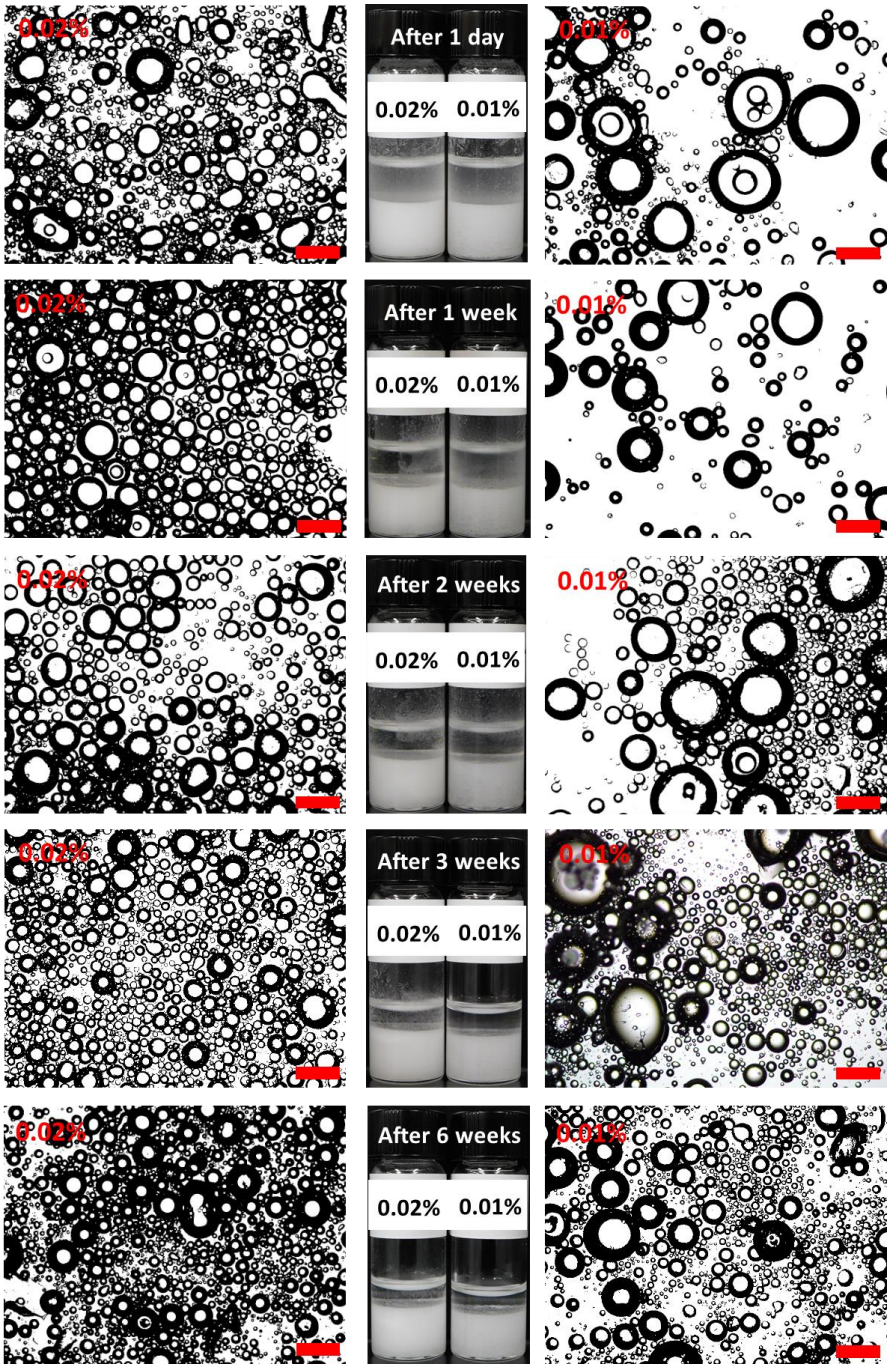

Figure 2.7. Long-term stability study of the emulsions stabilized by 0.02 wt% and 0.01 wt% MBB-$B_{0.51}E_{0.49}$ under the acidic conditions (pH = 4.0 for the aqueous phases). Optical micrograph of emulsion droplets from the 0.02 wt% emulsion (left), photo of two emulsions (middle), and optical micrograph of emulsion droplets from the 0.01 wt% emulsion after 1 day (top row), one week (2nd row), two weeks (3rd row), three weeks (4th row), and six weeks (5th row). Scale bars: 200 μm.

if the emulsions could be reversibly formed for multiple cycles. Note that each addition of HCl or NaOH to adjusting the pH of the aqueous phase will cause an accumulation of the salt in the aqueous phase, which could negatively impact the emulsion efficiency of the brush polymer because inorganic salts are commonly used to break emulsions. MBB-$B_{0.51}E_{0.49}$ was selected to investigate the repeatability of emulsion formation and breaking for its symmetric composition and its ability to function as an effective emulsifier at pH = 4.0. Four concentrations, 0.03, 0.02, 0.01, and 0.005 wt%, were tested for this brush polymer. Once the emulsions of toluene and the 1.0 mM phosphate aqueous buffer solution were generated at pH = 4.0 by vortexing, they were left for at least 6 h prior to taking photos by a digital camera and recording optical micrographs of emulsion droplets on an optical microscope. Subsequently, a calculated amount of a NaOH solution was added into the mixture to adjust the pH to 10.0 along with a magnetic stir bar to induce the breaking of the emulsions. The emulsions were then re-generated by vortexing after the addition of HCl to change the pH back to 4.0.

A total of 10 cycles were performed, and we found that for the three higher concentrations (i.e., 0.03, 0.02, and 0.01%), the mixtures were able to go through 10 full emulsion formation and breaking cycles (top two rows in Figure 2.8). For the mixture with the lowest concentration, 0.005 wt%, a stable emulsion was formed under the acidic condition after vortexing until the ninth cycle (i.e., no stable emulsion was observed in the ninth and tenth cycles) (second row in Figure 2.8). Despite the macroscopic observation of the formation of stable emulsions for all three concentrations after ten cycles, from the optical micrographs of emulsions droplets in the first and tenth cycles, the emulsion droplets were slightly larger after the tenth cycle for the concentrations of 0.02 and 0.01 wt%, while for the 0.03 wt% mixture the sizes of droplets were similar (bottom two rows in Figure 2.8). This could be attributed to the accumulation of the salt in the aqueous

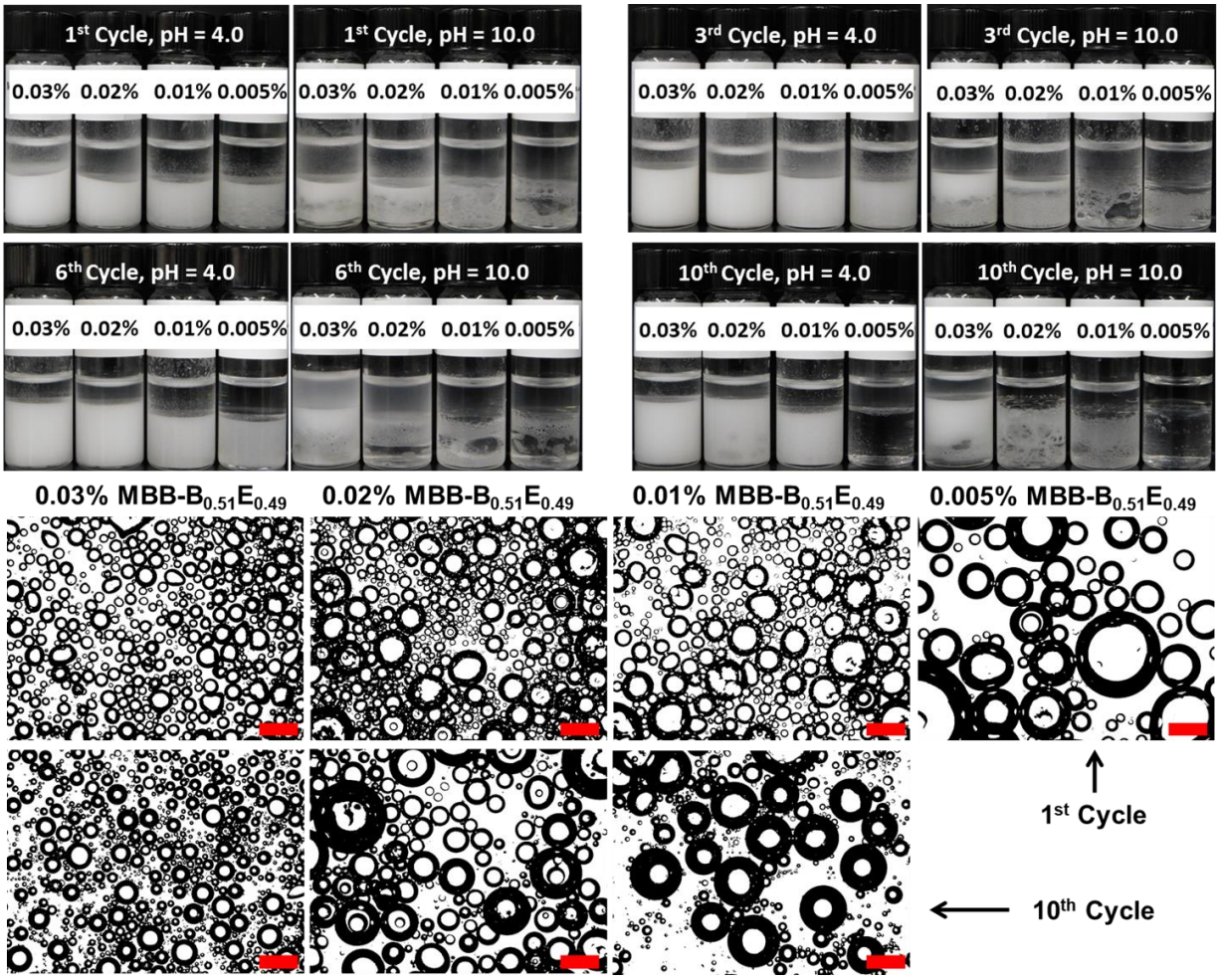

Figure 2.8. Digital optical photos (top two rows) of the mixtures of toluene, a 1.0 mM aqueous phosphate buffer solution, and MBB-$B_{0.51}E_{0.49}$ at concentrations of 0.03 wt%, 0.02 wt%, 0.01 wt%, and 0.005 wt% for the formation and breaking of emulsions from 1st cycle, 3rd cycle, 6th cycle, and 10th cycle, showing the repeatability of pH-induced formation and breaking of water-toluene emulsion. Note that starting in the 9th cycle, 0.005% brush polymer was unable to produce stable emulsions. The bottom two rows are optical micrographs of emulsion droplets from the 1st cycle and 10th cycle for different concentrations of the brush polymer. Scale bars in bottom two rows: 200 μm.

phase after the introduction of HCl and NaOH, which screened the charge interactions to some degree at the interface and thus reduced the emulsion stability. We also noticed that throughout the formation-breaking cycles the emulsion layer gradually became taller. At first, this might contradict the larger droplet sizes observed under the optical microscope, which should result in a smaller height for the emulsion layer. The taller emulsion layer was likely a result of the increased volume of the aqueous phase after multiple rounds of addition of HCl and NaOH solutions. Although only tens of microliters were added in each cycle, a total of 200 μL of aqueous solutions were injected into the vial after 10 cycles.

To examine if the brush molecules remained intact after ten cycles of the formation and breaking of emulsions, a small portion of the emulsion layer was taken out from the vial and deposited onto the surface of the subphase of a 1.0 mM aqueous phosphate buffer solution to prepare an AFM sample. Figure 2.9 shows a representative AFM height image and the corresponding phase image of the wormlike brush molecules of MBB-$B_{0.51}E_{0.49}$. (Additional images can be found in Appendix A, Figure A20.) Image analysis showed that the average length of 102 brushes was 100.8 ± 28.2nm, essentially the same as that of the original brush molecules (100.6 ± 25.7 nm) and very close to that of the brushes from the second cycle (98.2 ± 25.5 nm) shown in Figure 2.6. This indicates that there was no change to the brush polymer after ten rounds of vortexing.

2.3.5. Further Discussion on pH-Induced Formation and Breaking of Emulsion with Heterografted P*n*BA/PDEAEMA MBBs as a pH-Responsive Stabilizer

Our amphiphilic pH-responsive brush polymers with side chain compositions in a certain range showed abilities to function as pH-responsive emulsion stabilizers (Figures 2.2 and 2.4). At pH = 4.0, the PDEAEMA side chains are protonated and soluble in the aqueous solution, while the

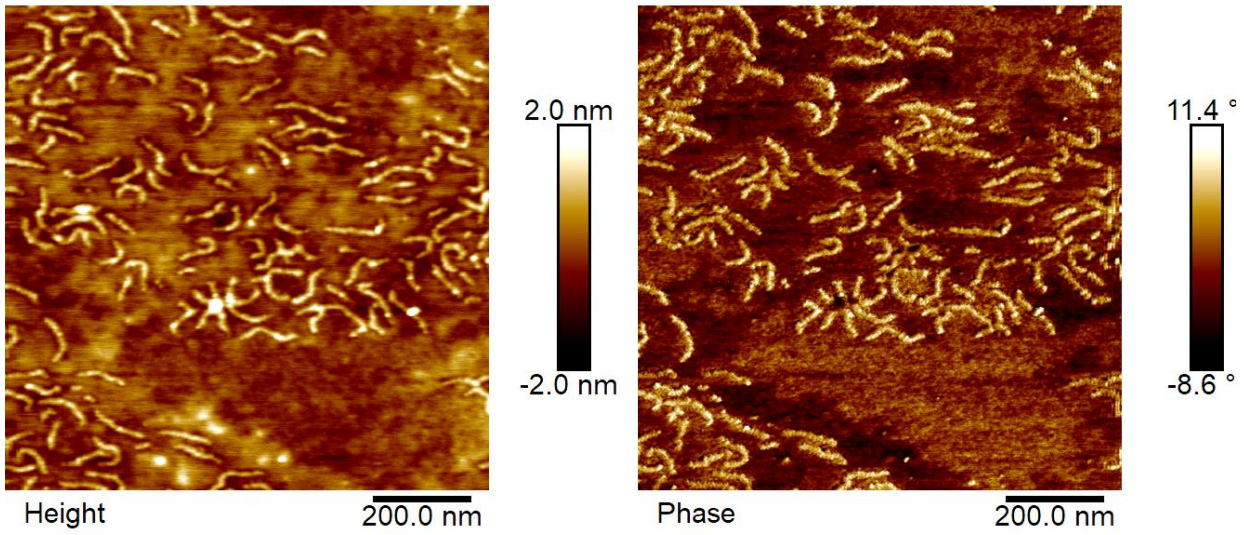

Figure 2.9. AFM height image (left) and corresponding phase image (right) of MBB-$B_{0.51}E_{0.49}$ after 10 cycles of emulsion formation and breaking.

hydrophobic P*n*BA side chains are only soluble in toluene. Consequently, the charged PDEAEMA side chains and the hydrophobic P*n*BA side chains can only extend into the acidic aqueous phase and the toluene phase, respectively. In other words, the heterografted P*n*BA/PDEAEMA brush molecules undergo spontaneous reconfiguration at the water-toluene interface, resulting in a perfect Janus structure (Scheme 2.2). The contrasting attractions of the two types of side chains for distinct phases and the large molecular size of the MBBs impart a strong affinity for the MBBs to the interface and thus a high stability of the emulsions. If the interfacial area is reduced, the high adsorption energy of the brush molecules at the interface would prevent them from desorbing from the interface, which would result in jamming of the brushes at the interface.

During the optical microscopy study of the emulsion droplets formed with the use of 0.03 wt% MBB-$B_{0.51}E_{0.49}$ as stabilizer under the acidic conditions, interestingly, we observed that with the evaporation of toluene and water from the glass slide the emulsion droplets crumpled, leaving behind a visible wrinkled thin polymer film (Figure 2.10). The formation of the wrinkled polymer film at the toluene-water interface evidenced that the charged, amphiphilic brush polymer molecules showed no ability to escape from the interface but were trapped at the interface.[42,43] This crumpling phenomenon is similar to the jamming of solid particles or electrostatically assembled nanostructures of poly(acrylic acid) molecular bottlebrushes and POSS-NH_2 at the interface reported by Russell et al.[36]

When the pH of the aqueous phase is changed to 10.0, the PDEAEMA side chains of MBBs are deprotonated and become insoluble in water, the brush molecules would retreat from the interface into the toluene phase and would exhibit a rather weak affinity to the interface. Consequently, the emulsions are broken (Scheme 2.2). Thus, this study shows that our amphiphilic

Scheme 2.2. Schematic Illustration of Formation and Breaking of Water-in-Oil Emulsion with pH-Responsive Amphiphilic Molecular Bottlebrushes as Emulsifier

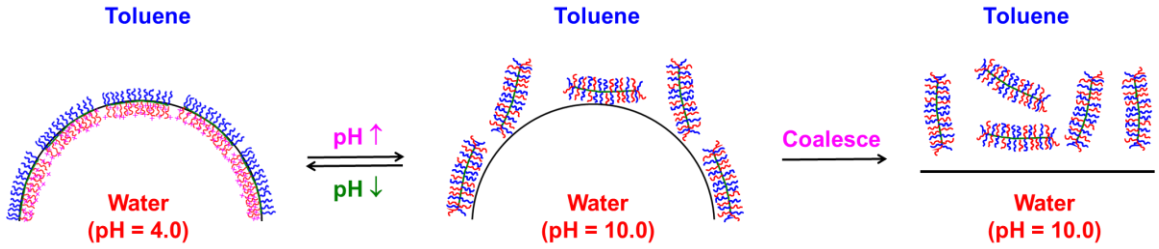

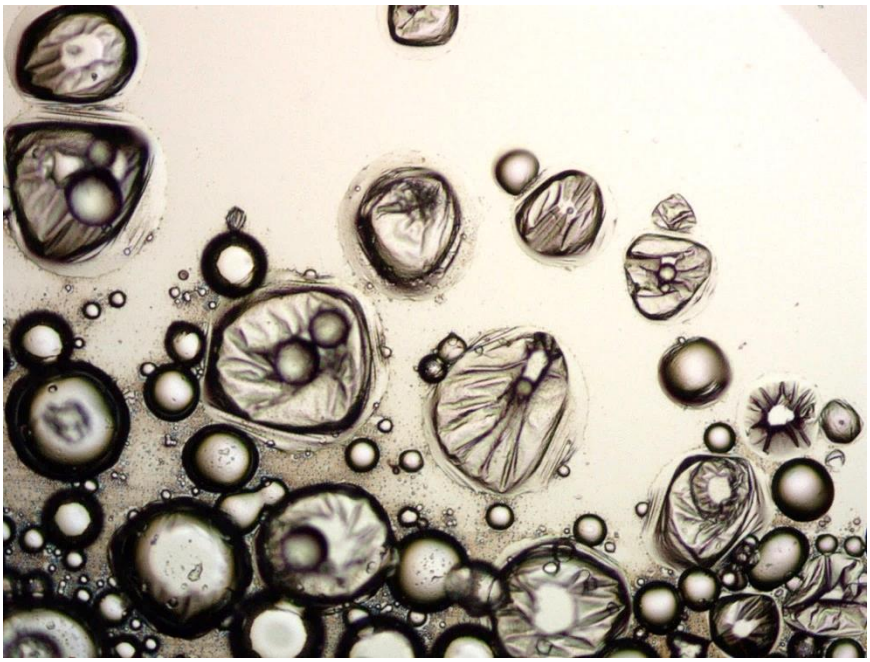

Figure 2.10. Optical micrograph of partially dried emulsion droplets from a 0.03 wt% MBB-$B_{0.51}E_{0.49}$-stabilized emulsion at pH = 4.0. As the toluene and water were evaporating, the droplets began to crumple on themselves, leaving behind a thin polymer film.

pH-responsive heterografted bicomponent MBBs with appropriate side chain compositions can function as effective and robust stimuli-responsive emulsion stabilizers, exhibiting the combined properties of particle stabilizers and the flexibility and responsiveness of block copolymer surfactants.

2.4. Conclusions

In summary, six brush polymers with different side chain compositions, including four heterografted MBBs and two homografted brush polymers, were synthesized in this study by grafting alkyne-end-functionalized side chain polymer(s) onto an azide-functionalized backbone polymer via the CuAAC click reaction and were fully purified and characterized. We showed that amphiphilic heterografted P*n*BA/PDEAEMA MBBs with appropriate side chain compositions were effective pH-responsive stabilizers for water-toluene emulsions. With the use of MBB-$B_{0.51}E_{0.49}$, the formation and breaking of emulsions can be repeated at least ten times by cycling the pH of the aqueous solution between 4.0 and 10.0 at the brush polymer concentrations of 0.01 wt% and above. The emulsions exhibited an excellent long-term stability, with no perceivable changes from the microscopic appearance and optical micrographs of emulsion droplets after six weeks. AFM imaging showed that the brush polymer remained intact after 10 cycles of emulsion formation and breaking and the average length was essentially the same as that of the original brush molecules. This study demonstrates a method to design MBBs as robust responsive emulsion stabilizers that combine the desired properties of particle emulsifiers and block copolymer surfactants, which may find potential applications in industry.

References

1. Zhang, M.; Müller, A. H. E., Cylindrical polymer brushes. *Journal of Polymer Science Part A: Polymer Chemistry* **2005,** *43* (16), 3461-3481.
2. Sheiko, S. S.; Sumerlin, B. S.; Matyjaszewski, K., Cylindrical molecular brushes: Synthesis, characterization, and properties. *Progress in Polymer Science* **2008,** *33* (7), 759-785.
3. Yuan, J.; Müller, A. H. E.; Matyjaszewski, K.; Sheiko, S. S., 6.06 - Molecular Brushes. In *Polymer Science: A Comprehensive Reference*, Matyjaszewski, K.; Möller, M., Eds. Elsevier: Amsterdam, 2012; pp 199-264.
4. Li, Z.; Tang, M.; Liang, S.; Zhang, M.; Biesold, G. M.; He, Y.; Hao, S.-M.; Choi, W.; Liu, Y.; Peng, J.; Lin, Z., Bottlebrush polymers: From controlled synthesis, self-assembly, properties to applications. *Progress in Polymer Science* **2021,** *116*, 101387.
5. Zhao, B., Shape-Changing Bottlebrush Polymers. *J. Phys. Chem. B* **2021**, 125 (24), 6373-6389.
6. Lee, H.-i.; Pietrasik, J.; Sheiko, S. S.; Matyjaszewski, K., Stimuli-responsive molecular brushes. Progress in Polymer Science 2010, 35 (1), 24-44.
7. Qi, H.; Liu, X.; Henn, D. M.; Mei, S.; Staub, M. C.; Zhao, B.; Li, C. Y., Breaking translational symmetry via polymer chain overcrowding in molecular bottlebrush crystallization. *Nature Communications* **2020,** *11* (1), 2152.
8. Xie, G.; Martinez, M. R.; Olszewski, M.; Sheiko, S. S.; Matyjaszewski, K., Molecular Bottlebrushes as Novel Materials. *Biomacromolecules* **2019,** *20* (1), 27-54.
9. Rzayev, J., Molecular Bottlebrushes: New Opportunities in Nanomaterials Fabrication. *ACS Macro Letters* **2012,** *1* (9), 1146-1149.

10. Daniel, W. F. M.; Xie, G.; Vatankhah Varnoosfaderani, M.; Burdyńska, J.; Li, Q.; Nykypanchuk, D.; Gang, O.; Matyjaszewski, K.; Sheiko, S. S., Bottlebrush-Guided Polymer Crystallization Resulting in Supersoft and Reversibly Moldable Physical Networks. *Macromolecules* **2017,** *50* (5), 2103-2111.
11. Liberman-Martin, A. L.; Chu, C. K.; Grubbs, R. H., Application of Bottlebrush Block Copolymers as Photonic Crystals. *Macromolecular Rapid Communications* **2017,** *38* (13), 1700058.
12. Banquy, X.; Burdyńska, J.; Lee, D. W.; Matyjaszewski, K.; Israelachvili, J., Bioinspired Bottle-Brush Polymer Exhibits Low Friction and Amontons-like Behavior. *Journal of the American Chemical Society* **2014,** *136* (17), 6199-6202.
13. Müllner, M., Molecular polymer bottlebrushes in nanomedicine: therapeutic and diagnostic applications. *Chemical Communications* **2022**.
14. Wang, M.-Q.; Zou, H.; Liu, W.-B.; Liu, N.; Wu, Z.-Q., Bottlebrush Polymers Based on RAFT and the "C1" Polymerization Method: Controlled Synthesis and Application in Anticancer Drug Delivery. *ACS Macro Letters* **2022,** *11* (2), 179-185.
15. Detappe, A.; Nguyen, H. V. T.; Jiang, Y.; Agius, M. P.; Wang, W.; Mathieu, C.; Su, N. K.; Kristufek, S. L.; Lundberg, D. J.; Bhagchandani, S.; Ghobrial, I. M.; Ghoroghchian, P. P.; Johnson, J. A., Molecular bottlebrush prodrugs as mono- and triplex combination therapies for multiple myeloma. *Nature Nanotechnology* **2023,** *18* (2), 184-192.
16. Zhang, Y.; Fu, L.; Martinez, M. R.; Sun, H.; Nava, V.; Yan, J.; Ristroph, K.; Averick, S. E.; Marelli, B.; Giraldo, J. P.; Matyjaszewski, K.; Tilton, R. D.; Lowry, G. V., Temperature-Responsive Bottlebrush Polymers Deliver a Stress-Regulating Agent In Vivo

for Prolonged Plant Heat Stress Mitigation. *ACS Sustainable Chemistry & Engineering* **2023,** *11* (8), 3346-3358.

17. Fournier, D.; Hoogenboom, R.; Schubert, U. S., Clicking polymers: a straightforward approach to novel macromolecular architectures. *Chemical Society Reviews* **2007,** *36* (8), 1369-1380.
18. Henn, D. M.; Fu, W.; Mei, S.; Li, C. Y.; Zhao, B., Temperature-Induced Shape Changing of Thermosensitive Binary Heterografted Linear Molecular Brushes between Extended Wormlike and Stable Globular Conformations. Macromolecules 2017, 50 (4), 1645-1656.
19. Henn, D. M.; Lau, C. M.; Li, C. Y.; Zhao, B., Light-triggered unfolding of single linear molecular bottlebrushes from compact globular to wormlike nano-objects in water. Polymer Chemistry 2017, 8 (17), 2702-2712.
20. Henn, D. M.; Holmes, J. A.; Kent, E. W.; Zhao, B., Worm-to-Sphere Shape Transition of Thermoresponsive Linear Molecular Bottlebrushes in Moderately Concentrated Aqueous Solution. The Journal of Physical Chemistry B 2018, 122 (27), 7015-7025.
21. Kent, E. W.; Henn, D. M.; Zhao, B., Shape-changing linear molecular bottlebrushes with dually pH- and thermo-responsive diblock copolymer side chains. Polymer Chemistry 2018, 9 (41), 5133-5144.
22. Kent, E. W.; Zhao, B., Stimuli-Induced Star-Globule Shape Transitions of Dually Responsive Binary Heterografted Three-Arm Star Molecular Brushes in Aqueous Solution. Macromolecules 2019, 52 (17), 6714-6724.
23. Kent, E. W.; Lewoczko, E. M.; Zhao, B., Effect of Buffer Anions on Pearl-Necklace Morphology of Tertiary Amine-Containing Binary Heterografted Linear Molecular Bottlebrushes in Acidic Aqueous Buffers. Langmuir 2020, 36 (44), 13320-13330.

24. Kent, E. W.; Lewoczko, E. M.; Zhao, B., pH- and chaotropic anion-induced conformational changes of tertiary amine-containing binary heterografted star molecular bottlebrushes in aqueous solution. Polymer Chemistry 2021, 12 (2), 265-276.

25. Lewoczko, E. M.; Kelly, M. T.; Kent, E. W.; Zhao, B., Effects of temperature on chaotropic anion-induced shape transitions of star molecular bottlebrushes with heterografted poly(ethylene oxide) and poly(*N*,*N*-dialkylaminoethyl methacrylate) side chains in acidic water. *Soft Matter* **2021**, *17 (27)*, 6566-6579.

26. Kelly, M. T.; Kent, E. W.; Zhao, B., Stepwise Conformational Transitions of Stimuli-Responsive Linear Ternary Heterografted Bottlebrush Polymers in Aqueous Solution. *Macromolecules* **2022**, *55(5)*, 1629-1641.

27. Gan, W.; Shi, Y.; Jing, B.; Cao, X.; Zhu, Y.; Gao, H., Produce Molecular Brushes with Ultrahigh Grafting Density Using Accelerated CuAAC Grafting-Onto Strategy. *Macromolecules* **2017,** *50* (1), 215-222.

28. Yan, Y.; Shi, Y.; Zhu, W.; Chen, Y., Highly efficient synthesis of cylindrical polymer brushes with various side chains via click grafting-onto approach. *Polymer* **2013,** *54* (21), 5634-5642.

29. Engler, A. C.; Lee, H.-i.; Hammond, P. T., Highly Efficient "Grafting onto" a Polypeptide Backbone Using Click Chemistry. *Angewandte Chemie International Edition* **2009,** *48* (49), 9334-9338.

30. Gao, H.; Matyjaszewski, K., Synthesis of Molecular Brushes by "Grafting onto" Method: Combination of ATRP and Click Reactions. *Journal of the American Chemical Society* **2007,** *129* (20), 6633-6639.

31. Obhi, N. K.; Peda, D. M.; Kynaston, E. L.; Seferos, D. S., Exploring the Graft-To Synthesis of All-Conjugated Comb Copolymers Using Azide–Alkyne Click Chemistry. *Macromolecules* **2018,** *51* (8), 2969-2978.

32. Li, Y.; Zou, J.; Das, B. P.; Tsianou, M.; Cheng, C., Well-Defined Amphiphilic Double-Brush Copolymers and Their Performance as Emulsion Surfactants. *Macromolecules* **2012,** *45* (11), 4623-4629.

33. Xie, G.; Krys, P.; Tilton, R. D.; Matyjaszewski, K., Heterografted Molecular Brushes as Stabilizers for Water-in-Oil Emulsions. *Macromolecules* **2017,** *50* (7), 2942-2950.

34. Seong, H.-G.; Chen, Z.; Emrick, T.; Russell, T. P., Reconfiguration and Reorganization of Bottlebrush Polymer Surfactants. *Angewandte Chemie International Edition* **2022,** *61* (19), e202200530.

35. Gao, Y.; Wu, X.; Xiang, Z.; Qi, C., Amphiphilic Double-Brush Copolymers with a Polyurethane Backbone: A Bespoke Macromolecular Emulsifier for Ionic Liquid-in-Oil Emulsion. *Langmuir* **2021,** *37* (7), 2376-2385.

36. Wang, B.; Liu, T.; Chen, H.; Yin, B.; Zhang, Z.; Russell, T. P.; Shi, S., Molecular Brush Surfactants: Versatile Emulsifiers for Stabilizing and Structuring Liquids. *Angewandte Chemie International Edition* **2021,** *60* (36), 19626-19630.

37. Tang, J.; Quinlan, P. J.; Tam, K. C., Stimuli-responsive Pickering emulsions: recent advances and potential applications. *Soft Matter* **2015,** *11* (18), 3512-3529.

38. Zhou, S.; Zeng, M.; Liu, Y.; Sui, X.; Yuan, J., Stimuli-Responsive Pickering Emulsions Regulated via Polymerization-Induced Self-Assembly Nanoparticles. *Macromolecular Rapid Communications* **2022,** *43* (11), 2200010.

39. Umar, A. A.; Saaid, I. B. M.; Sulaimon, A. A.; Pilus, R. B. M., A Review of Petroleum Emulsions and Recent Progress on Water-in-Crude Oil Emulsions Stabilized by Natural Surfactants and Solids. *Journal of Petroleum Science and Engineering* **2018,** *165*, 673-690.

40. Deirram, N.; Zhang, C.; Kermaniyan, S. S.; Johnston, A. P. R.; Such, G. K., pH-Responsive Polymer Nanoparticles for Drug Delivery. *Macromolecular Rapid Communications* **2019,** *40* (10), 1800917.

41. Hu, M.; Russell, T. P., Polymers with Advanced Architectures as Emulsifiers for Multi-Functional Emulsions. *Materials Chemistry Frontiers* **2021,** *5* (3), 1205-1220.

42. Datta, S. S.; Shum, H. C.; Weitz, D. A., Controlled Buckling and Crumpling of Nanoparticle-Coated Droplets. *Langmuir* **2010,** *26* (24), 18612-18616.

43. Liu, K.; Jiang, J.; Cui, Z.; Binks, B. P., pH-Responsive Pickering Emulsions Stabilized by Silica Nanoparticles in Combination with a Conventional Zwitterionic Surfactant. *Langmuir* **2017,** *33* (9), 2296-2305.

Appendix A

for

Chapter 2: Amphiphilic Heterografted Bottlebrush Polymers with Tertiary Amine-Containing Side Chains as Effective and Efficient pH-Responsive Emulsion Stabilizers

Scheme A1. Synthesis of PHEMA-TMS, PHEMA-Br, and PHEMA-N_3

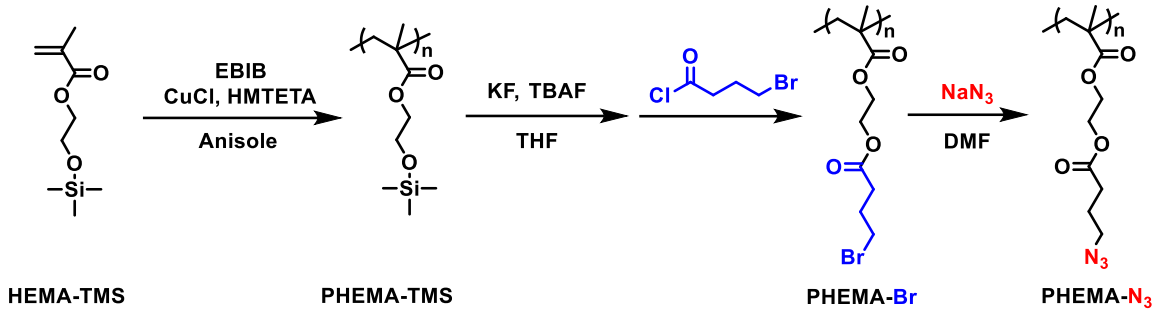

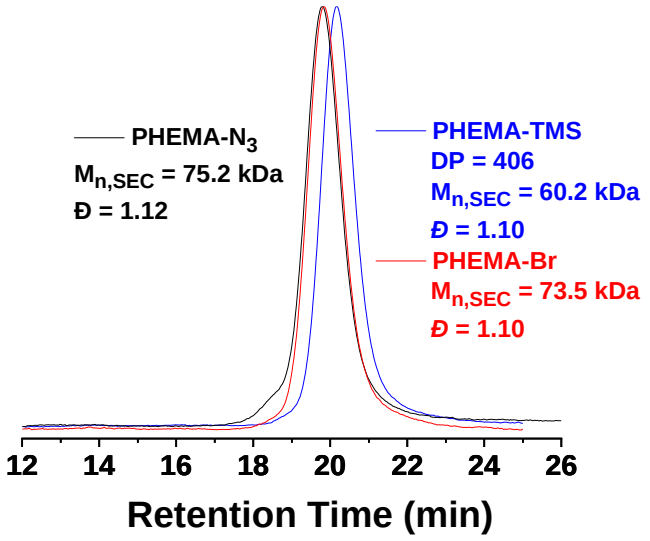

Figure A1. Size exclusion chromatography (SEC) curves of PHEMA-TMS, PHEMA-Br, and PHEMA-N_3. SEC analysis was performed using PL-GPC 50 plus equipped with GRAM columns and an RI detector using 50 mM LiBr as eluent.

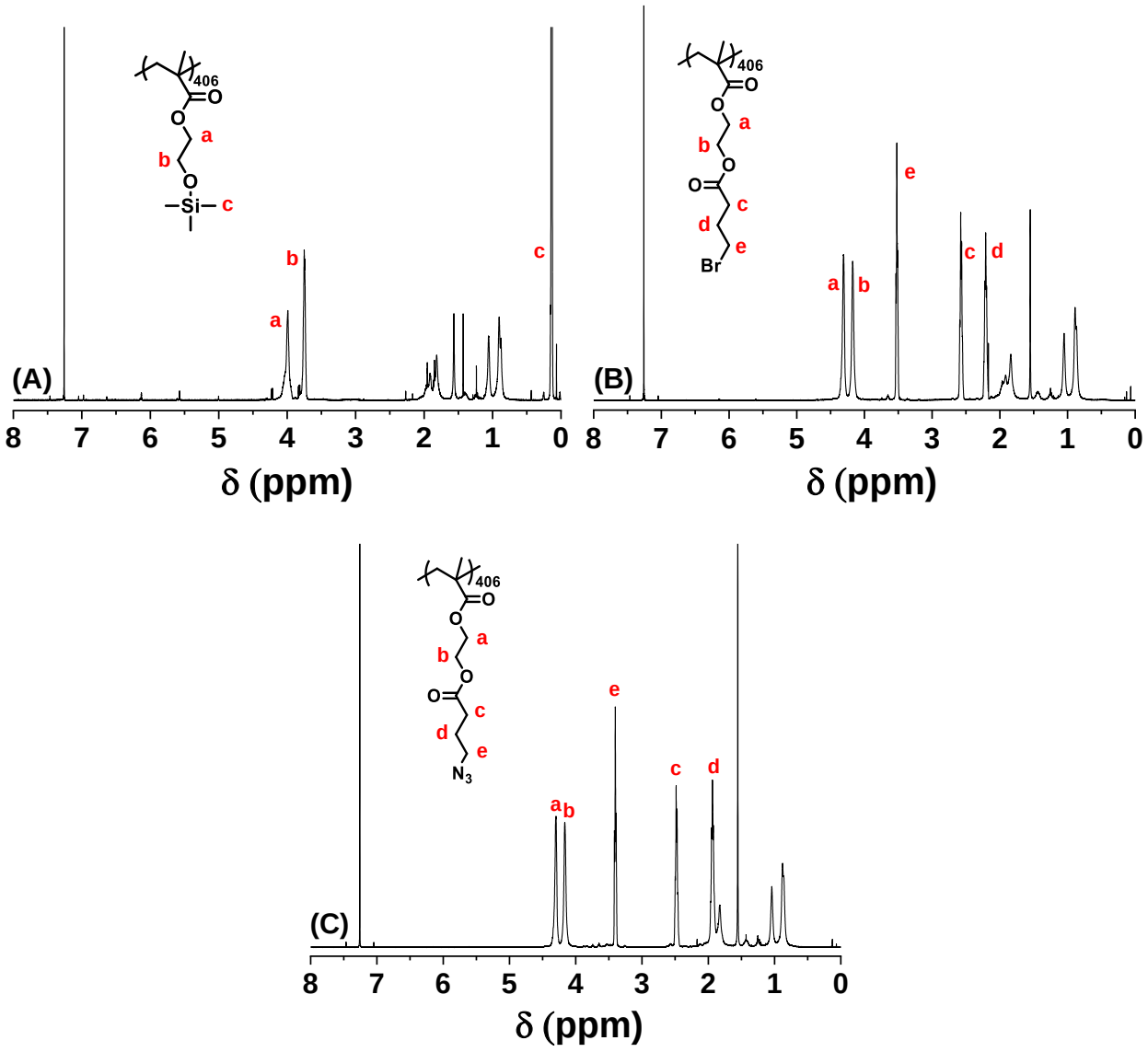

Figure A2. ^{1}H NMR spectra of purified PHEMA-TMS (A), PHEMA-Br (B), and PHEMA-N_3 (C) in $CDCl_3$.

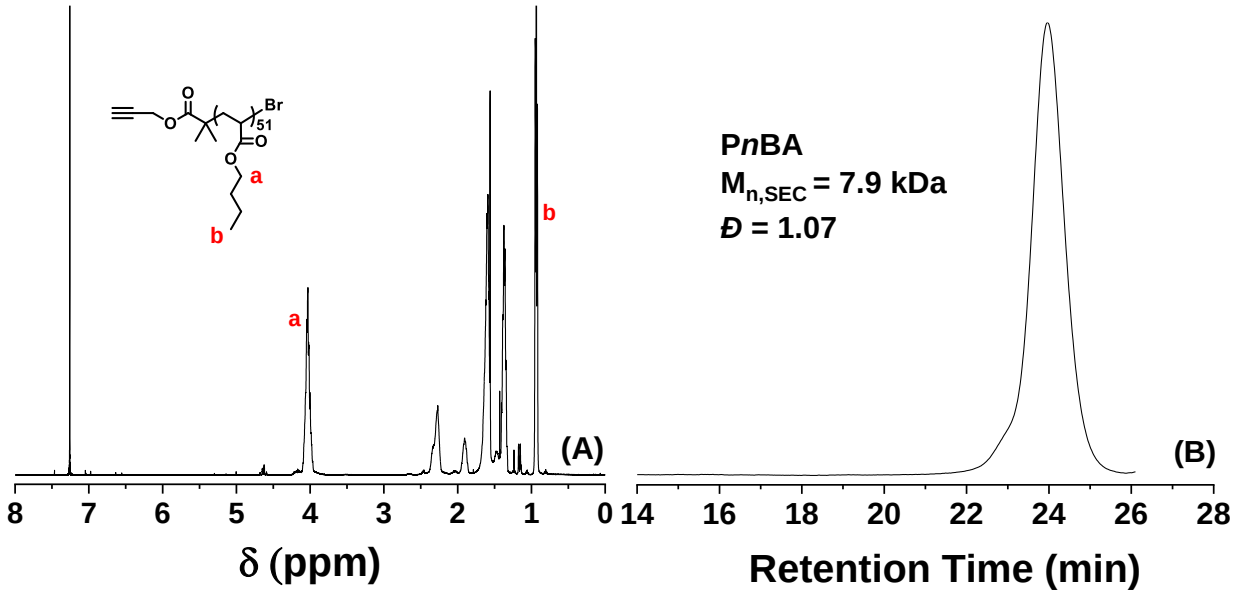

Figure A3. (A) ^{1}H NMR spectrum of the alkyne-end-functionalized P*n*BA side chain polymer in $CDCl_3$ and (B) size exclusion chromatography (SEC) trace of P*n*BA from SEC analysis using GRAM columns and DMF with 50 mM LiBr as eluent.

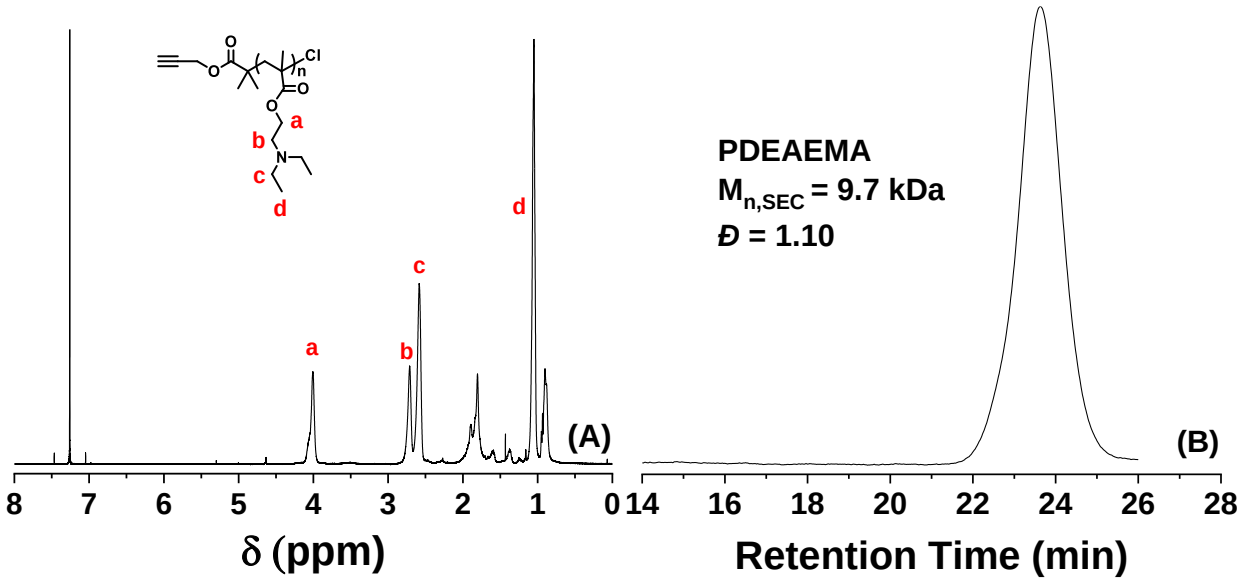

Figure A4. (A) ^{1}H NMR spectrum of the alkyne-end-functionalized PDEAEMA side chain polymer in $CDCl_3$ and (B) size exclusion chromatography (SEC) trace of PDEAEMA from SEC analysis using GRAM columns and DMF with 50 mM LiBr as eluent.

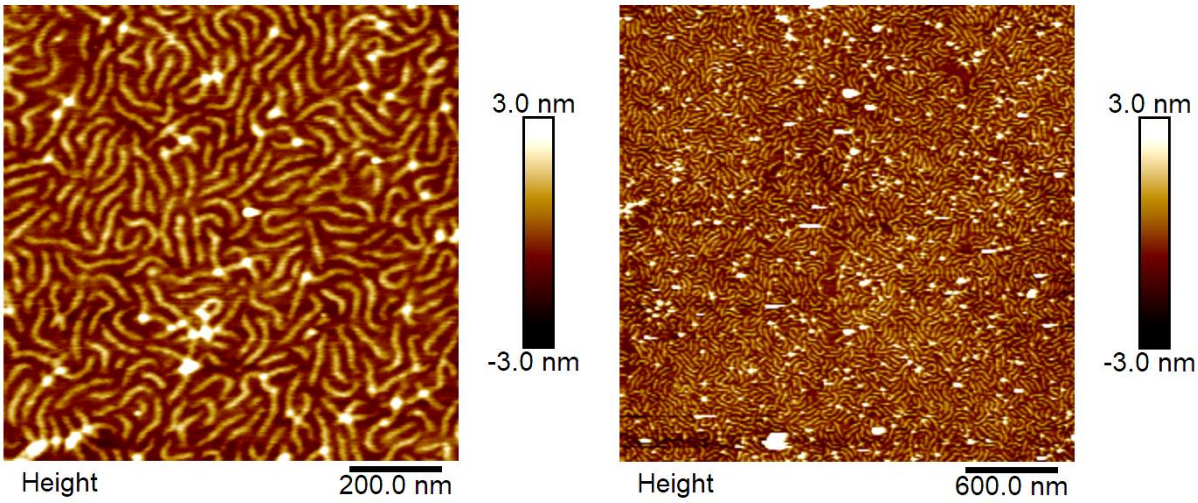

Figure A5. Additional AFM height images of MBB-$B_{0.80}E_{0.20}$. The AFM sample was prepared using a Langmuir-Blodgett trough with a pH of 4.0 for the aqueous subphase. The average length of 250 brush molecules was 100.6 ± 28.2 nm.

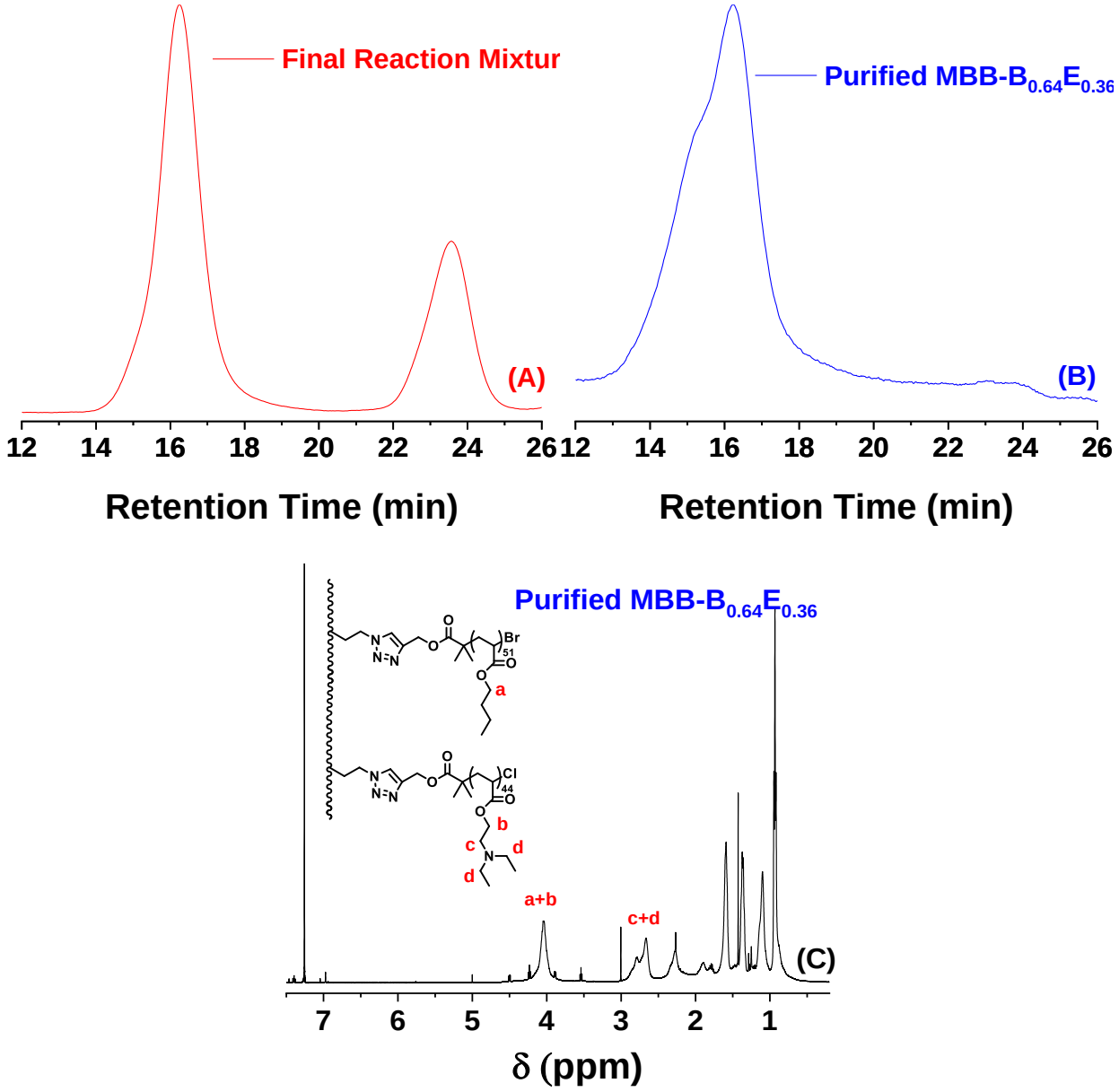

Figure A6. SEC traces of (A) the final reaction mixture for the synthesis of binary heterografted molecular bottlebrushes MBB-$B_{0.64}E_{0.36}$ and (B) after removal of residual side chain polymers, and (C) ^{1}H NMR spectrum of the purified MBB-$B_{0.64}E_{0.36}$ in $CDCl_3$.

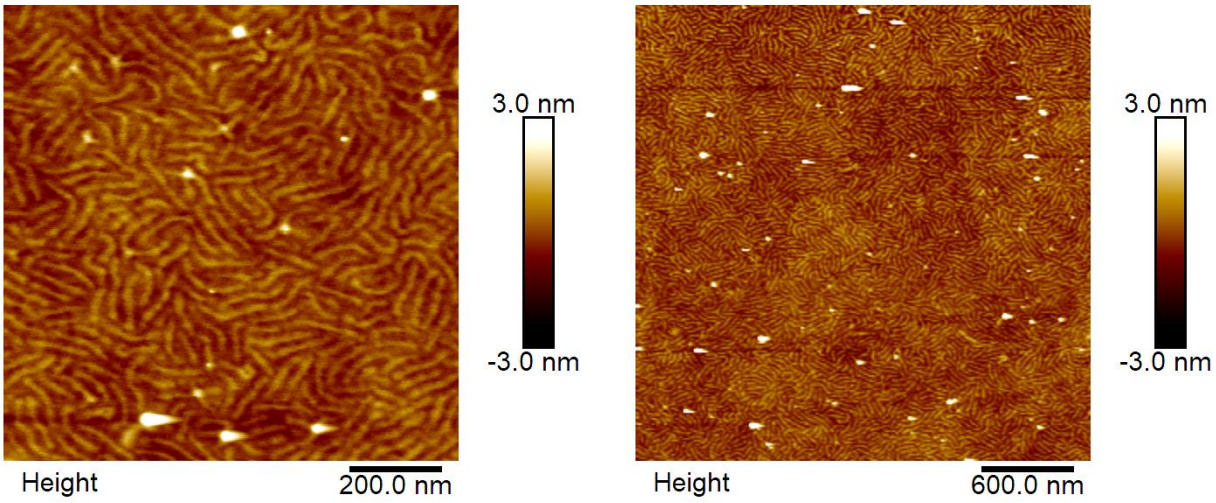

Figure A7. AFM height images of MBB-$B_{0.64}E_{0.36}$. The AFM sample was prepared using a Langmuir-Blodgett trough with a pH of 4.0 for the aqueous subphase. The average length of 217 measured brush molecules was 102.4 ± 26.4 nm.

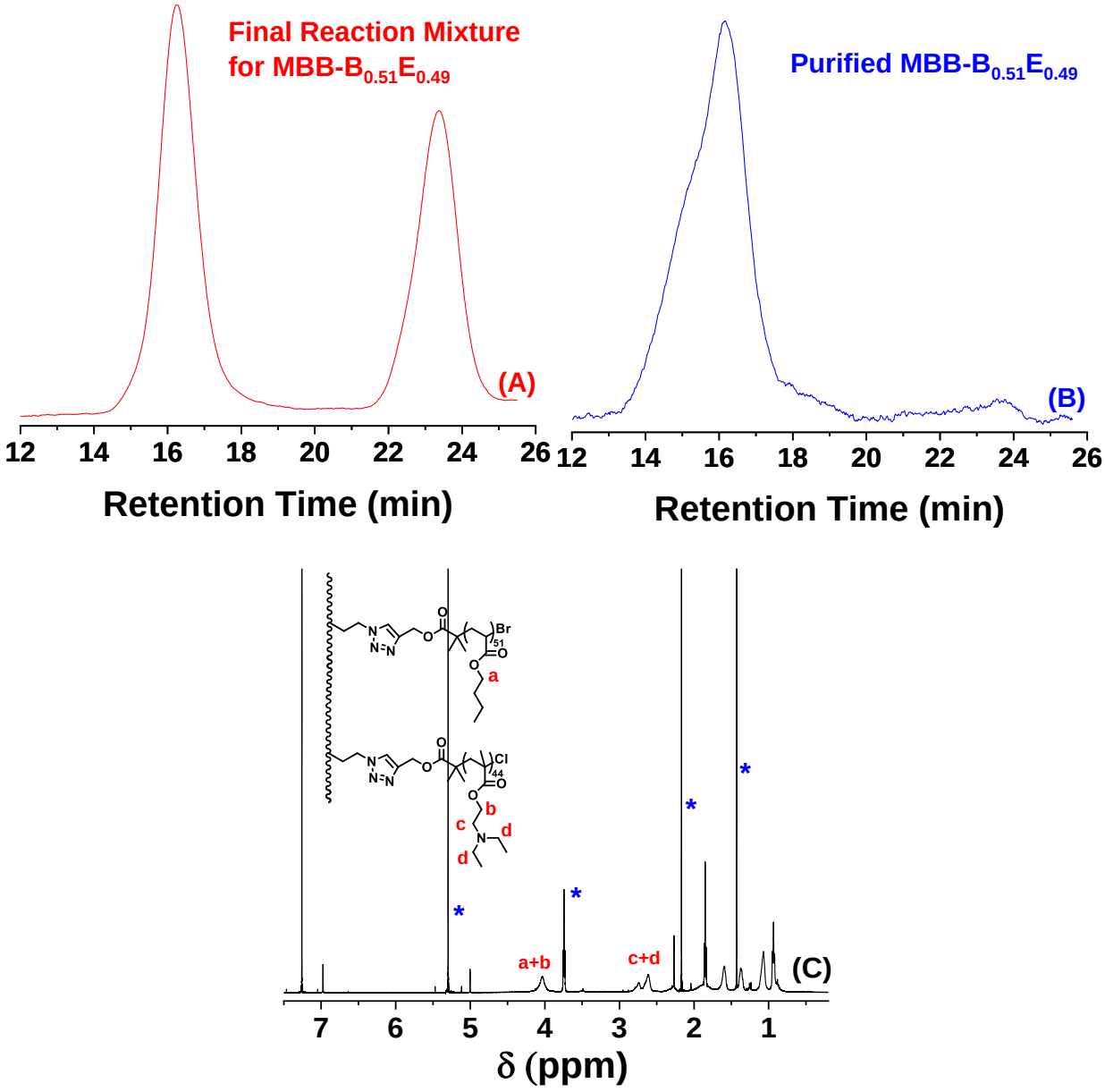

Figure A8. SEC traces of (A) the final reaction mixture for the synthesis of binary heterografted molecular bottlebrushes MBB-$B_{0.51}E_{0.49}$ and (B) after removal of residual side chain polymers, and (C) ^{1}H NMR spectrum of the purified MBB-$B_{0.51}E_{0.49}$ in $CDCl_3$.

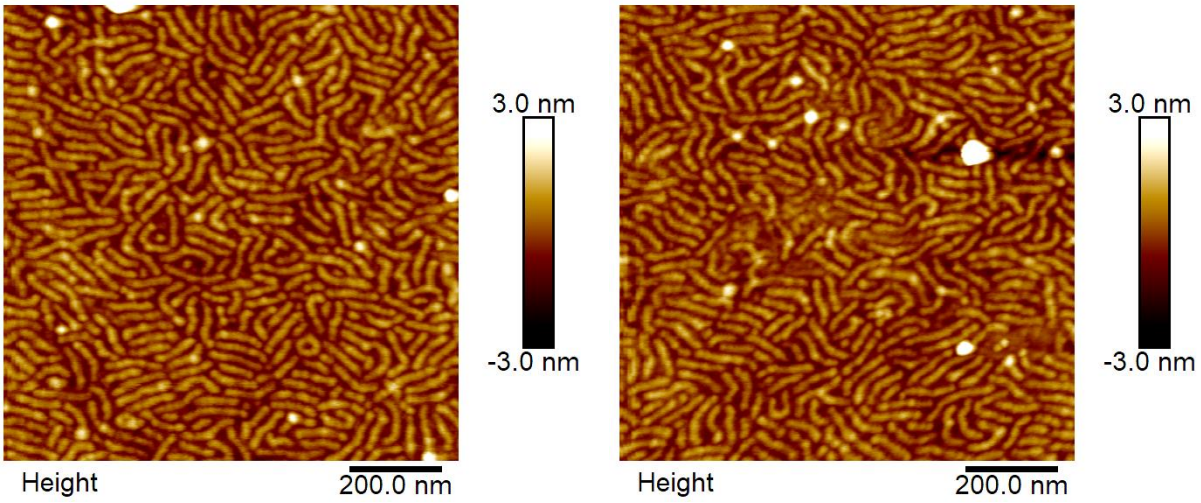

Figure A9. AFM height images of MBB-$B_{0.51}E_{0.49}$. The AFM sample was prepared using a Langmuir-Blodgett trough with a pH of 4.0 for the aqueous subphase. The average length of 287 brush molecules was 99.8 ± 26.9 nm.

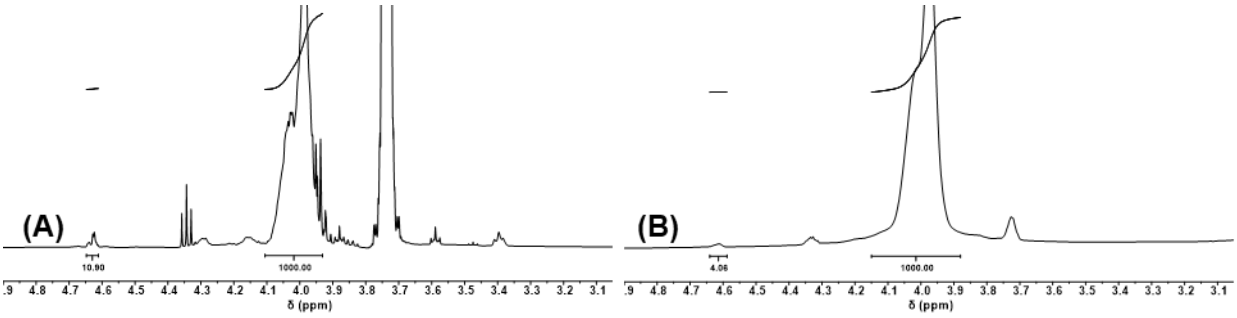

Figure A10. ^{1}H NMR spectra of (A) the initial reaction mixture and (B) the final reaction mixture for the synthesis of MBB-$B_{0.24}E_{0.76}$ for estimating the grafting density of MBB-$B_{0.24}E_{0.76}$. The initial feed molar ratio of the alkyne-end-functionalized side chains to the azide groups is 1.38. Therefore, the grafting density is estimated to be $1.38 \times [1 - (4.06/10.9)] = 86.7\%$.

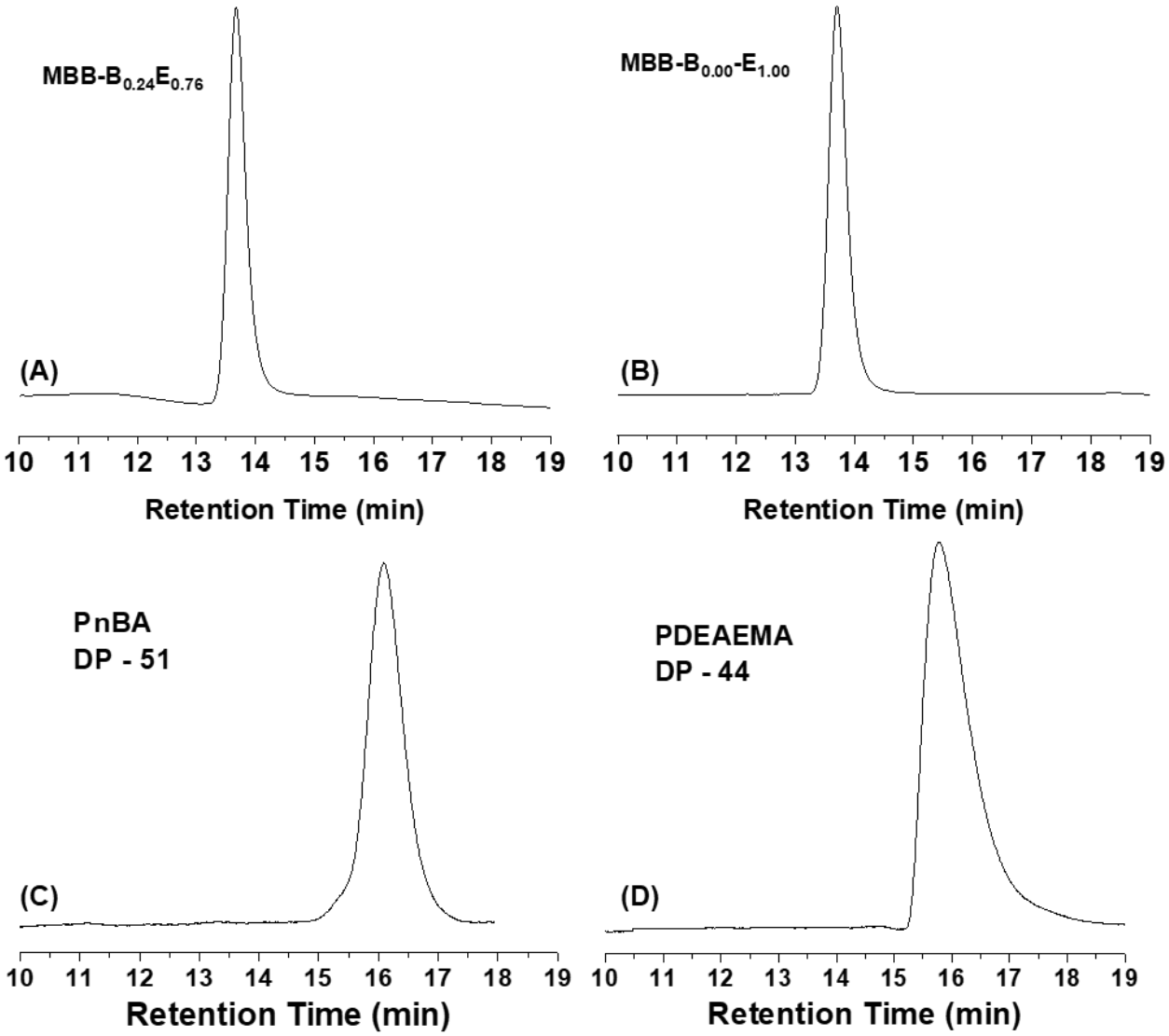

Figure A11. SEC analysis of (A) a mixture of MBB-$B_{0.24}E_{0.76}$ (3 mg) and a 100 kDa PMMA standard (3 mg) dissolved in THF (2 mL), (B) a mixture of MBB-$B_{0.00}E_{1.00}$ (3 mg) and a 100 kDa PMMA standard (3 mg) dissolved in THF (2 mL), (C) alkyne end-functionalized side chain polymer P*n*BA, and (D) alkyne end-functionalized side chain polymer PDEAEMA using the THF GPC system. MBB-$B_{0.24}E_{0.76}$ and MBB-$B_{0.00}E_{1.00}$ cannot be eluted out from our THF GPC system, but P*n*BA and PDEAEMA can be analyzed by this GPC system. To confirm the removal of unreacted side chain polymers, a 100 kDa PMMA standard was added into the purified brush polymer with similar amounts. As can be seen from (A) and (B), the PMMA standard can be seen but not any side chain polymers, proving that they were completely removed.

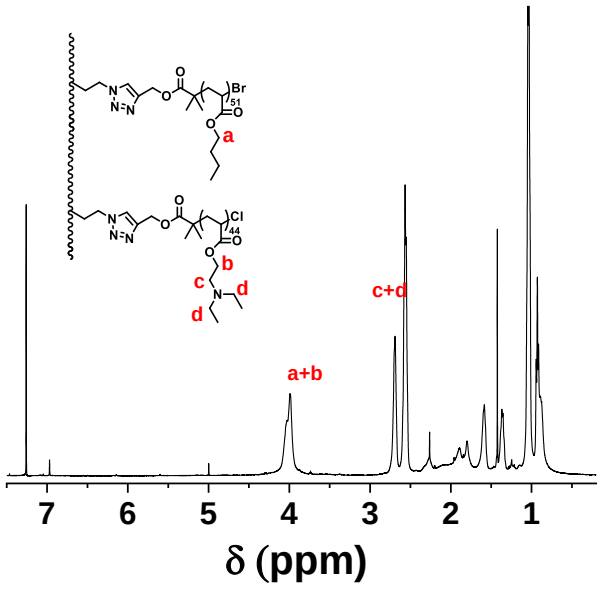

Figure A12. ^{1}H NMR spectrum of the purified MBB-$B_{0.24}E_{0.76}$ in $CDCl_3$.

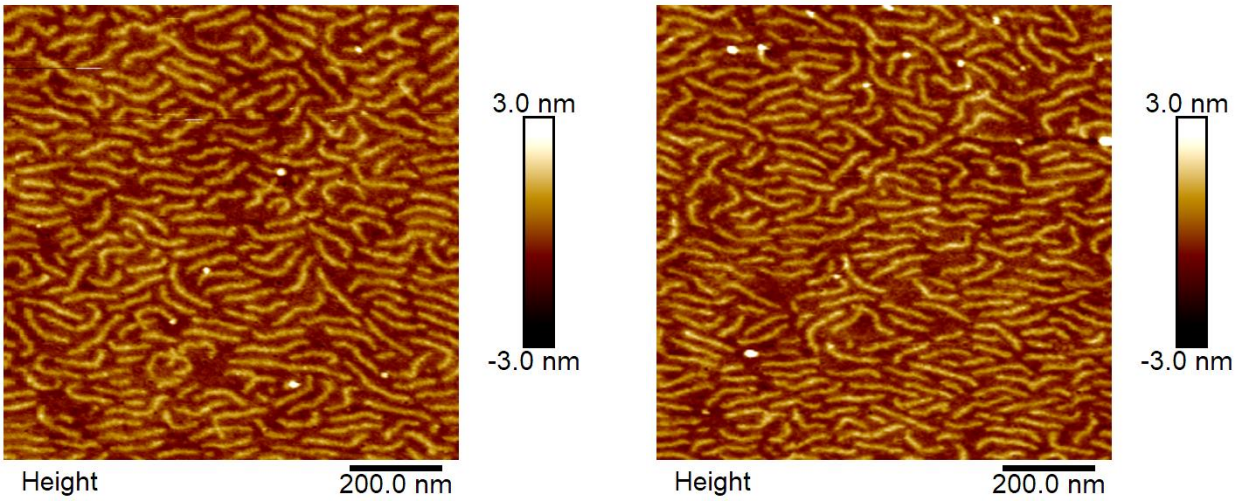

Figure A13. AFM height images of MBB-$B_{0.24}E_{0.76}$. The AFM sample was prepared using a Langmuir-Blodgett trough with a pH of 4.0 for the aqueous subphase. The average length of 234 measured brush molecules was 99.2 ± 30.2 nm.

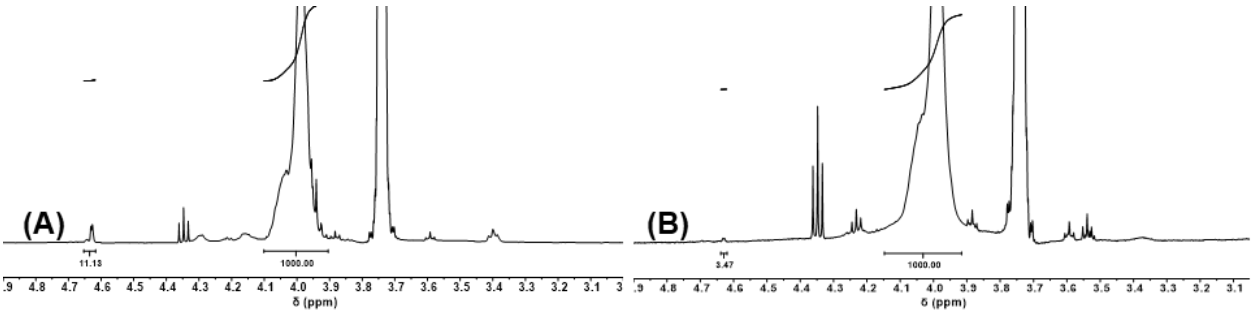

Figure A14. ^{1}H NMR spectra of (A) the initial reaction mixture and (B) the final reaction mixture for the synthesis of MBB-$B_{0.00}E_{1.00}$ for estimating the grafting density of MBB-$B_{0.00}E_{1.00}$. The initial feed molar ratio of the alkyne-end-functionalized side chains to the azide groups is 1.29. Therefore, the grafting density is estimated to be 1.29 × [1 – (3.47/11.13)] = 88.8%.

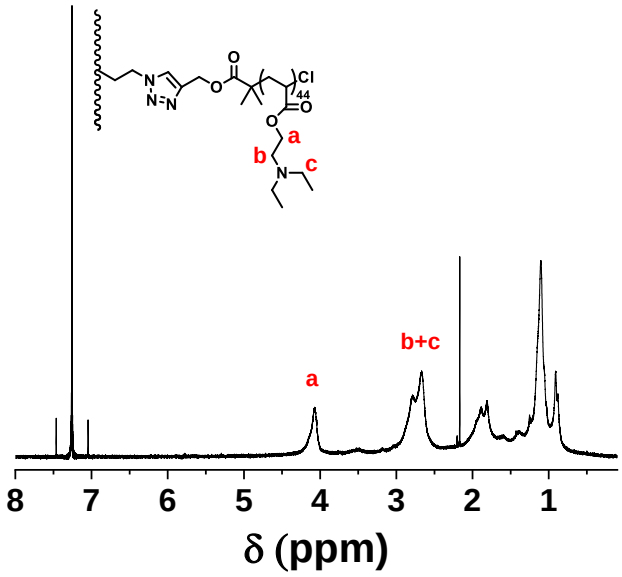

Figure A15. ^{1}H NMR spectrum of the purified homografted molecular bottlebrushes MBB-$B_{0.00}E_{1.00}$ in $CDCl_3$.

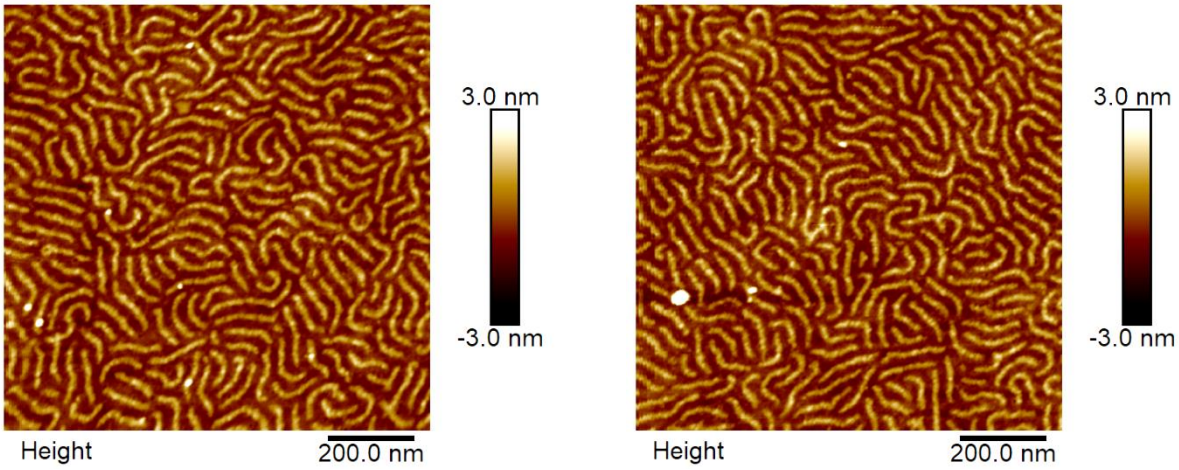

Figure A16. AFM height images of MBB-$B_{0.00}E_{1.00}$. The AFM sample was prepared using a Langmuir-Blodgett trough with a pH of 10.0 for the aqueous subphase. The average length of 211 measured brush molecules was 109.2 ± 26.5 nm.

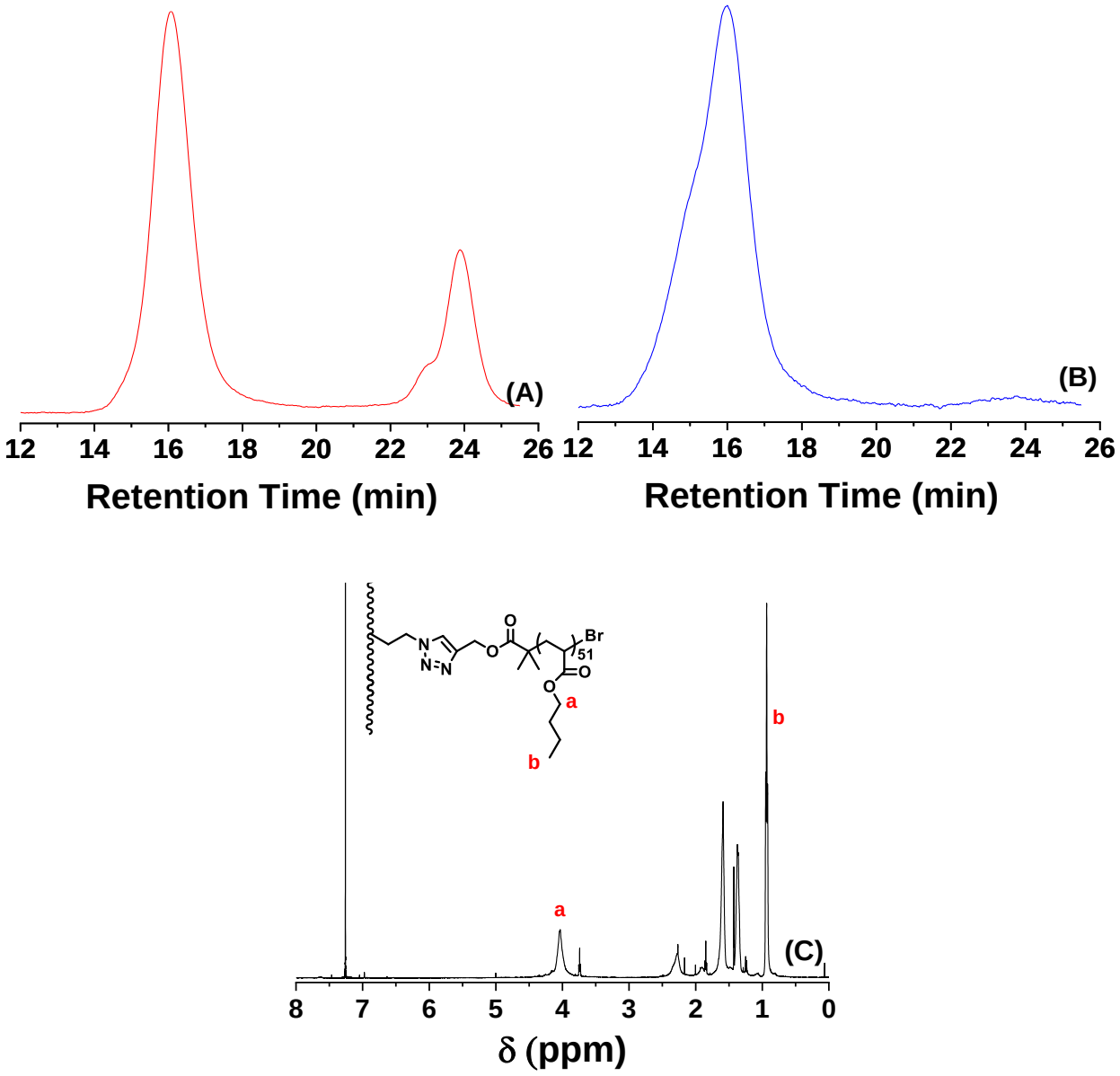

Figure A17. SEC traces of (A) the final reaction mixture for the synthesis of homografted P*n*BA molecular bottlebrushes MBB-$B_{1.00}E_{0.00}$ and (B) after removal of residual side chain polymers, and (C) ^{1}H NMR spectrum of the purified MBB-$B_{1.00}E_{0.00}$ in $CDCl_3$.

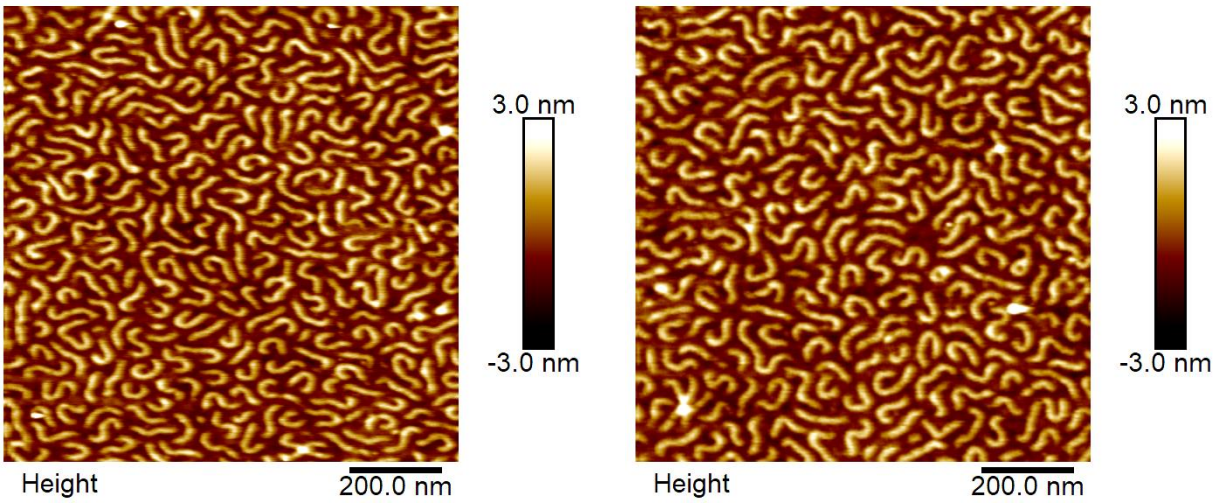

Figure A18. AFM height images of homografted P*n*BA molecular bottlebrushes MBB-$B_{1.00}E_{0.00}$. The AFM sample was prepared using a Langmuir-Blodgett trough using Milli-Q water as the subphase. The average length of 251 measured brush molecules was 100.1 ± 23.6 nm.

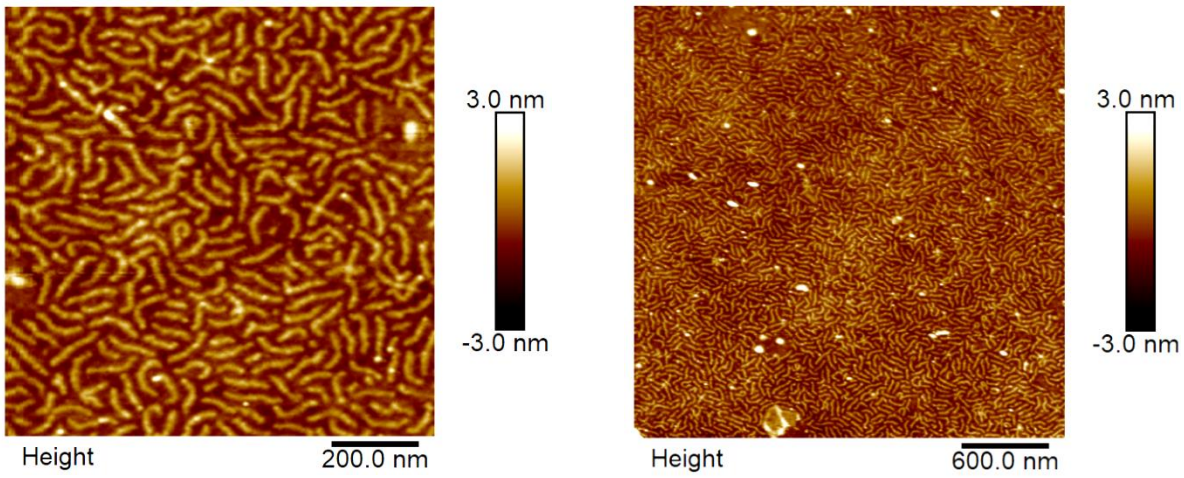

Figure A19. Additional AFM height images of the brush polymer MBB-$B_{0.51}E_{0.49}$ on a glass disc from the water-in-toluene emulsion at pH = 4.00 formed in the second cycle with 0.02 wt% of MBB-$B_{0.51}E_{0.49}$ as stabilizer. The AFM sample was prepared by depositing 25 µL of the emulsion layer onto the surface of the subphase of 1.0 mM phosphate buffer with pH of 4.0 in a Langmuir-Blodgett trough. After 20 min, the barriers were compressed at a rate of 10 mm/min until a surface pressure of 0.5 mN/m was reached. Once the pressure stabilized the monolayer was transferred on a glass coverslip at a rate of 2 mm/min.

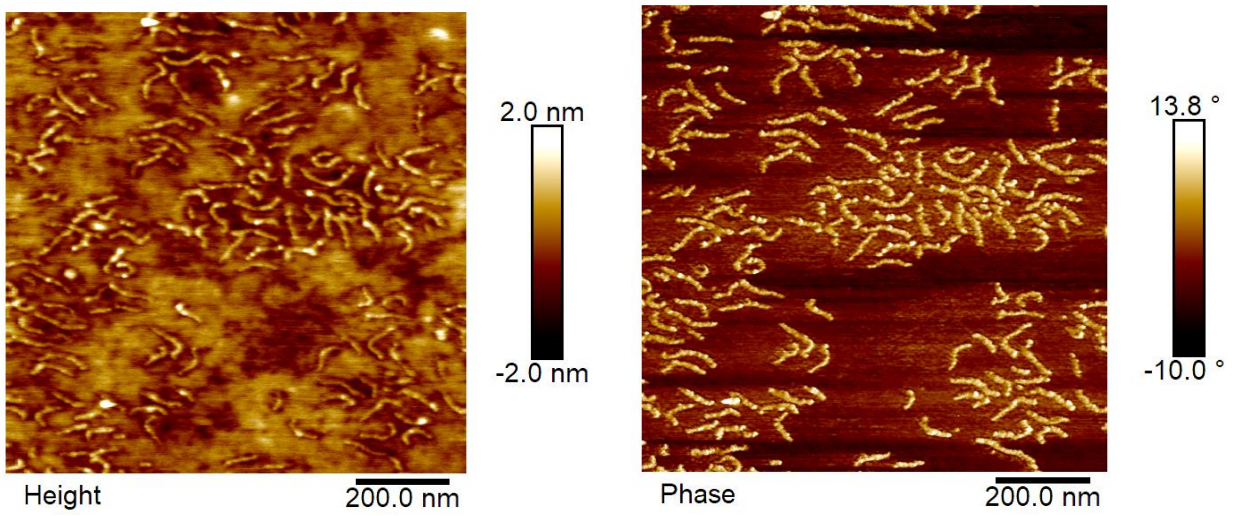

Figure A20. Additional AFM height images of the brush polymer MBB-$B_{0.51}E_{0.49}$ on a glass disc from the water-in-toluene emulsion at pH = 4.00 formed in the tenth cycle with 0.02 wt% of MBB-$B_{0.51}E_{0.49}$ as stabilizer. The AFM sample was prepared by depositing 25 μL of the emulsion layer onto the surface of the subphase of 1.0 mM phosphate buffer with pH of 4.0 in a Langmuir-Blodgett trough. After 20 min, the barriers were compressed at a rate of 10 mm/min until a surface pressure of 0.5 mN/m was reached. Once the pressure stabilized the monolayer was transferred on a glass coverslip at a rate of 5 mm/min as described in the experimental section.

Chapter 3. Effects of Side Chain Composition and pH on Reduction of Toluene-Water Interfacial Tension by Amphiphilic pH-Responsive Binary Heterografted Bottlebrush Polymers

Abstract

This Chapter presents a systematic study on the effects of side chain composition and solution pH on reduction of toluene-water interfacial tension (γ) by four heterografted poly(*n*-butyl acrylate) (P*n*BA)/poly(2-(*N*,*N*-diethylamino)ethyl methacrylate) (PDEAEMA) brush polymers and two corresponding homografted brushes. The interfacial tensions between toluene and aqueous solutions were measured as a function of time by injecting a toluene droplet, containing a 0.2 mg/g brush polymer, into the aqueous solution with a pH of 4.0 or 10.0 using pendant drop tensiometry. The γ for toluene and pure water is 35 mN/m. At pH = 4.0, the lowest value of γ was observed to decrease to ≤ 5.0 mN/m when the molar fraction of PDEAEMA ($\chi_{PDEAEMA}$) in the side chains of heterografted MBBs was ≥ 0.36, which was attributed to the protonation of PDEAEMA side chains increasing the amphiphilicity of the MBBs and improving their packing at the interface. At pH = 10.0, γ was found to decrease to similar values, in the range of 12.8 to 14.1 mN/m, when $\chi_{PDEAEMA}$ was ≥ 0.36. Although MBBs with $\chi_{PDEAEMA}$ ≥ 0.76 at pH 4.0 and all PDEAEMA-containing brush polymers at pH = 10.0 showed significant interfacial tension reductions, they had no ability to stabilize water-toluene emulsions because their bonding to the interface was weak, which was confirmed by the jamming test experiments. When the toluene droplet was withdrawn from the acidic aqueous solution or the emulsion droplets were allowed for solvent evaporation to reduce the interfacial area, wrinkled interfaces were only observed for the brush polymers containing 20%, 36%, and 49% PDEAEMA in the side chains, indicating the strong adsorption of these three MBBs to the interface at pH 4.0, which correlated well with their abilities to stabilize water-toluene emulsions. This study showed that for amphiphilic bicomponent brush polymers to function as effective emulsion stabilizers, it is critical that the brush molecules strongly adsorb to the interface.

3.1. Introduction

Molecular bottlebrush (MBB) polymers heterografted with hydrophilic and hydrophobic polymeric side chains exhibit amphiphilicity and can be used as emulsifiers for generation and stabilization of emulsions.[1-11] Compared with small molecule surfactants and linear flexible amphiphilic diblock copolymers, the stiffening of the backbone and the large molecular size impart particle-like characteristics to the amphiphilic brush polymers, which could result in higher effectiveness and higher efficiencies of MBBs as emulsion stabilizers. In addition, there is greater flexibility in the design of MBBs, and one can tune various molecular parameters of MBBs, including backbone and side chain lengths, grafting density, molar ratio and distributions of hydrophilic and hydrophobic side chains, to achieve optimal performances.[4-11]

The use of amphiphilic MBBs as emulsion stabilizers has been reported in the literature. In general, researchers found that MBB-stabilized emulsions exhibited enhanced stability, and the brush polymers were efficient in emulsifying mixtures of water and organic liquids even at rather low concentrations.[8-14] An early example was reported by Cheng et al.; they prepared polynorbornene-based bottlebrush polymers with a combination of polyethylene oxide (PEO) and poly(lactic acid) grafts on each repeat unit.[7] The brush molecules had little tendency to undergo intermolecular self-assembly and showed an excellent ability as surfactants for the generation of miniemulsions. Matyjaszewski et. al synthesized a series of heterografted MBBs with a combination of PEO and poly(*n*-butyl acrylate) (P*n*BA) grafts.[9] They studied the effects of several architectural parameters of MBBs in their ability to stabilize water-in-oil type emulsions and found that MBBs were able to stabilize emulsions at concentrations as low as 0.005 wt%. Pendant drop experiments showed that the interfacial tension between water and xylene was lowered from 37.2 mN/m to ~ 20 – 25 mN/m and ~ 12 – 20 mN/m with the addition of 0.01 wt% and 0.1 wt% of their

PEO/P*n*BA brush polymers, respectively. However, the interfacial tension lowering did not precisely correlate with the emulsifying efficiency of different MBBs.

By exploiting the electrostatic interactions between water-soluble poly(acrylic acid) MBBs and toluene-soluble amine-functionalized polyhedral oligomeric silsesquioxane (POSS-NH_2) at the water-toluene interface, Shi et al. reported the formation of various types of stable emulsions in a one-step process and the jamming of molecular assemblies at the interface.[12] The interfacial assemblies exhibited "solid-like" characteristics as evidenced by the wrinkling of the interface when the interfacial area of the droplet in a pendant drop experiment was reduced to compress the interfacial assembly. This property was utilized for printing 3D liquid structures. A subsequent study found a similar phenomenon when the same system was applied to the *N*,*N*-dimethylformamide-octane interface, and stable oil-in-oil type emulsions could be formed.[13] Seong et al. recently reported a systematic study of amphiphilic bottlebrush polymers with a combination of PEO and poly(dimethylsiloxane) (PDMS) grafts at the water-toluene interfaces by pendant drop tensiometry.[14] The time-dependence of the dynamic interfacial tension between water and toluene suggested that amphiphilic PEO/PDMS bottlebrush molecules adsorbed onto the interface to reduce the interfacial tension via three distinct steps: induction, reconfiguration/adsorption, and reorganization when the polymer concentration was low.

In Chapter 2, we showed that amphiphilic heterografted P*n*BA/poly(2-(*N*,*N*-diethylamino)ethyl methacrylate) (PDEAEMA) MBBs with appropriate side chain compositions were efficient and pH-responsive emulsifiers for the mixtures of toluene and a 1.0 mM aqueous phosphate buffer solution with a pH of 4.0. Stable emulsions were readily formed by vortexing even with the use of 0.005 wt% MBBs. When a brush polymer with a symmetric side chain composition was employed at concentrations of 0.01 wt% and above, the formation and breaking

of emulsions can be repeated for at least 10 times by changing the pH between 4.0 and 10.0 back and forth. At pH = 4.0, the PDEAEMA side chains were protonated and only soluble in the acidic aqueous solution, while P*n*BA is only soluble in toluene, and thus our MBBs spontaneously reconfigured into a genuine Janus structure. This contrasts with the previously reported amphiphilic brush polymers with PEO side chains,[8,9,14] where we believe PEO is actually distributed into water and toluene on both sides of the water-organic interface, although all schematic illustrations showed a Janus structure. The large molecular size with hundreds of side chains per brush molecule and the Janus structure of our amphiphilic MBBs with certain side chain compositions result in strong adsorption at the interface. At pH = 10.0, the brushes are deprotonated and retreat to the toluene phase, and emulsion droplets coalesce, causing the emulsion to break.

The adsorption of our MBBs at pH = 4.0 at the interface and the desorption at pH = 10.0 would cause changes in interfacial tension (γ). To better understand the behavior of our brush polymers at the interface between toluene and water, we conducted two types of pendant drop experiments: (i) time-dependence of dynamic interfacial tension through the droplet shape analysis and (ii) withdrawing of pendant drops to examine if MBBs are jammed at the interface. All six brush polymers described in Chapter 2, MBB-$B_{1.00}E_{0.00}$, and MBB-$B_{0.80}E_{0.20}$, MBB-$B_{0.64}E_{0.36}$, MBB-$B_{0.51}E_{0.49}$, MBB-$B_{0.24}E_{0.76}$, and MBB-$B_{0.00}E_{1.00}$, were studied at both pH values of 4.0 and 10.0.

3.2. Experimental Section

3.2.1. Materials

Toluene (Certified ACS) was purchased from Fisher Scientific and used as received. Milli-Q water was obtained from a Millipore Milli-Q lab water system. The synthesis, purification, and

characterization of six brush polymers, MBB-$B_{1.00}E_{0.00}$, and MBB-$B_{0.80}E_{0.20}$, MBB-$B_{0.64}E_{0.36}$, MBB-$B_{0.51}E_{0.49}$, MBB-$B_{0.24}E_{0.76}$, and MBB-$B_{0.00}E_{1.00}$, used in this work are detailed in Chapter 2. Aqueous solutions with pH values of 4.00 and 10.00 were prepared using Milli-Q water with 0.1 M HCl and 0.1 M NaOH solutions, and the pH values were confirmed using an Accumet AB150 pH meter (Fisherbrand). Toluene solutions of molecular brushes were prepared by transferring a known amount of a brush polymer from a toluene stock solution to a vial and diluting it with toluene to the desired concentration.

3.2.2. Toluene-Water Interfacial Tension Measurements by Pendant Drop Tensiometry

Interfacial tension measurements were performed using an OCA 15plus (DataPhysics) by pendant drop tensiometry. Stock solutions of each brush polymer in toluene were prepared at desired concentrations. The measurements were conducted by introducing a toluene droplet containing MBBs (7 µL, dispensed at a rate of 2 mm/min) from a glass syringe into a large glass cuvette containing 10 mL of a pH 4.00 or 10.00 aqueous solution. A J-shape needle was used so that the droplet was suspended upwards towards the surface of the water. Prior to beginning each measurement, the glass syringe, needle, and cuvette were thoroughly rinsed with toluene, isopropanol, and acetone and then dried by a nitrogen stream to avoid contamination. Interfacial tensions were calculated using SCA 20 software by analyzing the contour of a pendant drop over time. Multiple measurements were recorded for each condition to ensure that the interfacial tension values were reliable and reproducible. The interfacial assembly of brush molecules was assessed by withdrawing pendant drops and recording the change in the droplet morphology.

3.2.3. Optical Micrographs of Emulsion Drops

The morphology of emulsion droplets was studied using an Olympus BX51 optical microscope equipped with a digital camera (Amscope). Emulsion droplets were transferred to a clean glass

microscope slide with a small amount of toluene using a mechanical pipette. Images and videos were acquired to study the initial droplet morphology and the effect of solvent evaporation on droplet morphology. The preparation of MBB-$B_{0.51}E_{0.49}$- and sodium dodecyl sulfate (SDS)-stabilized emulsions was similar, and the following shows the process for the brush polymer. To a 1-dram vial, 1.00 g of a 1.0 mM aqueous phosphate buffer with a pH of 4.0 was added, and a certain amount of a 0.1 M HCl solution was added to the vial to account for protonation of PDEAEMA side chains based on the control experiment as described in Chapter 2. The brush polymer MBB-$B_{0.51}E_{0.49}$ was then added from the toluene stock solution, and additional toluene was injected to have a total of 1.00 g of toluene. The concentration of the brush polymer was 0.3 wt% considering the mass of both phases. The emulsion was generated by using a vortex mixer (Fisherbrand Analog Vortex Mixer, max 3200 rpm) at a setting of 8 out of 10 for a total of 60 s, performed in two 30 s intervals within 10 min. The pH of the MBB emulsion was then adjusted by adding a calculated amount of a 0.1 M NaOH solution and gently shaking the vial for 10 sec.

3.3. Results and Discussion

3.3.1. Interfacial Tensions Between Toluene Solutions of MBBs and Aqueous Solutions with pH of 4.0 and 10.0 Measured by Pendant Drop Tensiometry

Pendant drop tensiometry was used to evaluate the interfacial activities of heterografted P*n*BA/PDEAEMA MBBs along with two homografted analogues at toluene-aqueous interfaces with pH values of 4.0 and 10.0 for the aqueous solutions. A toluene droplet containing 0.2 mg/g MBBs with volume of 7 μL was injected into an aqueous phase with a pH value of either 4.0 or 10.0, and the interfacial tension (γ), determined through drop shape analysis by computer, was monitored as a function of time. For reference, γ for the pure water-toluene interface is 35 mN/m.[14]

Figure 3.1 shows the time-dependences of γ for all six brush polymers at pH values of 4.0 (Figure 3.1A) and 10.0 (Figure 3.1B) for the aqueous solutions. The homografted P*n*BA bottlebrushes, MBB-$B_{1.00}E_{0.00}$, showed minimal interfacial tension reductions at both pH values as expected, and γ leveled off to 27.2 mN/m for pH = 4.0 and 25.5 mN/m for pH = 10.0. This means that even if P*n*BA was insoluble in water, the brush molecules still exhibited a small affinity to the water-toluene interface, which in some sense similar to the behavior of particles. However, this affinity is not sufficient for forming stable emulsions as noted in Chapter 2.

Compared with MBB-$B_{1.00}E_{0.00}$, all heterografted P*n*BA/PDEAEMA MBBs and the homografted PDEAEMA brushes exhibited larger interfacial tension reductions at both acidic and basic pH values, which appeared to occur in two stages: an initial rapid decrease stage and a subsequent slow change stage (Figure 3.1). At pH = 4.0, the extent of the initial decrease for MBBs appeared to be directly related to and increased with the mole fraction of PDEAEMA ($\chi_{PDEAEMA}$) in the side chains. For example, MBB-$B_{0.00}E_{1.00}$ and MBB-$B_{0.24}E_{0.76}$ showed large decreases in γ within 20 s, at which point γ reached ~ 15 mN/m, while in that same time frame γ only decreased to ~ 26 mN/m for MBB-$B_{0.80}E_{0.20}$. The initial fast decrease likely reflected the initial attachment of brush molecules from the toluene phase to the liquid/liquid interface, indicating that more PDEAEMA side chains made the attachment of brush molecules to the interface easier. After the initial fast decrease, the homografted PDEAEMA brushes quickly reached a quasi-equilibrium interfacial tension (γ_s) at ~ 9.5 mN/m, which remained relatively constant over the course of 20 min. Such a large interfacial tension reduction by MBB-$B_{0.00}E_{1.00}$ was unexpected because the fully protonated PDEAEMA brushes were soluble in water, and we reported in Chapter 2 that this brush polymer could not stabilize water-toluene emulsions at both pH = 4.0 and 10.0. It is possible that this observation is a transient state of MBB-$B_{0.00}E_{1.00}$ moving across the interface from the toluene

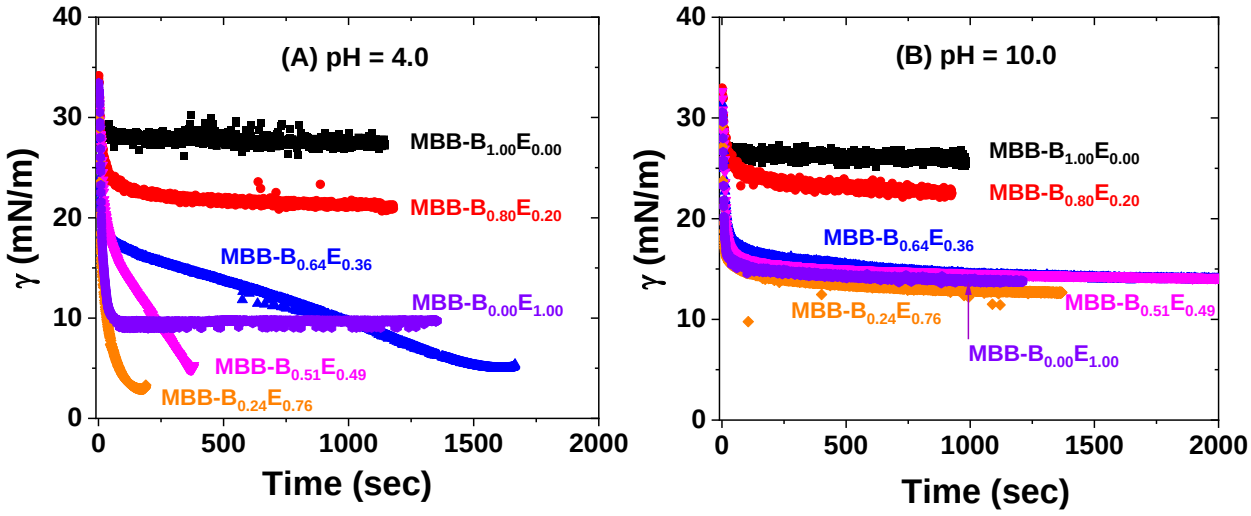

Figure 3.1. Time dependence of interfacial tension a toluene solution of a brush polymer with a concentration of 0.2 mg/g and an aqueous solution with a pH value of 4.0 (A) and 10.0 (B) measured by pendant drop tensiometry for six brush polymers (MBB-$B_{1.00}E_{0.00}$, and MBB-$B_{0.80}E_{0.20}$, MBB-$B_{0.64}E_{0.36}$, MBB-$B_{0.51}E_{0.49}$, MBB-$B_{0.24}E_{0.76}$, and MBB-$B_{0.00}E_{1.00}$). A 7 μL drop of a 0.2 mg/g solution of a brush polymer toluene was injected into the aqueous solution (10 mL).

phase to the aqueous phase. Once the brushes "bump" into the interface, the tertiary amine groups of PDEAEMA become protonated; given the length of the brush molecules (~ 100 nm), the protonation would be not be finished instantaneously, and the interface would be packed with many partially protonated brush molecules. However, because there are no hydrophobic P*n*BA side chains present to permanently anchor the brush polymer at the interface. Once the protonation is complete, it is very likely that the bottlebrushes would detach from the interface to the acidic aqueous phase, and the next brush molecule would start the process. If given enough time, it may be possible to see a gradual increase in γ as the brush molecules in the toluene droplet are exhausted.

Figure 3.1A also shows that the four heterografted brush polymers behaved very differently after the initial fast drop. For MBB-$B_{0.80}E_{0.20}$, γ leveled off quickly and reached a γ_s value of ~ 21 mN/m after 20 min. The overall interfacial tension reduction was not very large, which was not unreasonable given that the polymer contained only 20 mol% of PDEAEMA in the side chains. This can be attributed to the somewhat weak overall driving forces for MBBs toward the acidic phase due to the relative abundance of P*n*BA side chains. The other three brush polymers, MBB-$B_{0.24}E_{0.76}$, MBB-$B_{0.51}E_{0.49}$, MBB-$B_{0.64}E_{0.36}$, never reached a clear quasi equilibrium. Instead, γ continued to decrease until the approximate experimental limit of ~ 5 mN/m was reached, at which the point the pendant drops were observed to pinch off spontaneously from the needle tip. The slight upward turn at the end of each curve for these three heterografted brush polymers reflects the "pinch-off" of the droplet. The rate of decrease in the second stage increased with increasing $\chi_{PDEAEMA}$ in the side chains of the brushes as can be seen from the slope magnitudes. The lowest γ value observed decreased with the increase in $\chi_{PDEAEMA}$ in the side chains, from 21.0 mN/m for MBB-$B_{0.80}E_{0.20}$, to 5.0 mN/m for MBB-$B_{0.64}E_{0.36}$, 4.9 mN/m for MBB-$B_{0.51}E_{0.49}$, and 2.9 mN/m

for MBB-$B_{0.24}E_{0.76}$, and the times to reach the minimum γ value for the latter three MBBs were about 3, 6, and 25 min, respectively. Note that despite the largest interfacial reductions observed for MBB-$B_{0.24}E_{0.76}$, this brush polymer could not form stable emulsions at pH = 4.0. Similarly, MBB-$B_{0.00}E_{1.00}$ showed a large decrease in γ at pH = 4.0 but also could not stabilize the emulsion at this pH value. On the other hand, MBB-$B_{0.80}E_{0.20}$ only decreased the interfacial tension to 21.0 mN/m, but it showed an ability to emulsify the mixture of toluene and the acidic aqueous solution. Thus, reducing the interfacial tension is a necessary condition for the formation of stable emulsions but not a sufficient condition.

At pH = 10.0, the time-dependence of γ for MBB-$B_{0.80}E_{0.20}$ was similar to that at pH = 4.0 and γ_s was found to be 22.5 mN/m (Figure 3.1B), which was only slightly higher than that at pH 4.0 (γ_s = 21.0 mN/m). For other three heterografted MBBs, γ decreased very slowly after the initial rapid reduction, unlike the observations at pH = 4.0 shown in Figure 3.1A. The homografted PDEAEMA brushes behaved similarly. These four brush polymers reduced the toluene-water interfacial free energy to similar values, in the range of 12.8 to 14.1 mN/m. Considering the interfacial tension of 35 mN/m for pure water and toluene, the interfacial tension reductions observed here were quite large; however, all of these MBBs could not generate stable emulsions as described in Chapter 2. An interfacial tension decrease is not sufficient to produce stable emulsions for our MBBs to act as emulsifiers. Note that even if the PDEAEMA homografted brush polymer was not soluble in the basic aqueous solution with a pH of 10.0, it exhibited a quite high interfacial activity, significantly higher than that of MBB-$B_{1.00}E_{0.00}$.

The lowest interfacial tensions (γ_{lowest}) of each brush polymer at both pH 4.0 and 10.0 were plotted against the mole fraction of PDEAEMA in the side chains as shown in Figure 3.2. While

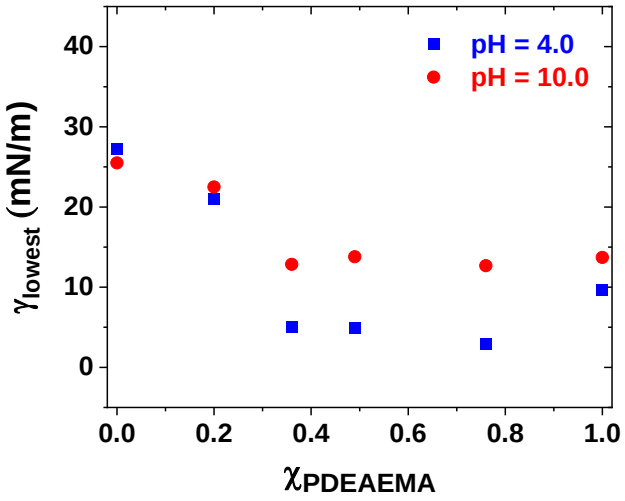

Figure 3.2. Plot of the lowest interfacial tension, obtained from Figure 3.1, versus the mole fraction of PDEAEMA in the side chains of MBBs.

the difference in the observed lowest γ values between 4.0 and 10.0 for MBB-$B_{1.00}E_{0.00}$ and MBB-$B_{0.80}E_{0.20}$ were quite small (< 2 mN/m), the changes for MBB-$B_{0.64}E_{0.36}$, MBB-$B_{0.51}E_{0.49}$, and MBB-$B_{0.24}E_{0.76}$ were large (~ 8 – 10 mN/m). On the other hand, the interface tension increased by ~ 4 mN/m for the homografted PDEAEMA bottlebrushes. Recall in Chapter 2 that only three out of these six brush polymers, MBB-$B_{0.80}E_{0.20}$, MBB-$B_{0.64}E_{0.36}$, and MBB-$B_{0.51}E_{0.49}$, can act as pH-responsive emulsion stabilizers. At pH 4.0, they produced stable emulsions, and when the pH was adjusted to pH 10.0, the emulsions were broken. The small difference in γ between the two pH values for MBB-$B_{0.80}E_{0.20}$ is puzzling, probably because the measurement time was short (~ 20 min) while the breaking of emulsions in Chapter 2 was performed under the stirring conditions.

3.3.2. Assembly Dynamics of MBBs at the Interfaces Between Toluene and Aqueous Solutions with pH of 4.0 and 10.0

Besides the interfacial tension reduction, we were also interested in how the PDEAEMA-containing brush polymers were adsorbed to the interface between toluene and the aqueous solution with pH values of 4.0 and 10.0. To gain further insight into the assembly dynamics of the PDEAEMA-containing MBBs, we plotted the data from Figure 3.1 as a semi-log form (linear γ vs. log time) as shown in Figure 3.3. Previously, Russell et al. showed that the assembly of amphiphilic polynorbornene-based brush polymers with PEO and polydimethylsiloxane at the water-toluene interface consisted of three steps: diffusion to the interface, reconfiguration/adsorption, and reorganization when the polymer concentration was low.[14] Figure 3.1 shows that at a concentration of 0.2 mg/g, all PDEAEMA-containing brush polymers exhibited an almost immediate decrease from the reported interfacial tension of a pure water-toluene interface at both pH values of 4.0 and 10.0. From the semi-log plots in Figure 3.3, we observed a short, nearly flat region for each brush polymer that lasted for a few seconds before γ decreased

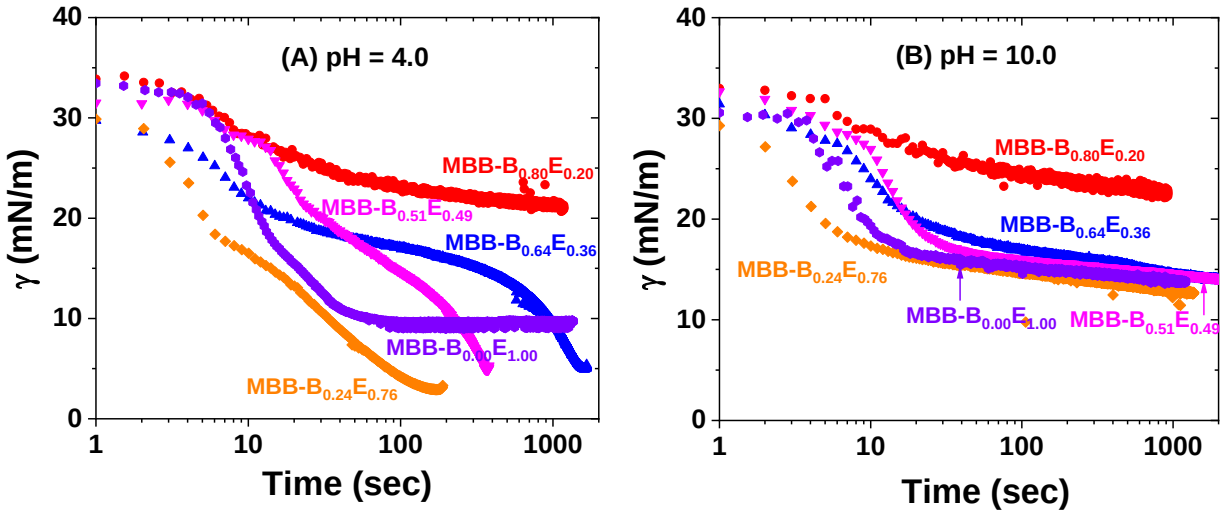

Figure 3.3. Interfacial tension between a toluene solution of a brush polymer with a concentration of 0.2 mg/g and an aqueous solution with a pH value of 4.0 (A) and 10.0 (B) versus time (log) for six brush polymers.

quickly, which could be attributed to the diffusion of brush molecules to the interface. The following fast drop of the interfacial tension is believed to be caused by the absorption of the brush molecules to the interface and the reconfiguration of their conformations into a Janus arrangement. For MBB-$B_{0.80}E_{0.20}$ at pH = 4.0 and all five brush polymers at pH = 10.0, the rapid decrease in γ was followed by a slower continuous reduction of γ in an almost linear fashion with time on a logarithmic scale. This was the reorganization of brush molecules at the water-toluene interface to achieve more close-packing and to minimize the uncovered water-toluene interfacial area; the relaxation times seemed to be very large.

At pH = 4.0, for MBB-$B_{0.00}E_{1.00}$, after the rapid drop region, there was a slower decrease region between 15 seconds and 40 seconds, which appeared to be an exponential decay and likely is associated with the relaxation of the brushes to achieve better packing at the interface. Afterwards, γ was very stable, and there seemed to be little changes. The time scale for the reorganization of MBB-$B_{0.24}E_{0.76}$ at the interface seemed to be similar to that for MBB-$B_{0.00}E_{1.00}$ (Figure 3.3A). For MBB-$B_{0.64}E_{0.36}$ and MBB-$B_{0.51}E_{0.49}$ at pH = 4.0, the reorganization occurred at a larger time scale, several hundreds to 1000 seconds for the former and ~ 100 to 300 seconds for the latter. There seemed to be a trend that the reorganization of the brush molecules at the interface became faster with increasing the molar content of PDEAEMA in the side chains. Note that MBB-$B_{0.51}E_{0.49}$ showed an additional step at around 10 seconds at both pH values of 4.0 and 10.0. We were unsure what was happening and could not provide an explanation for this observation. Note that we repeated the measurements for all five PDEAEMA-containing brush polymers at both pH values, and the data included in Appendix B showed that they were reproducible.

3.3.3. Jamming Test Experiments by Reducing Interfacial Area of Droplets

We further studied the interfacial bonding of MBBs at the toluene-aqueous solution interfaces at pH = 4.0 and 10.0 by withdrawing of the pendant drop containing a brush polymer at a concentration of 0.2 mg/g to reduce the volumes and by solvent evaporation to decrease the interfacial area to examine if the brush molecules would be jammed at the interface. These experiments are analogous to lateral compression of MBBs at the interface. Russell et al. previously reported that the interface became wrinkled when the particles were jammed at the interface, evidencing the strong interfacial adsorption. In Chapter 2, when studying the morphology of emulsion droplets, we accidentally noticed the interfacial wrinkling of emulsion droplets when the solvents were evaporating. As mentioned in the last section, for MBB-$B_{0.64}E_{0.36}$, MBB-$B_{0.51}E_{0.49}$, and MBB-$B_{0.24}E_{0.76}$, the toluene droplet spontaneous pinched off from the tip of the needle at pH = 4.0 when γ decreased to very low values, e. g., 5 mN/m and below. Therefore, for these polymers, we chose to withdraw the toluene droplet at a bit higher interfacial tension (18 – 23 mN/m) to compress the brush molecules at the interface before γ became too low. Figures 3.4 and 3.5 show the optical images of toluene droplets in the initiate state and at the point where it was about to be withdrawn into the syringe for six brush polymers at pH values of 4.0 and 10.0, respectively. These images were cropped from videos recorded during the pendant drop experiments.

At pH = 4.0, only three brush polymers, MBB-$B_{0.80}E_{0.20}$ (Figure 3.4B), MBB-$B_{0.64}E_{0.36}$ (Figure 3.4C), and MBB-$B_{0.51}E_{0.49}$ (Figure 3.4D), showed a wrinkled interface when the droplet was about to be withdrawn into the syringe, demonstrating that these bottlebrush molecules were strongly bonded to the interface and could not be forced to desorb from it. This is likely because of the Janus arrangement of the two types of side chains on the two sides of the interface, and one side

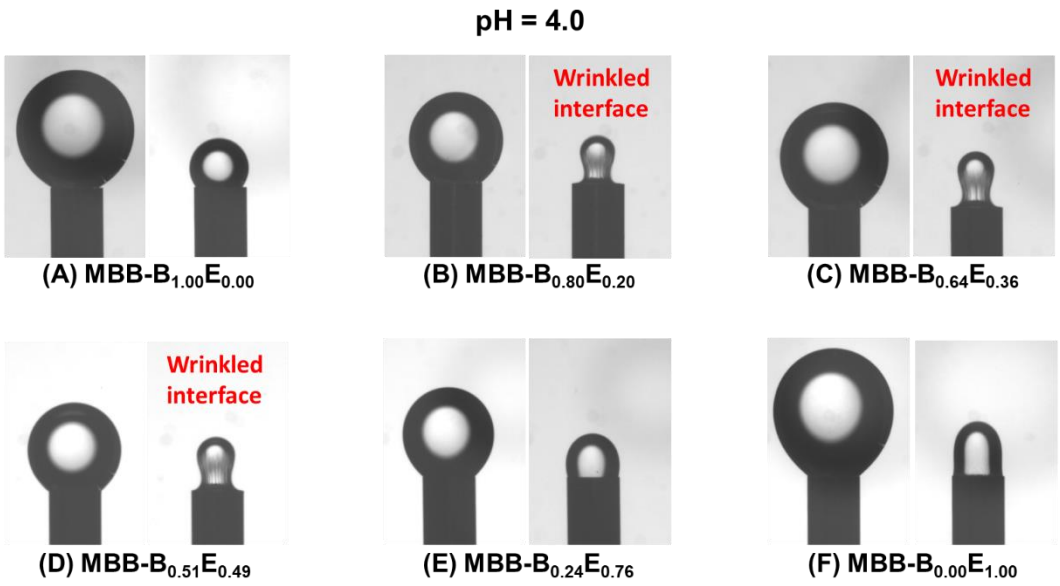

Figure 3.4. Photos of a toluene droplet containing 0.2 mg/g MBBs injected into a pH 4.0 aqueous solution and then gradually withdrawn for MBB-$B_{1.00}E_{0.00}$ (A), MBB-$B_{0.80}E_{0.20}$ (B) (withdrawn at γ = 23 mN/m), MBB-$B_{0.64}E_{0.36}$ (C) (withdrawn at γ = 20 mN/m), MBB-$B_{0.51}E_{0.49}$ (D) (withdrawn at γ = 18 mN/m), MBB-$B_{0.24}E_{0.76}$ (E), and MBB-$B_{0.00}E_{1.00}$ (F). For each sample, the left photo shows the initial state and the right photo shows the droplet before being fully withdrawn into the syringe.

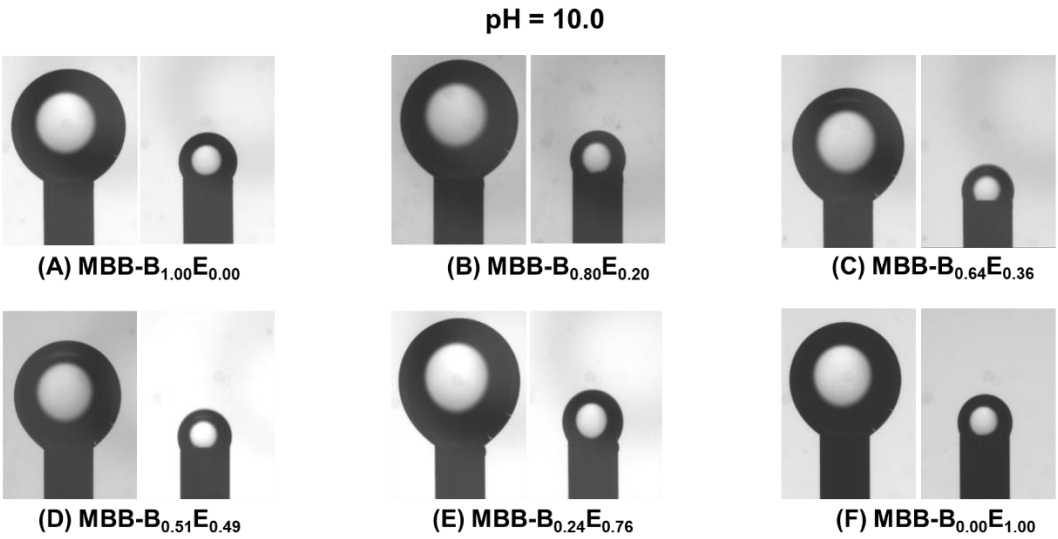

Figure 3.5. Photos of a toluene droplet containing 0.2 mg/g MBBs injected into a pH 10.0 aqueous solution and then gradually withdrawn for MBB-$B_{1.00}E_{0.00}$ (A), MBB-$B_{0.80}E_{0.20}$ (B), MBB-$B_{0.64}E_{0.36}$ (C), MBB-$B_{0.51}E_{0.49}$ (D), MBB-$B_{0.24}E_{0.76}$ (E), and MBB-$B_{0.00}E_{1.00}$ (F). For each sample, the left photo shows the initial state and the right photo shows the droplet before being fully withdrawn into the syringe.

chain polymer could only be soluble in one liquid phase, in contrast to the reports in the literature where one of the side chains is soluble in both liquids.[8.12] We note here that this is the first report that MBBs are jammed at the interface, resulting in a wrinkled interface. MBB-$B_{1.00}E_{0.00}$ was only very weakly associated with the interface (Figure 3.1). Although a large interfacial reduction was observed for and MBB-$B_{0.00}E_{1.00}$ at pH = 4.0 as shown in Figure 3.1A, the molecules can be easily ejected from the interface because it is soluble in water. MBB-$B_{0.24}E_{0.76}$ contained 76 mol% PDEAEMA side chains, and the brushes might transform into unimolecular micelles in water after the desorption, which may not require a large amount of energy. At pH = 10.0, no droplet showed a wrinkled interface when the interfacial area was reduced, although significant interfacial tension reductions were observed for five PDEAEMA-containing MBBs.

To further confirm these observations, we prepared an emulsion of toluene and the 1.0 mM aqueous phosphate buffer solution with a pH of 4.0 using 0.03 wt% MBB-$B_{0.51}E_{0.49}$ as emulsifier by vortexing and transferred a small portion of the emulsion layer to a microscope slide for observation under an optical microscope. As can be seen from the top row in Figure 3.6, with the evaporation of solvents, the interface wrinkled and crumpled, indicating the very strong adsorption of MBB-$B_{0.51}E_{0.49}$ to the interface. After nearly all the solvents evaporated, a very thin polymer film remained behind. For the same brush polymer, as described in Chapter 2, no stable emulsion could be generated at pH = 10.0. We vortexed the mixture and examined the droplets quickly under an optical microscope; no wrinkling was observed when the solvents evaporated (the middle row of Figure 3.6). As another control, we used 0.03 wt% sodium dodecyl sulfonate (SDS) as the surfactant to make an emulsion of toluene and an acidic aqueous solution under the same conditions. However, the emulsion was found to be a toluene-in-water emulsion. The toluene droplet clearly shrank in size with time and then disappeared, and no interfacial wrinkling was

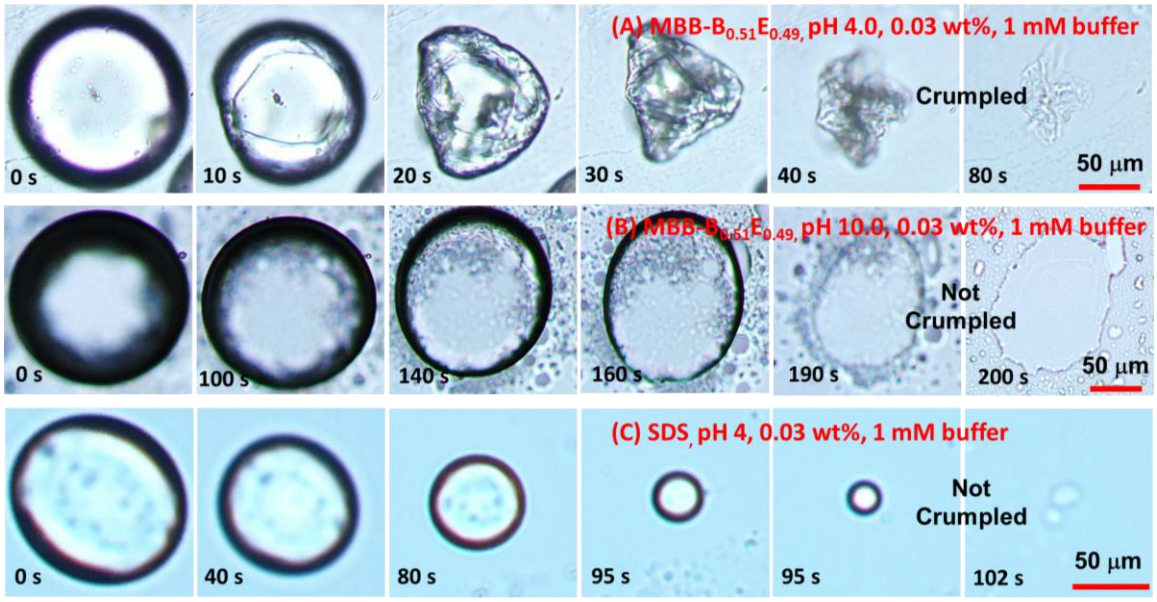

Figure 3.6. The images show screenshots of videos recorded using an optical microscope to study emulsion droplet morphology at different timepoints. (A) Emulsion droplet, stabilized by MBB-$B_{0.51}E_{0.49}$ at a concentration of 0.03 wt% with a pH of 4.0 for the aqueous phase. (B) Unstable emulsion droplet, formed with the use of 0.03 wt% MBB-$B_{0.51}E_{0.49}$ at a pH of 10.0 for the aqueous phase. (C) Emulsion droplet, stabilized by sodium dodecyl sulfonate (SDS) at a concentration of 0.03 wt% and a pH of 4.0 for an aqueous phase.

found. Although SDS is an effective surfactant, it is not strongly bound to the interface; as the toluene evaporated, the SDS was ejected from the interface into either the water or toluene phase. These experimental observations confirmed that the MBBs with appropriate chemical compositions are strongly adsorbed to and could not desorb from the interface at pH = 4.0.

These experimental observations correlated well with the emulsification behaviors of six MBBs described in Chapter 2, where only those three brush polymers showed an ability to stabilize the water-toluene emulsions at pH = 4.0 and no brush polymers could produce stable emulsions at pH = 10.0. Clearly, even if MBB-$B_{0.24}E_{0.76}$ and MBB-$B_{0.00}E_{1.00}$ dramatically reduced the interfacial tension at pH = 4.0 and all PDEAEMA-containing MBBs showed an ability to lower γ significantly at pH = 10.0, the brush molecules were not tightly bonded to the interface under those conditions. When the interfacial area was reduced, the molecules were forced to desorb from the interface. Therefore, this study revealed that for MBBs to function as effective emulsion stabilizers, it is important that they have an ability to reduce the interfacial tension and it is critical that they are strongly adsorbed to the interface.

3.4. Conclusions

In summary, we measured the time-dependences of the interfacial tension between toluene and an aqueous solution by injecting a toluene droplet, containing a brush polymer at a concentration of 0.2 mg/g, into the aqueous solution with a pH of either 4.0 or 10.0 using pendant drop tensiometry. At pH = 4.0, the lowest value of γ was observed to decrease with increasing the molar content of PDEAEMA in the side chains for the four heterografted brush polymers, from 21.0 mN/m for MBB-$B_{0.80}E_{0.20}$ to 5.0 mN/m for MBB-$B_{0.64}E_{0.36}$, 4.9 mN/m for MBB-$B_{0.51}E_{0.49}$, and 2.9 mN/m for MBB-$B_{0.24}E_{0.76}$. At pH = 10.0, γ was found to decrease to similar values, in the range of

12.8 to 14.1 mN/m, when the mole fraction of PDEAEMA was 0.36 and above. Although MBB-$B_{0.24}E_{0.76}$ and MBB-$B_{0.00}E_{1.00}$ significantly reduced the interfacial tension, they showed no ability to stabilize water-toluene emulsions because their bonding to the interface was rather weak, which was confirmed by the jamming test experiments. When the toluene droplet was gradually withdrawn to reduce the interfacial area, only MBB-$B_{0.80}E_{0.20}$, MBB-$B_{0.64}E_{0.36}$, and MBB-$B_{0.51}E_{0.49}$ showed the wrinkled interface, indicating the strong adsorption of these three MBBs to the interface, which correlated well with their abilities to stabilize the water-toluene emulsions.

References

1. Zhang, M.; Müller, A. H. E., Cylindrical polymer brushes. *Journal of Polymer Science Part A: Polymer Chemistry* **2005,** *43* (16), 3461-3481.
2. Sheiko, S. S.; Sumerlin, B. S.; Matyjaszewski, K., Cylindrical molecular brushes: Synthesis, characterization, and properties. *Progress in Polymer Science* **2008,** *33* (7), 759-785.
3. Yuan, J.; Müller, A. H. E.; Matyjaszewski, K.; Sheiko, S. S., 6.06 - Molecular Brushes. In *Polymer Science: A Comprehensive Reference*, Matyjaszewski, K.; Möller, M., Eds. Elsevier: Amsterdam, 2012; pp 199-264.
4. Li, Z.; Tang, M.; Liang, S.; Zhang, M.; Biesold, G. M.; He, Y.; Hao, S.-M.; Choi, W.; Liu, Y.; Peng, J.; Lin, Z., Bottlebrush polymers: From controlled synthesis, self-assembly, properties to applications. *Progress in Polymer Science* **2021,** *116*, 101387.
5. Xie, G.; Martinez, M. R.; Olszewski, M.; Sheiko, S. S.; Matyjaszewski, K., Molecular Bottlebrushes as Novel Materials. *Biomacromolecules* **2019,** *20* (1), 27-54.
6. Hu, M.; Russell, T. P., Polymers with advanced architectures as emulsifiers for multi-functional emulsions. *Materials Chemistry Frontiers* **2021,** *5* (3), 1205-1220.
7. Li, Y.; Zou, J.; Das, B. P.; Tsianou, M.; Cheng, C., Well-Defined Amphiphilic Double-Brush Copolymers and Their Performance as Emulsion Surfactants. *Macromolecules* **2012,** *45* (11), 4623-4629.
8. Xie, G.; Krys, P.; Tilton, R. D.; Matyjaszewski, K., Heterografted Molecular Brushes as Stabilizers for Water-in-Oil Emulsions. *Macromolecules* **2017,** *50* (7), 2942-2950.
9. Chen, X.; Yang, X.; Song, D.-P.; Men, Y.-F.; Li, Y., Discovery and Insights into Organized Spontaneous Emulsification via Interfacial Self-Assembly of Amphiphilic Bottlebrush Block Copolymers. *Macromolecules* **2021,** *54* (8), 3668-3677.

10. Gao, Y.; Wu, X.; Xiang, Z.; Qi, C., Amphiphilic Double-Brush Copolymers with a Polyurethane Backbone: A Bespoke Macromolecular Emulsifier for Ionic Liquid-in-Oil Emulsion. *Langmuir* **2021,** *37* (7), 2376-2385.
11. Wang, B.; Liu, T.; Chen, H.; Yin, B.; Zhang, Z.; Russell, T. P.; Shi, S., Molecular Brush Surfactants: Versatile Emulsifiers for Stabilizing and Structuring Liquids. *Angewandte Chemie International Edition* **2021,** *60* (36), 19626-19630.
12. Wang, B.; Zhang, Z.; Feng, W.; Luo, J.; Shi, S., Stabilizing and structuring oil–oil interfaces by molecular brush surfactants. *Aggregate* **2022,** *3* (6), e292.
13. Seong, H.-G.; Chen, Z.; Emrick, T.; Russell, T. P., Reconfiguration and Reorganization of Bottlebrush Polymer Surfactants. *Angewandte Chemie International Edition* **2022,** *61* (19), e202200530.
14. Ito, K.; Sauer, B. B.; Skarlupka, R. J.; Sano, M.; Yu, H., Dynamic interfacial properties of poly(ethylene oxide) and polystyrene at toluene/water interface. *Langmuir* **1990,** *6* (8), 1379-1388.

Appendix B

for

Chapter 3. Effects of Side Chain Composition and pH on Reduction of Toluene-Water Interfacial Tension by Amphiphilic pH-Responsive Binary Heterografted Bottlebrush Polymers

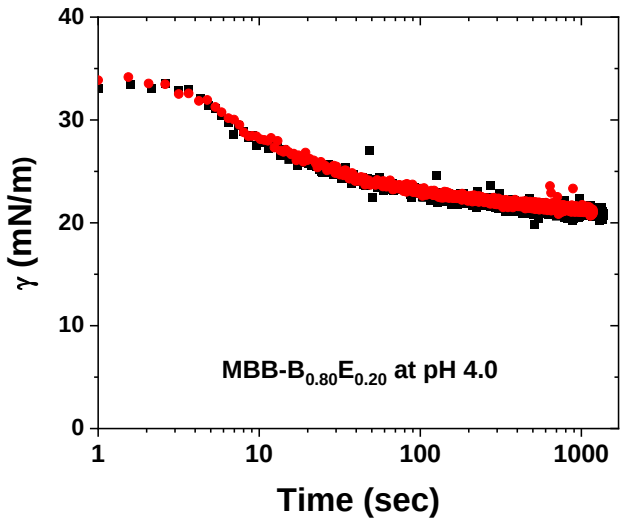

Figure B1. Interfacial tension (γ) between a toluene solution of 0.2 mg/g $MBB_{0.80}E_{0.20}$ and a pH 4.0 aqueous solution on a linear scale versus time on a semi-log scale for two repeated measurements.

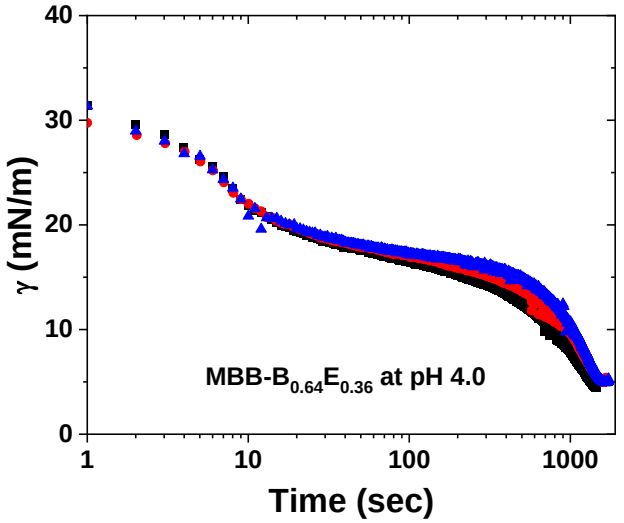

Figure B2. Interfacial tension (γ) between a toluene solution of 0.2 mg/g $MBB_{0.64}E_{0.36}$ and a pH 4.0 aqueous solution on a linear scale versus time on a semi-log scale for three repeated measurements.

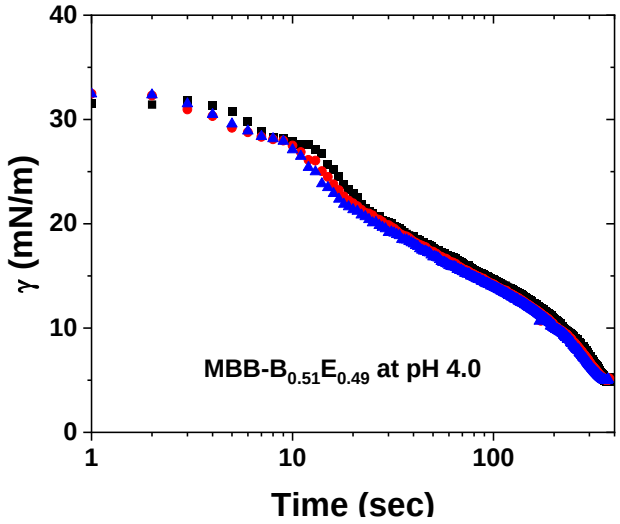

Figure B3. Interfacial tension (γ) between a toluene solution of 0.2 mg/g $MBB_{0.51}E_{0.49}$ and a pH 4.0 aqueous solution on a linear scale versus time on a semi-log scale for three repeated measurements.

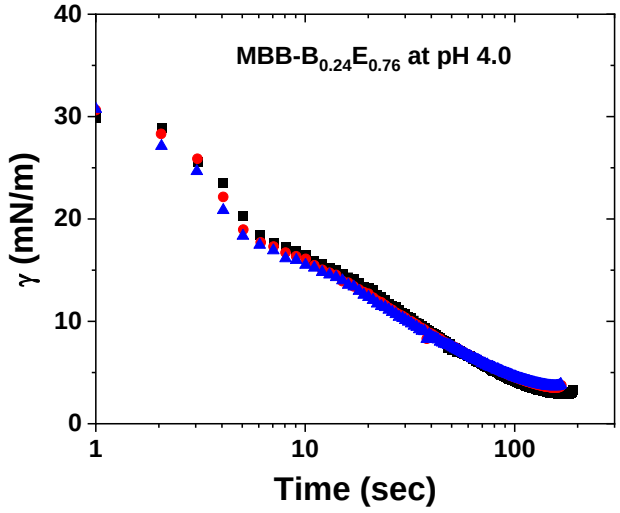

Figure B4. Interfacial tension (γ) between a toluene solution of 0.2 mg/g $MBB_{0.24}E_{0.76}$ and a pH 4.0 aqueous solution on a linear scale versus time on a semi-log scale for three repeated measurements.

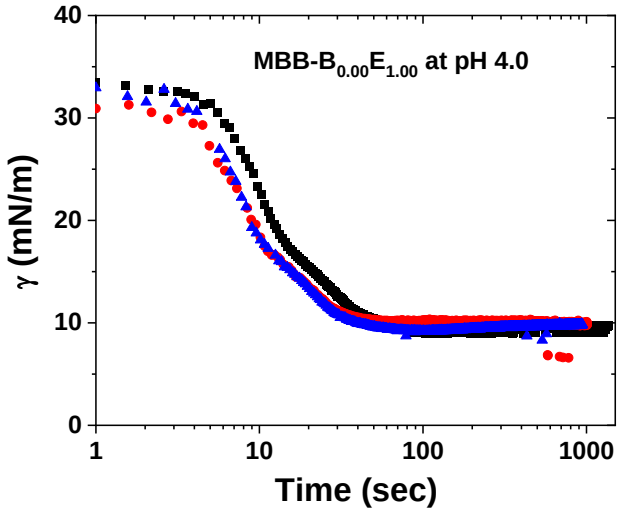

Figure B5. Interfacial tension (γ) between a toluene solution of 0.2 mg/g $MBB_{0.00}E_{1.00}$ and a pH 4.0 aqueous solution on a linear scale versus time on a semi-log scale for three repeated measurements.

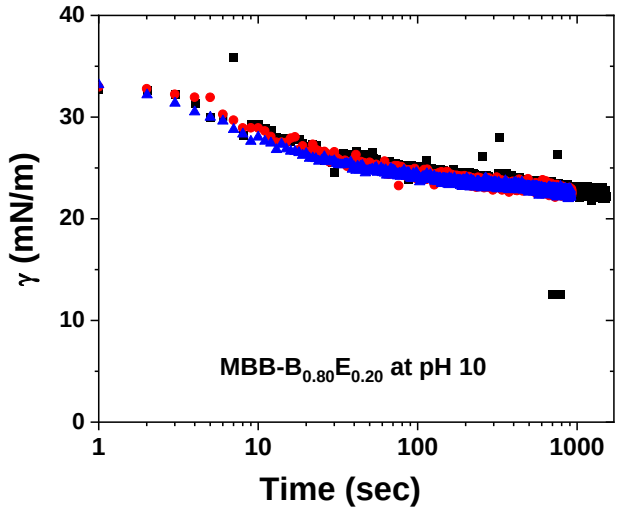

Figure B6. Interfacial tension (γ) between a toluene solution of 0.2 mg/g $MBB_{0.80}E_{0.20}$ and a pH 10.0 aqueous solution on a linear scale versus time on a semi-log scale for three repeated measurements.

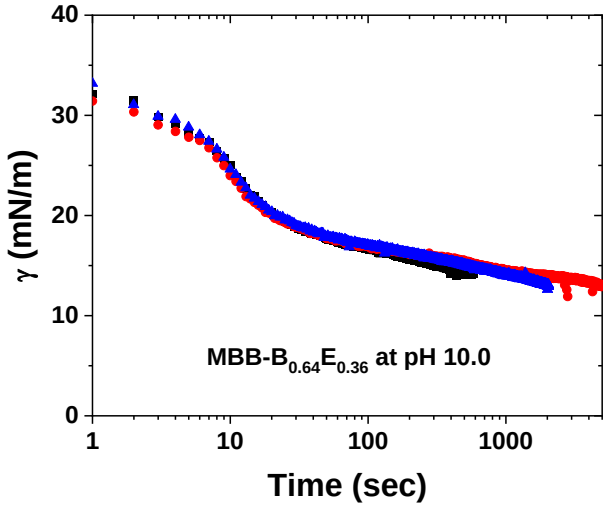

Figure B7. Interfacial tension (γ) between a toluene solution of 0.2 mg/g $MBB_{0.64}E_{0.36}$ and a pH 10.0 aqueous solution on a linear scale versus time on a semi-log scale for three repeated measurements.

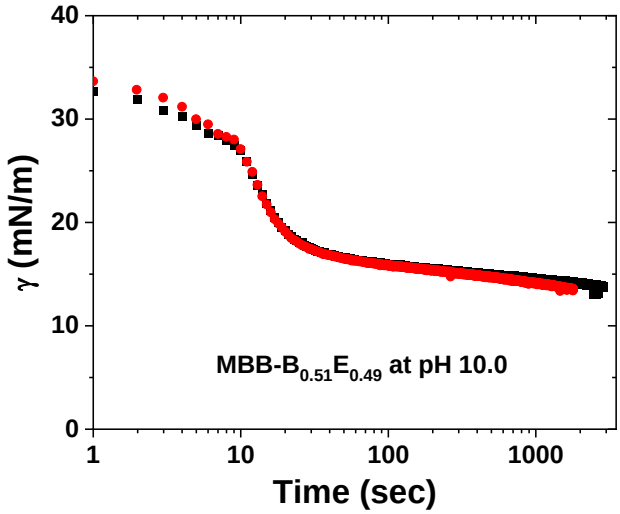

Figure B8. Interfacial tension (γ) between a toluene solution of 0.2 mg/g $MBB_{0.51}E_{0.49}$ and a pH 10.0 aqueous solution on a linear scale versus time on a semi-log scale for two repeated measurements.

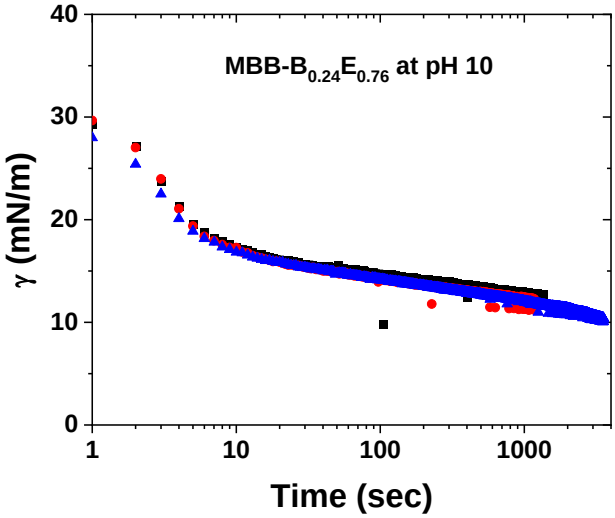

Figure B9. Interfacial tension (γ) between a toluene solution of 0.2 mg/g $MBB_{0.24}E_{0.76}$ and a pH 10.0 aqueous solution on a linear scale versus time on a semi-log scale for three repeated measurements.

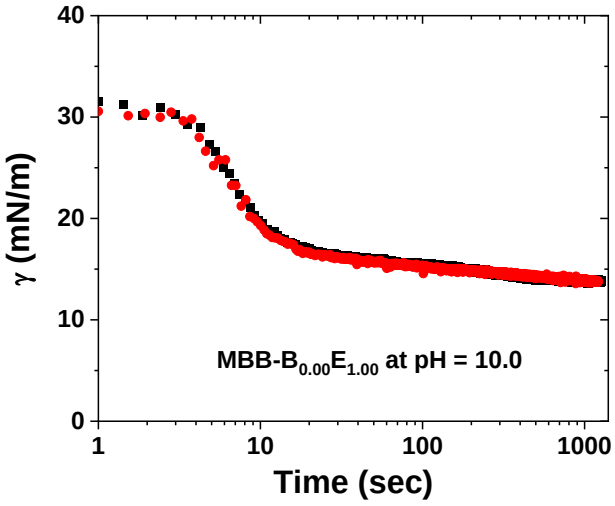

Figure B10. Interfacial tension (γ) between a toluene solution of 0.2 mg/g $MBB_{0.00}E_{1.00}$ and a pH 10.0 aqueous solution on a linear scale versus time on a semi-log scale for two repeated measurements.

Chapter 4. Conformational Behavior of Tertiary Amine-Containing Binary Heterografted Molecular Bottlebrushes at Planar Air-Water Interfaces In Response to Lateral Compression and pH Changes

Abstract

The conformational behavior of a series of amphiphilic pH-responsive binary heterografted and two homografted molecular bottlebrushes (MBBs) at air-water interfaces in response to pH changes and lateral compression was investigated using a Langmuir-Blodgett trough and atomic force microscopy. The two side chain polymers used in these MBBs are pH-responsive poly(2-(*N*,*N*-diethylamino)ethyl methacrylate) (PDEAEMA) with a pK_a of 7.4 and poly(*n*-butyl acrylate). All the PDEAEMA-containing MBBs exhibited wormlike morphologies on the surfaces of aqueous solutions with pH of 4.0 and 10.0 and a surface pressure of 0.5 mN/m. Upon compression at a pH of 4.0, MBBs with the mole fraction of PDEAEMA in the side chains ($\chi_{PDEAEMA}$) < 0.50 underwent reversible wormlike-globular conformational transitions. However, with increasing $\chi_{PDEAEMA}$, there was an increasing tendency for globular MBBs to be associated with each other. At $\chi_{PDEAEMA}$ = 0.76, the molecules remained in the wormlike state even under high compression. These observations are likely caused by the repulsions among protonated PDEAEMA side chains in the aqueous subphase that increased with increasing $\chi_{PDEAEMA}$, hampering the conformational changes of individual MBBs. On the surface of an aqueous solution with a pH of 10.0, MBBs with $\chi_{PDEAEMA}$ < 0.50 showed a lower tendency to change the wormlike conformations upon compression but a higher tendency to undergo aggregation compared with their behavior at pH 4.0. No shape transitions were observed for the MBBs with $\chi_{PDEAEMA}$ of 0.76 and 1.00. These observations can be attributed to the relatively higher affinity of nonprotonated PDEAEMA toward water compared with P*n*BA, and the desorption of PDEAEMA side chains upon lateral compression was less energetically favorable, effectively preventing conformational changes. This study revealed for the first time the conformational behavior of amphiphilic pH-responsive binary heterografted MBBs at air-aqueous solution interfaces, providing a foundation for future design of

MBBs for potential interface-related applications, such as stimuli-responsive emulsions and foams.

4.1. Introduction

Molecular bottlebrushes (MBBs) are a special type of graft copolymers in which polymeric side chains are densely end-tethered on a backbone polymer, which is typically much longer than the side chains.[1-5] This brush structure imposes strong steric interactions among the closely grafted polymeric side chains, forcing the backbone of MBBs to assume an extended conformation. When the aspect ratio, that is, N_{BB}/N_{SC}, where N_{BB} is the backbone's degree of polymerization (DP) and N_{SC} is the DP of side chains, is sufficiently large, MBBs exhibit cylindrical conformations, resembling, as suggested by the name, bottlebrush flowers and brushes for bottles and pipes.[1-3, 6] Bottlebrush polymers have attracted considerable interest in recent years, from synthesis to structures and properties; many intriguing unique characteristics have been revealed, such as large and tunable persistent length, no or low main chain entanglements, and unusual crystal habits.[7-10] A variety of potential applications of MBBs have been demonstrated in diverse areas, ranging from photonic crystals to drug delivery systems, lubricants, and emulsion stabilizers.[11-22]

Of particular interest to us is large and abrupt, often reversible, conformational changes between worm- or rod-like and globular displayed by high-aspect-ratio MBBs in response to external stimuli, which have been observed both in solution and at interfaces.[4, 23] Shape-changing bottlebrush polymers are not only scientifically interesting but also have implications in technologies, e.g., for triggered delivery of substances and stimuli-responsive emulsions. Using a Langmuir-Blodgett trough, Sheiko et al. were the first to report reversible rod-globule transitions of MBBs with densely grafted poly(*n*-butyl acrylate) (P*n*BA) side chains on the water surface via lateral compression and expansion.[24] Without compression, P*n*BA side chains spread readily on the water interface due to their amphiphilic nature, and presumably the ester groups were in direct contact with water while the butyl tails pointed toward air.[24-26] Upon lateral compression to reduce

the interfacial area, a portion of P*n*BA side chains desorbed from the air-water interface and coiled into globular conformations, and the rodlike bottlebrush molecules transformed unimolecularly into globules stabilized by the remaining adsorbed side chains on the water surface.[24] Coexistence of wormlike and spherical brush molecules at constant pressure and temperature was observed, suggesting that the rod-sphere shape transition of P*n*BA MBBs on the water surface was a first-order phase transition. Subsequently, rod-globule conformational transitions of P*n*BA MBBs were also induced at air-liquid interfaces by changing the subphase's surface tension and on solid substrates by exposing the brushes to different vapors.[27-29]

On the other hand, Schmidt et al. observed temperature-induced wormlike-globular conformational transitions by MBBs with thermoresponsive with poly(*N*-isopropylacrylamide) side chains by atomic force microscopy (AFM).[30] However, the collapsed globular PNIPAm brush molecules were unstable and eventually aggregated and precipitated out from water. This issue is particularly severe for pH-responsive poly(2-(*N*,*N*-dimethylamino)ethyl methacrylate) (PDEAEMA) brush polymers, which precipitated out immediately even at a concentration of 0.002 mg/g when the pH of the aqueous solution was increased from below to above its pK_a of ~ 7.4).[31] By introducing a second water-soluble polymer into the side chains, either as a second set of homopolymer side chains in heterografted MBBs or as the outer block of diblock copolymer side chains in homografted MBBs, to function as a stabilizer, our research group achieved wormlike/starlike-stable globular shape transitions in dilute aqueous solutions as well as in moderately concentrated solutions.[31-38]

In Chapter 2, we demonstrated that linear amphiphilic heterografted P*n*BA/PDEAEMA MBBs with appropriate side chain compositions were effective and efficient pH-responsive emulsion stabilizers. At pH = 4.0, PDEAEMA was protonated and soluble in water; the brushes tightly

adsorbed at the water-toluene interface, with charged PDEAEMA side chains extending into the aqueous phase and P*n*BA side chains remaining stretched in toluene, resulting in stable emulsions even at rather low polymer concentrations. When the pH was adjusted to 10.0, PDEAEMA was deprotonated and became insoluble in water but soluble in toluene, the bottlebrush molecules retreated to the toluene phase from the interface, triggering the breaking of the emulsions. The formation and breaking of emulsions with P*n*BA/PDEAEMA MBBs as stabilizers can be repeated at least 10 times, showing the pH dependence of the interfacial activity of the MBBs. Considering the adsorption and detachment of these brush polymers at the water-toluene interface, several questions have emerged. Do amphiphilic P*n*BA/PDEAEMA brush molecules collapse into a globular conformation when the pH was raised to above the pK_a of PDEAEMA as water-soluble stimuli-responsive MBBs do in aqueous solutions? Or, do the brush molecules simply gradually detach from the interface when the tertiary amine groups of PDEAEMA are deprotonated while remaining in the wormlike shape? In addition, we observed in Chapter 2 wrinkled films formed on the surface of emulsion droplets when the solvents were evaporating and in Chapter 3 wrinkled interfaces when the toluene droplets were withdrawn from the acidic aqueous solution into the syringe in a pendant drop experiment. In these two situations, the brush molecules were stuck at the interface while being squeezed due to the decrease in interfacial area. Do they change their conformations from wormlike to globular to accommodate the reduced interfacial area available to them? In Chapter 3, we studied the adsorption and detachment of MBBs at the water-toluene interface by measuring the interfacial tensions between the two phases using a pendant drop tensiometry method. However, these measurements did not provide any information about the conformations of the brush molecules at the interfaces.

Motivated by the aforementioned questions, in this Chapter, we investigate the conformational behavior of four linear binary heterografted P*n*BA/PDEAEMA bottlebrush polymers as well as two homografted MBBs at planar air-water interfaces in a Langmuir-Blodgett (LB) trough in response to pH changes of the aqueous subphase and lateral compression and expansion (Scheme 4.1). Although this study does not directly correlate with the stimuli-responsive water-toluene emulsion research in Chapter 2 and the pendant drop experiments in Chapter 3, the results presented here, we believe, will provide insights into the behavior of heterografted P*n*BA/PDEAEMA MBBs at the two-dimensional (2D) interface and will guide our future research endeavors on MBBs at other interfaces.

4.2. Experimental Section

4.2.1. Materials

Toluene (certified ACS) and monobasic potassium phosphate (99+%, Acros) were purchased from Fisher Scientific. Absolute ethanol (100%) was purchased from Decon Labs. Water was purified by a Millipore filtration device (Milli-Q). 1.0 mM aqueous phosphate buffer solution was prepared using appropriate amounts of potassium phosphate and Milli-Q water. The brush polymers used in this work are the same as those detailed in Chapter 2, and they are MBB-$B_{1.00}E_{0.00}$, MBB-$B_{0.80}E_{0.20}$, MBB-$B_{0.64}E_{0.36}$, MBB-$B_{0.51}E_{0.49}$, MBB-$B_{0.24}E_{0.76}$, and MBB-$B_{0.00}E_{1.00}$, where B and E represent P*n*BA and PDEAEMA side chains, and the subscripts correspond to the mole fractions of the two side chain polymers.

4.2.2. Langmuir-Blodgett Lateral Compression and Sample Transfer

The compression/decompression isotherm and dipping experiments were performed using a KSV NIMA Langmuir-Blodgett Trough (Biolin Scientific). Prior to each experiment, the

Scheme 4.1. Conformational Behavior of Amphiphilic Linear Heterografted P*n*BA/PDEAEMA Molecular Bottlebrushes at Planar Air-Water Interfaces in Response to pH Changes and Lateral Compression and Expansion

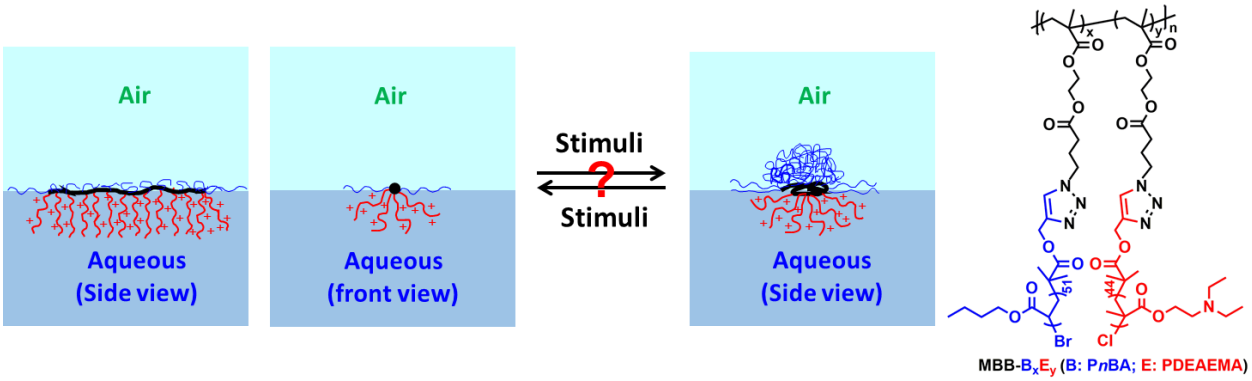

Langmuir-Blodgett trough and barriers were cleaned by gently brushing the surfaces with ethanol, rinsing with Milli-Q water, and then nitrogen flow and an aspirator were used to remove any residual water. The platinum Wilhelmy plate was cleaned by first rinsing sequentially with ethanol and water, and then being held in the flame of a Bunsen burner for several seconds until the plate was red-hot. The LB trough was assembled, and the subphase was gently poured in. If necessary, the pH of the aqueous subphase was adjusted prior to addition to the trough using 1.0 M HCl and NaOH solutions and monitored by a pH meter (Accument AB-15, calibrated at room temperature using a series of buffer standards with the pH values of 4.01, 7.00, and 10.01). To ensure the water surface was sufficiently clean, the barriers were compressed several times and an aspirator was used to remove any possible surface contaminants. The surface was considered sufficiently clean if the surface pressure increase was less than 0.3 mN/m during the compression process. For dipping experiments, the MBBs were transferred to 12 mm cover glasses (Fisherbrand), which had been previously cleaned in a piranha solution, rinsed thoroughly with Milli-Q water, and stored in isopropanol.

MBB solutions were prepared by dissolving the MBBs in chloroform and adjusting the concentration to 0.5 mg/mL. When the brush solutions were not being used, they were stored in a freezer (-20 °C) to minimize solvent evaporation. In a typical experiment 40 µL of MBB solution was deposited gently on the surface dropwise using a microsyringe. To ensure evaporation of the chloroform and ensure uniform spread of the brush molecules the system was equilibrated for 15 min prior to compression. The barriers were then compressed at a rate of 10 mm/min. For isotherm experiments the barriers were compressed to a desired mean molecular area, then the barriers were expanded, and then followed by an additional cycle. For dipping experiments the barriers were compressed to a desired surface pressure value. Once the surface pressure reading was steady, the

glass coverslip was lifted out of the subphase at a rate of 5 mm/min, and the surface pressure was held constant. The coverslip was transferred to a stainless-steel disc with double sided tape to prepare for AFM imaging.

4.2.2. Atomic Force Microscopy (AFM)

MBB monolayers were imaged by AFM using a Digital Instruments Multimode IIIa Scanning Probe Microscope in tapping mode at ambient conditions. Silicon AFM probes with a reflective aluminum coating (Tap300Al-G, BudgetSensors) were used with a tip radius of 10 nm, force constant of 40 N/m, and resonance frequency of 300 kHz. For each AFM sample, several 3 × 3 μm and 1 × 1 μm images were taken to ensure that the collected images were representative of the MBBs' morphology on the substrate. The collected images were flattened, and the height scale was adjusted using Nanoscope Analysis 2.0 (Bruker). The height and length of MBBs were measured using Nanoscope Analysis and ImageJ, respectively.

4.3. Results and Discussion

4.3.1. Amphiphilic pH-Responsive Heterografted MBBs at Interfaces between Air and Aqueous Solutions in a LB Trough at a Surface Pressure of 0.5 mN/m: pH Effect

Four amphiphilic heterografted P*n*BA/PDEAEMA linear bottlebrush polymers with different side chain compositions, MBB-$B_{0.80}E_{0.20}$, MBB-$B_{0.64}E_{0.36}$, MBB-$B_{0.51}E_{0.49}$, and MBB-$B_{0.80}E_{0.20}$, are used in this study (see Scheme 4.1 for molecular structures), along with two homografted MBBs, MBB-$B_{1.00}E_{0.00}$ and MBB-$B_{0.00}E_{1.00}$, where B denotes P*n*BA, E represents PDEAEMA, and subscripts stand for mole fractions of the two side chain polymers. These brush polymers are the same as those in Chapters 2 and 3, and their synthesis and characterization data can be found in Chapter 2.

We first investigated if pH changes would induce wormlike-globular conformational transitions of heterografted P*n*BA/PDEAEMA MBBs on the water surface. To this end, we prepared a solution of each brush polymer in chloroform at a concentration of 0.5 mg/mL and used a microsyringe to deposit a small amount of a brush polymer solution, typically 40 μL, onto the surface of a 1.0 mM phosphate buffer with a pH of either 4.0 or 10.0. After the evaporation of chloroform, the monolayer of bottlebrush molecules was compressed slightly to a small surface pressure of 0.5 mN/m and transferred to a "Piranha" solution-cleaned round glass disk at a transfer rate of 5 mm/min. The brush molecules were imaged in a tapping mode using an atomic force microscope, and the results are shown in Figures 4.1 and C1. Note that Sheiko et al. previously argued that the observed molecular conformations of MBBs transferred to a solid substrate corresponded to those at the air-water interface,[24] and from our own experiments, we also believe that this is the case, as discussed later in this Chapter.

Wormlike molecules were observed for all four brush polymers at both pH 4.0 (Figure 4.1A,C,E,G) and 10.0 (Figure 4.1B,D,F,I). The bottlebrushes appeared to be stretched to similar degrees. Image analysis of > 100 molecules for each sample showed the average length of wormlike bottlebrush molecules was 103.3 ± 22.9 nm for MBB-$B_{0.80}E_{0.20}$ at pH = 4.0 (196 molecules), 104.6 ± 26.5 nm for MBB-$B_{0.80}E_{0.20}$ at pH = 10.0 (183 molecules), 105.5 ± 20.1 nm for MBB-$B_{0.64}E_{0.36}$ at pH = 4.0 (218 molecules), 100.4 ± 20.4 nm for MBB-$B_{0.64}E_{0.36}$ at pH = 10.0 (194 molecules), 107.4 ± 25.1 nm for MBB-$B_{0.51}E_{0.49}$ at pH = 4.0 (238 molecules) , 102.9 ± 21.8 nm for MBB-$B_{0.51}E_{0.49}$ at pH = 10.0 (167 molecules), 99.8 ± 27.3 nm for MBB-$B_{0.24}E_{0.76}$ at pH = 4.0 (181 molecules), and 97.8 ± 19.9 nm for MBB-$B_{0.24}E_{0.76}$ at pH = 10.0 (205 molecules). The typical height at pH 4.0 was 1.6 ± 0.3 nm for MBB-$B_{0.80}E_{0.20}$, 1.1 ± 0.2 nm for MBB-$B_{0.64}E_{0.36}$, 1.5 ± 0.3 nm for MBB-$B_{0.51}E_{0.49}$, and 1.7 ± 0.2 nm for MBB-$B_{0.24}E_{0.76}$, while at pH 10.0 it was 1.5

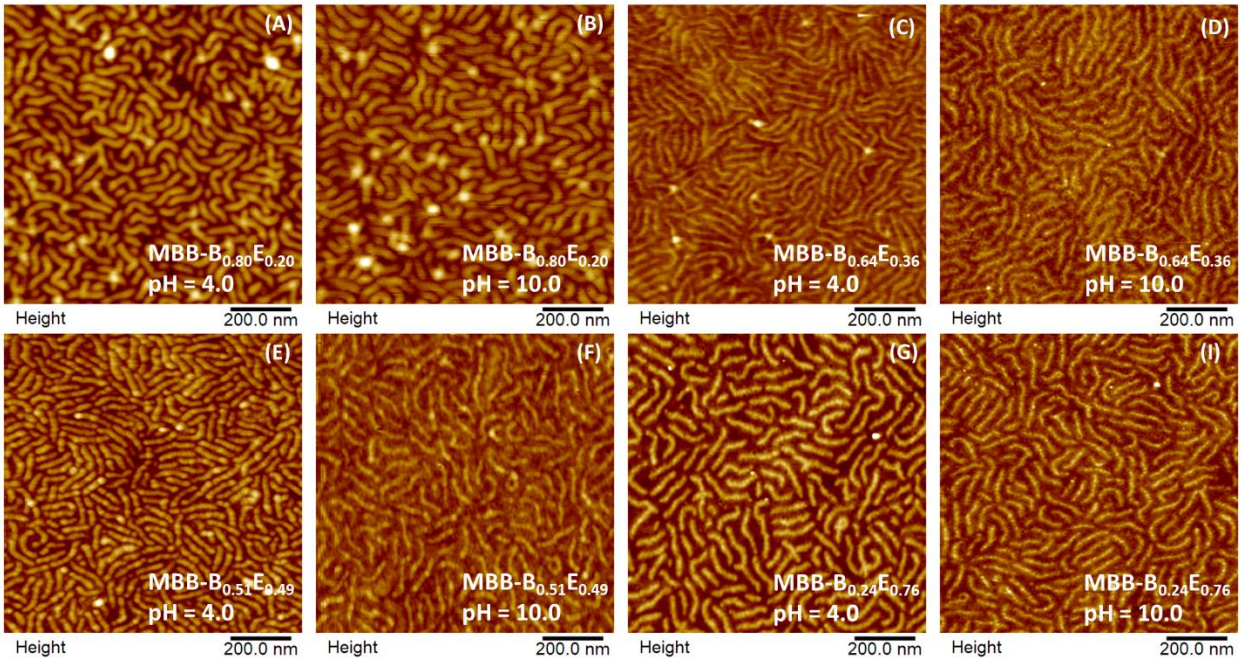

Figure 4.1. AFM height images of MBB-$B_{0.80}E_{0.20}$ (A,B), MBB-$B_{0.64}E_{0.36}$ (C,D), MBB-$B_{0.51}E_{0.49}$ (E,F), MBB-$B_{0.24}E_{0.76}$ (G,I) transferred onto "Piranha" solution-cleaned glass disks from the interface between air and a 1.0 mM aqueous phosphate buffer solution with a pH of 4.0 (A,C,E,G) or 10.0 (B,D,F,I) at a surface pressure of 0.5 mN/m using a Langmuir-Blodgett trough.

± 0.3 nm for MBB-$B_{0.80}E_{0.20}$, 1.2 ± 0.2 nm for MBB-$B_{0.64}E_{0.36}$, 1.4 ± 0.2 nm for MBB-$B_{0.51}E_{0.49}$, and 1.5 ± 0.3 nm for MBB-$B_{0.24}E_{0.76}$. There were no significant differences in the average length and height of each brush polymer at acidic and basic pH values, and the slight variations in height could likely be attributed to the AFM tip. These results indicate that linear heterografted P*n*BA/PDEAEMA MBBs did not exhibit wormlike-globular conformation transitions at the air-water interfaces when the pH of the subphase was increased from pH 4.0 to 10.0, crossing the pK_a of PDEAEMA, which was reported to be ~ 7.4.[39, 40] This is further corroborated by the observation of a wormlike morphology of MBB-$B_{0.00}E_{1.00}$, the homografted brush polymer with the same PDEAEMA side chains at in heterografted MBBs, at the air-water interface with pH = 10.0 for the subphase transferred at a surface pressure of 0.5 mN/m (Figures 4.2 and C2). Analysis showed that the average length of wormlike MBB-$B_{0.00}E_{1.00}$ molecules was 111.1 ± 21.2 nm with a typical brush height of 1.6 ± 0.2 nm. There does appear to be a trend that the MBBs adopt a more rod like morphology as the mole fraction of PDEAEMA increases, which is likely caused by the larger actual molecular weight. Note that we did not attempt to transfer the bottlebrushes of MBB-$B_{0.00}E_{1.00}$ because this homografted brush polymer would become soluble after protonation in acidic water.

As mentioned early, we previously observed that PDEAEMA homografted bottlebrushes aggregated and precipitated out immediately from the aqueous solution, even at a concentration as low as 0.002 mg/g, when the pH was changed from acidic to basic.[31] When a soluble polymer was introduced into the side chains as a stabilizer, the collapsed brushes took on a globular conformation. These observations suggest that the pH-induced soluble-insoluble transition of PDEAEMA side chains is a very strong driving force for minimizing the contact area with water.

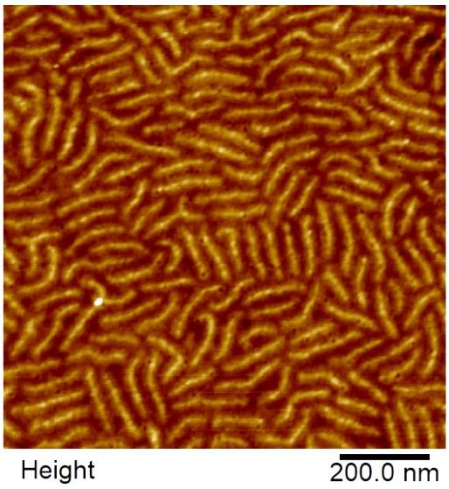

Figure 4.2. AFM height image of homografted MBB-$B_{0.00}E_{1.00}$ transferred to a "Piranha" solution-cleaned glass disk from the interface between air and a 1.0 mM phosphate aqueous buffer solution with a pH of 10.0 at a surface pressure of 0.5 mM/m using a Langmuir-Blodgett trough.

However, no wormlike-globular shape transition was observed for the amphiphilic heterografted P*n*BA/PDEAEMA brush polymers at the air-water interface when the pH of the aqueous subphase was changed from 4.0 to 10.0, and the homografted PDEAEMA bottlebrush molecules assumed wormlike conformations on the surface of a basic aqueous solution with a pH of 10.0. These observations indicate that the globular conformation is not the lowest energy state on the surface of the pH 10.0 aqueous solution. Instead, the spreading of the PDEAEMA side chains on the surface of a basic aqueous solution is favored (Figure 4.2), that is, the spreading coefficient of nonprotonated PDEAEMA on the surface of basic water $S = \gamma_{water\text{-}air} - (\gamma_{water\text{-}PDEAEMA} + \gamma_{PDEAEMA\text{-}air}) > 0$, where $\gamma_{water\text{-}air}$ is the surface tension of the basic aqueous subphase, $\gamma_{water\text{-}PDEAEMA}$ is the interfacial free energy between the basic aqueous solution and nonprotonated PDEAEMA, and $\gamma_{PDEAEMA\text{-}air}$ is the surface free energy of nonprotonated PDEAEMA. This can be attributed to the amphiphilicity of nonprotonated PDEAEMA on the surface of the aqueous solution with a pH of 10.0 because both the ester group and the tertiary amine moiety can have dipole-dipole interactions and hydrogen bonding with water molecules. By examining the molecular structures of P*n*BA and PDEAEMA, we believe that P*n*BA is more hydrophobic than PDEAEMA. Given that P*n*BA bottlebrushes adopt wormlike conformation on the water surface due to the interactions between the polar ester group and water, it is not surprising to see that the nonprotonated PDEAEMA side chains have a tendency to spread on the surface of the pH 10.0 aqueous solution.

4.3.2. Lateral Compression-Induced Reversible Worm-Sphere Conformational Transitions of Homografted P*n*BA Bottlebrushes, MBB-$B_{1.00}E_{0.00}$, at the Air-Water Interface in a Langmuir-Blodgett Trough

We previously showed that at pH = 4.0 heterografted P*n*BA/PDEAEMA MBBs were jammed at the water-toluene interfaces when the emulsion droplets or the pendant toluene drop was

shrinking (caused by evaporation of solvents or withdrawing of the droplet), resulting in wrinkled interfaces. Under both conditions, the brush molecules assumed a Janus-type structure at the liquid-liquid interface, with P*n*BA side chains extending into the toluene phase and protonated PDEAEMA side chains residing in the acidic aqueous solution. When the interfacial area was reduced, the brush molecules were pushed together and squeezed at the interface because they could not desorb. This situation is analogous to the lateral mechanical compression of the bottlebrushes at the 2D interface, which may cause conformational changes. Herein, we use a Langmuir-Blodgett trough to investigate how amphiphilic heterografted P*n*BA/PDEAEMA MBBs at the air-water interface respond to lateral mechanical compression and expansion with the pH of the aqueous subphase at 4.0 and 10.0. Although this study does not correspond directly to the MBBs at the water-toluene interface, we expect that the data will provide insights into the behavior of multicomponent MBBs at 2D interfaces in general upon compression.

We first examined the behavior of the homografted P*n*BA brush polymer, MBB-$B_{1.00}E_{0.00}$, on the water surface in a Langmuir-Blodgett trough as P*n*BA bottlebrushes with sufficiently long P*n*BA side chains were reported by Sheiko et al. to undergo reversible rod-globule conformational transitions upon lateral compression.[24] Figure 4.3A shows the surface pressure (π)-mean area per molecule (A) isotherms for two cycles of lateral compression and decompression. No difference was observed between the 1st and 2nd cycle. Upon compression, the surface pressure began to increase at $A_0 = 2.57 \times 10^3$ nm^2/molecule, and increased rapidly and almost linearly with decreasing A until an inflection point at about ~ 1800 nm^2/molecule. A plateau was observed after that, and a second one occurred when A was decreased to about 1300 nm^2/molecule. Note that the mean surface area per brush molecule was calculated based on the mass of the sample deposited on the water surface and the calculated molecular weight of the brush polymer (Table 2.1).

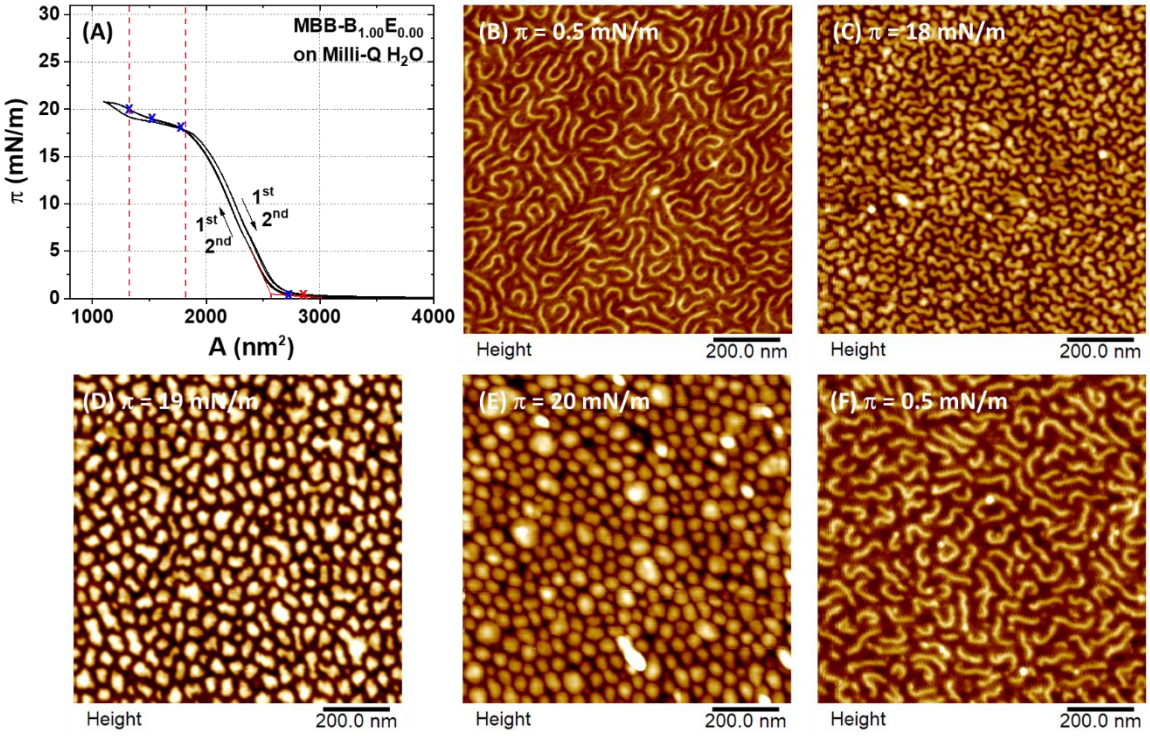

Figure 4.3. (A) Isotherm plots of surface pressure (π) vs mean area per brush (A) from two cycles of lateral compression and expansion for MBB-$B_{1.00}E_{0.00}$ on Milli-Q water and AFM images at different compression-expansion stages: (B) π = 0.5 mN/m, (C) π = 18 mN/m, (D) π = 19 mN/m, (E) π = 20 mN/m, and (E) π = 0.5 mN/m again.

AFM samples were prepared by transferring the brush monolayer onto glass disks at different degrees of lateral compression (i.e., at different surface pressures). At a surface pressure of 0.50 mN/m, the P*n*BA brushes were wormlike (Figure 4.3B). When the pressure was increased to 18 mN/m (Figure 4.3C), just past the inflection point on the isotherm, the molecules shrank significantly and were about to collapse. In the middle of the first plateau at π = 19 mN/m, AFM imaging revealed that the vast majority of bottlebrushes collapsed into globules, although not very round. Some molecules can be seen to remain in the wormlike morphology, while others exhibit tadpole-like conformations, suggesting that the worm-to-globule shape transition appeared to be initiated from the end of the molecule. The coexistence of wormlike and spherical brush molecules indicated that the worm-globule shape transition is a first-order phase transition, much like the coexistence of liquid and crystalline water during the melting transition at constant temperature and pressure, as first reported by Sheiko et al.[24] When the surface pressure reached 20 mN/m, near the end the first plateau, all molecules completed the conformational transition. A few molecules appeared to aggregate with each other, which is probably because the degree of lateral compression is at the transition from the first plateau to the second plateau. Further increasing the surface pressure likely will result in more aggregation. Upon decompression to π = 0.50 mN/m, the MBBs resumed wormlike conformations, however, the molecules appeared to be wavier than the initial conformation, which may be an artifact of the unfolding process. Overall the behavior of the P*n*BA MBBs at the air-water interface are very similar to those reported by Sheiko et al.[24-26]

4.3.3. Conformational Behavior of Amphiphilic pH-Responsive Binary Heterografted MBBs at Interface between Air and a 1.0 mM Aqueous Phosphate Buffer Solution with pH of 4.0 in Response to Lateral Compression and Decompression

The conformational behavior of four heterografted brush polymers at the air-water interface with a subphase pH of 4.0 was then investigated. The subphase was a 1.0 mM aqueous phosphate buffer solution whose pH was adjusted to 4.0 before being poured into the Langmuir-Blodgett trough. Figure 4.4 shows the LB isotherms for two cycles of compression and expansion and AFM height images at different surface pressures for MBB-$B_{0.80}E_{0.20}$. Similar to MBB-$B_{1.00}E_{0.00}$, three stages with two plateaus can be discerned from the LB isotherms for this heterografted P*n*BA/PDEAEMA brush polymer, although the second plateau at high surface pressures is short and moved to a lower average area per brush molecule, ~ 1100 nm^2/molecule. In the first compression, π started to increase at A_0 = 2500 nm^2/brush. Unlike MBB-$B_{1.00}E_{0.00}$, a large hysteresis occurred after expansion; the surface pressure did not return to nearly 0 mN/m but stayed at ~ 3 mN/m. This hysteresis was very likely caused by the loose attachment of bottlebrush molecules containing charged PDEAEMA side chains on the platinum Wilhelmy plate possibly through charge-image charge interactions. AFM imaging showed that the brush molecules were worm- or rodlike at a surface pressure of 0.50 mN/m (Figure 4.4B) and appeared to be closer to each other than MBB-$B_{1.00}E_{0.00}$ brush molecules shown in Figure 4.3B at the same surface pressure. Here, on the surface of the acidic aqueous solution with a pH of 4.0, 20% of the side chains in the brush polymer are charged PDEAEMA, extending into the solution. Once transferred onto the glass disk, these positively charged side chains interact strongly with the substrate, and the brush molecules are likely pinned on the substrate immediately. At the surface pressure of 19 mN/m (Figure 4.4C), which was at the beginning of the first plateau, some brushes already

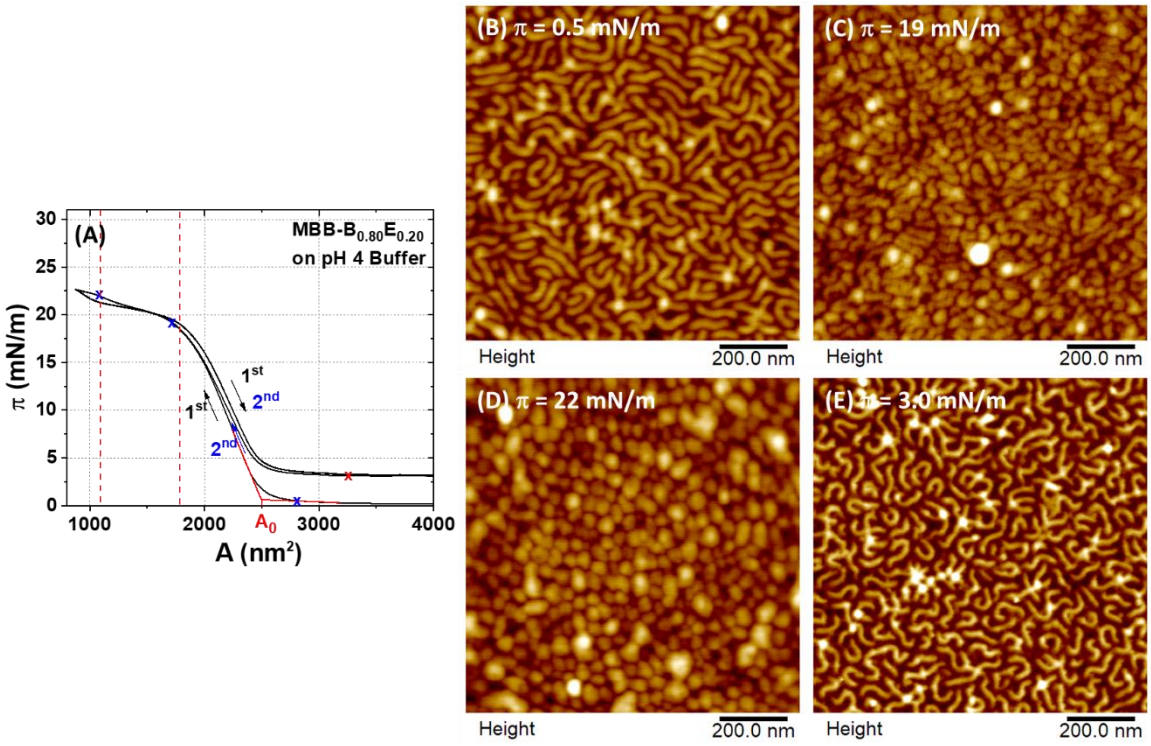

Figure 4.4. (A) Isotherm plots of surface pressure (π) vs mean area per brush (A) from two cycles of compression and expansion for MBB-$B_{0.80}E_{0.20}$ on the surface of a 1.0 mM phosphate buffer aqueous solution with a pH of 4.0 and AFM height images of MBB-$B_{0.80}E_{0.20}$ at different surface pressures: (B) π = 0.5 mN/m, (C) π = 19 mN/m, (D) π = 22 mN/m, and (E) π = 3 mN/m.

transformed into a globular shape, while many other molecules remained in the wormlike state. Upon further increasing the surface pressure to 22 mN/m, which is at the end of the first plateau, nearly all bottlebrushes transformed into spheres (Figure 4.4D). Upon decompression to 3.0 mN/m, the brushes resumed a wormlike morphology (Figure 4.4E). By comparing Figures 4.3 and 4.4, we can see this polymer behaved similarly to MBB-$B_{1.00}E_{0.00}$ to some degree, with the only distinct difference being the hysteresis observed for MBB-$B_{0.80}E_{0.20}$.

Figure 4.5A shows the isotherm π-A plots from two cycles of compression and expansion for MBB-$B_{0.64}E_{0.36}$. While the first plateau was clearly visible, we only saw the beginning of the transition from the 1st plateau to a possible second one. AFM revealed that the brushes were wormlike at π = 0.5 mN/m (Figure 4.5B) and 20 mN/m (Figure 4.5C), where the molecular worms were more closely packed at π = 20 mN/m as expected. The molecules changed to globular at π = 23 mN/m (Figure 4.5D). However, the globules were less defined and less round than those in Figures 4.3E and 4.4D and some molecules were in a partially collapsed state, despite the surface pressure being at the end of the plateau. Upon expansion, the brushes resume their wormlike state.

Further increasing the molar content of PDEAEMA in the side chains of MBB to 0.49 (i.e., MBB-$B_{0.51}E_{0.49}$), the L-B isotherm plot showed an even weaker transition from the rapid increase region to the plateau, as evidenced by the more upward pointing plateau, with a larger magnitude of the slope, in the range from A = ~ 1700 to ~ 1100 nm^2/molecule (Figure 4.6A). There seems no sign that the second plateau will appear if the molecules continue to be compressed. AFM images showed that the MBB-$B_{0.51}E_{0.49}$ molecules were wormlike at π = 0.5 mN/m (Figure 4.6B) as for other brush polymers and were about to collapse at π = 21 mN/m (Figure 4.6C). In the center of the upward-pointing plateau at π = 24 mN/m, the bottlebrush molecules were globular but more connected (Figure 4.6D); individual molecules were even harder to be discerned than MBB-

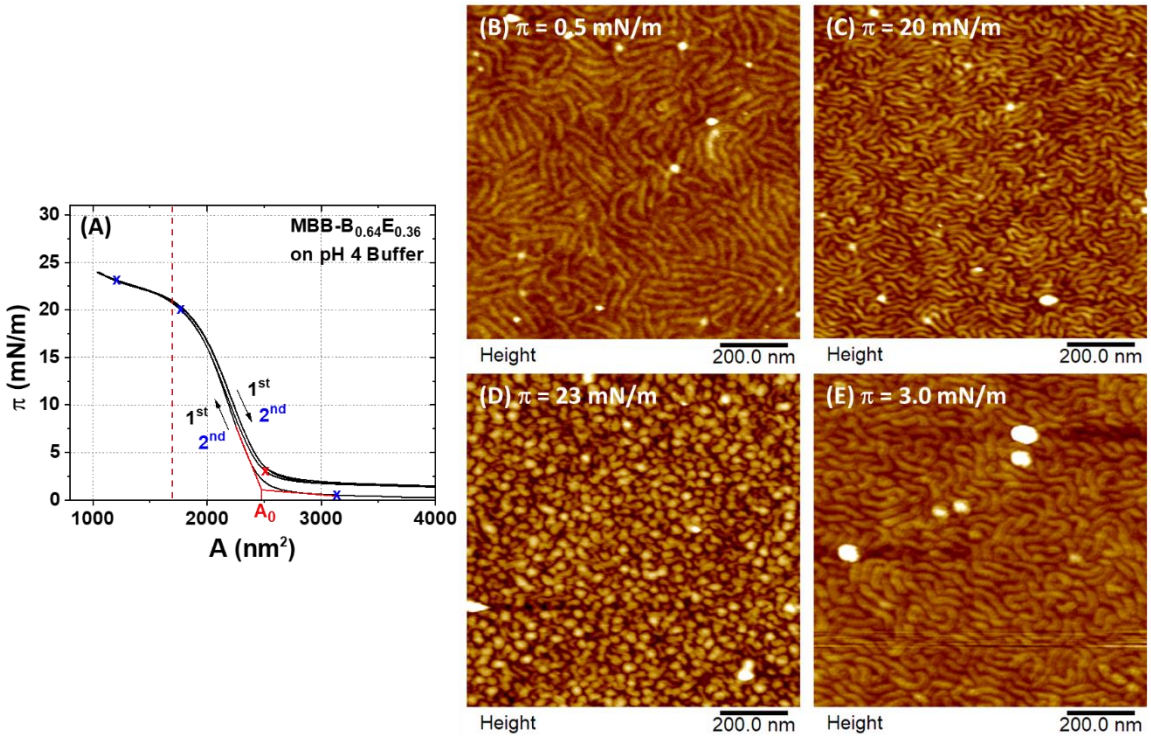

Figure 4.5. (A) Isotherm plots of surface pressure (π) vs mean area per brush (A) from two cycles of compression and expansion for MBB-$B_{0.64}E_{0.36}$ on the surface of a 1.0 mM phosphate buffer aqueous solution with a pH of 4.0 and AFM height images of MBB-$B_{0.64}E_{0.36}$ at different surface pressures: (B) π = 0.5 mN/m, (C) π = 20 mN/m, (D) π = 23 mN/m, and (E) π = 3.0 mN/m.

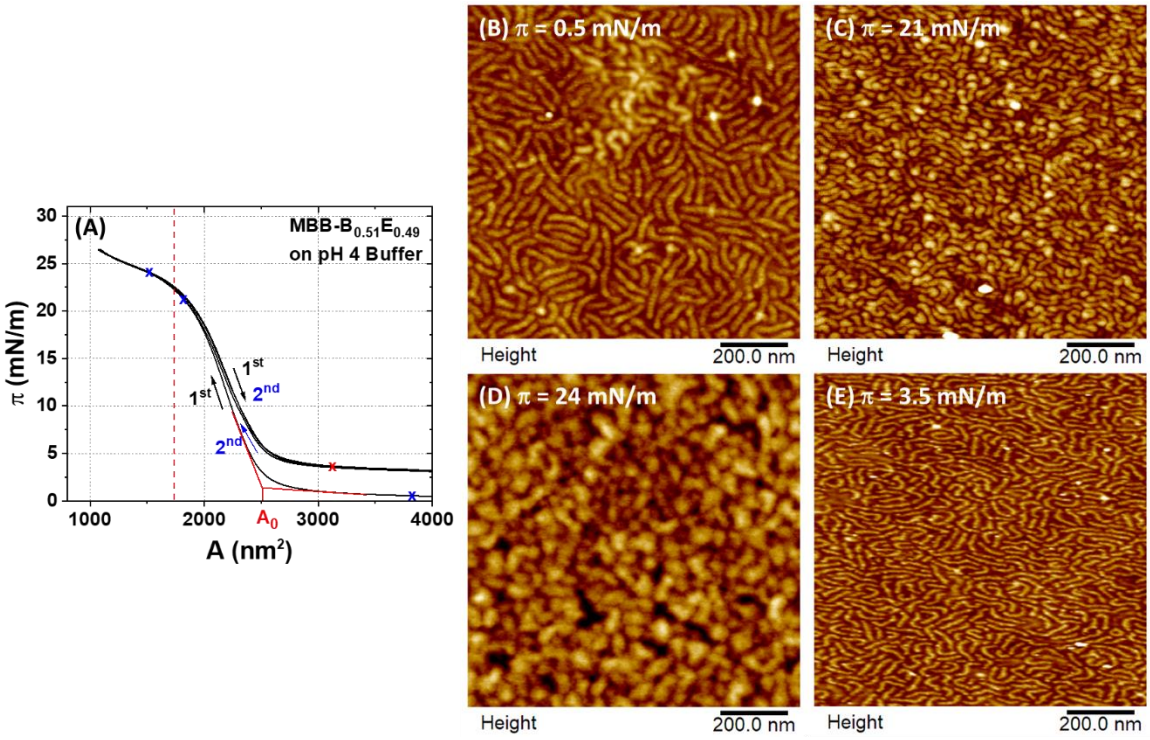

Figure 4.6. (A) Isotherm plots of surface pressure (π) vs mean area per brush (A) from two cycles of compression and expansion for MBB-$B_{0.51}E_{0.49}$ on the surface of a 1.0 mM phosphate buffer aqueous solution with a pH of 4.0 and AFM height images of MBB-$B_{0.51}E_{0.49}$ bottlebrush molecules at different surface pressures: (B) π = 0.5 mN/m, (C) π = 21 mN/m, (D) π = 24 mN/m, and (E) π = 3.5 mN/m.

$B_{0.64}E_{0.36}$ in Figure 4.5D. Despite the observation that the molecules seemingly aggregated at π = 24 mN/m in Figure 4.6D, they returned to the wormlike state upon lateral decompression to π = 3.5 mN/m (Figure 4.6E).

For MBB-$B_{0.24}E_{0.76}$ with 76% of side chains being PDEAEMA, no transition in the π-A plot was observed upon compression on the surface of the 1.0 mM phosphate buffer aqueous solution with a pH of 4.0 (Figure 4.7A). The isotherm showed a sharp, monotonous increase in surface pressure with reducing the surface area. Similar to other PDEAEMA-containing heterografted MBBs, there was a large hysteresis in the isotherm in the first compression-decompression cycle, and the surface pressure did not come back to nearly zero. However, the hysteresis was negligible in the second cycle. From AFM height images, the brush molecules stayed in the cylindrical wormlike state from π = 0.5 mN/m to 30 mN/m (Figure 4.7B,C,D); they were closer to each other at high surface pressures and seemed to become smoother. Unexpectedly, no molecular worms could be clearly visualized by AFM upon expansion, and the bottlebrushes appeared to "fuse" into a featureless film (Figure 4.7E). We repeated the LB and AFM experiments and confirmed the observations.

To summarize the behavior of four heterografted P*n*BA/PDEAEMA brush polymers on the surface of an acidic aqueous solutions in response to lateral compression and decompression, we can see several trends. (i) In contrast to the homografted P*n*BA brushes, all the four heterografted MBBs exhibited a large hysteresis in surface pressure in the first compression-decompression cycle, and the surface pressure did not return to ~ 0 mN/m upon expansion. (ii) With increasing the molar content of PDEAEMA in the side chains, the transition in the π-A isotherm from the rapid increase region to a plateau became weaker and eventually disappeared. (iii) With the increase PDEAEMA side chains in MBBs, the tendency to undergo a unimolecular worm-to-

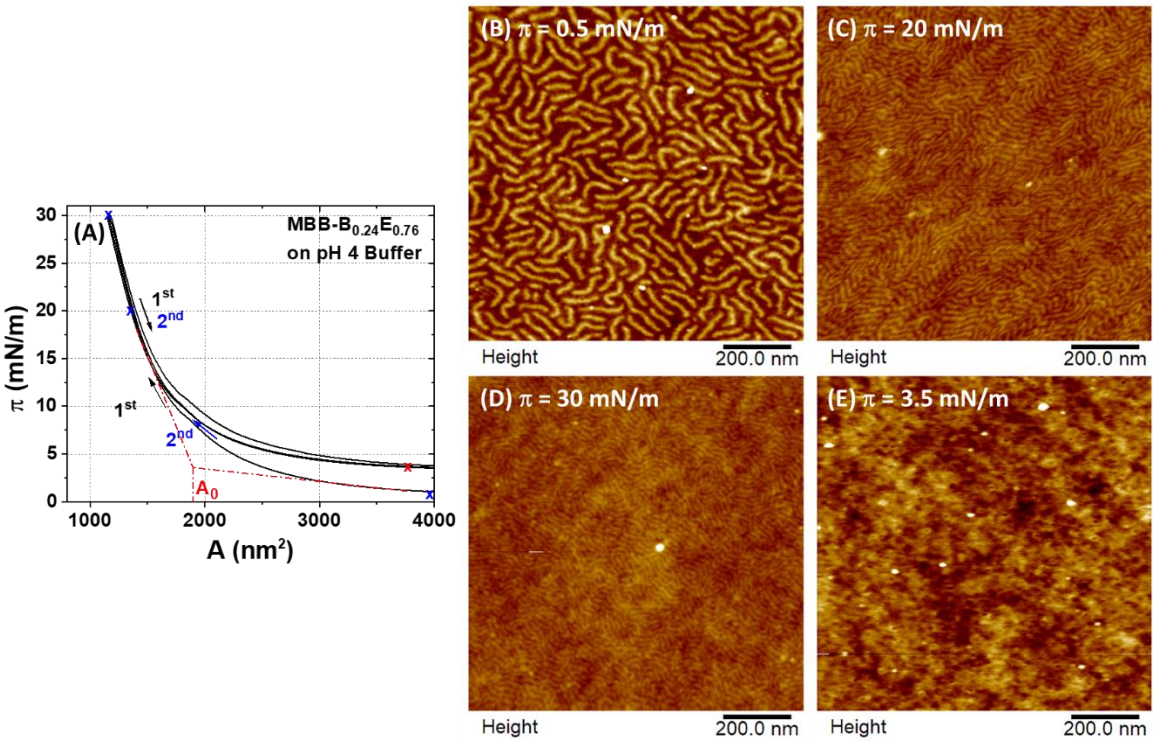

Figure 4.7. (A) Isotherm plots of surface pressure (π) vs mean area per brush (A) from two cycles of compression and expansion for MBB-$B_{0.24}E_{0.76}$ on the surface of a 1.0 mM phosphate buffer aqueous solution with a pH of 4.0 and AFM height images of MBB-$B_{0.24}E_{0.76}$ bottlebrush molecules at different surface pressures: (B) π = 0.5 mN/m, (C) π = 20 mN/m, (D) π = 30 mN/m, and (E) π = 3.5 mN/m.

globule shape transition in response to compression decreases, and the tendency for brush molecules to aggregate initially increases and then decreases. (iv) When the majority of the side chains are P*n*BA, the brush molecules are more likely to undergo reversible individual worm-globule shape transitions with no obvious aggregation. (v) When the molar content of PDEAEMA is sufficiently high, the bottlebrushes showed no tendency to change their shape.

4.3.4. Conformational Behavior of Amphiphilic pH-Responsive Heterografted P*n*BA/PDEAEMA MBBs at the Interface Between Air and a 1.0 mM Aqueous Phosphate Buffer Solution with a pH of 10.0 in Response to Lateral Compression and Expansion

In Chapter 2, we showed that heterografted P*n*BA/PDEAEMA MBBs were effective and efficient pH-responsive emulsion stabilizers. At pH = 4.0, the brushes were tightly bonded to the interface, acting similarly to Janus particles, and stabilized the water-toluene emulsions. When the pH was increased to 10.0, the PDEAEMA side chains of MBBs were deprotonated and became insoluble in water. This caused a decrease in interfacial activity of MBBs, and the brush molecules were only weakly associated with the interface, resulting in the breaking of the emulsions. Considering that nonprotonated PDEAEMA is also amphiphilic, we were interested in how MBBs with P*n*BA and nonprotonated PDEAEMA side chains on the surface of a basic aqueous solution with a pH of 10.0 responded to lateral compression and decompression in a Langmuir-Blodgett trough. To be consistent with the work described in Chapter 2, we adjusted the pH of a 1.0 mM phosphate buffer aqueous solution to 10.0 and poured it into the Langmuir-Blodgett trough as a subphase. A dilute solution of a brush polymer in chloroform was carefully deposited onto the surface of the basic aqueous solution, and then chloroform was allowed to evaporate from the interface.

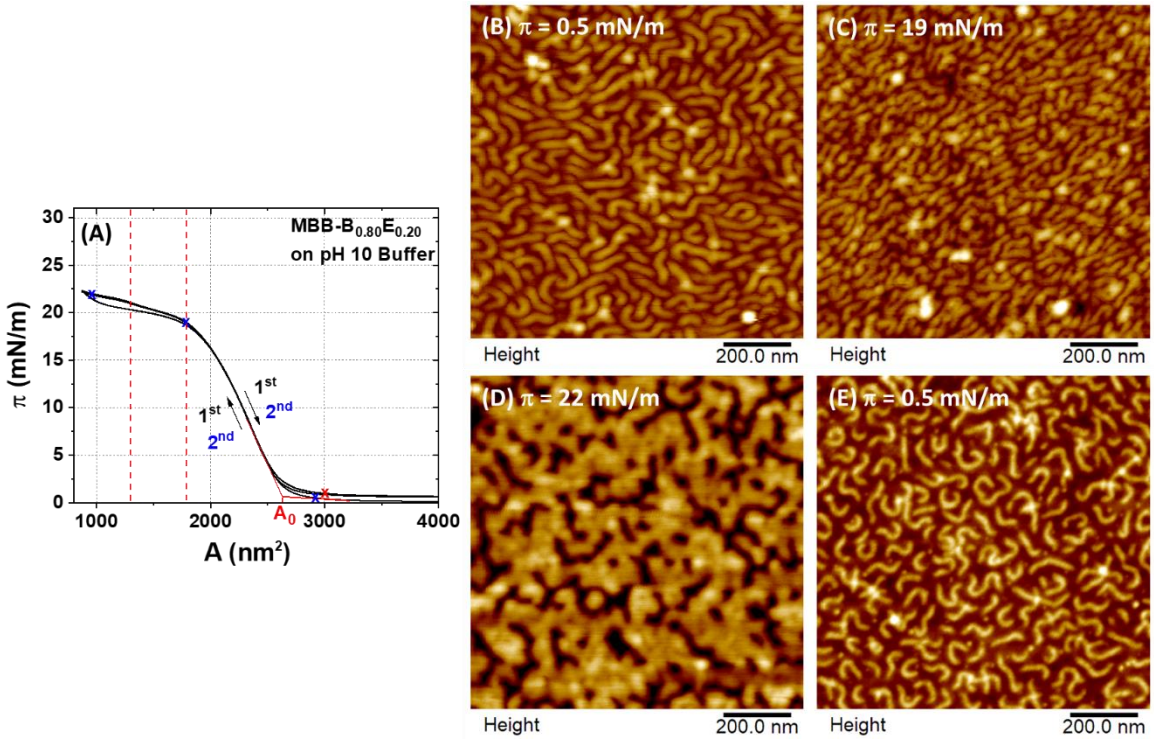

Figure 4.8. (A) LB isotherm plots of surface pressure (π) vs mean area per brush (A) from two cycles of compression and expansion for MBB-$B_{0.80}E_{0.20}$ on the surface of a 1.0 mM phosphate buffer aqueous solution with a pH of 10.0 and AFM height images of MBB-$B_{0.80}E_{0.20}$ bottlebrush molecules at different surface pressures: (B) π = 0.5 mN/m, (C) π = 19 mN/m, (D) π = 22 mN/m, and (E) π = 1.0 mN/m.

Figure 4.8A shows the π-A isotherms of MBB-$B_{0.80}E_{0.20}$ on the surface of the pH 10.0 solution, which are quite similar to that of the same brush polymer on the acidic aqueous solution shown in Figure 4.4A. Two plateaus can be seen at the high surface pressure region, although the transition from the first one to the second is not very pronounced. The value of A_0 was 2600 nm^2/molecule, slightly higher than that (2500 nm^2/molecule) at pH 4.0. A marked difference for the isotherms of MBB-$B_{0.80}E_{0.20}$ at pH = 10.0 from those at pH = 4.0 is the much smaller hysteresis after lateral decompression, although π did not completely decrease to ~ 0 mN/m. This indicates that even on the surface of the pH 10 aqueous solution, the brushes still have a small number of charges, unlike MBB-$B_{1.00}E_{0.00}$ for which the isotherm returned to 0 mN/m. Similarly, at π = 0.5 mN/m, the molecules were wormlike (Figure 4.8B), while at π = 19 mN/m, the bottlebrushes were about to collapse or partially collapsed (Figure 4.8C). When the surface pressure was 22 mN/m (Figure 4.8D), which was at the upper end of the 2nd plateau, the brushes molecules aggregated, likely caused by the overcompression of the brushes at the air-water interface. We will prepare another AFM sample by transferring the molecules onto a glass disk at 20 mN/m, which is in the middle of the 1st plateau, for AFM imaging. Given the similarity of the isotherms at pH = 4.0 and 10.0, we believe that there is a good chance that the brushes are in a globular state at π = 20 mN/m. After the surface pressure was lowered to ~ 0.5 mN/m, the brushes changed back to wormlike (Figure 4.8E).

The π-A isotherms of MBB-$B_{0.64}E_{0.36}$ at pH = 10.0 shown in Figure 4.9A were also similar to those at pH = 4.0. The value of A_0 from extrapolation was 2650 nm^2/brush, larger than that at pH = 4.0 (2470 nm^2/brush). AFM showed that the brushes assumed a cylindrical conformation at π = 0.5 mN/m (Figure 4.9B) and wormlike at π = 20 mN/m upon compression (Figure 4.9C) and π = 2.5 mN/m (Figure 4.9E). However, at the surface pressure of 23 mN/m, the collapsed bottlebrush

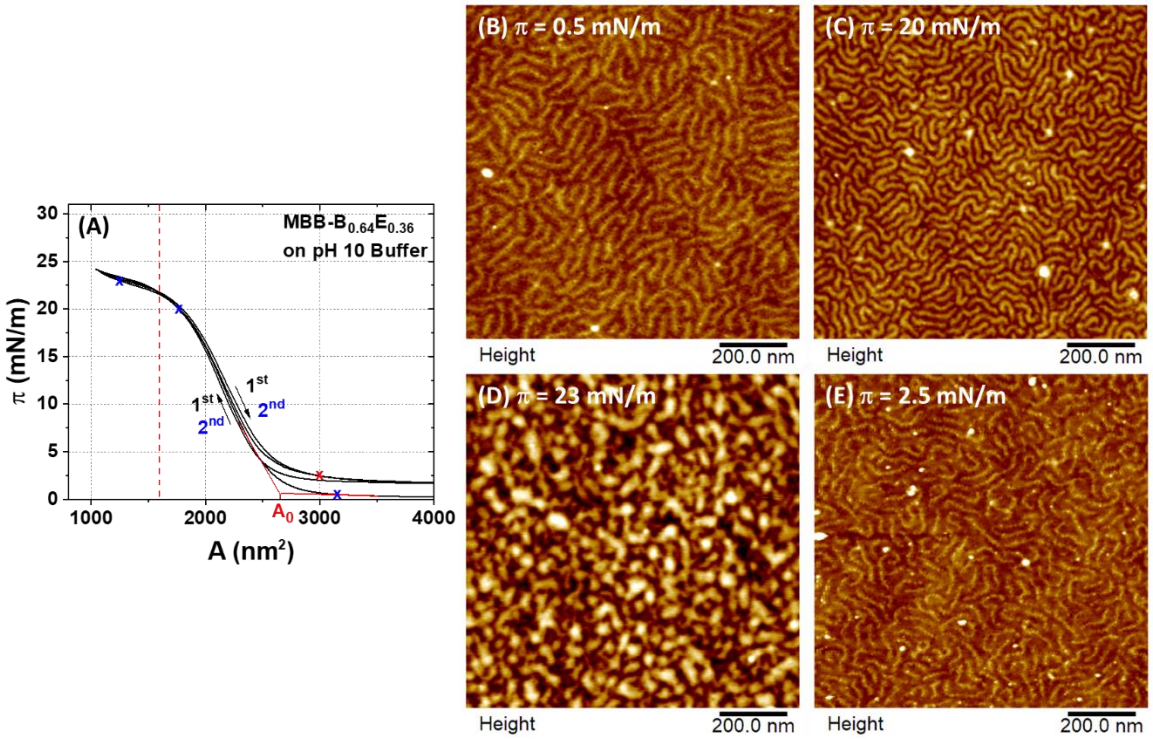

Figure 4.9. (A) Isotherm plots of surface pressure (π) vs mean area per brush (A) from two cycles of compression and expansion for MBB-$B_{0.64}E_{0.36}$ on the surface of a 1.0 mM phosphate buffer aqueous solution with a pH of 10.0 and AFM height images of MBB-$B_{0.64}E_{0.36}$ bottlebrush molecules at different surface pressures: (B) π = 0.5 mN/m, (C) π = 20 mN/m, (D) π = 23 mN/m, and (E) π = 2.5 mN/m.

molecules aggregated (Figure 4.9D), which is different from the same brush polymer at the same surface pressure on the acidic water surface (Figure 4.5D). Considering the observations in Figures 4.8D and 4.9D, the brush polymers seemed to have a greater tendency to undergo aggregation at pH = 10.0 than at pH = 4.0, although both polymers also exhibited a tendency to change the conformation from wormlike to globular.

For MBB-$B_{0.51}E_{0.49}$, the isotherms at pH 10 were also similar to those at pH 4, with a weaker transition from the rapid rise region to the more upward pointing plateau (Figure 4.10A). The brush polymer was wormlike before compression and after decompression as well as at π = 21 mN/m (Figure 4.10B,C,E). When the brush polymer monolayer was compressed to a surface pressure of 24 mN/m, the majority of brush molecules appeared to be in the wormlike state. However, some molecules already started form large aggregates (Figure 4.10D). This is somewhat different from the same polymer at pH of 4.0, where almost all the bottlebrushes changed to globular conformations and some globular molecules aggregated. This once again showed that at pH = 10.0 the heterografted P*n*BA/PDEAEMA brush polymers had a lower tendency to undergo shape transitions but a higher tendency to aggregate.

A large hysteresis was observed for MBB-$B_{0.24}E_{0.76}$ between the two cycles of compression and expansion (Figure 4.11A). However, in each cycle, the hysteresis between compression and decompression was quite small. Similar to the isotherms at pH = 4.0, the surface pressure increased sharply and monotonously upon compression. The onset value of mean surface area per brush (A_0) was hard to determine but was estimated to be 3680 nm^2/molecule from the first cycle. AFM showed no shape transitions upon lateral mechanical compression (Figures 4.11B,C,D), even at a surface pressure of 30 mN/m (Figure 4.11D). Unlike at pH = 4.0, where wormlike molecules could

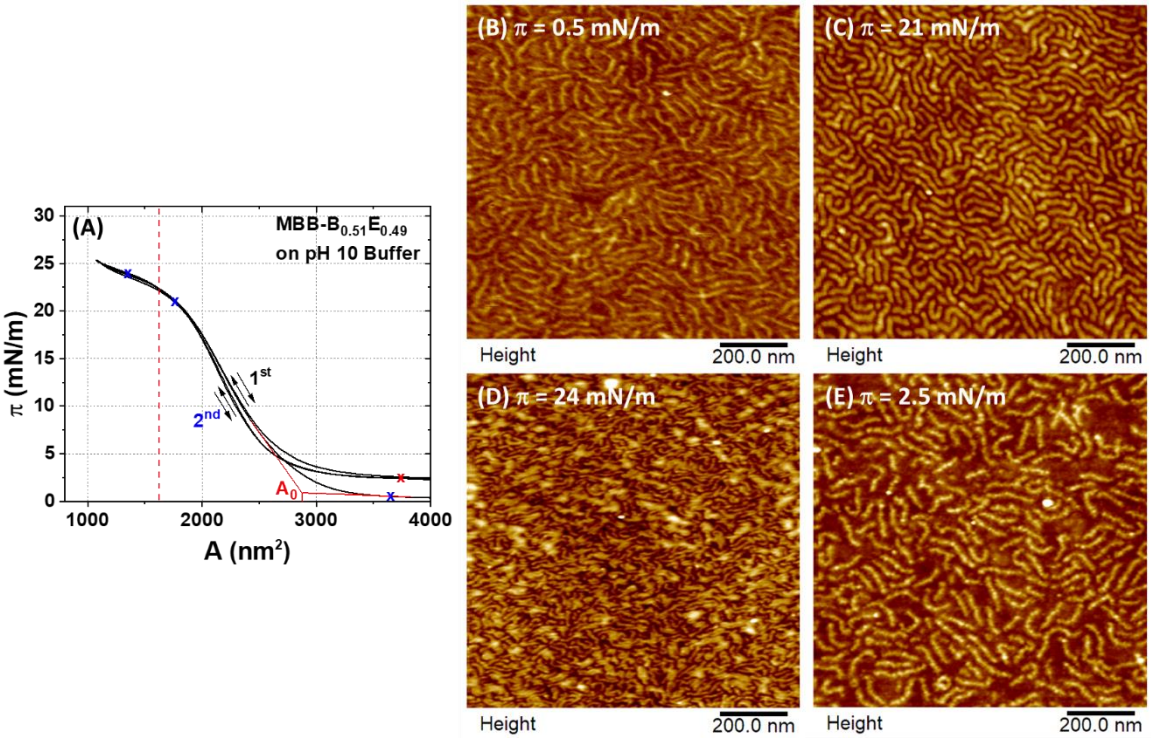

Figure 4.10. (A) Isotherm plots of surface pressure (π) vs mean area per brush (A) from two cycles of compression and expansion for MBB-$B_{0.51}E_{0.49}$ on the surface of a 1.0 mM phosphate buffer aqueous solution with a pH of 10.0 and AFM height images of MBB-$B_{0.51}E_{0.49}$ bottlebrush molecules at different surface pressures: (B) π = 0.5 mN/m, (C) π = 21 mN/m, (D) π = 24 mN/m, and (E) π = 2.5 mN/m.

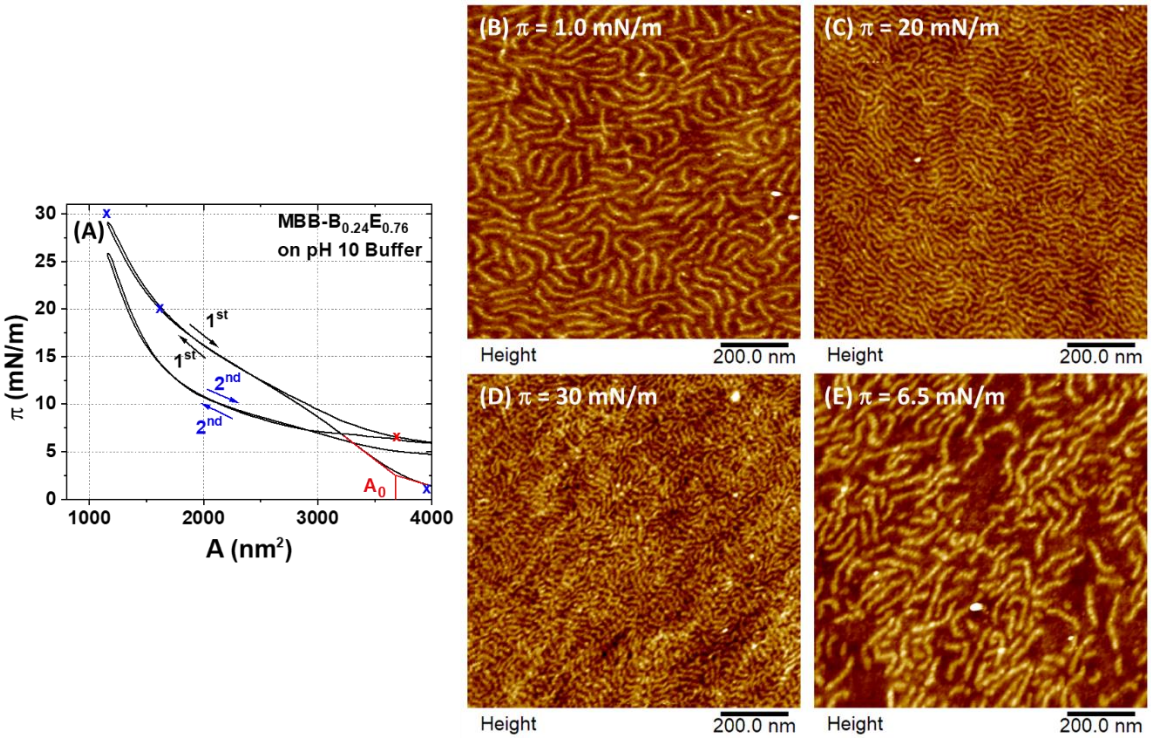

Figure 4.11. (A) Isotherm plots of surface pressure (π) vs mean area per brush (A) from two cycles of compression and expansion for MBB-$B_{0.24}E_{0.76}$ on the surface of a 1.0 mM phosphate buffer aqueous solution with a pH of 10.0 and AFM height images of MBB-$B_{0.24}E_{0.76}$ bottlebrush molecules at different surface pressures: (B) π = 1.0 mN/m, (C) π = 20 mN/m, (D) π = 30 mN/m, and (E) π = 6.5 mN/m.

not be discerned after expansion and likely fused into a featureless film, individual linear brushes can be easily seen after decompression on the basic solution surface (Figure 4.11E).

In summary for this section, a few trends can be seen. (i) Generally, each brush polymer behaved similarly at the two pH values. (ii) The same brush polymer appeared to have a lower tendency to transform from a wormlike to a globular shape but a higher tendency to undergo aggregation.

4.3.5. Conformational Behavior of MBB-$B_{0.00}E_{1.00}$ at Interface between Air and a 1.0 mM Phosphate Aqueous Buffer Solution with pH = 10.0 in Response to Lateral Compression and Decompression in a Langmuir-Blodgett Trough

Since MBB-$B_{0.00}E_{1.00}$, the homografted PDEAEMA bottlebrush polymer, is insoluble in the basic aqueous solution, for comparison, we also investigated the behavior of this brush polymer at the interface of air and a 1.0 mM aqueous phosphate buffer solution with a pH of 10.0. The isotherms from two compression-decompression cycles were found to be similar to those of MBB-$B_{0.24}E_{0.76}$ at pH = 10.0 (see Figures 4.11A and 4.12A). A_0 from the first compression MBB-$B_{0.00}E_{1.00}$ was 3800 nm^2/brush, the largest value seen in this study. AFM revealed no shape transition upon lateral mechanical compression for this brush polymer, same as MBB-$B_{0.24}E_{0.76}$.

4.3.6. Further Discussion on Different Conformational Behavior of MBB-$B_{1.00}E_{0.00}$ and MBB-$B_{0.00}E_{1.00}$ at Air-Aqueous Solution Interfaces in Response to Lateral Compression

While MBB-$B_{1.00}E_{0.00}$ underwent reversible worm-sphere shape transitions on the water surface upon lateral compression as shown in Figure 4.3 and reported in the literature,[26] MBB-$B_{0.00}E_{1.00}$ exhibited no tendency to change the wormlike conformations when compressed on the surface of a 1.0 mM phosphate buffer solution with a pH of 10.0. Given that the reported pK_a value of protonated PDEAEMA is ~ 7.4, there should be very small amount charges on the brushes. (If

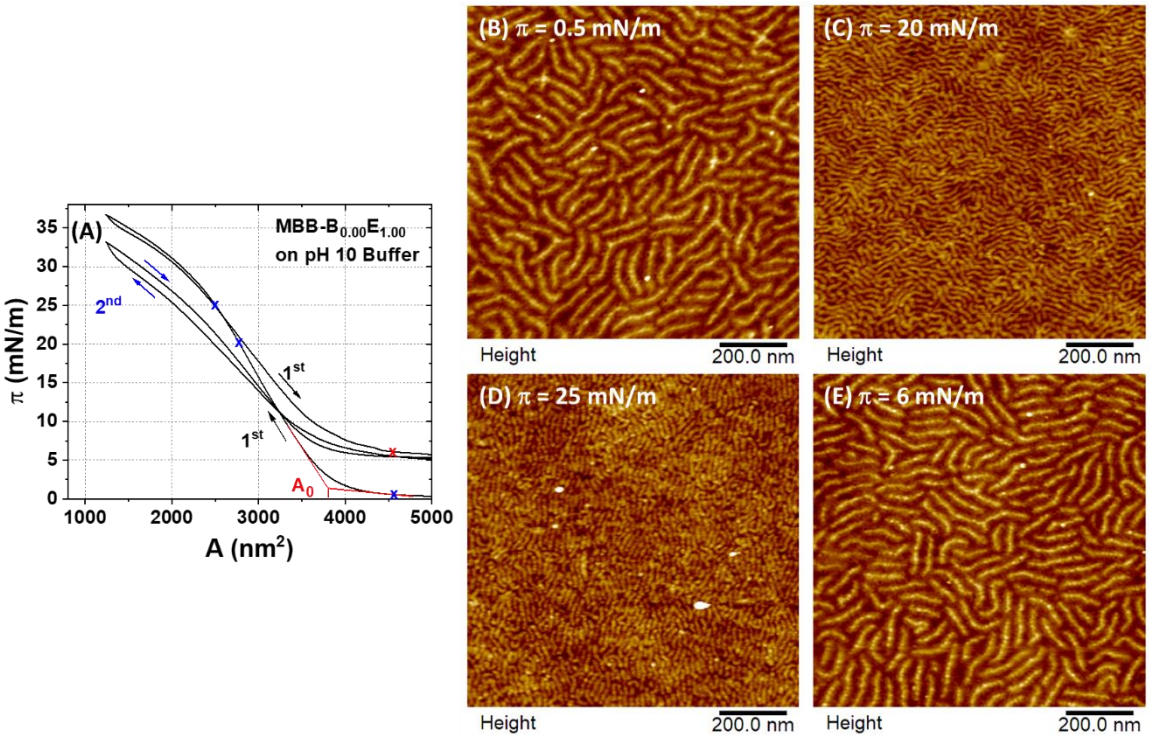

Figure 4.12. (A) Isotherm plots of surface pressure (π) vs mean area per brush (A) from two cycles of compression and expansion for MBB-$B_{0.00}E_{1.00}$ on the surface of a 1.0 mM phosphate buffer aqueous solution with a pH of 10.0 and AFM height images of MBB-$B_{0.00}E_{1.00}$ bottlebrush molecules at different surface pressures: (B) π = 0.5 mN/m, (C) π = 20 mN/m, (D) π = 25 mN/m, and (E) π = 6.0 mN/m after expansion.

the Henderson–Hasselbalch equation can be applied, the molar ratio of nonprotonated to protonated tertiary amine groups at pH = 10.0 would be 398, i.e., 0.25% tertiary amine groups would be charged.) As mentioned earlier, both the ester group and the -$N(C_2H_5)_2$ can have dipole-dipole interactions and hydrogen bonding with water, which likely result in relatively strong attractive forces between PDEAEMA side chains with water, although PDEAEMA is insoluble in the aqueous solution with a pH of 10.0. For P*n*BA bottlebrushes, the desorption of side chains from the water surface, which is essential for the transition to a globular conformation, is facilitated by the rather weak interactions with water because only the ester group in each repeat unit can interact with water and the hydrophobic longer butyl tail points away from the water surface. Thus, PDEAEMA likely has stronger attractive interactions with water than P*n*BA. In addition, the T_g of P*n*BA is significantly below room temperature (~ – 50 °C), which means that P*n*BA has a high mobility. On the other hand, we found from our own experiment that the pure PDEAEMA side chain polymer was glassy at room temperature (~ 20 °C) after drying under high vacuum and therefore has a lower segmental mobility than P*n*BA. Consequently, the homografted PDEAEMA brushes remained in the wormlike state even at rather high degrees of compression. The observed differences in the conformational behavior of MBB-$B_{1.00}E_{0.00}$ and MBB-$B_{0.00}E_{1.00}$ at the air-water interface in response to lateral compression will be useful to us in future design of shape-changing bottlebrush polymers at the interfaces.

4.3.7. Further Discussion on Conformational Behaviors of Four Heterografted P*n*BA/PDEAEMA MBBs at Air-Aqueous Solution Interfaces with Subphase pH of 4.0 and 10.0 in Response to Lateral Mechanical Compression

The A_0 values for the four heterografted brush polymers at pH = 4.0 and 10.0 were estimated from the first compression isotherms and are plotted again the mole fraction of PDEAEMA in the

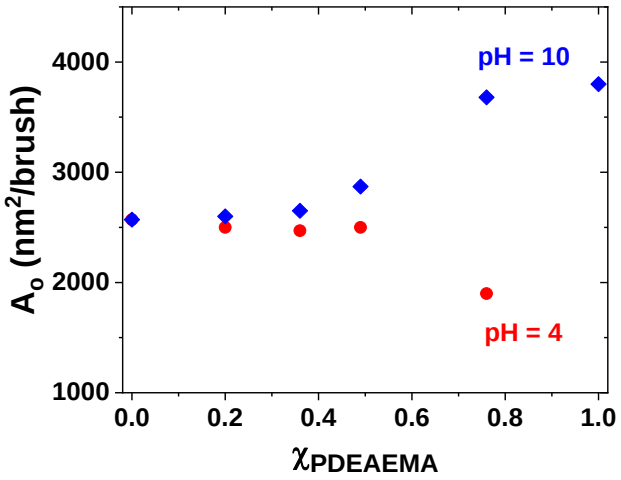

Figure 4.13. Plot of A_0 (nm^2/brush) versus mole fraction of PDEAEMA side chains in the brush polymer.

side chains of each brush polymer (Figure 4.13). Note that the DP of P*n*BA is 51 and the DP of PDEAEMA is 44. The molar mass is 128.17 g/mol for *n*-butyl acrylate and 185.26 g/mol for DEAEMA. Thus, based on the DPs, the calculated $M_{n,cal}$ value is 6537 g/mol for P*n*BA and 8151 g/mol for PDEAEMA, excluding the chain ends from the initiator. At pH = 4.0, A_0 was initially similar when the mole fraction of PDEAEMA ($\chi_{PDEAEMA}$) in the side chains was increased from 0 to 0.49 and then dropped noticeably when $\chi_{PDEAEMA}$ reached 0.76. This is likely because the protonated PDEAEMA side chains were soluble in water and thus extended into the aqueous subphase. When $\chi_{PDEAEMA}$ was < 0.50, the A_0 value was not significantly affected as the P*n*BA side chains were still closely, tightly packed at the air-water interface while spreading on the water surface. At the higher $\chi_{PDEAEMA}$ value of 0.76, the brush molecules can be packed more tightly on the surface of the acidic subphase because of less P*n*BA side chains spreading on the water surface, resulting in a low A_0. In contrast, at pH = 10, A_0 was observed to increase with increasing $\chi_{PDEAEMA}$. Note that the PDEAEMA side chains at pH 10.0 were deprotonated and became insoluble in the basic aqueous solution, and thus all the side chains of P*n*BA and PDEAEMA were located at the interface. The relatively strong interactions with water drove the PDEAEMA side chains to spread on the water surface. The much larger nominal A_0 values for MBB-$B_{0.24}E_{0.76}$ and MBB-$B_{0.00}E_{1.00}$ should be related to the large hysteresis observed in the isotherms; it is possible that the brushes were not packed tightly but formed a percolated two-dimensional network at the air-water interface making A_0 appear to be much larger than expected.

As can be seen from Figure 4.3, P*n*BA side chains can be forced to desorb from the water surface, driving the worm-globule shape transition of the homografted P*n*BA brushes. At pH = 4.0, the PDEAEMA side chains are protonated and water-soluble, causing the homografted PDEAEMA bottlebrushes to be dissolved in the aqueous solution. On the other hand, when the pH

of the aqueous subphase is 10.0, the nonprotonated PDEAEMA side chains spread on the water surface and have a relatively higher affinity toward water than P*n*BA and cannot be forced by lateral compression to desorb from the water surface, making the homografted PDEAEMA bottlebrushes pinned in the wormlike state. Thus, whether heterografted MBBs can undergo worm-globule shape transition on the water surface depends on the competition between the two side chain polymers. However, the situations at pH 4.0 and 10.0 are slightly different and will be further discussed separately in the following.

When the subphase's pH was 4.0, the protonated PDEAEMA side chains extended from the backbone into the subphase and were presumably uniformly distributed in the half-cylindrical region along the backbone on the water side due to the electrostatic repulsive interactions among the charged side chains and the osmotic pressure. When the brush molecules are compressed in the Langmuir-Blodgett trough, the surface area available for each brush molecule is reduced. Some P*n*BA side chains are desorbed from the water surface and coiled up in air. Accordingly, the volume available to each protonated PDEAEMA side chain in water is also reduced, and these charged side chains are forced to be closer to each other and could interdigitate with those from neighboring brush molecules. Consequently, the electrostatic repulsive forces increase, as well as the osmotic pressure. When the mole fraction of PDEAEMA in the side chains is around 0.50 and below, the electrostatic repulsive interactions among the charged side chains and osmotic pressure are not sufficiently large to prevent the coil-up of the backbone and the worm-globule shape transition, as seen from MBB-$B_{0.80}E_{0.20}$, MBB-$B_{0.64}E_{0.36}$, and MBB-$B_{0.51}E_{0.49}$. However, with the increase of the mole fraction of PDEAEMA side chains in MBBs, the transition from the rapid-rise region to the plateau in the LB isotherms occur at a higher surface pressure, i.e., greater compression is needed to drive the conformational transition. Consequently, at a lower $\chi_{PDEAEMA}$,

individual worm-globule shape transition is observed as in the cases of MBB-$B_{0.80}E_{0.20}$ and MBB-$B_{0.64}E_{0.36}$; for MBB-$B_{0.51}E_{0.49}$, the globular bottlebrushes appeare to be more connected, and it becomes more difficult for P*n*BA side chains to spread on the water surface to stabilize individual globular brush molecules. For MBB-$B_{0.24}E_{0.76}$, the coil-up of the backbone is prevented by the very strong electrostatic repulsive forces; the bottlebrushes are compressed to be so close to each other that the charged PDEAEMA side chains are highly interdigitated, resulting in molecules being fused together (Figure 4.7D). After expansion, only a thin film was seen and individual molecules could not be discerned (Figure 4.7E).

At pH = 10.0, both P*n*BA and nonprotonated PDEAEMA side chains are spread on the water surface. MBB-$B_{0.80}E_{0.20}$, MBB-$B_{0.64}E_{0.36}$, and MBB-$B_{0.51}E_{0.49}$ all appear to be more reluctant to change the conformations and show a higher tendency to undergo aggregation. For MBB-$B_{0.80}E_{0.20}$, the brush molecules already become connected at π = 22 mN/m (Figure 4.8D), but some wormlike molecules can still be seen, even though the polymer film might be overcompressed (see Figure 4.8A). Similarly, MBB-$B_{0.63}E_{0.36}$ molecules are more associated with each other at pH = 10.0 than at 4.0 under the same surface pressures (Figures 4.5D and 4.9D). For MBB-$B_{0.63}E_{0.36}$, the vast majority of the molecules are in the wormlike state at π = 24 mN/m, while at pH 4.0 almost all bottlebrushes have changed to globular conformations, though somewhat aggregated. Both MBB-$B_{0.24}E_{0.76}$ and MBB-$B_{0.00}E_{1.00}$ remain in the wormlike state even at very high degrees of compression. This can be attributed to the high affinity of nonprotonated PDEAEMA side chains to water, and consequently lateral compression cannot desorb them from the water interface.

4.4. Conclusions

Using a Langmuir-Blodgett trough and AFM, we systematically investigated the conformational behavior of four amphiphilic pH-responsive heterografted P*n*BA/PDEAEMA bottlebrush polymers of different side chain compositions with $\chi_{PDEAEMA}$ being 0.20, 0.36, 0.49, and 0.76 on the surface of 1.0 mM aqueous phosphate buffer solutions with pH of 4.0 and 10.0 in response to lateral compression and expansion. For comparison, homografted P*n*BA brushes (MBB-$B_{1.00}E_{0.00}$) on Milli-Q water and homografted PDEAEMA brushes (MBB-$B_{0.00}E_{1.00}$) on the surface of the buffer solution with a pH of 10.0 were also studied. No worm-globule conformational changes were observed for all heterografted brush polymers on the air-water interface when the pH of the subphase was changed from 4.0 to 10.0 at a surface pressure of 0.5 mN/m, which was further confirmed by the revelation of a wormlike conformation of MBB-$B_{0.00}E_{1.00}$ on the surface of the pH 10.0 solution. For MBBs on the surface of the aqueous buffer solution with pH 4.0, reversible conformational transitions from wormlike to globular were observed for individual molecular bottlebrushes upon compression when the $\chi_{PDEAEMA}$ was < 0.50, although globular brushes MBB-$B_{0.51}E_{0.49}$ were somewhat more connected with each other. At $\chi_{PDEAEMA}$ = 0.76, i.e., MBB-$B_{0.24}E_{0.76}$, the bottlebrushes remained in the wormlike state. These observations can be attributed to the electrostatic repulsive interactions among protonated PDEAEMA side chains in water hampering the conformational changes of MBBs when $\chi_{PDEAEMA}$ was 0.76. On the surface of the basic aqueous solution, the brushes showed a lower tendency to change the wormlike conformations but a higher tendency to undergo aggregation when $\chi_{PDEAEMA}$ was < 0.50. No conformational transitions and no aggregation were observed for MBB-$B_{0.24}E_{0.76}$ and MBB-$B_{0.00}E_{1.00}$. These can be attributed to the higher affinity of nonprotonated PDEAEMA side chains toward water preventing them from desorbing from the surface. This study revealed

for the first time the conformational behavior of amphiphilic pH-responsive bicomponent heterografted bottlebrush polymers at the air-water interface with different pH values for the subphase. The insight gained here will guide us in future design of stimuli-responsive MBBs for potential applications related to interfaces, such as emulsion and foam stabilizers, surface coating, and lubrication.

References

1. Sheiko, S. S.; Sumerlin, B. S.; Matyjaszewski, K., Cylindrical molecular brushes: Synthesis, characterization, and properties. *Progress in Polymer Science* **2008,** *33* (7), 759-785.
2. Yuan, J.; Müller, A. H. E.; Matyjaszewski, K.; Sheiko, S. S., 6.06 - Molecular Brushes. In *Polymer Science: A Comprehensive Reference*, Matyjaszewski, K.; Möller, M., Eds. Elsevier: Amsterdam, 2012; pp 199-264.
3. Zhang, M.; Müller, A. H. E., Cylindrical polymer brushes. *Journal of Polymer Science Part A: Polymer Chemistry* **2005,** *43* (16), 3461-3481.
4. Zhao, B., Shape-Changing Bottlebrush Polymers. *J Phys Chem B* **2021,** *125* (24), 6373-6389.
5. Li, Z.; Tang, M.; Liang, S.; Zhang, M.; Biesold, G. M.; He, Y.; Hao, S.-M.; Choi, W.; Liu, Y.; Peng, J.; Lin, Z., Bottlebrush polymers: From controlled synthesis, self-assembly, properties to applications. *Progress in Polymer Science* **2021,** *116*, 101387.
6. Zhang, B.; Gröhn, F.; Pedersen, J. S.; Fischer, K.; Schmidt, M., Conformation of Cylindrical Brushes in Solution: Effect of Side Chain Length. *Macromolecules* **2006,** *39* (24), 8440-8450.
7. Haugan, I. N.; Maher, M. J.; Chang, A. B.; Lin, T.-P.; Grubbs, R. H.; Hillmyer, M. A.; Bates, F. S., Consequences of Grafting Density on the Linear Viscoelastic Behavior of Graft Polymers. *ACS Macro Letters* **2018,** *7* (5), 525-530.
8. Daniel, W. F. M.; Burdyńska, J.; Vatankhah-Varnoosfaderani, M.; Matyjaszewski, K.; Paturej, J.; Rubinstein, M.; Dobrynin, A. V.; Sheiko, S. S., Solvent-free, supersoft and superelastic bottlebrush melts and networks. *Nature Materials* **2016,** *15* (2), 183-189.
9. Daniel, W. F. M.; Xie, G.; Vatankhah Varnoosfaderani, M.; Burdyńska, J.; Li, Q.; Nykypanchuk, D.; Gang, O.; Matyjaszewski, K.; Sheiko, S. S., Bottlebrush-Guided Polymer

Crystallization Resulting in Supersoft and Reversibly Moldable Physical Networks. *Macromolecules* **2017,** *50* (5), 2103-2111.

10. Qi, H.; Liu, X.; Henn, D. M.; Mei, S.; Staub, M. C.; Zhao, B.; Li, C. Y., Breaking translational symmetry via polymer chain overcrowding in molecular bottlebrush crystallization. *Nature Communications* **2020,** *11* (1), 2152.
11. Xie, G.; Martinez, M. R.; Olszewski, M.; Sheiko, S. S.; Matyjaszewski, K., Molecular Bottlebrushes as Novel Materials. *Biomacromolecules* **2019,** *20* (1), 27-54.
12. Liberman‐Martin, A. L.; Chu, C. K.; Grubbs, R. H., Application of Bottlebrush Block Copolymers as Photonic Crystals. *Macromolecular Rapid Communications* **2017,** *38* (13), 1700058.
13. Müllner, M., Molecular polymer bottlebrushes in nanomedicine: therapeutic and diagnostic applications. *Chemical Communications* **2022**.
14. Johnson, J. A.; Lu, Y. Y.; Burts, A. O.; Xia, Y.; Durrell, A. C.; Tirrell, D. A.; Grubbs, R. H., Drug-Loaded, Bivalent-Bottle-Brush Polymers by Graft-through ROMP. *Macromolecules* **2010,** *43* (24), 10326-10335.
15. Detappe, A.; Nguyen, H. V. T.; Jiang, Y.; Agius, M. P.; Wang, W.; Mathieu, C.; Su, N. K.; Kristufek, S. L.; Lundberg, D. J.; Bhagchandani, S.; Ghobrial, I. M.; Ghoroghchian, P. P.; Johnson, J. A., Molecular bottlebrush prodrugs as mono- and triplex combination therapies for multiple myeloma. *Nature Nanotechnology* **2023,** *18* (2), 184-192.
16. Banquy, X.; Burdyńska, J.; Lee, D. W.; Matyjaszewski, K.; Israelachvili, J., Bioinspired Bottle-Brush Polymer Exhibits Low Friction and Amontons-like Behavior. *Journal of the American Chemical Society* **2014,** *136* (17), 6199-6202.

17. Adibnia, V.; Olszewski, M.; De Crescenzo, G.; Matyjaszewski, K.; Banquy, X., Superlubricity of Zwitterionic Bottlebrush Polymers in the Presence of Multivalent Ions. *Journal of the American Chemical Society* **2020,** *142* (35), 14843-14847.

18. Faivre, J.; Shrestha, B. R.; Xie, G.; Delair, T.; David, L.; Matyjaszewski, K.; Banquy, X., Unraveling the Correlations between Conformation, Lubrication, and Chemical Stability of Bottlebrush Polymers at Interfaces. *Biomacromolecules* **2017,** *18* (12), 4002-4010.

19. Faivre, J.; Shrestha, B. R.; Xie, G.; Olszewski, M.; Adibnia, V.; Moldovan, F.; Montembault, A.; Sudre, G.; Delair, T.; David, L.; Matyjaszewski, K.; Banquy, X., Intermolecular Interactions between Bottlebrush Polymers Boost the Protection of Surfaces against Frictional Wear. *Chemistry of Materials* **2018,** *30* (12), 4140-4149.

20. Xie, G.; Krys, P.; Tilton, R. D.; Matyjaszewski, K., Heterografted Molecular Brushes as Stabilizers for Water-in-Oil Emulsions. *Macromolecules* **2017,** *50* (7), 2942-2950.

21. Wang, B.; Liu, T.; Chen, H.; Yin, B.; Zhang, Z.; Russell, T. P.; Shi, S., Molecular Brush Surfactants: Versatile Emulsifiers for Stabilizing and Structuring Liquids. *Angewandte Chemie International Edition* **2021,** *60* (36), 19626-19630.

22. Seong, H.-G.; Chen, Z.; Emrick, T.; Russell, T. P., Reconfiguration and Reorganization of Bottlebrush Polymer Surfactants. *Angewandte Chemie International Edition* **2022,** *61* (19), e202200530.

23. Lee, H.-i.; Pietrasik, J.; Sheiko, S. S.; Matyjaszewski, K., Stimuli-responsive molecular brushes. *Progress in Polymer Science* **2010,** *35* (1), 24-44.

24. Sheiko, S. S.; Prokhorova, S. A.; Beers, K. L.; Matyjaszewski, K.; Potemkin, I. I.; Khokhlov, A. R.; Möller, M., Single Molecule Rod−Globule Phase Transition for Brush Molecules at a Flat Interface. *Macromolecules* **2001,** *34* (23), 8354-8360.

25. Boyce, J. R.; Shirvanyants, D.; Sheiko, S. S.; Ivanov, D. A.; Qin, S.; Börner, H.; Matyjaszewski, K., Multiarm Molecular Brushes: Effect of the Number of Arms on the Molecular Weight Polydispersity and Surface Ordering. *Langmuir* **2004,** *20* (14), 6005-6011.

26. Lord, S. J.; Sheiko, S. S.; LaRue, I.; Lee, H.-I.; Matyjaszewski, K., Tadpole Conformation of Gradient Polymer Brushes. *Macromolecules* **2004,** *37* (11), 4235-4240.

27. Sun, F.; Sheiko, S. S.; Möller, M.; Beers, K.; Matyjaszewski, K., Conformational Switching of Molecular Brushes in Response to the Energy of Interaction with the Substrate. *The Journal of Physical Chemistry A* **2004,** *108* (45), 9682-9686.

28. Gallyamov, M. O.; Tartsch, B.; Khokhlov, A. R.; Sheiko, S. S.; Börner, H. G.; Matyjaszewski, K.; Möller, M., Reversible Collapse of Brushlike Macromolecules in Ethanol and Water Vapours as Revealed by Real-Time Scanning Force Microscopy. *Chemistry – A European Journal* **2004,** *10* (18), 4599-4605.

29. Gallyamov, M. O.; Tartsch, B.; Khokhlov, A. R.; Sheiko, S. S.; Börner, H. G.; Matyjaszewski, K.; Möller, M., Real-Time Scanning Force Microscopy of Macromolecular Conformational Transitions. *Macromolecular Rapid Communications* **2004,** *25* (19), 1703-1707.

30. Li, C.; Gunari, N.; Fischer, K.; Janshoff, A.; Schmidt, M., New Perspectives for the Design of Molecular Actuators: Thermally Induced Collapse of Single Macromolecules from Cylindrical Brushes to Spheres. *Angewandte Chemie International Edition* **2004,** *43* (9), 1101-1104.

31. Kent, E. W.; Henn, D. M.; Zhao, B., Shape-changing linear molecular bottlebrushes with dually pH- and thermo-responsive diblock copolymer side chains. *Polymer Chemistry* **2018,** *9* (41), 5133-5144.

32. Henn, D. M.; Fu, W.; Mei, S.; Li, C. Y.; Zhao, B., Temperature-Induced Shape Changing of Thermosensitive Binary Heterografted Linear Molecular Brushes between Extended Wormlike and Stable Globular Conformations. *Macromolecules* **2017,** *50* (4), 1645-1656.

33. Henn, D. M.; Lau, C. M.; Li, C. Y.; Zhao, B., Light-triggered unfolding of single linear molecular bottlebrushes from compact globular to wormlike nano-objects in water. *Polymer Chemistry* **2017,** *8* (17), 2702-2712.

34. Henn, D. M.; Holmes, J. A.; Kent, E. W.; Zhao, B., Worm-to-Sphere Shape Transition of Thermoresponsive Linear Molecular Bottlebrushes in Moderately Concentrated Aqueous Solution. *The Journal of Physical Chemistry B* **2018,** *122* (27), 7015-7025.

35. Kent, E. W.; Zhao, B., Stimuli-Induced Star-Globule Shape Transitions of Dually Responsive Binary Heterografted Three-Arm Star Molecular Brushes in Aqueous Solution. *Macromolecules* **2019,** *52* (17), 6714-6724.

36. Kent, E. W.; Lewoczko, E. M.; Zhao, B., pH- and chaotropic anion-induced conformational changes of tertiary amine-containing binary heterografted star molecular bottlebrushes in aqueous solution. *Polymer Chemistry* **2021,** *12* (2), 265-276.

37. Lewoczko, E. M.; Kelly, M. T.; Kent, E. W.; Zhao, B., Effects of temperature on chaotropic anion-induced shape transitions of star molecular bottlebrushes with heterografted poly(ethylene oxide) and poly(N,N-dialkylaminoethyl methacrylate) side chains in acidic water. *Soft Matter* **2021,** *17* (27), 6566-6579.

38. Kelly, M. T.; Kent, E. W.; Zhao, B., Stepwise Conformational Transitions of Stimuli-Responsive Linear Ternary Heterografted Bottlebrush Polymers in Aqueous Solution. *Macromolecules* **2022**, *55(5),* 1629-1641.

39. Zhou, K.; Wang, Y.; Huang, X.; Luby-Phelps, K.; Sumer, B. D.; Gao, J., Tunable, Ultrasensitive pH-Responsive Nanoparticles Targeting Specific Endocytic Organelles in Living Cells. *Angewandte Chemie International Edition* **2011,** *50* (27), 6109-6114.

40. Henn, D. M.; Wright, R. A. E.; Woodcock, J. W.; Hu, B.; Zhao, B., Tertiary-Amine-Containing Thermo- and pH-Sensitive Hydrophilic ABA Triblock Copolymers: Effect of Different Tertiary Amines on Thermally Induced Sol–Gel Transitions. *Langmuir* **2014,** *30* (9), 2541-2550.

Appendix C

for

Chapter 4. Conformational Behavior of Tertiary Amine-Containing Binary Heterografted Molecular Bottlebrushes at Planar Air-Water Interfaces In Response to Lateral Compression and pH Changes

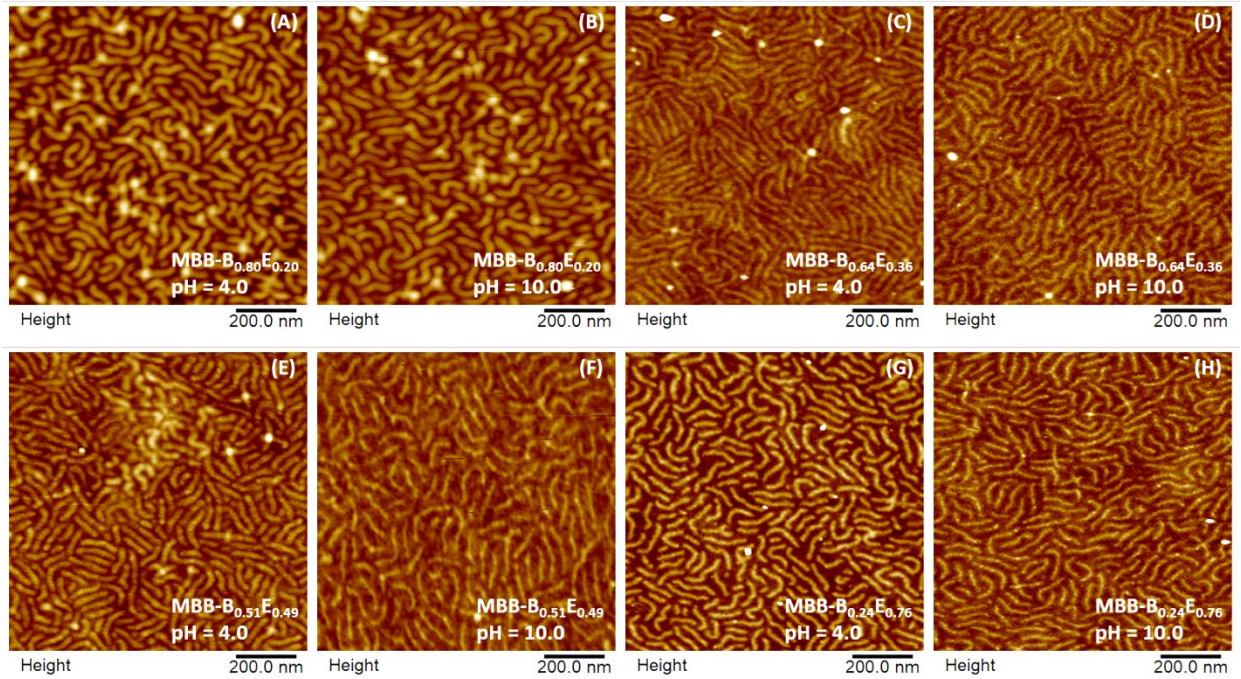

Figure C1. Additional AFM height images of MBB-$B_{0.80}E_{0.20}$ (A,B), MBB-$B_{0.64}E_{0.36}$ (C,D), MBB-$B_{0.51}E_{0.49}$ (E,F), MBB-$B_{0.24}E_{0.76}$ (G,I) transferred onto "Piranha" solution-cleaned glass disks from the interface between air and a 1.0 mM aqueous phosphate buffer solution with a pH of 4.0 (A,C,E,G) or 10.0 (B,D,F,I) at a surface pressure of 0.5 mN/m using a Langmuir-Blodgett trough.

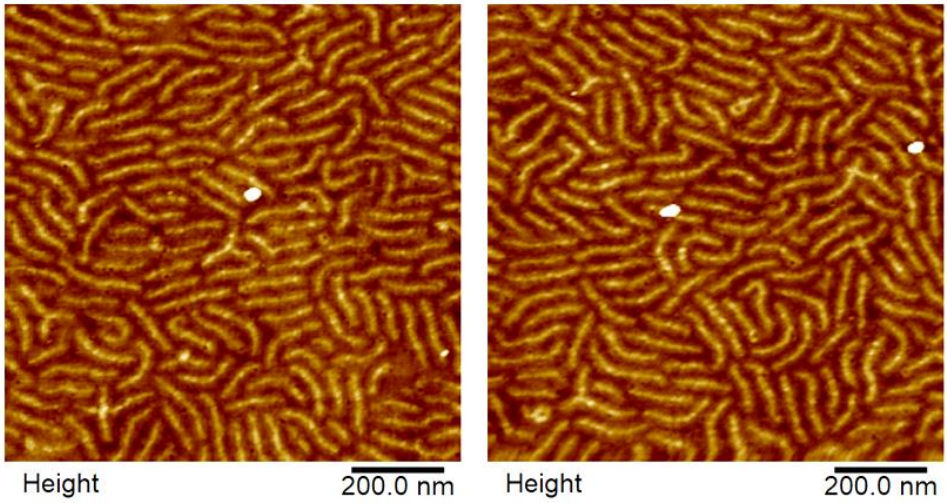

Figure C2. Additional AFM height images of homografted MBB-$B_{0.00}E_{1.00}$ transferred to a "Piranha" solution-cleaned glass disk from the interface between air and a 1.0 mM phosphate aqueous buffer solution with a pH of 10.0 at a surface pressure of 0.5 mM/m using a Langmuir-Blodgett trough.

Chapter 5. Stepwise Conformational Transitions of Stimuli-Responsive Linear Ternary Heterografted Bottlebrush Polymers in Aqueous Solution

The work presented in this chapter has been published as a journal article in *Macromolecules* **2022**, *55* (5), 1629–1641. I synthesized all the side chain and molecular bottlebrush polymers presented in this work and performed all the corresponding molecular and physical characterizations. Coauthor Dr. Ethan W. Kent synthesized and characterized the azide functionalized backbone and provided feedback on the manuscript. Prof. Bin Zhao advised this work.

Abstract

Stepwise conformational transitions of molecular bottlebrushes (MBBs) from extended wormlike to partially collapsed and stable globular in aqueous solution were realized with the use of two distinct stimuli-responsive polymers and poly(ethylene oxide) (PEO) as the side chains, where PEO served as a stabilizer when the responsive side chains became insoluble. Three dually responsive brush polymers, composed of either two distinct pH-responsive or two different thermoresponsive or one pH- and one thermoresponsive polymers along with PEO randomly grafted on the backbone polymer, were synthesized by a click grafting to method. Dynamic light scattering studies showed that all three brush polymers displayed two successive steplike size transitions in aqueous solutions in response to application of external stimuli, with overall size decreases of 27 – 29 %. ^{1}H NMR spectroscopy analysis confirmed that the size transitions of MBBs originated from the pH-induced soluble-to-insoluble and/or the temperature-triggered lower critical solution temperature transitions of responsive side chain polymers in the brushes. Atomic force microscopy revealed stepwise conformational changes from extended wormlike (with and without a pearl-necklace morphology) to partially collapsed (shrunken wormlike or wavelike or C-/S-shaped) and globular nano-objects stabilized by PEO side chains. As a demonstration of

potential applications, Nile Red was encapsulated in the dually pH-responsive globular MBBs as a hydrophobic model drug and its stepwise release was achieved upon gradually decreasing pH.

5.1. Introduction

Molecular bottlebrushes (MBBs), also termed bottlebrush polymers, are a special type of graft copolymers in which relatively short polymer chains are covalently grafted on a long backbone polymer with a sufficiently high grafting density that the backbone is forced to take on stretched conformations.[1-6] These architecturally complex polymers have attracted considerable attention in the past years, and their potential applications have been demonstrated in a wide variety of areas, including drug delivery,[7,8] photonic crystals,[9-11] supersoft elastomers,[12] biological tissue-inspired advanced organic materials,[13] and surface coating for lubrication.[14] Due to the dense grafting of macromolecular side chains, MBBs exhibit many intriguing characteristics and behavior, including high persistence length, no backbone entanglement, large conformational changes (i.e., shape transitions), and unusual crystal habit.[1-6,15] Among these, stimuli-triggered shape transitions of MBBs are particularly interesting.[2,3,6] While bottlebrush polymers adopt a cylindrical or wormlike shape under conditions favorable for side chains (e.g., in good solvents), they can exhibit pronounced and abrupt shape changes and take on different conformations (e.g., spherical) when the interactions of the side chains with the environment become unfavorable. Shape-changing MBBs may find applications in areas such as delivery of substances, regulation of molecular interactions, and templated synthesis of nanomaterials with controlled morphologies.[6,8,16]

Stimuli-induced shape transitions of MBBs from wormlike to globular or from starlike to disklike were demonstrated at interfaces.[17-21] Sheiko and coworkers showed that linear and star MBBs with homografted poly(*n*-butyl acrylate) (P*n*BA) side chains underwent reversible rod-to-sphere and star-to-disk shape transitions, respectively, at the air-water interface by lateral compression and decompression.[17,18] MBBs with stimuli-responsive polymers as the side chains can undergo shape transitions in solution in response to environmental stimuli, which are more

relevant to potential applications. A variety of stimuli-responsive polymers, including thermosensitive water-soluble polymers, pH- and light-responsive polymers as well as polyelectrolytes, have been employed to construct stimuli-responsive MBBs.[6,16,22-36] Li et al. reported that thermosensitive MBBs with poly(*N*-isopropylacrylamide) (PNIPAm) side chains collapsed from a wormlike to a globule shape upon heating from below to above the lower critical solution temperature (LCST) of PNIPAm.[22] The collapsed globular PNIPAm MBBs, however, were unstable at high temperatures; the brush molecules were found to aggregate and eventually precipitate out from water. Polyelectrolyte MBBs can change their conformations in water in response to the addition of surfactants, salts, and oppositely charged polyelectrolytes.[28-31] For example, unusual helical conformations of MBBs with polyelectrolyte side chains were found in highly dilute aqueous solutions upon the addition of multivalent ions or surfactants.[28,29] Multiple wormlike-globular shape transitions for cationic MBBs with quaternary ammonium polyelectrolyte side chains in dilute aqueous solutions were observed when sodium dodecyl sulfate (SDS), β-cyclodextrin, and 1-adamantylammonium chloride were added sequentially into the solution.[30] However, at a slightly higher concentration (e.g., 1 mg/mL), the bottlebrush polymer precipitated out immediately after the addition of SDS.

The collapsed globular MBBs in solution can be stabilized against aggregation by introducing a second polymer into the side chains, either as a second set of side chains in heterografted brushes or as the outer block of block copolymer side chains in homografted MBBs.[6,8,16,37-44] When the responsive side chains or the inner blocks of bicomponent MBBs become insoluble in water, driving the shape transitions from worm- or starlike to globular, the second polymer in the side chains serves as a stabilizer. The resultant core-shell globular nano-objects are in fact unimolecular spherical micelles. If the binary heterografted brush polymers are composed of two distinct types

of stimuli-responsive polymeric side chains, two stable globular states with different polymers in the core can be obtained under different conditions.[40] Our bicomponent MBBs were synthesized by a grafting to method using the highly efficient copper(I)-catalyzed alkyne-azide cycloaddition (CuAAC) click reaction to graft alkyne-end-functionalized polymers onto an azide-functionalized backbone polymer.[6,16,37-42] This approach is modular,[8,16,37-42,45-50] allowing for separate synthesis and characterization of backbone and side chain polymers, simultaneous incorporation of different polymers into the side chains, and facile tuning of the molar ratios of different side chain polymers.

In the present work, we show that stepwise conformational transitions of linear MBBs from wormlike to partially collapsed and globular can be achieved with the use of two distinct stimuli-responsive polymers along with poly(ethylene oxide) (PEO) as the side chains. PEO is introduced to stabilize the brush molecules against aggregation when the responsive side chains become insoluble.[16] Three dually responsive linear ternary MBBs were constructed by the click grafting to method using thermosensitive poly(ethoxydi(ethylene glycol) acrylate) (PDEGEA) with an LCST of 9 °C,[51,52] thermosensitive poly(methoxydi(ethylene glycol) acrylate) (PDEGMA) with an LCST of 38 °C,[53] pH-responsive poly(2-(*N*,*N*-diethylamino)ethyl methacrylate) (PDEAEMA) with a pK_a of 7.4, and pH-responsive poly(2-(*N*,*N*-di(*n*-butyl)amino)ethyl methacrylate) (PDBAEMA) with a pK_a of 5.1,[54,55] along with 5 kDa PEO (Scheme 5.1). The three ternary MBB samples are: (i) MBB-PP composed of PEO and two pH-responsive polymers (PDEAEMA and PDBAEMA), (ii) MBB-TT consisting of PEO and two thermoresponsive polymers (PDEGEA and PDEGMA), and (iii) MBB-TP comprising PEO and two different stimuli-responsive polymers (PDEGEA and PDEAEMA) as the side chains, where T and P represent a thermosensitive and a pH-responsive polymer, respectively. The stimuli-induced conformational changes of these MBBs in aqueous solutions were studied by dynamic light scattering (DLS), ^{1}H NMR spectroscopy analysis, and

Scheme 5.1. Synthesis of Dually Responsive Linear Ternary Heterografted Molecular Bottlebrushes, MBB-PP, -TT, and -TP, and Stimuli-Induced Stepwise Collapse in Aqueous Solution

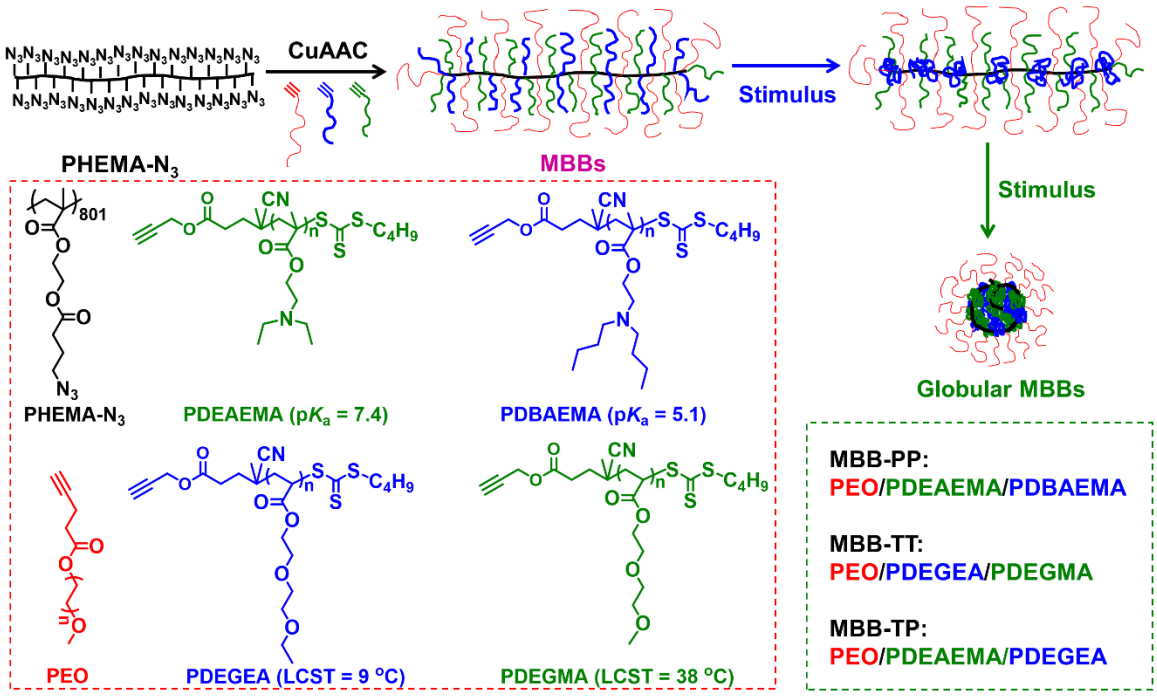

atomic force microscopy (AFM). In addition, as a demonstration of potential applications, MBB-PP was used to encapsulate Nile Red in the globular form, and stepwise release of this hydrophobic model drug from the collapsed globular brushes was achieved upon gradually decreasing pH.

5.2. Experimental Section

See Appendix D.

5.3. Results and Discussion

5.3.1. Synthesis and Characterization of Dually Responsive Ternary MBBs

Three linear MBBs composed of randomly grafted 5 kDa PEO and two stimuli-responsive polymers were prepared by a grafting-to approach via the CuAAC reaction (Scheme 5.1). This method is particularly suitable for the preparation of multicomponent brush polymers, which not only can produce high grafting density brushes but also allows for convenient tuning of the side chain composition. Stimuli-responsive alkyne-end-functionalized side chain polymers, PDEAEMA, PDBAEMA, PDEGEA, and PDEGMA (Scheme 5.1), were prepared by reversible addition-fragmentation chain transfer (RAFT) polymerization[56] of respective monomers in anisole using an alkyne-functionalized trithiocarbonate compound (CTA-Alkyne, Figure D1) as the chain transfer agent and 2,2′-azobis(2-methylpropionitrile) as the initiator. The details can be found in Appendix D, and the characterization data for all side chain polymers are summarized in Table 5.1. Size exclusion chromatography (SEC) analysis showed that the dispersities ($Đ$) of these polymers were in the range of 1.12 to 1.16 with a unimodal peak (Figures D2-D6), indicating that the RAFT polymerizations were well controlled. The degrees of polymerization (DPs) of these polymers were in the range of 43 to 57, calculated from the monomer conversions determined by ^{1}H NMR spectroscopy analysis and the initial molar ratios. Alkyne-end-

Table 5.1. Characterization Data for Side Chain Polymers Used for Synthesizing MBBs

Side Chain Polymer	Molecular Weight	*Đ*	DP
PEO	M_n = 5 kDa [a]	1.04 [b]	114 [c]
PDEAEMA-45	$M_{n,SEC}$ = 6.9 kDa [d]	1.14 [d]	45 [e]
PDEAEMA-56	$M_{n,SEC}$ = 7.8 kDa [d]	1.14 [d]	56 [e]
PDBAEMA	$M_{n,SEC}$ = 9.9 kDa [d]	1.12 [d]	43 [e]
PDEGEA	$M_{n,SEC}$ = 10.3 kDa [d]	1.16 [d]	57 [e]
PDEGMA	$M_{n,SEC}$ = 9.3 kDa [d]	1.15 [d]	55 [e]

[a] Molecular weight from the vendor. [b] Dispersity (*Đ*) was determined by a PL-GPC 20 system relative to polystyrene standards. [c] Degree of polymerization (DP) was calculated from the M_n. [d] Number-average molecular weight ($M_{n,SEC}$) and *Đ* were determined using a PL-GPC 20 system relative to polystyrene standards. [e] Calculated from the initial monomer-to-CTA molar ratio and the monomer conversion.

functionalized PEO was synthesized by reacting 5 kDa poly(ethylene oxide) monomethyl ether with 4-pentynoic acid using 1-(3-dimethylaminopropyl)-3-ethylcarbodiimide hydrochloride and 4-(dimethylamino)pyridine as the catalysts.[16] The linear azide-functionalized backbone polymer with a DP of 801 and a degree of azide functionalization of 96.7%, PHEMA-N_3, was prepared by atom transfer radical polymerization of 2-(trimethylsilyloxy)ethyl methacrylate and post-polymerization modifications, including the deprotection of trimethylsilyl groups, reaction with 4-bromobutyryl chloride, and substitution of pendant bromine atoms with azide, as described previously.[50]

The click reactions for the synthesis of the three brush polymers were carried out in tetrahydrofuran (THF) at ambient temperature using CuCl and *N*,*N*,*N*′,*N*″,*N*‴-pentamethyldiethylenetriamine as the catalyst and ligand, respectively. In order to achieve high grafting density MBBs, excess side chain polymers were employed with a feed molar ratio of ~ 1.5 : 1 for the side chain polymers to the azide groups. At the end of the click reaction, benzyl propargyl ether was added to cap the possible remaining unreacted azide groups on the backbone to mitigate potential issues in the subsequent purification and study. The MBBs were purified by a combination of precipitation/fractionation and centrifugal filtration using an Amicon 50 kDa MWCO filter. The complete removal of excess side chain polymers from the MBBs was confirmed by SEC analysis (Figures D7-D9), and ^{1}H NMR analysis showed that the molar ratios of different side chain polymers in the purified brushes were similar to the feed ratios. Using the SEC peak area percentages of the brushes and the unreacted side chain polymers in the final reaction mixture and the side chain composition from ^{1}H NMR analysis along with the feed masses and the DPs of the side chain polymers, the grafting densities of MBB-TT and MBB-TP were estimated to be 93.0% and 90.4%, respectively. The absolute $M_{w,expt}$ values of these two brush polymers measured

by a SEC-multiangle light scattering (SEC-MALS) system were 7.92×10^6 Da and 7.81×10^6 Da, respectively, which were close to the calculated $M_{w,calc}$ values, 7.51×10^6 Da and 7.29×10^6 Da, based on the grafting densities and the calculated $M_{w,calc}$ values of the backbone and the side chain polymers (M_n calculated from DP × $Đ$). The grafting density of MBB-PP, however, could not be estimated by the above method because PDBAEMA was insoluble in DMF. SEC-MALS analysis of purified MBB-PP in DMF, prepared by gradually adding DMF into a dilute THF solution of MBB-PP and then evaporating the solvents to an appropriate concentration, showed that the $M_{w,expt}$ of MBB-PP was 7.13×10^6 Da (Figure D10), similar to the $M_{w,expt}$ values of MBB-TP and -TT. This $M_{w,expt}$, however, is higher than the calculated $M_{w,calc}$ value for a hypothetical brush polymer with the same side chain composition and a full grafting density (i.e., 96.7% - the degree of azide functionalization) ($M_{w,calc} = 6.38 \times 10^6$ Da, see Appendix D), which could be due to the loss of lower molecular weight brush molecules during the purification. The characterization data for the three bottlebrush polymers are summarized in Table 5.2 along with the aforementioned calculated values.

5.3.2. pH-Induced Stepwise Conformational Transitions of MBB-PP in Aqueous Solution

MBB-PP is composed of 51.0 mol% PEO and two different pH-responsive polymers, 29.2 mol% PDEAEMA-45 (DP = 45) with a pK_a of 7.4 and 19.8 mol% PDBAEMA with a pK_a of 5.1,[54,55] densely and randomly grafted on the backbone polymer as the side chains. The two tertiary-amine-containing polymethacrylates are insoluble in water at pH > pK_a and undergo soluble-insoluble transitions in different pH ranges. Figure 5.1A shows the plot of the apparent hydrodynamic diameter (D_h) of 0.2 mg/g MBB-PP in a 25 mM phosphate buffer at 25 °C versus pH. At pH = 3.50, the D_h was 80.8 nm. Upon increasing pH, two steplike size-reduction transitions

Table 5.2. Characterization Data and Calculated Values for MBBs

MBBs	Side Chain Polymer 1 and Molar Percentage [a]	Side Chain Polymer 2 and Molar Percentage [a]	Side Chain Polymer 3 and Molar Percentage [a]	Grafting Density [b]	$M_{w,expt.}$ [c] (Da)	$M_{w,calc.}$ [d] (Da)
MBB-PP	PEO, 51.0%	PDEAEMA-45, 29.2%	PDBAEMA, 19.8%	NA	7.13×10^6	6.38×10^6 (for a grafting density of 96.7%)
MBB-TT	PEO, 34.4%	PDEGEA, 32.9%	PDEGMA, 32.7%	93.0%	7.92×10^6	7.51×10^6
MBB-TP	PEO, 40.4%	PDEGEA, 32.2%	PDEAEMA-56, 27.4%	90.4%	7.81×10^6	7.29×10^6

[a] Molar percentages of side chain polymers of MBBs were determined by ^{1}H NMR analysis. [b] Grafting density was estimated using the SEC data, feed masses, and side chain composition. [c] Experimental absolute M_w ($M_{w,expt}$) was measured using a SEC-MALS system. [d] Calculated absolute M_w ($M_{w,calc}$) was obtained by considering the M_w values of the azide-carrying backbone and side chain polymers, calculated from DPs and dispersities ($M_{n,calc} \times Đ$), and the grafting density.

were observed. The first one occurred in the pH range of 4.50 (D_h = 79.4 nm) to 5.26 (D_h = 71.8 nm), around the pK_a of PDBAEMA, which was attributed to the collapse of PDBAEMA side chains caused by the deprotonation of the pendant charged di(*n*-butyl)aminoethyl groups. This was followed by a plateau in the pH range from ~5.3 to ~6.0, where the size decreased only slightly. The second transition was observed at pH = ~7.0; the D_h decreased from 68.5 nm at pH = 6.50 to 60.3 nm at pH = 7.50 and leveled off to 57.5 nm at pH = 9.50. The overall size change from pH 3.50 to 9.50 was 23.3 nm (~29%), i.e., the hydrodynamic volume decreased by 64.0%. The size transitions were reversible; decreasing the pH to 8.00, 5.98, and 4.00 resulted in D_h values right on the curve (Figure 5.1A). Throughout the processes of changing pH, the hydrodynamic size distributions were unimodal and narrow as can be seen from the three curves shown in the inset of Figure 5.1A. We note here that without PEO as a stabilizer, MBBs with homografted PDEAEMA side chains precipitated out immediately at pH > pK_a.[39]

^{1}H NMR spectroscopy was employed to confirm that the steplike size transitions observed from DLS measurements were driven by the solubility changes of the two pH-responsive side chain polymers. As shown in Figure 5.1B, the peak of -$CH_2CH_2CH_2CH_3$ from PDBAEMA at ~1.0 ppm was visible at pH 3.50 but nearly disappeared at pH 5.00, which matched the first transition observed by DLS (Figure 5.1A). Note that the disappearance or the decrease in intensity of the peak in the NMR spectra is caused by the loss of mobility.[40] With further increasing pH, the peak of -CH_2CH_3 from PDEAEMA at ~ 1.4 ppm decreased significantly in intensity at pH = 7.00 and completely disappeared at pH = 8.00, corresponding to the second size reduction transition from DLS measurements.

AFM was performed to study the morphologies of the brushes at different pH values. The samples were prepared by spin casting the phosphate buffer solutions of 0.050 mg/g MBB-PP at

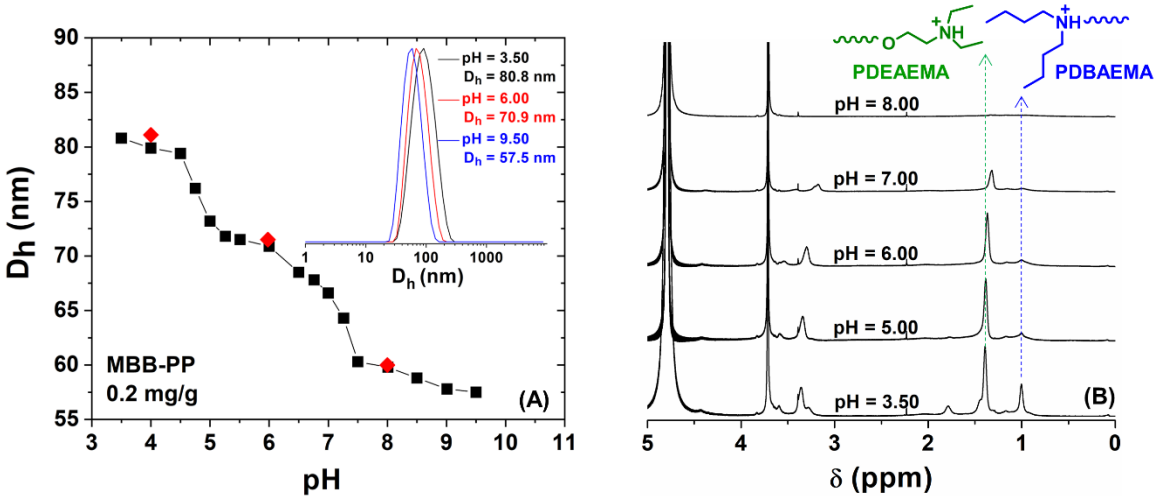

Figure 5.1. (A) Apparent hydrodynamic diameter (D_h) of 0.2 mg/g MBB-PP in a 25 mM phosphate buffer at 25 °C upon increasing pH. The three red diamond data points were collected from the process of decreasing pH from pH = 9.50. The inset shows hydrodynamic size distributions of MBB-PP at pH values of 3.50, 6.00, and 9.50. (B) ^{1}H NMR spectra of 4.0 mg/g MBB-PP in a 10 mM phosphate buffer prepared using D_2O at various pH values. The ^{1}H NMR spectra were normalized against the HDO peak at 4.79 ppm.

pH 4.00, 6.00, and 9.50 on PMMA-coated mica disks at room temperature. At pH = 4.00, MBB-PP assumed wormlike conformations with a pearl-necklace morphology comprising a string of beads along the backbone (Figures 5.2A and C5.11). The height, length, and width of a representative bead marked by an arrow in Figure 5.2A were 3.0, 23.7, 19.1 nm, respectively. Image analysis showed that the average length of 131 brush molecules was 171.1 ± 42.6 nm, which represents a degree of stretching of 85% considering the maximum length of the brushes with a backbone DP of 801. The high degree of stretching can be attributed to the repulsive electrostatic interactions between protonated side chains. The pearl-necklace morphology presumably resulted from the microphase separation between protonated PDEAEMA and PDBAEMA and neutral PEO side chains. Similar pearl-necklace morphologies were reported in the literature for bicomponent MBBs, either with homografted core-shell diblock copolymer side chains or heterografted two distinct homopolymer side chains,[40,50,57,58] and we are not aware of MBBs with one-component homopolymer side chains exhibiting such a morphology. When the solution pH was raised to 6.00 at which PDBAEMA side chains became insoluble in water and PDEAEMA was still protonated, the pearl-necklace morphology was maintained for longer brush molecules, whereas shorter brushes appeared to transform into a roughly globular or short rodlike shape (Figures 5.2B and C5.12). The height, length, and width of the representative bead marked with an arrow in Figure 5.2B were slightly larger (3.8, 25.4, and 25.1 nm, respectively). The average length of 144 brush molecules was 110.9 nm ± 44.3 nm, significantly shorter than that at pH = 4.00 (171.1 ± 42.6 nm) due to the collapse of PDBAEMA side chains. Further increasing the pH to 9.50 caused all of the brushes to collapse into globules (Figures 5.2C and D13), with an average diameter of 48.9 ± 9.3 nm from the measurements of 75 MBB molecules (two measurements for each in perpendicular

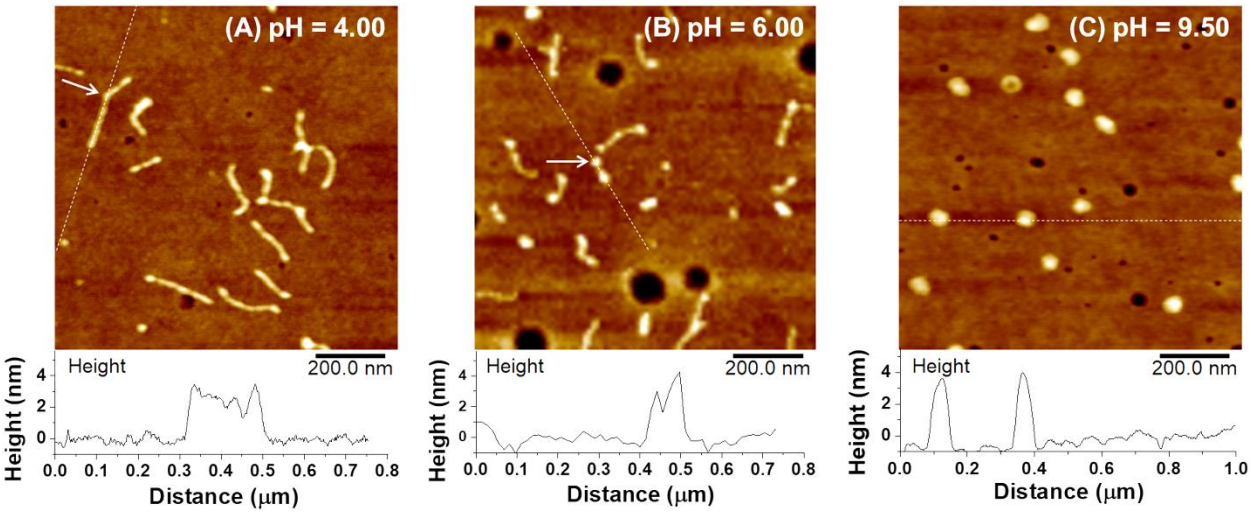

Figure 5.2. AFM height images of MBB-PP spin cast on PMMA-coated mica from a 0.050 mg/g solution of MBB-PP in a 10 mM phosphate buffer with a pH of 4.00 (A), 6.00 (B), and 9.50 (C). The plot in the bottom of each image shows the cross-sectional profile along the dashed line.

directions) and a representative height of 5 nm. The results from the AFM study were consistent with the large size drops observed from the DLS study when the pH was increased from 4.00 (D_h = 79.9 nm) to 6.00 (70.9 nm) and 9.50 (D_h = 57.5 nm). Note that even when the height of globular MBB-PP brushes at pH = 9.50 from the AFM study was ~ 5 nm, the average diameter (48.9 nm) was still smaller than the D_h from the DLS measurements (57.5 nm); we believe that this is because the hydrophilic 5 kDa PEO side chains remained well solvated in the solution. We also note here that the morphologies of MBBs observed by AFM in the dry state can be different from those in the solution. Nevertheless, all the AFM samples were prepared on PMMA-coated mica using the same spin-casting process.

5.3.3. Temperature-Induced Stepwise Conformational Transitions of MBB-TT in Aqueous Solution

MBB-TT contained two thermoresponsive polymers, 32.9 mol% PDEGEA with an LCST of 9 °C and 32.7 mol% PDEGMA with an LCST of 38 °C, in the side chains along with 34.4 mol% PEO. Unlike MBB-PP, where stepwise conformational changes were induced through the addition of a basic or an acidic solution to adjust the pH, MBB-TT represents an opportunity to realize stepwise collapse of side chains solely by changing temperature. Figure 5.3A shows the D_h of MBB-TT in Milli-Q water at a concentration of 1.0 mg/g as a function of temperature upon heating from 1 °C to 65 °C from DLS measurements. When the temperature was 1 °C, the D_h of MBB-TT was 66.7 nm. With increasing temperature, two size transitions were observed; the first one began at 10 °C, around the LCST of PDEGEA, and continued over a temperature range of ~10 °C, where the D_h decreased from 65.0 nm at 10 °C to 56.3 nm at 22 °C. In the following temperature range of 22 to 37 °C, the D_h exhibited little changes. The second steplike size transition occurred in the temperature range of 37 to 52 °C, with an onset temperature of 37 °C, close to the LCST of

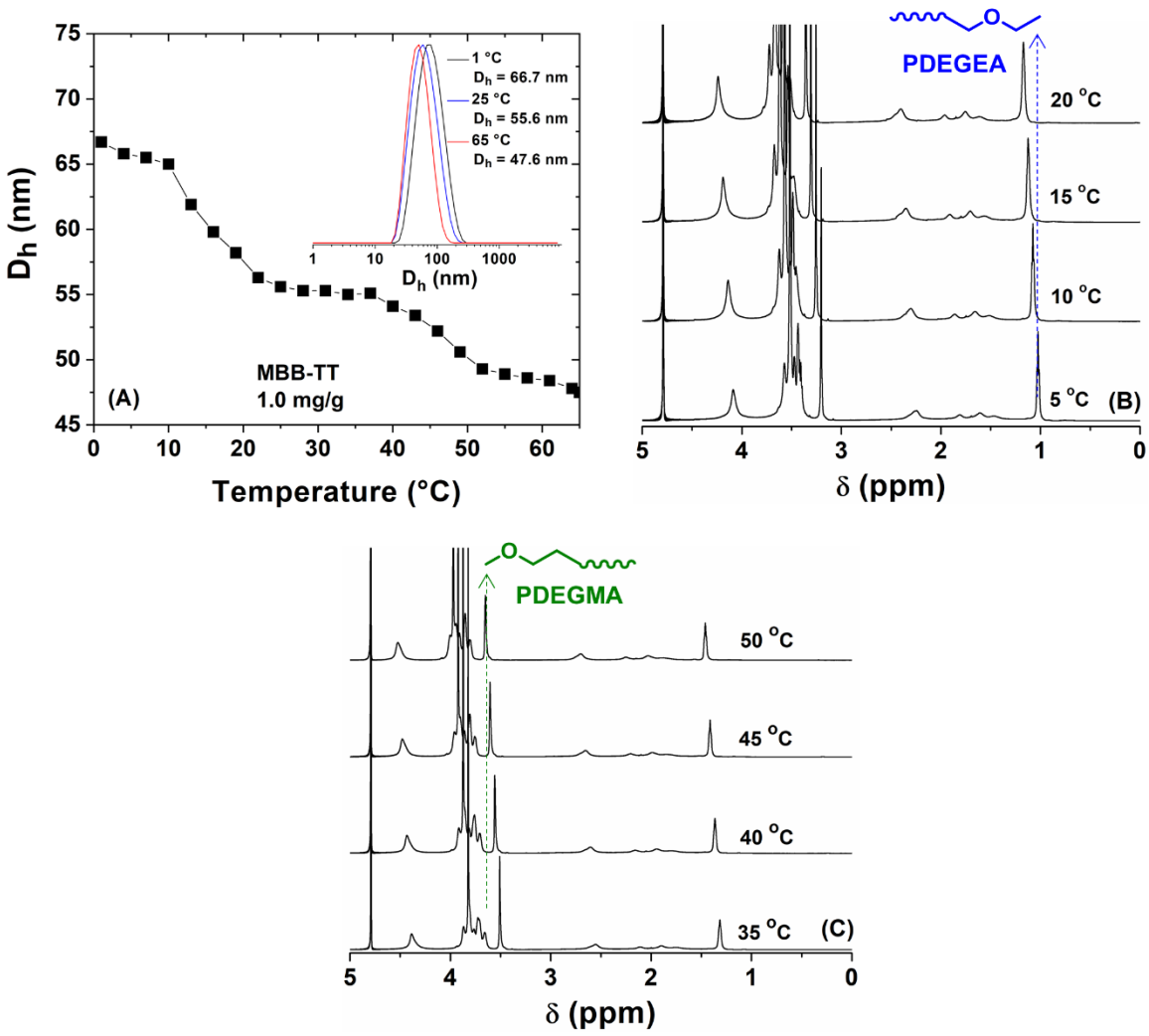

Figure 5.3. (A) Plot of D_h of 1.0 mg/g MBB-TT in Milli-Q water versus temperature in a heating process from a DLS study. The inset shows hydrodynamic size distributions at 1, 25, and 65 °C, and variable temperature ^{1}H NMR spectra of MBB-TT in D_2O with a concentration of 4.0 mg/g in the temperature ranges of 5 to 20 °C (B) and of 35 to 50 °C (C). The ^{1}H NMR spectra were normalized again the HDO peak at 4.79 ppm.

PDEGMA. The D_h decreased from 55.1 nm at 37 °C to 49.3 nm at 52 °C and then leveled off above 52 °C, reaching 47.6 nm at 65 °C. Again, a single narrow size distribution was observed at each selected temperature (see the three hydrodynamic size distributions at 1, 25, and 65 °C in the inset of Figure 5.3A). We note here that the D_h values of MBB-TT at two different concentrations, 1.0 and 0.2 mg/g, at 1 °C, were essentially the same, and so were the D_h values at 65 °C (Figure C5.14), suggesting unimolecular collapse of MBB-TT at the concentration of 1.0 mg/g upon heating.

Variable temperature ^{1}H NMR spectroscopy was performed to study the LCST transitions of the two thermoresponsive side chain polymers in MBB-TT upon heating, which are presumably responsible for the stepwise size transitions in Figure 5.3A. Figure 5.3B and C shows the ^{1}H NMR spectra of MBB-TT in D_2O at a concentration of 4.0 mg/g in the temperature ranges of 5 to 20 °C and 35 to 50 °C, respectively. Upon heating from 10 to 15 °C, the peak at ~1.0 ppm, which is from the -OCH_2CH_3 of PDEGEA, decreased and broaden slightly (Figure 5.3B). This temperature-induced change was much less pronounced than the pH-induced soluble-to-insoluble transitions of PDEAEMA and PDBAEMA side chains in MBB-PP (Figure 5.1B). This could be attributed to (i) the nature of the liquid-liquid phase separation of thermosensitive polymers in water above the LCSTs[59,60] and (ii) the influence of the strongly hydrated PEO and PDEGMA side chains.[40] For PDEGMA side chains, upon heating from 35 to 50 °C, the peak at 3.50 ppm (-$OCH_2CH_2OCH_3$) decreased noticeably, consistent with the expected LCST transition of PDEGMA.

AFM showed that MBB-TT brushes spin cast on PMMA-coated mica at 0 °C were wormlike (Figures 5.4 and C5.15). The average length of 106 MBB brush molecules was 169.2 ± 37.5 nm, and the typical height was ~1 nm (see the cross-sectional profile at the bottom of Figure 5.4A). When the temperature was raised to 30 °C, the brushes shrank noticeably (Figures 5.4B and

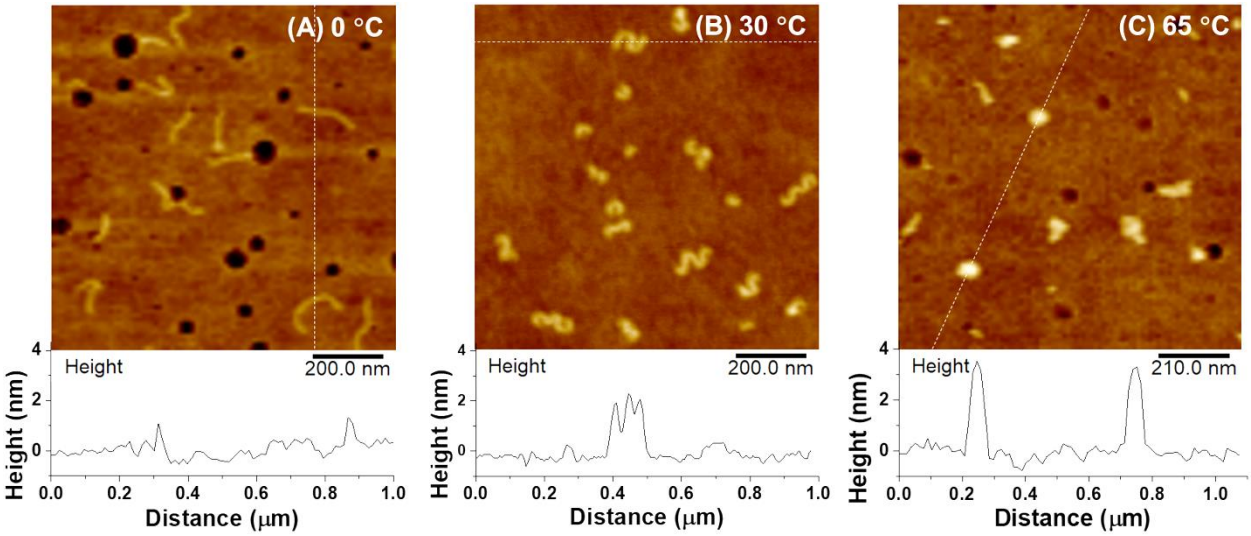

Figure 5.4. AFM height images of MBB-TT spin cast on PMMA-coated mica from a 0.050 mg/g solution of MBB-PP in Milli-Q water at T = 0 °C (A), 30 °C (B), and 65 °C (C). The plot in the bottom of each image shows the cross-sectional profile along the dashed line.

C5.16). Interestingly, longer brushes took on wavelike conformations, while short ones assumed C or S shapes, which is likely due to the requirement for locally collapsed and aggregated PDEGEA side chains to minimize the contact with water along the backbone under the conditions that PEO and PDEGMA are still highly hydrated. Note that C- and S-shaped brush molecules were previously reported in the literature for P*n*BA MBBs at the air-water interface after lateral decompression and were theoretically explained as that the uneven distribution of side chains on the two sides of the backbone resulted in a decrease of the elastic energy of the side chains.[17,61] The brush height was ~2.5 nm, in contrast to ~1 nm at 0 °C, and the average cross-length (from one side to another) of 152 MBB molecules from image analysis was 124.8 ± 42.4 nm. Further heating to 65 °C, the brushes were found to be mostly globular (Figures 5.4C and D17), though some molecules appeared to be unfolded on the substrate, which could be due to the shearing force in the sample preparation process. The average dimension of 66 globular MBB brushes (two measurements for each in perpendicular directions) was 52.1 ± 15.2 nm, and the typical height was ~ 4 nm. Thus, the results from AFM analysis agreed with the DLS data (Figure 5.3A).

5.3.4. pH- and Temperature-Induced Stepwise Conformational Changes of MBB-TP in Aqueous Solution

MBB-TP comprised 32.2 mol% thermoresponsive PDEGEA, 27.4 mol% pH-responsive PDEAEMA-56 (DP = 56), and 40.4 mol% PEO side chains. The stepwise collapse of stimuli-responsive side chains in this brush polymer can be induced through two routes: (i) increasing pH from below to above the pK_a of PDEAEMA at a temperature below the LCST of PDEGEA, followed by heating to collapse the thermoresponsive side chains; (ii) raising temperature across the LCST of PDEGEA while PDEAEMA side chains are protonated, following by changing the pH from below to above the pK_a of PDEAEMA. Figure 5.5 shows the DLS results for route (i). A

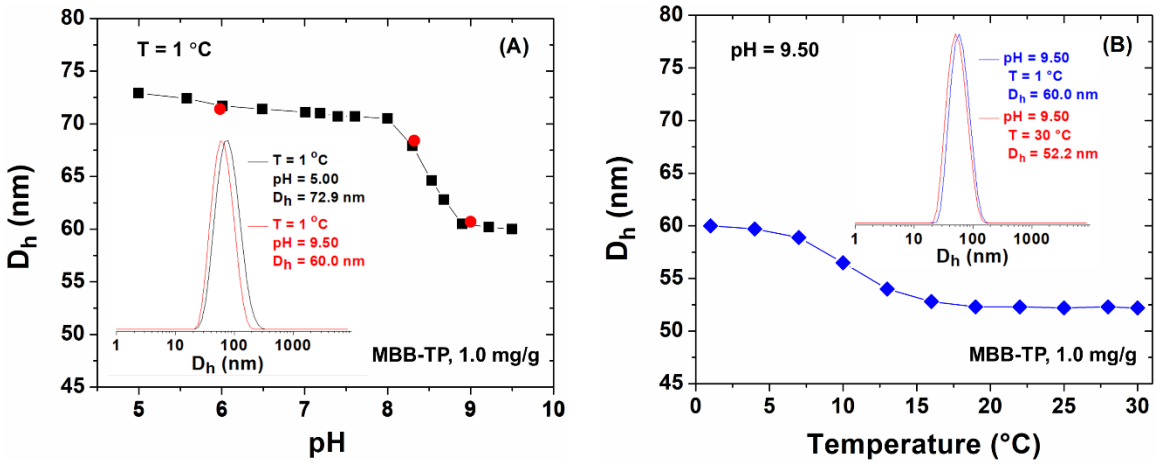

Figure 5.5. (A) Plot of D_h of 1.0 mg/g MBB-TP in a 10 mM phosphate buffer at 1 °C versus pH from DLS measurements. The inset shows the hydrodynamic size distributions of MBB-TP at T = 1 °C and two pH values (5.00 and 9.50). (B) Plot of D_h of 1.0 mg/g MBB-TP in a 10 mM phosphate buffer at pH = 9.50 versus temperature. The inset shows the hydrodynamic size distributions of MBB-TP at pH = 9.50 and two different temperatures (1 and 30 °C).

1.0 mg/g solution of MBB-TP in a 10 mM phosphate buffer with a pH of 5.00 was prepared in an ice/water bath, and the D_h at 1 °C was found to be 72.9 nm. With increasing pH to 8.00 at 1 °C, the D_h decreased slightly to 70.5 nm, followed by a sharp drop to 60.5 nm at pH = 8.90, beyond which the size levelled off. The overall size reduction from pH 5.00 to 9.50 was 12.9 nm (~ 18%). We previously observed that for pH-induced full collapse of binary MBBs (i.e., from wormlike/starlike to globular) the size decreased by ~ 30%.[39,40] Thus, the overall decrease in the D_h of MBB-TP here implied partial collapse of the brushes. The pH-induced shrinking of MBB-TP was reversible upon lowering pH, as can be seen from the red circles in Figure 5.5A. Similar to MBB-PP, the hydrodynamic size distributions of MBB-TP remained narrow and unimodal throughout the pH-changing process, suggesting unimolecular collapse. Note that the pH-induced size transition of MBB-TP at 1 °C occurred in the pH range of 8.00 to 8.90, with the mid-point at pH = 8.45, much higher than the reported pK_a of PDEAEMA.[54,55] This is different from the observation for PDEAEMA side chains of MBB-PP at 25 °C in Figure 5.1A, but similar to our previous report for binary heterografted three-arm star MBBs,[40] which exhibited a sharp size decrease at pH = ~ 8.1 at 1 °C. The delayed size transition can be attributed to two factors. (i) The pH values were measured in an ice/water bath, whereas the pK_a values are usually determined at 25 °C or ambient temperature. We calibrated the pH meter at 0 °C using pH = 4.01, 7.00, and 10.01 standard buffer solutions, whose pH values at 0 °C were 4.00, 7.11 and 10.32, slightly different from the values at 25 °C. (ii) Figure 5.5A shows the D_h values of MBB-TP upon increasing pH, not the solubility change of PDEAEMA side chains. The fully hydrated PEO and PDEGEA side chains of MBB-TP at 1 °C were believed to keep the brushes in the wormlike state to higher pH values above the pK_a of PDEAEMA until more monomer units were deprotonated to

drive the shrinking of MBB-TP. As a result, the size reduction transition was delayed to a slightly higher pH range.

The sample was then gradually heated at pH = 9.50; the D_h exhibited a second size reduction transition, from 58.9 nm at 7 °C to 54.0 nm at 13 °C (Figure 5.5B), above which the D_h decreased slightly and reached 52.2 nm at 30 °C. The temperature-triggered size transition occurred at ~10 °C, almost the same as the reported LCST of PDEGEA (~9 °C). The overall decrease of D_h was 20.7 nm (~28%), from 72.9 nm at T = 1 °C and pH = 5.00 to 52.2 nm at T = 30 °C and pH = 9.50, corresponding to a hydrodynamic volume reduction by 63.3%. This indicated that the brushes likely fully collapsed at T = 30 °C and pH = 9.50. The single narrow size distributions shown in Figure 5.5B suggested that the brushes remained molecularly dispersed thanks to the steric stabilization provided by the PEO side chains.

Figure 5.6 shows the DLS results for the second route, that is, heating at a lower pH from below to above the LCST of PDEGEA and then increasing the pH from below to above the pK_a of PDEAEMA. At pH = 5.00, PDEAEMA side chains of MBB-TP were fully protonated and strongly hydrated, and only a small size decrease, yet appreciable, was observed upon heating, from 73.1 nm at 1 °C to 67.8 nm at 16 °C (Figure 5.6A). The transition occurred in a temperature range similar to that in Figure 5.5B, but the magnitude was smaller, only 3.6 nm from 7 to 16 °C, in contrast to 6.1 nm in Figure 5.5B in the same temperature range. This smaller D_h change was presumably caused by the highly hydrated protonated PDEAEMA side chains along with PEO side chains that kept the brushes in the wormlike form despite the temperature-induced collapse of PDEGEA side chains. At 19 °C, the pH of the solution was then gradually increased, and a large drop in D_h, ~13 nm, was observed in the pH range around the pK_a of PDEAEMA (Figure 5.6B). Above pH = 8.0, the D_h decreased only slightly and reached 53.4 nm at pH = 9.50. This D_h value

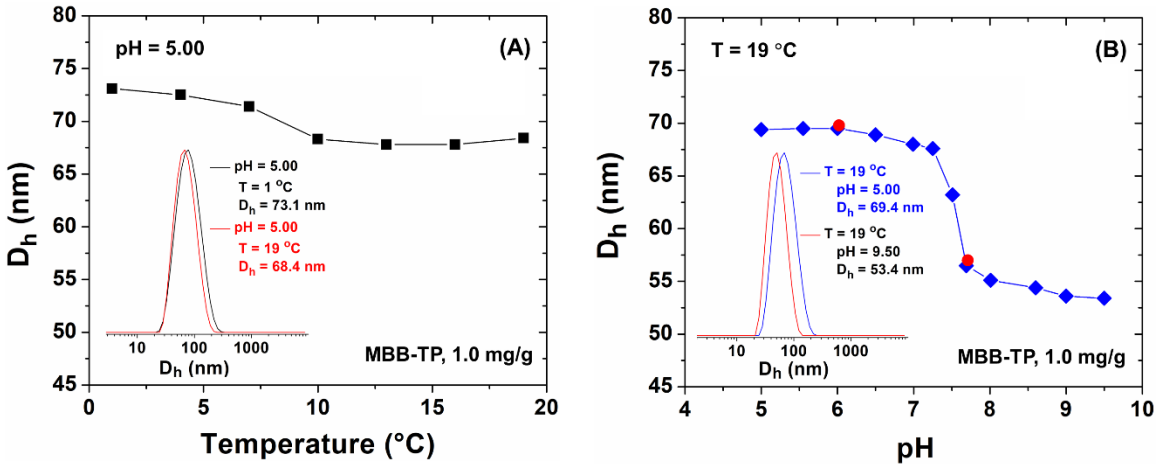

Figure 5.6. (A) Plot of D_h of 1.0 mg/g MBB-TP in a 10 mM phosphate buffer at pH = 5.00 versus temperature from DLS measurements upon heating. The inset shows the hydrodynamic size distributions of MBB-TP at pH = 5.00 and two temperatures (T = 1 and 19 °C). (B) Plot of D_h of 1.0 mg/g MBB-TP in a 10 mM phosphate buffer at T = 19 °C versus pH. The inset shows the hydrodynamic size distributions of MBB-TP at T = 19 °C and two pH values (5.00 and 9.50).

is similar to that at the end of the first route (52.2 nm at T = 30 °C and pH = 9.50), also suggesting that the brushes were likely fully collapsed. The overall size reduction of MBB-TP in route (ii) was 19.7 nm (i.e., ~27%). Similarly, the pH-induced size transition was reversible with negligible hysteresis, as can be seen from the red circles in Figure 5.6B from decreasing pH, which fell right on the curve obtained from the process of increasing pH.

The observed stepwise side transitions originated from the collapse of PDEGEA and PDEAEMA side chains of MBB-TP in water in response to heating and pH increases, respectively, which were verified by ^{1}H NMR analysis of MBB-TP following the changes in both routes. Figure 5.7A shows the ^{1}H NMR spectra of MBB-TP in a 10 mM phosphate buffer prepared with D_2O at 4 °C with increasing pH from 5.00 to 9.50; clearly, the peak at 1.2 ppm, which was from -$HN^{+}(CH_2C\mathit{H}_3)_2$ of PDEAEMA side chains and visible at pH 5.00 to 7.50, completely disappeared at pH = 8.00 and 9.50. It was interesting to observe that the same peak almost disappeared at pH = 7.00 for MBB-PP in Figure 5.1B but still visible at pH = 7.50 for MBB-TP here, which could be caused by the temperature effect as discussed earlier. Note that the DLS measurements showed that the size transition began at pH = 8.00 at 1 °C and continued till about 8.90 (Figure 5.5A). This is likely because slightly higher pH might be necessary to drive the decrease in D_h, while the NMR signal reflects the mobility of the group. Figure 5.7B shows the variable temperature ^{1}H NMR spectra obtained at pH = 9.50 upon heating from 4 to 16 °C. The peak of -$OCH_2C\mathit{H}_3$ from PDEGEA decreased significantly, with the transition occurring at ~10 °C, consistent with the LCST of PDEGEA. In the 2nd route, at pH = 5.00, the peak of -$OCH_2C\mathit{H}_3$ from PDEGEA decreased only slightly upon heating from 7 to 10 °C (Figure 5.7C) due to the protonated PDEAEMA side chains as discussed earlier for the observation in Figure 5.6A. At 25 °C, the peak of -$HN^{+}(CH_2C\mathit{H}_3)_2$ of PDEAEMA at 1.2 ppm disappeared at pH = 8.00 (Figure 5.7D); interestingly,

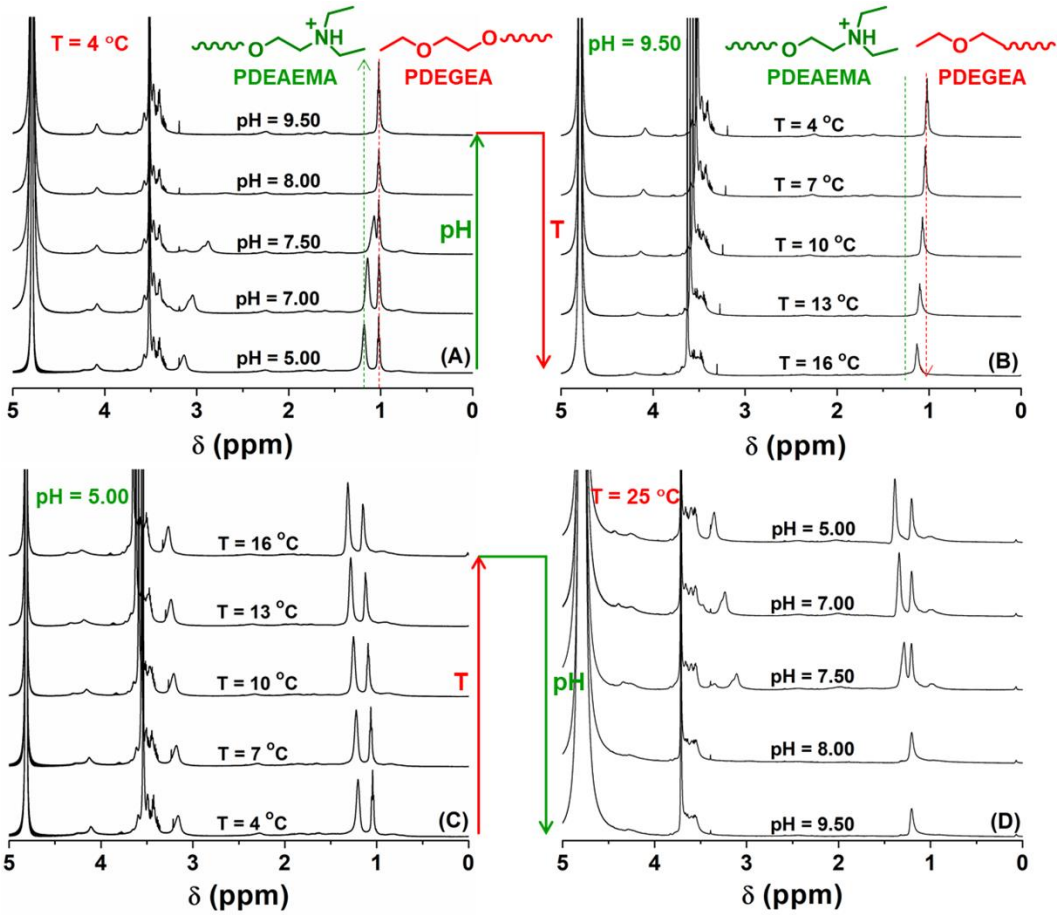

Figure 5.7. ^{1}H NMR spectra of a 4.0 mg/g solution of MBB-TP in a 10 mM phosphate buffer made with D_2O at 4 °C with increasing pH value from 5.00 to 9.50 (A), at pH = 9.50 with increasing temperature from 4 to 16 °C (B), at pH = 5.00 and various temperatures upon heating (C), and at 25 °C with increasing pH value from 5.00 to 9.50 (D). The ^{1}H NMR spectra were normalized against the HDO peak at 4.79 ppm.

the peak of -OCH_2CH_3 of PDEGEA at ~1.1 ppm became smaller noticeably, indicating the effects of the protonated and deprotonated PDEAEMA side chains on the signal of PDEGEA.

To visualize the changes of MBB-TP under different conditions, AFM was performed. The AFM samples were prepared by spin casting 0.05 mg/g brush solutions on PMMA-coated mica disks immediately after the equilibration of the brush solutions, mica disks, and the spin stage of the spin coater at desired temperatures. Figure 5.8 shows the AFM height images of MPP-TP at different temperatures and pH values from both routes. At T = 0 °C and pH = 5.00, the brushes assumed a wormlike conformation with a pearl-necklace nanostructure composed of a number of beads (Figures 5.8A and C5.18), similar to but more pronounced than the morphology of MBB-PP at pH = 4.00 in Figure 5.2A. The representative bead marked with an arrow in Figure 5.8A had a length of 19.4 nm (along the backbone), a width of 12.9 nm, and a height of 3.7 nm. The height of the brushes showed undulations of ~1 nm, as can be seen from the cross-sectional profile at the bottom of Figure 5.8A. This peculiar morphology is also believed to be a result of microphase separation between the charged PDEAEMA side chains and the neutral PEO and PDEGEA side chains. The average length of 142 MBB molecules was 179.5 ± 41.7 nm, representing a degree of stretching of 89%. Upon increasing pH to 9.50 at 0 °C, the PDEAEMA side chains were deprotonated, and AFM imaging showed that height variations along the backbone were significantly smaller (< 0.5 nm) (Figures 5.8B and D19), although beadlike nanostructures were still visible. This observation suggested that the microphase separation of the side chains along the backbone were significantly weakened upon increasing pH to deprotonate the charged PDEAEMA side chains. Analysis showed that the average length of 246 brushes was 160.8 ± 40.7 nm, which was slightly shorter than that at pH = 5.00 and T = 0 °C (179.5 ± 41.7 nm). When the temperature was raised to 20 °C at pH 9.50, the brushes collapsed into a roughly globular shape, with a folded

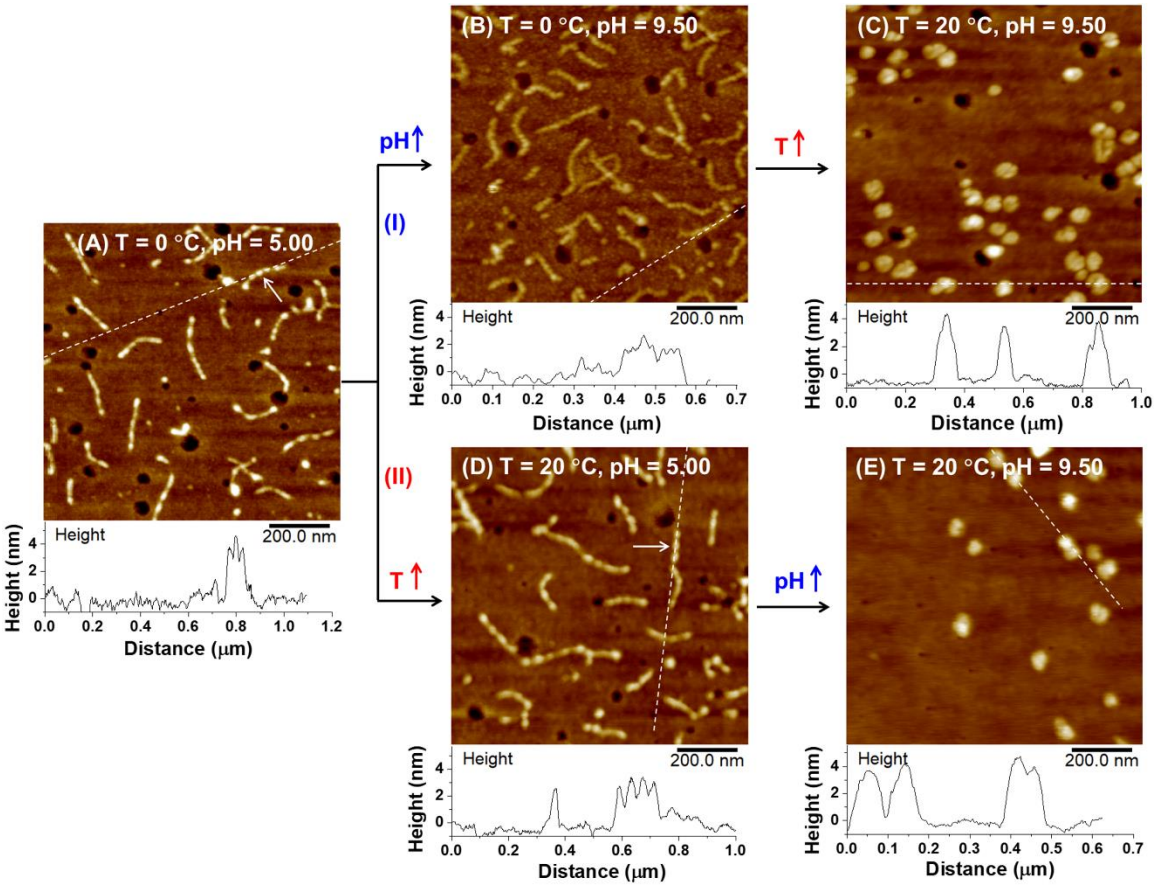

Figure 5.8. AFM height images of MBB-TP spin cast on PMMA-coated mica from a 0.050 mg/g solution of MBB-TP in a 5 mM phosphate buffer at T = 0 °C and pH = 5.00 (A), T = 0 °C and pH = 9.50 (C), T = 20 °C and pH = 9.50 (C), T = 20 °C and pH = 5.00 (D), and T = 20 °C and pH = 9.50 (E). The plot in the bottom of each AFM micrograph shows the cross-sectional profile along the dashed line in the height image.

backbone being clearly visible for many globules in Figures 5.8C and D20. The typical height of folded brushes was ~4 nm, and the average diameter from the image analysis of 100 globular molecules (two measurements for each in perpendicular directions) was 54.5 ± 9.7 nm.

When the MBB-TP solution with a pH of 5.00 was heated from 0 to 20 °C, AFM showed that the pronounced pearl-necklace morphology was maintained (Figures 5.8D and D21), with the typical bead (marked with an arrow) of a similar height (3.4 nm), a slightly larger length (26.4 nm) and width (21.3 nm) than the bead in Figure 5.8A. Image analysis showed that the average length of 211 brush molecules was 167.1 nm ± 36.4 nm, slightly shorter that at the conditions of pH = 5.00 and T = 0 °C (179.5 ± 41.7 nm). This suggests that the heating-induced collapse of PDEGEA at pH = 5.00 had a rather small influence on the overall conformation and the pearl-necklace morphology of the brushes, consistent with the small changes in the D_h from DLS (Figure 5.6A) and in the intensity of the characteristic peak from ^{1}H NMR analysis (Figure 5.7C), which could be attributed to the strong hydration of PEO and protonated PDEAEMA side chains. Nevertheless, the collapse of PDEGEA side chains enhanced the microphase separation along the backbone as reflected by the larger beads in the pearl-necklace nanostructures in Figure 5.8D.

When the pH was increased from 5.00 to 9.50 at 20 °C, both responsive side chain polymers collapsed as can be seen from the ^{1}H NMR spectrum in Figure 5.7D, the brushes transformed into a globular shape stabilized by PEO side chains (Figures 5.8E and D22); the typical height was ~ 4-5 nm, similar to the collapsed brushes shown in Figure 5.8C. The average diameter of 93 globular brushes measured (two measurements for each in perpendicular directions) was 51.8 ± 9.9 nm, slightly smaller than the average size of the globular brushes from the first route (54.5 ± 9.7 nm), likely because the brushes in Figure 5.8C appeared to spread slightly on the surface. Thus, studies by DLS, NMR, and AFM showed that MBB-TP exhibited stepwise collapse of side chains in

response to external stimuli and eventually transformed into globular shapes stabilized by the PEO side chains. Subtle differences were observed from different routes for the stepwise conformational transitions of MBB-TP in aqueous solutions.

5.3.5. Stepwise Release of Hydrophobic Model Drug, Nile Red, from Collapsed Globular MBB-PP

Shape-changing MBBs have potential application in many areas, including manipulation of molecular interactions, delivery of substances, and templated synthesis of inorganic nanoparticles of different morphologies via shape transitions. In particular, ternary MBBs with two distinct stimuli-responsive polymers in the side chains provide a unique opportunity to achieve stepwise release of hydrophobic substances encapsulated in the globular brushes. Nile Red is commonly used as a hydrophobic fluorescence probe for study of block copolymer micellization in water because its fluorescence is negligible in water but increases significantly in the hydrophobic core of micelles.[62] As a demonstration, we encapsulated Nile Red in the globular MBB-PP in a phosphate buffer with pH of 9.50. The pH of the solution was then gradually decreased, and fluorescence emission spectra were recorded at selected pH values with an excitation wavelength of 540 nm. Figure 5.9A shows the fluorescence emission spectra at pH values ranging from 9.50 to 3.50. The maximum fluorescence emission intensity decreased substantially from 400 a.u. at pH = 9.50 to 87 a.u. at pH = 3.50. A two-step release profile of Nile Red can be seen in Figure 5.9B. The first one occurred in the pH range of 7.5 to 6.5, corresponding to the insoluble-to-soluble transition of PDEAEMA (pK_a = 7.4); the second sharp decrease was observed upon reducing the pH of the solution from ~5.0 to ~4.0, corresponding to the pK_a of PDBAEMA. Note that it is unclear why the fluorescence emission intensity increased with the pH decreasing from 6.0 to 5.0, but this was repeatedly observed in our experiments. The stepwise intensity changes observed here

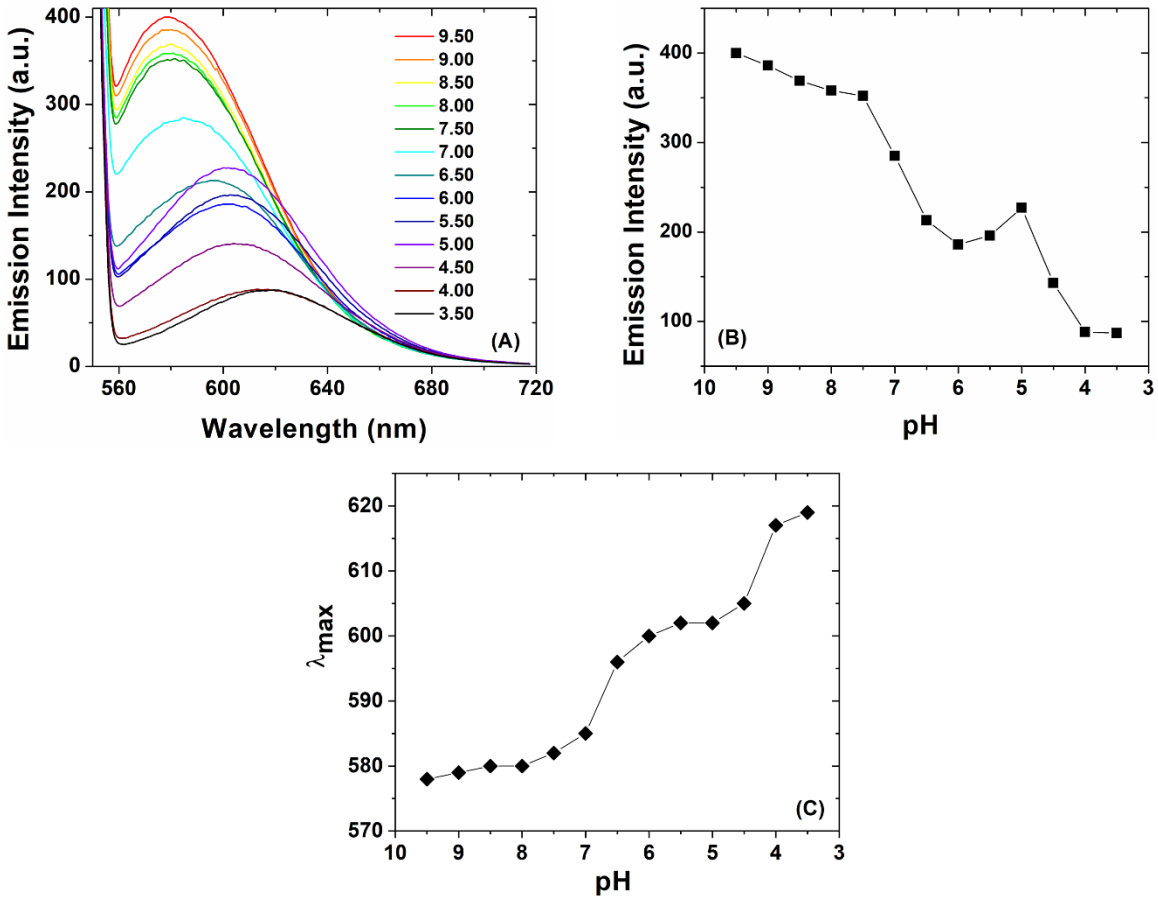

Figure 5.9. (A) Fluorescence emission spectra of Nile Red in a 4.0 mL solution of 0.2 mg/g MBB-PP in a 25 mM phosphate buffer with decreasing pH from 9.50 to 3.50. The nominal concentration of Nile Red was 6.7×10^{-7} M. The pH of the solution was decreased at a step of 0.50 pH unit, and at each pH the sample was equilibrated for 10 min before the fluorescence emission spectrum was taken. The excitation wavelength is 540 nm, and the spectra were recorded from 550 to 720 nm. (B) Plot of fluorescent emission intensity at the maximum peak versus pH. (C) Plot of λ_{max} versus pH.

correlated well with the size reduction transitions from DLS measurements (Figure 5.1A), indicating that the stepwise release of hydrophobic Nile Red from MBB-PP was triggered by the pH-induced conformation changes of MBB-PP. In addition, the maximum peak exhibited a red shift with decreasing pH, from λ_{max} = 578 nm at pH = 9.50 to λ_{max} = 619 nm pH = 3.50, which also indicated that the Nile Red molecules were released from a hydrophobic to a hydrophilic environment. Interestingly, stepwise changes in λ_{max} were also observed, suggesting stepwise polarity changes in the microenvironment of Nile Red with decreasing pH.

5.4. Conclusions

Three dually responsive linear ternary heterografted MBBs were synthesized by a grafting to method via the CuAAC click reaction: MBB-PP with two different pH-responsive polymers, MBB-TT with two distinct thermoresponsive polymers, and MBB-TP with one pH-responsive polymer and one thermoresponsive polymer along with 5 kDa PEO as the side chains. DLS studies showed that all three brush polymers exhibited two steplike size reduction transitions in aqueous solution in response to external stimuli, resulting in overall hydrodynamic size decreases by 27% to 29 % (61% to 64 % decrease in hydrodynamic volume). The size transitions were driven by the pH-induced soluble-to-insoluble and/or temperature-triggered LCST transitions of responsive side chain polymers of the brushes in aqueous solution, which were confirmed by ^{1}H NMR spectroscopy analysis. AFM imaging revealed stepwise conformational changes from extended wormlike brushes (with and without a pearl-necklace morphology) to partially collapsed nanostructures (shrunken wormlike or wavelike or C-/S-shaped) to globular nano-objects stabilized by PEO side chains. This work shows that it is possible to achieve controllable stepwise conformational transitions of multicomponent MBBs while maintaining the stability of brush

molecules against aggregation in solution, opening up more opportunities for potential applications in diverse areas such as drug delivery, stimuli-responsive emulsions, and controlled templated synthesis of nanomaterials. As a demonstration, MBB-PP was used to encapsulate Nile Red as a hydrophobic model drug in the globular state, and a stepwise release profile was achieved upon gradually decreasing pH.

References

1. Zhang, M. F.; Müller, A. H. E. Cylindrical Polymer Brushes. *J. Polym. Sci. Part A: Polym. Chem.* **2005**, *43*, 3461-3481.
2. Sheiko, S. S.; Sumerlin, B. S.; Matyjaszewski, K. Cylindrical Molecular Brushes: Synthesis, Characterization, and Properties. *Prog. Polym. Sci.* **2008**, *33*, 759-785.
3. Lee, H.-I.; Pietrasik, J.; Sheiko, S. S.; Matyjaszewski, K. Stimuli-Responsive Molecular Brushes. *Prog. Polym. Sci.* **2010**, *35*, 24-44.
4. Rzayev, J. Molecular Bottlebrushes: New Opportunities in Nanomaterials Fabrication. *ACS Macro Lett.* **2012**, *1*, 1146-1149.
5. Xie, G.; Martinez, M. R.; Olszewski, M.; Sheiko, S. S.; Matyjaszewski, K. Molecular Bottlebrushes as Novel Materials. *Biomacromolecules* **2019**, *20*, 27-54.
6. Zhao, B. Shape-Changing Bottlebrush Polymers. *J. Phys. Chem. B* **2021**, *125*, 6373-6389.
7. Liao, L.; Liu, J.; Dreaden, E. C.; Morton, S. W.; Shopsowitz, K. E.; Hammond, P. T.; Johnson, J. A. A Convergent Synthetic Platform for Single-Nanoparticle Combination Cancer Therapy: Ratiometric Loading and Controlled Release of Cisplatin, Doxorubicin, and Camptothecin. *J. Am. Chem. Soc.* **2014**, *136*, 5896–5899.
8. Luo, H.; Szymusiak, M.; Garcia, E. A.; Lock, L. L.; Cui, H.; Liu, Y.; Herrera-Alonso, M. Solute-Triggered Morphological Transitions of an Amphiphilic Heterografted Brush Copolymer as a Single-Molecule Drug Carrier. *Macromolecules* **2017**, *50*, 2201-2206.
9. Runge, M. B.; Bowden, N. B. Synthesis of High Molecular Weight Comb Block Copolymers and Their Assembly into Ordered Morphologies in the Solid State. *J. Am. Chem. Soc.* **2007**, *129*, 10551-10560.

10. Xia, Y.; Olsen, B. D.; Kornfield, J. A.; Grubbs, R. H. Efficient Synthesis of Narrowly Dispersed Brush Copolymers and Study of Their Assemblies: The Importance of Side Chain Arrangement. *J. Am. Chem. Soc.* **2009**, *131*, 18525-18532.

11. Liberman-Martin, A. L.; Chu, C. K.; Grubbs, R. H. Application of Bottlebrush Block Copolymers as Photonic Crystals. *Macromol. Rapid Commun.* **2017**, *38*, 1700058.

12. Daniel , W. F.; Burdynska, J.; Vatankhah-Varnoosfaderani, M.; Matyjaszewski, K.; Paturej, J.; Rubinstein, M.; Dobrynin, A. V.; Sheiko, S. S. Solvent-Free, Supersoft and Superelastic Bottlebrush Melts and Networks. *Nat. Mater.* **2016**, 15, 183-189.

13. Sheiko, S. S.; Dobrynin, A. V. Architectural Code for Rubber Elasticity: From Supersoft to Superfirm Materials. *Macromolecules* **2019**, *52*, 7531-7546.

14. Banquy, X.; Burdyńska, J.; Lee, D. W.; Matyjaszewski, K.; Israelachvili, J. Bioinspired Bottle-Brush Polymer Exhibits Low Friction and Amontons-Like Behavior. *J. Am. Chem. Soc.* **2014**, *136*, 6199 -6202.

15. Qi, H.; Liu, X. T.; Henn, D. M.; Mei, S.; Staub, M. C.; Zhao, B.; Li, C. Y. Breaking Translational Symmetry via Polymer Chain Overcrowding in Molecular Bottlebrush Crystallization. *Nature Communications* **2020**, *11*, 2152.

16. Henn, D. M.; Fu, W. X.; Mei, S.; Li, C. Y.; Zhao, B. Temperature-Induced Shape Changing of Thermosensitive Binary Heterografted Linear Molecular Brushes between Extended Worm-Like and Stable Globular Conformations. *Macromolecules* **2017**, *50*, 1645-1656.

17. Sheiko, S. S.; Prokhorova, S. A.; Beers, K. L.; Matyjaszewski, K.; Potemkin, I. I.; Khokhlov, A. R.; Möller, M. Single Molecule Rod−Globule Phase Transition for Brush Molecules at a Flat Interface. *Macromolecules* **2001,** *34*, 8354-8360.

18. Boyce, J. R.; Shirvanyants, D.; Sheiko, S. S.; Ivanov, D. A.; Qin, S. H.; Börner, H.; Matyjaszewski, K. Multiarm Molecular Brushes: Effect of the Number of Arms on the Molecular Weight Polydispersity and Surface Ordering. *Langmuir* **2004**, *20*, 6005-6011.

19. Sun, F.; Sheiko, S. S.; Moeller, M.; Beers, K.; Matyjaszewski, K. Conformational Switching of Molecular Brushes in Response to the Energy of Interaction with the Substrate. *J. Phys. Chem. A* **2004**, *108*, 9682–9686.

20. Gallyamov, M. O.; Tartsch, B.; Khokhlov, A. R.; Sheiko, S. S.; Börner, H. G.; Matyjaszewski, K.; Möller, M. Reversible Collapse of Brushlike Macromolecules in Ethanol and Water Vapours as Revealed by Real-Time Scanning Force Microscopy. *Chem. Eur. J.* **2004,** *10*, 4599-4605.

21. Gallyamov, M. O.; Tartsch, B.; Khoklov, A. R.; Sheiko, S. S.; Börner, H. G.; Matyjaszewski, K.; Möller, M. Real-Time Scanning Force Microscopy of a Macromolecular Conformational Transitions. *Macromol. Rapid Comm.* **2004**, *25*, 1703-1707.

22. Li, C.; Gunari, N.; Fischer, K.; Janshoff, A.; Schmidt, M. New Perspectives for the Design of Molecular Actuators: Thermally Induced Collapse of Single Macromolecules from Cylindrical Brushes to Spheres. *Angew. Chem. Int. Ed.* **2004**, *43*, 1101-1104.

23. Lee, H.-I.; Pietrasik, J.; Matyjaszewski, K. Phototunable Temperature-Responsive Molecular Brushes Prepared by ATRP. *Macromolecules* **2006**, *39*, 3914–3920.

24. Lee, H.-I.; Boyce, J.R.; Nese, A.; Sheiko, S. S.; Matyjaszewski, K. pH-Induced Conformational Changes of Loosely Grafted Molecular Brushes Containing Poly(acrylic acid) Side Chains. *Polymer* **2008**, *49*, 5490-5496.

25. Yamamoto, S.-i.; Pietrasik, J.; Matyjaszewski, K. ATRP Synthesis of Thermally Responsive Molecular Brushes from Oligo(ethylene oxide) Methacrylates. *Macromolecules* **2007**, *40*, 9348-9353.

26. Pietrasik, J.; Sumerlin, B.S.; Lee, R.Y.; Matyjaszewski, K. Solution Behavior of Temperature-Responsive Molecular Brushes Prepared by ATRP. *Macromol. Chem. Phys.* **2007**, *208*, 30–36.

27. Stephan, T.; Muth, S.; Schmidt, M. Shape Changes of Statisical Copolymacromomers: From Wormlike Cylinders to Horseshoe- and Meanderlike Structures. *Macromolecules* **2002**, *35*, 9857-9860.

28. Gunari, N.; Cong, Y.; Zhang, B.; Fischer, K.; Janshoff, A.; Schmidt, M. Surfactant-Induced Helix Formation of Cylindrical Brush Polymers with Poly(L-lysine) Side Chains. *Macromol. Rapid Commun.* **2008**, *29*, 821-825.

29. Xu, Y.; Bolisetty, S.; Drechsler, M.; Fang, B.; Yuan, J.; Harnau, L.; Ballauff, M.; Müller, A. X. E. Manipulating Cylindrical Polyelectrolyte Brushes on the Nanoscale by Counterions: Collapse Transition to Helical Structures. *Soft Matter* **2009**, *5*, 379–384.

30. Xu, Y.; Bolisetty, S.; Ballauff, M.; Müller, A. H. E. Switching the Morphologies of Cylindrical Polycation Brushes by Ionic and Supramolecular Inclusion Complexes. *J. Am. Chem. Soc.* **2009**, *131*, 1640–1641.

31. Xu, Y.; Borisov, O. V.; Ballauff, M.; Muller, A. H. Manipulating the Morphologies of Cylindrical Polyelectrolyte Brushes by Forming Interpolyelectrolyte Complexes with Oppositely Charged Linear Polyelectrolytes: an AFM Study. *Langmuir* **2010,** *26*, 6919-6926.

32. Weller, D.; McDaniel, J. R.; Fischer, K.; Chilkoti, A.; Schmidt, M. Cylindrical Polymer Brushes with Elastin-Like Polypeptide Side Chains. *Macromolecules* **2013**, *46*, 4966-4971.

33. Li, X.; ShamsiJazeyi, H.; Pesek, S. L.; Agrawal, A.; Hammouda, B.; Verduzco, R. Thermoresponsive PNIPAAM Bottlebrush Polymers with Tailored Side-Chain Length and End-Group Structure. *Soft Matter* **2014**, *10*, 2008-2015.

34. Kutnyanszky, E.; Hempenius, M. A.; Vancso, G. J. Polymer Bottlebrushes with a Redox Responsive Backbone Feel the Heat: Synthesis and Characterization of Dual Responsive Poly(ferrocenylsilane)s with PNIPAM Side Chains. *Polym. Chem.* **2014**, *5*, 771-783.

35. Zhu, X. M.; Zhang, J.; Miao, C.; Li, S. Y.; Zhao, Y. L. Synthesis, Thermoresponsivity and Multi-Tunable Hierarchical Self-assembly of Multi-Responsive $(AB)_mC$ Miktobrush-Coil Terpolymers. *Polym. Chem.* **2020**, *11*, 3003-3017.

36. Yan, Y. Y.; Gao, C.; Li, J. J.; Zhang, T.; Yang, G.; Wang, Z. K.; Hua, Z. Modulating Morphologies and Surface Properties of Nanoparticles from Cellulose-Grafted Bottlebrush Copolymers Using Complementary Hydrogen-Bonding between Nucleobases. *Biomacromolecules* **2020**, *21*, 613-620.

37. Henn, D. M.; Lau, C. M.; Li, C. Y.; Zhao, B. Light-Triggered Unfolding of Single Linear Molecular Bottlebrushes from Compact Globular to Wormlike Nano-Objects in Water. *Polym. Chem.* **2017**, *8*, 2702-2712.

38. Henn, D. M.; Holmes, J. A.; Kent, E. W.; Zhao, B. Worm-to-Sphere Shape Transition of Thermoresponsive Linear Molecular Bottlebrushes in Moderately Concentrated Aqueous Solution. *J. Phys. Chem. B* **2018**, *122*, 7015-7025.

39. Kent, E. W.; Henn, D. M.; Zhao, B. Shape-Changing Linear Molecular Bottlebrushes with Dually pH- and Thermo-Responsive Diblock Copolymer Side Chains. *Polym. Chem.* **2018**, *9*, 5133-5144.

40. Kent, E. W.; Zhao, B. Stimuli-Induced Star-Globule Shape Transitions of Dually Responsive Binary Heterografted Three-Arm Star Molecular Brushes in Aqueous Solution. *Macromolecules* **2019**, *52(17)*, 6714-6724.

41. Kent, E. W.; Lewoczko, E. M.; Zhao, B. pH- and Chaotropic Anion-Induced Conformational Changes of Tertiary Amine-Containing Binary Heterografted Star Molecular Bottlebrushes in Aqueous Solution. *Polymer Chemistry* **2021**, *12*, 265-276.

42. Lewoczko, E. M.; Kelly, M. T.; Kent, E. W.; Zhao, B. Effects of Temperature on Chaotropic Anion-Induced Shape Transitions of Star Molecular Bottlebrushes with Heterografted Poly(ethylene oxide) and Poly(N,N-dialkylaminoethyl methacrylate) Side Chains in Acidic Water. *Soft Matter* **2021**, *17*, 6566-6579.

43. Gumus, B.; Herrera-Alonso, M.; Ramírez-Hernández, A. Kinetically-Arrested Single-Polymer Nanostructures from Amphiphilic Mikto-Grafted Bottlebrushes in Solution: a Simulation Study. *Soft Matter* **2020**, *16*, 4969-4979.

44. Gumerov, R. A.; Potemkin, I. I. Computer Simulations of Comb-Like Macromolecules with Responsive Diblock Copolymer Side Chains. *Colloid Polym. Sci.* **2021**, *299*, 407-418.

45. Gao, H. F.; Matyjaszewski, K. Synthesis of Molecular Brushes by "Grafting onto" Method: Combination of ATRP and Click Reactions. *J. Am. Chem. Soc.* **2007**, *129*, 6633– 6639.

46. Tang, H.; Li, Y.; Lahasky, S. H.; Sheiko, S. S.; Zhang, D. Core−Shell Molecular Bottlebrushes with Helical Polypeptide Backbone: Synthesis, Characterization, and Solution Conformations. *Macromolecules* **2011**, *44*, 1491-1499.

47. Han, D.; Tong, X.; Zhao Y. One-Pot Synthesis of Brush Diblock Copolymers through Simultaneous ATRP and Click Coupling. *Macromolecules* **2011**, *44*, 5531-5536.

48. Zhao, P.; Yan, Y.; Feng, X.; Liu, L.; Wang, C.; Chen, Y. Highly Efficient Synthesis of Polymer Brushes with PEO and PCL as Side Chains via Click Chemistry. *Polymer* **2012**, *53*, 1992-2000.

49. Li, Y.; Themistou, E.; Zou, J.; Das, B. P.; Tsianou, M.; Cheng, C. Facile Synthesis and Visualization of Janus Double-Brush Copolymers. *ACS Macro Lett.* **2012**, *1*, 52–56.

50. Kent, E. W.; Lewoczko, E. M.; Zhao, B. Effect of Buffer Anions on Pearl-Necklace Morphology of Tertiary Amine-Containing Binary Heterografted Linear Molecular Bottlebrushes in Acidic Aqueous Buffers. *Langmuir* **2020**, *36*, 13320-13330.

51. Jin, N. X.; Woodcock, J. W., Xue, C. M.; O'Lenick, T. G.; Jiang, X. G.; Jin, S.; Dadmun, M. D.; Zhao, B. Tuning of Thermo-Triggered Gel-to-Sol Transition of Aqueous Solution of Multi-Responsive Diblock Copolymer Poly(methoxytri(ethylene glycol) acrylate-*co*-acrylic acid)-*b*-poly(ethoxydi(ethylene glycol) acrylate). *Macromolecules* **2011**, *44*, 3556-3566.

52. Woodcock, J. W., Jiang, X. G.; Wright, R. A. E.; Zhao, B. Enzyme-Induced Formation of Thermoreversible Micellar Gels from Aqueous Solutions of Multiresponsive Hydrophilic ABA Triblock Copolymers. *Macromolecules* **2011**, *44*, 5764-5775.

53. Hua, F. J.; Jiang, X. G.; Li, D. J.; Zhao, B. Well-Defined Thermosensitive, Water-Soluble Polyacrylates and Polystyrenics with Short Pendant Oligo(ethylene glycol) Groups Synthesized by Nitroxide-Mediated Radical Polymerization. *J. Polym. Sci. Part A: Polym. Chem.* **2006**, *44*, 2454-2467.

54. Zhou, K. J.; Wang, Y. G.; Huang, X. N.; Luby-Phelps, K.; Sumer, B. D.; Gao, J. M. Tunable, Ultrasensitive pH-Responsive Nanoparticles Targeting Specific Endocytic Organelles in Living Cells. *Angew. Chem., Int. Ed.* **2011**, *50*, 6109 -6114

55. Henn, D. M.; Wright, R. A. E.; Woodcock, J. W.; Hu, B.; Zhao, B. Tertiary Amine-Containing Thermo- and pH-Sensitive Hydrophilic ABA Triblock Copolymers: Effect of Different Tertiary Amines on Thermally Induced Sol-Gel Transitions. *Langmuir* **2014**, *30*, 2541–2550.

56. Chiefari, J.; Chong, Y. K.; Ercole, F.; Krstina, J.; Jeffery, J.; Le, T. P. T.; Mayadunne, R. T. A.; Meijs, G. F.; Moad, C. L.; Moad, G.; Rizzardo, E.; Thang, S. H. Living Free-Radical Polymerization by Reversible Addition-Fragmentation Chain Transfer: The RAFT Process. *Macromolecules* **1998**, *31*, 5559-5562.

57. Zhang, M.; Drechsler, M.; Müller, A. H. E. Template-Controlled Synthesis of Wire-Like Cadmium Sulfide Nanoparticle Assemblies within Core−Shell Cylindrical Polymer Brushes. *Chem. Mater.* **2004**, *16*, 537–543.

58. Zhang, M.; Estournès, C.; Bietsch, W.; Müller, A. H. E. Superparamagnetic Hybrid Nanocylinders. *Adv. Funct. Mater.* **2004**, *14*, 871–882.

59. Schild, H. G. Poly(*N*-isopropylacrylamide): Experiment, Theory and Application. *Prog. Polym. Sci.* **1992**, *17*, 163-249.

60. Lewoczko, E. M.; Wang, N.; Lundberg, C. E.; Kelly, M. T.; Kent, E. W.; Wu, T.; Chen, M.-L.; Wang, J.-H.; Zhao, B. Effects of *N*-Substituents on Solution Behavior of Poly(sulfobetaine methacrylate)s in Water: UCST and LCST. *ACS Applied Polymer Materials* **2021**, *3*, 867-878.

61. Potemkin, I. I.; Khokhlov, A. R.; Prokhorova, S.; Sheiko, S. S.; Möller, M.; Beers, K. L.; Matyjaszewski, K. Spontaneous Curvature of Comblike Polymers at a Flat Interface. *Macromolecules* **2004**, *37*, 3918-3923.

62. Jiang, X. G.; Lavender, C. A.; Woodcock, J. W.; Zhao, B. Multiple Micellization and Dissociation Transitions of Thermo- and Light-Sensitive Poly(ethylene oxide)-*b*-poly(ethoxytri(ethylene glycol) acrylate-*co*–*o*-nitrobenzyl acrylate) in Water. *Macromolecules* **2008**, *41*, 2632-2643.

Appendix D

for

Chapter 5. Stepwise Conformational Transitions of Stimuli-Responsive Linear Ternary Heterografted Bottlebrush Polymers in Aqueous Solution

D5. Experimental Section

D5.1. Materials

CuCl (99%, Sigma-Aldrich) was stirred in glacial acetic acid overnight, collected by vacuum filtration, washed thoroughly with absolute ethanol and diethyl ether, and then dried under high vacuum. *N*,*N*,*N*′,*N*″,*N*‴-Pentamethyldiethylenetriamine (PMDETA, 99%, Acros) was dried over calcium hydride, purified by vacuum distillation, and stored in a desiccator. 2,2′-Azobis(2-methylpropionitrile) (AIBN, 98%, Aldrich) was recrystallized in ethanol, filtered, and dried under high vacuum. 2-(*N*,*N*-Diethylamino)ethyl methacrylate (DEAEMA, 98.5%, TCI) and 2-(2-ethoxyethoxy)ethyl acrylate (DEGEA, 98%, TCI) were passed through a basic alumina (top)/silica gel (bottom) column to remove the inhibitor prior to polymerization. Di(ethylene glycol) methyl ether acrylate (DEGMA) was prepared by the reaction of di(ethylene glycol) monomethyl ether with acryloyl chloride and purified by vacuum distillation.[C1] 2-(*N*,*N*-Di(*n*-butyl)amino)ethyl methacrylate (DBAEMA) was prepared by the reaction of *N*,*N*-di(*n*-butyl)aminoethanol with methacryloyl chloride and purified by column chromatography and vacuum distillation.[C2,C3] 4-(((Butylthio)carbonothioyl)thio)-4-cyanopentanoic acid (CTA-COOH) and alkyne-end-functionalized 5 kDa poly(ethylene oxide) (PEO) were prepared using procedures from the literature.[C4,C5] 1-(3-Dimethylaminopropyl)-3-ethylcarbodiimide hydrochloride (Arcos, 98%) and 4-dimethylaminopyridine (TCI, 99.0%) were used as received. All other chemicals were purchased from either Sigma-Aldrich or Fisher and used directly. The synthesis of the linear azide-functionalized backbone polymer with a degree of polymerization (DP) of 801, PHEMA-N_3, was reported previously.[S6] ^{1}H NMR spectroscopy analysis indicated that the degree of azide functionalization was 96.7%. Size exclusion chromatography (SEC) analysis, using a SEC system with PSS GRAL columns and 50 mM LiBr-containing *N*,*N*-dimethylformaide (DMF) as the eluent

at 50 °C, showed that the $M_{n,SEC}$ of PHEMA-N_3 was 121.1 kDa and the dispersity (*Đ*) was 1.13, relative to polystyrene standards.

D5.2. General Characterization

^{1}H and ^{13}C NMR spectra were recorded on either a Varian VNMRS 500 NMR or a Varian VNMRS 600 spectrometer. The stimuli-responsive behavior of three dually responsive brush polymers in aqueous solutions was studied using a Varian VNMRS 600 spectrometer equipped with a temperature controller (FTS Systems, Inc.). Aqueous solutions of MBBs with a concentration of 4.0 mg/g were prepared in D_2O (for MBB-TT) or in a 10 mM phosphate buffer made with D_2O (for MBB-PP and -TP). The pH values of the buffer solutions were measured with a pH meter (Accument AB-15, calibrated using pH = 4.01, 7.00, and 10.01 standard buffer solutions) at either 0 °C (MBB-TP) or 20 °C (MBB-PP) and adjusted using 0.1 M HCl and 0.1 M NaOH solutions in D_2O. For variable temperature ^{1}H NMR experiments, the samples were equilibrated for 5 min at each selected temperature before the data acquisition.

SEC of alkyne end-functionalized side chain polymers was performed at ambient temperature using a PL-GPC 20 (an integrated GPC/SEC system from Polymer Laboratories, Inc.) with a differential refractive index (RI) detector, one PLgel 5 μm guard column (50 × 7.5 mm, Agilent Technologies), and two PL gel 5μm mixed-C columns (each 300 × 7.5 mm, linear range of molecular weights from 200 to 2 000 000 Da, Agilent Technologies). The mobile phase was tetrahydrofuran (THF) with a flow rate of 1.0 mL/min, and the system was calibrated with a set of narrow disperse linear polystyrene standards (Scientific Polymer Products, Inc.). SEC of the MBBs was performed using a PL-GPC 50 Plus system (an integrated GPC/SEC system from Polymer Laboratories, Inc.) with an RI detector, one PSS GRAL 10 μm guard column (50 × 8 mm, Polymer Standards Service-USA, Inc.), and two PSS GRAL 10 μm linear columns (each 300 × 8 mm, linear

range of molecular weight from 500 to 1 000 000 Da, PSS-USA, Inc.) at 50 °C or the PL-GPC 20 system described above. For the PL-GPC 50 Plus system, DMF with 50 mM LiBr was used as the eluent at a flow rate of 1.0 mL/min. The absolute weight-average molecular weights ($M_{w,expt}$) of the MBBs were determined by a SEC-multiangle light scattering (SEC-MALS) system comprising one PSS GRAM 10 μm guard column (8 × 50 mm, PSS-USA, Inc.), three PSS GRAM 10 μm linear columns (8 × 300 mm; 100, 1000, and 3000 Å, PSS-USA, Inc.), an Agilent model 1260 Infinity pump, a Rheodyne model 7725 manual injector with a 200 μL loop, and a Varian 390 LC detector system consisting of an RI detector and a two-angle light scattering detector (15° and 90°). The mobile phase was DMF with 100 mM LiBr, and the analysis was carried out at 50 °C.

D5.3. Dynamic Light Scattering (DLS) Study of MBBs in Aqueous Solutions

DLS studies of MBBs in aqueous solutions at a concentration of 1.0 mg/g or 0.2 mg/g were performed using a Malvern Zetasizer Nano ZS instrument equipped with a He-Ne 633 nm laser and a temperature controller at a scattering angle of 173 °C. Each DLS sample was prepared using a wet-transfer method from a stock solution of MBBs in THF with a known concentration. A portion of the stock solution with a known concentration was weighed into a round bottom flask and then diluted with a calculated amount of Milli-Q water (for MBB-TT) or a 10 mM (for MBB-TP) or 25 mM (for MBB-PP) phosphate buffer. The solution was concentrated under vacuum to remove THF and subsequently diluted to the desired concentration with Milli-Q water. To study the pH-responsive behavior of MBB-PP and -TP, the pH of the solution was gradually adjusted using 0.1 M NaOH and 0.1 M HCl solutions and monitored by an Accument AB-15 pH meter calibrated with pH = 4.01, 7.00, and 10.01 standard buffer solutions at 0 °C (for MBB-TP) or 20 °C (for MBB-PP). After equilibrating for 10 min at the desired pH, the solution was transferred directly into a cuvette and loaded into the DLS instrument pre-set to the desired temperature.

Temperature ramps were performed by gradually changing the temperature at pre-set increments and allowing the sample to equilibrate for 5 min before the measurements. Each reported DLS value was an average of 3 measurements, each of which was comprised of 10 runs; z-average hydrodynamic diameters (D_h) were used.

D5.4. Atomic Force Microscopy (AFM) Study of MBBs

The MBBs were studied by AFM using a Digital Instruments Multimode IIIa Scanning Probe Microscope in the tapping mode under ambient conditions. Reflective Al-coated Si probes (Budget Sensors) with a resonant frequency of 300 kHz and a force constant of 40 N/m were used. Poly(methyl methacrylate) (PMMA)-coated mica substrates were prepared by cleaving a fresh layer of mica disks with Scotch tape and spin casting three drops of a 1.0 wt% solution of PMMA (M_n = 38.0 kDa) in $CHCl_3$ on the disks at 3000 rpm (P-6000 Spin Coater, Specialty Coating Systems, Inc.). To prepare AFM samples, aqueous solutions of 0.20 mg/g MBBs were diluted with Milli-Q water or a phosphate buffer to 0.05 mg/g and spin-cast onto the PMMA-coated mica substrates (3000 rpm). The pH values of aqueous solutions of MBB-PP and -TP were monitored using a pH meter (Accument AB-15) and adjusted using 0.1 M HCl and 0.1 M NaOH solutions. For the AFM samples prepared at 0 °C, the brush solutions were equilibrated in an ice/water bath while the spin stage and the PMMA-coated mica disk were cooled in a refrigerator (4 °C) and used immediately. For the AFM samples prepared at above ambient temperature, an oven was set to the desired temperature and used to equilibrate the MBB solution, the PMMA-coated mica disk, and the stage for 30 min. After equilibrating, the spin stage was quickly placed on the spin coater, and the MBB solution was spin cast promptly on the mica disk.

D5.5. Fluorescence Spectroscopy Study of Stepwise Release of Nile Red from Collapsed MBB-PP in Aqueous Solution

Nile Red was used as a model hydrophobic drug to demonstrate the pH-induced stepwise release from MBB-PP in an aqueous solution. A stock solution of Nile Red in acetone with a concentration of 0.021 mg/mL was prepared, and a microsyringe was used to transfer 50 µL of this stock solution to a vial. After the solution was dried under high vacuum for 5 h, a 0.2 mg/g MBB-PP solution in 25 mM phosphate buffer (5.00 g) was added to the vial. The pH of the solution was adjusted to 9.50 at room temperature, and the solution was allowed to equilibrate two days. The calculated molar concentration of Nile Red in the solution was 6.7×10^{-7} M. The fluorescence emission spectra of Nile Red were acquired at room temperature using a Perkin Elmer LS 55 fluorescence spectrometer equipped with a 20 kW Xenon discharge lamp. The excitation wavelength used was 540 nm, the slit width was 10 nm, and the emission spectra were collected from 550 to 720 nm. The pH of the Nile Red-containing MBB-PP solution was adjusted using 0.1 M HCl and 0.1 M NaOH solutions and monitored with an Accument AB-15 pH meter; once a desired pH was reached, the sample was equilibrated for 10 min before the new fluorescence emission spectrum was collected.

D5.6. Synthesis of Alkyne-Functionalized Chain Transfer Agent, Prop-2-yn-1-yl 4-(((Butylthio)carbonothioyl)thio)-4-cyanopentanoate (CTA-Alkyne)

4-(((Butylthio)carbono-thioyl)thio)-4-cyanopentanoic acid (CTA-COOH) (1.344 g, 4.61 mmol), propargyl alcohol (0.371 g, 6.61 mmol), and dichloromethane (10 mL) were added into a 50 mL two-necked round bottom flask under nitrogen. The flask was then placed in an ice/water bath and stirred with a magnetic stir bar. 1-(3-Dimethylaminopropyl)-3-ethylcarbodiimide hydrochloride (1.332 g, 6.95 mmol) and 4-dimethylaminopyridine (0.0637 g, 0.521 mmol) were

dissolved in dichloromethane (10 mL) and added dropwise into the flask via an addition funnel. The reaction mixture gradually warmed to room temperature and was stirred overnight. Dichloromethane was removed under reduced pressure, and the crude product was purified by column chromatography using a mixture of hexanes and ethyl acetate (10/1, v/v) as eluent. The final product was dried under high vacuum, yielding an orange oil as the pure product (1.183 g, 77.8% yield). ^{1}H NMR δ (ppm, $CDCl_3$) = 4.71 (d, -OC*H*$_2$C≡CH, 2H), 3.34 (t, $CH_3CH_2CH_2CH_2$S-, 2H), 2.68 (m, -SC(CH_3)(CN)CH_2CH_2CO-, 2H), 2.58-2.38 (m, -SC(CH_3)(CN)C*H*$_2CH_2$CO- 2H), 2.49 (t, -C≡C*H*, 1H), 1.88 (s, -SC(C*H*$_3$)(CN)CH_2-, 3H), 1.69 (m, $CH_3CH_2CH_2CH_2$S-, 2H), 1.43 (m, $CH_3CH_2CH_2CH_2$S-, 2H), 0.94 (t, C*H*$_3CH_2CH_2CH_2$S-, 3H). ^{13}C NMR δ (ppm, $CDCl_3$) = 216.73 (-CH_2S*C*(=S)S-), 170.57 (-CH_2*C*OOCH_2C≡CH), 118.81 (-*C*N), 77.14 (-CH_2*C*≡CH), 75.20 (-CH_2C≡*C*H), 53.26 (-O*C*H_2C≡CH), 46.17 (-S*C*(CH_3)(CN)CH_2CH_2CO-), 36.67 ($CH_3CH_2CH_2$*C*H_2S*C*(=S)S-), 33.55 (-SC(CH_3)(CN)*C*H_2CH_2CO-), 29.61 (-SC(CH_3)(CN)CH_2*C*H_2CO-), 29.46 (CH_3CH_2*C*H_2CH_2S*C*(=S)S-), 24.75 (CH_3*C*$H_2CH_2CH_2$S*C*(=S)S-), 21.98 (-SC(C*H*$_3$)(CN)CH_2-), 13.49 (*C*$H_3CH_2CH_2CH_2$S-).

D5.7. Synthesis of Alkyne-End-Functionalized Side Chain Polymers

Alkyne-end-functionalized PDEGEA, PDEGMA, PDEAEMA, and PDBAEMA were prepared by reversible addition-fragmentation chain transfer (RAFT) polymerization using CTA-Alkyne. The following shows the details for the synthesis of the alkyne-end-functionalized PDEGEA with a degree of polymerization (DP) of 57. CTA-Alkyne (52.4 mg, 0.159 mmol), DEGEA (3.041 g, 16.12 mmol), AIBN (2.64 mg, 0.0161 mmol, from a 1.81 mg/g stock solution in anisole), and anisole (5.618 g total) were added to a 25 mL two-necked round bottom flask along with a magnetic stir bar. The reaction mixture was degassed by three cycles of freeze pump-thaw, and the flask was placed immediately in an oil bath with the temperature preset at 65 °C. After 4

h, the reaction mixture was removed from the oil bath, opened to air, and diluted with THF (10 mL). The solution was concentrated by rotary evaporation, and the polymer was precipitated into hexanes (75 mL) from THF at room temperature. After two additional rounds of precipitation, the purified polymer was dried under high vacuum, yielding a viscous yellow polymer (1.581 g, 52.0%). The monomer conversion was determined to be 56.0% using the ^{1}H NMR spectrum of the final reaction mixture by comparing the integrals of the peaks at 4.36-4.31 ppm (-COOC*H*$_2$- of DEGEA) and at 4.28-4.15 ppm (-COOC*H*$_2$- of PDEGEA). The DP of PDEGEA was calculated to be 57, from the initial monomer-to-CTA molar ratio (101.6:1) and the monomer conversion. SEC analysis using the PL-GPC 20 system gave a $M_{n,SEC}$ of 10.3 kDa and a $Đ$ of 1.16 relative to polystyrene standards. Alkyne-end-functionalized PDEGMA with a DP of 55 was synthesized using the same procedure as for PDEGEA. SEC showed $M_{n,SEC}$ = 9.3 kDa and $Đ$ = 1.15, with respect to polystyrene standards.

Alkyne-end-functionalized PDEAEMA and PDBAEMA were also prepared by the same procedure except the use of 70 °C as the polymerization temperature. PDEAEMA was purified by precipitation into hexanes from THF three times in a dry ice/acetone bath. The monomer conversion was calculated using the integrals of the peaks at 4.26-4.21 ppm (-COOC*H*$_2$- of DEAEMA) and at 4.15-3.96 ppm (-COOC*H*$_2$- of PDEAEMA) from the ^{1}H NMR spectrum of the final reaction mixture, and the DP was calculated from the monomer conversion and the initial molar ratio of monomer-to-CTA Alkyne. Two PDEAEMA polymers were made, one having a DP of 56, denoted as PDEAEMA-56, and the other having a DP of 45, denoted as PDEAEMA-45. SEC analysis of PDEAEMA-56 showed that the values of $M_{n,SEC}$ and $Đ$ were 7.8 kDa and 1.14, respectively, relative to polystyrene standards. The $M_{n,SEC}$ and $Đ$ of PDEAEMA-45 were 6.9 kDa and 1.14, respectively. Alkyne-end-functionalized PDBAEMA was purified by precipitation into

methanol three times at room temperature, and a centrifuge was used to maximize the recovery of the product. The monomer conversion was calculated from the ^{1}H NMR analysis of the final reaction mixture using the integrals of the peaks at 4.24-4.19 ppm (-COOC*H*$_2$- of DBAEMA) and at 4.08-3.94 ppm (-COOC*H*$_2$- of PDBAEMA), and the DP of PDBAEMA was 43. SEC using the PL-GPC 20 system yielded $M_{n,SEC}$ = 9.9 kDa and $Đ$ = 1.12, relative to polystyrene standards.

D5.8. Synthesis of Ternary MBBs

Three ternary brush polymers, MBB-TT, -PP, and -TP, were synthesized by the CuAAC click reaction using similar procedures. The following shows the synthesis, purification, and characterization of MBB-TP composed of PEO, PDEGEA and PDEAEMA-56 side chains. PHEMA-N_3 (5.03 mg, delivered by 0.466 g of a 10.81 mg/g stock solution in THF, 2.08 $\times 10^{-2}$ mmol of the azide groups assuming 100% azide functionalization), PDEGEA (115.5 mg, 1.05 $\times$ 10^{-2} mmol, delivered via 1.106 g of a 104.4 mg/g stock solution in THF), PDEAEMA-56 (110.9 mg, 1.04 $\times$ 10^{-2} mmol, delivered via 1.285 g of a 86.3 mg/g stock solution in THF), PEO (53.0 mg, 1.04 $\times$ 10^{-2} mmol), CuCl (2.4 mg, 2.43 $\times$ 10^{-2} mmol), and THF (4 mL) were added to a 2 dram vial equipped with a magnetic stir bar. The vial was sealed with a rubber septum and the reaction mixture was bubbled with nitrogen gas for 15 min. PMDETA (6.0 µL, 2.87 $\times$ 10^{-2} mmol) was then injected by a microsyringe. After 20 h, benzyl propargyl ether (BPE) (25.0 µL) was injected to attempt to cap unreacted azide groups. After an additional 2 h, an aliquot of the reaction mixture was taken for SEC analysis to estimate the grafting density, and the remaining mixture was diluted with THF and passed through a basic alumina/silica gel column to remove the copper catalyst. To ensure that all azide groups had reacted, a second round of CuAAC with BPE was performed as detailed below. The reaction mixture was concentrated to ~5 mL, followed by the addition of CuCl (2.5 mg) and BPE (25 µL). The mixture was then bubbled with nitrogen gas for 15 min, and

PMDETA (5.0 μL) was injected. After 5 h, the solution was passed through a basic alumina/silica gel column, and a rotary evaporator was used to concentrate the solution to ~2 mL. Two rounds of fractionation were performed using THF as a good solvent and hexanes as a poor solvent to remove a portion of the unreacted side chain polymers. The remaining excess side chain polymers were removed by 4 rounds of centrifugal filtration using an Amicon 50 kDa MWCO filter and a mixture of ethanol and water (50/50, v/v) at 4500 rpm. The complete removal of unreacted side chain polymers was confirmed by SEC analysis using the PL-GPC 50 Plus system. The molar composition of brush side chains was calculated using the integrals of the peaks at 4.30-4.13 ppm (-COOCH_2-) of PDEGEA, 4.13-3.96 ppm (-COOCH_2-) of PDEAEMA-56, and 3.38 ppm (-OCH_3) of PEO and the DP of each polymer. The molar contents of PDEGEA, PDEAEMA-56, and PEO side chains in MBB-TP were 32.2%, 27.4%, and 40.4%, respectively. The experimental absolute weight-average molecular weight ($M_{w,expt}$) of MBB-TP was 7.81×10^6 Da, measured by a SEC-MALS system. The grafting density of MBB-TP was calculated to be 90.4% using a combination of SEC analysis of the final reaction mixture, feed masses, and the side chain composition of the brush polymer as described below.

The peak area percentages were 59.0% for the MBBs and 41.0% for the unreacted side chain polymers from the SEC analysis of the final reaction mixture and were assumed to be the same as the respective mass percentages. The calculated absolute $M_{n,calc}$ values of PDEGEA and PDEAEMA-56 from the DPs and the molecular weight of CTA end groups were 11058 and 10704 Da, respectively. As mentioned earlier, the molar contents of PDEGEA, PDEAEMA-56, and PEO side chains were 32.2%, 27.4%, and 40.4%, respectively, from the ^{1}H NMR analysis. Based on the calculated $M_{n,calc}$ values and the molar composition, the mass percentages were 41.7% PDEGEA, 34.3% PDEAEMA-56, and 24.0% PEO. Using the area percentage of MBB-TP from

the SEC analysis of the final reaction mixture and multiplying it by the total feed mass of the backbone and side chain polymers yielded 162.8 mg of side chain polymers in the initial feed that had reacted. Therefore, the total amounts of side chains that were grafted onto the azide backbone were 67.9 mg PDEGEA, 55.8 mg PDEAEMA-56, and 39.1 mg of PEO. The total molar amount of the reacted side chain polymers was 0.0188 mmol compared to 0.0208 mmol of backbone azide (assuming 100% azide functionalization). The grafting density was calculated by dividing the total moles of the reacted side chain polymers by the moles of the backbone repeat units, which was 90.4%.

MBB-PP was synthesized using PEO, PDEAEMA-45, and PDBAEMA via a similar procedure. After the click reaction, the mixture was passed through an alumina column and concentrated to ~1 mL using a rotary evaporator. The unreacted PDBAEMA was first removed by three rounds of precipitation in methanol from THF. The unreacted PDEAEMA-45 and PEO were eliminated by several rounds of centrifugal filtration using an Amicon 50 kDa MWCO filter with a mixture of ethanol and water (60/40, v/v) at 4500 rpm. SEC analysis using the PL-GPC 50 Plus system with DMF as the eluent was employed to confirm the removal of PDEAEMA-45 and PEO side chain polymers, which showed no side chain polymers after the purification. Because PDBAEMA was not soluble in DMF and could not be eluted out from the DMF GPC columns, we used the PL-GPC 20 with mixed-C columns and THF as the mobile phase to verify the removal of PDBAEMA. A known amount of purified MBB-PP, from a stock solution in THF, was weighed into a vial along with a similar amount of PMMA (M_n = 100 kDa, a PMMA standard). The SEC trace showed that the peak of the PMMA standard was observed at the retention time of 13.8 min and no PDBAEMA was found, which would be eluted out at the retention time of 15.9 min. Control SEC analysis of a mixture of PDBAEMA and PMMA with similar amounts using the same SEC

system showed that both polymers appeared in the SEC chromatogram, thus confirming the complete removal of unreacted PDBAEMA. ^{1}H NMR spectroscopy analysis of MBB-PP revealed that the side chain molar composition was 19.8% PDBAEMA, 29.2% PDEAEMA-45, and 51.0 % PEO, calculated by considering the DPs of the side chain polymers and the integrals of the peaks at 4.17-3.91 ppm for -COOCH_2- of PDEAEMA-45 and PDBAEMA, 3.38 ppm for -OCH_3 of PEO, and 2.51-2.42 ppm for -N(CH_2CH$_2$CH$_2$CH$_3$)$_2$ of PDBAEMA. The absolute $M_{w,expt}$ of MBB-PP was determined to be 7.13×10^6 Da using a SEC-MALS system with DMF containing 100 mM LiBr as the eluent. The sample for SEC-MALS analysis was prepared by gradually adding DMF (10 mL) into a solution of MBB-PP in THF (10 mL, concentration = 0.10 mg/mL) and then evaporating THF under a stream of nitrogen. The final concentration of MBB-PP in DMF was 0.43 mg/g, and DLS measurements showed that the D_h was 67.9 nm with a polydispersity index (PDI) of 0.16. A repeated SEC-MALS measurement of another SEC sample of MBB-PP with a slightly different concentration (0.48 mg/g) gave a $M_{w,expt}$ of 7.22×10^6 Da, which is essentially the same. These observations suggested that brush molecules remained molecularly dissolved in DMF in the sample preparation process.

The $M_{w,expt}$ values from SEC-MALS were higher than the absolute $M_{w,calc}$ of a hypothetical bottlebrush polymer with the same side chain composition as MBB-PP and a full grafting density (i.e., 96.7% – the degree of azide functionalization of PHEMA-N$_3$) calculated as follows. The calculated $M_{n,calc}$ values of PDBAEMA, PDEAEMA-45, and PEO were 10709, 8666, and 5100 Da considering the DPs and the molecular weights of the end groups. Using the corresponding $Đ$ values from SEC analysis, the calculated $M_{w,calc}$ values for PDBAEMA, PDEAEMA-45, and PEO were 11994, 9878, and 5304 Da, respectively, and the $M_{w,calc}$ of the azide-functionalized backbone polymer (DP = 801) was 2.22×10^5 Da. The molar composition of the side chain polymers from

^{1}H NMR analysis was 19.8% PDBAEMA, 29.2% PDEAEMA-45, and 51.0% PEO. By taking into account the DP and the degree of azide functionalization (96.7%) of the backbone polymer, the hypothetical bottlebrush polymer consists of 153 PDBAEMA, 226 PDEAEMA-45, and 395 PEO side chains. Using the $M_{w,calc}$ values of side chain polymers and the backbone polymer, the $M_{w,calc}$ is calculated to be 6.38×10^6 Da.

MBB-TT was synthesized using alkyne-end-functionalized PEO, PDEGEA, and PDEGMA and purified similarly to MBB-TP. The crude brushes were dissolved in a mixture of ethanol and water (50/50, v/v), and the remaining unreacted side chain polymers were removed by centrifugal filtration using an Amicon centrifugal filter unit with a 50 kDa MWCO filter. The complete removal of unreacted side chain polymers was confirmed by SEC analysis. The absolute $M_{w,expt}$ measured by SEC-MALS was 7.92×10^6 Da. The side chain molar composition of MBB-TT was 32.9% PDEGEA, 32.7% PDEGMA, and 34.4 % PEO from the ^{1}H NMR analysis by comparing the integrals of the peaks at 4.30-4.07 ppm (-COOCH_2- of PDEGEA and PDEGMA), 3.42-3.30 ppm (-OCH_3 of PDEGMA and PEO), and 1.24-1.12 ppm (-OCH$_2$CH_3 of PDEGEA) and considering the DPs of the side chain polymers. The grafting density of MBB-TT was calculated to be 93.0% by using the SEC peak area fractions of the brushes and the unreacted side chains in the final reaction mixture, the feed masses, and the side chain composition as for MBB-TP.

References:

D1. Hua, F. J.; Jiang, X. G.; Li, D. J.; Zhao, B. Well-Defined Thermosensitive, Water-Soluble Polyacrylates and Polystyrenics with Short Pendant Oligo(ethylene glycol) Groups Synthesized by Nitroxide-Mediated Radical Polymerization. *J. Polym. Sci. Part A: Polym. Chem.* **2006**, *44*, 2454-2467.

D2. Zhou, K. J.; Wang, Y. G.; Huang, X. N.; Luby-Phelps, K.; Sumer, B. D.; Gao, J. M. Tunable, Ultrasensitive pH-Responsive Nanoparticles Targeting Specific Endocytic Organelles in Living Cells. *Angew. Chem., Int. Ed.* **2011**, *50*, 6109 -6114

D3. Henn, D. M.; Wright, R. A. E.; Woodcock, J. W.; Hu, B.; Zhao, B. Tertiary Amine-Containing Thermo- and pH-Sensitive Hydrophilic ABA Triblock Copolymers: Effect of Different Tertiary Amines on Thermally Induced Sol-Gel Transitions. *Langmuir* **2014**, *30*, 2541–2550.

D4. Seymour, B. T.; Wright, R. A. E.; Parrott, A. C.; Gao, H. Y.; Martini, A.; Qu, J.; Dai, S.; Zhao, B. Poly(alkyl methacrylate) Brush-Grafted Silica Nanoparticles as Oil Lubricant Additives: Effects of Alkyl Pendant Groups on Oil Dispersibility, Stability, and Lubrication Property. *ACS Appl. Mater. Interfaces*, **2017**, *9*, 25038–25048.

D5. Henn, D. M.; Fu, W. X.; Mei, S.; Li, C. Y.; Zhao, B. Temperature-Induced Shape Changing of Thermosensitive Binary Heterografted Linear Molecular Brushes between Extended Worm-Like and Stable Globular Conformations. *Macromolecules* **2017**, *50*, 1645-1656.

D6. Kent, E. W.; Lewoczko, E. M.; Zhao, B. Effect of Buffer Anions on Pearl-Necklace Morphology of Tertiary Amine-Containing Binary Heterografted Linear Molecular Bottlebrushes in Acidic Aqueous Buffers. *Langmuir* **2020**, *36*, 13320-13330.

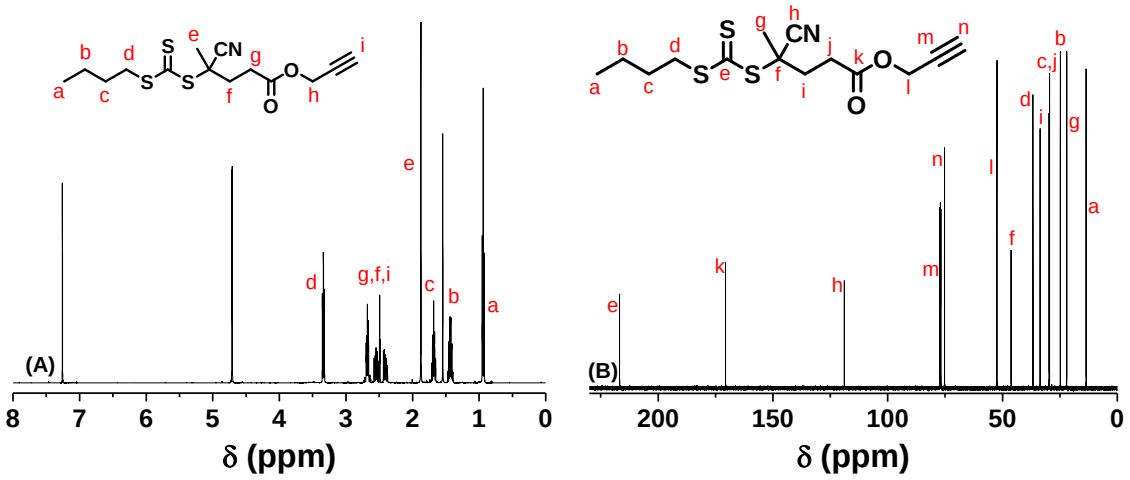

Figure D1. ^{1}H (A) and ^{13}C (B) NMR spectra of CTA-Alkyne in $CDCl_3$.

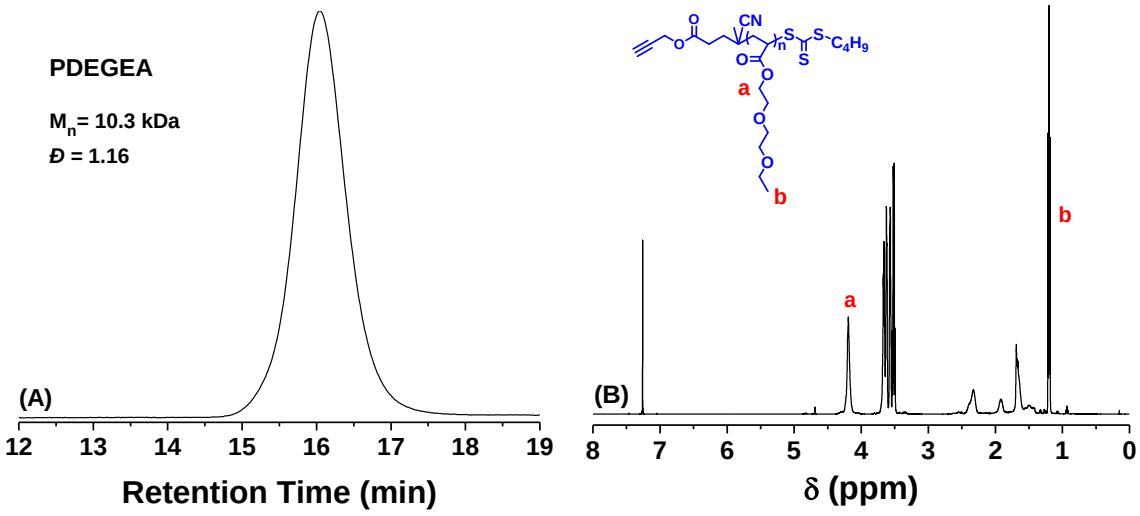

Figure D2. (A) SEC chromatogram of alkyne-end-functionalized PDEGEA with a DP of 57 from SEC analysis using a PL-GPC 20 with mixed-C columns and THF as the eluent and (B) ^{1}H NMR spectrum of PDEGEA in $CDCl_3$.

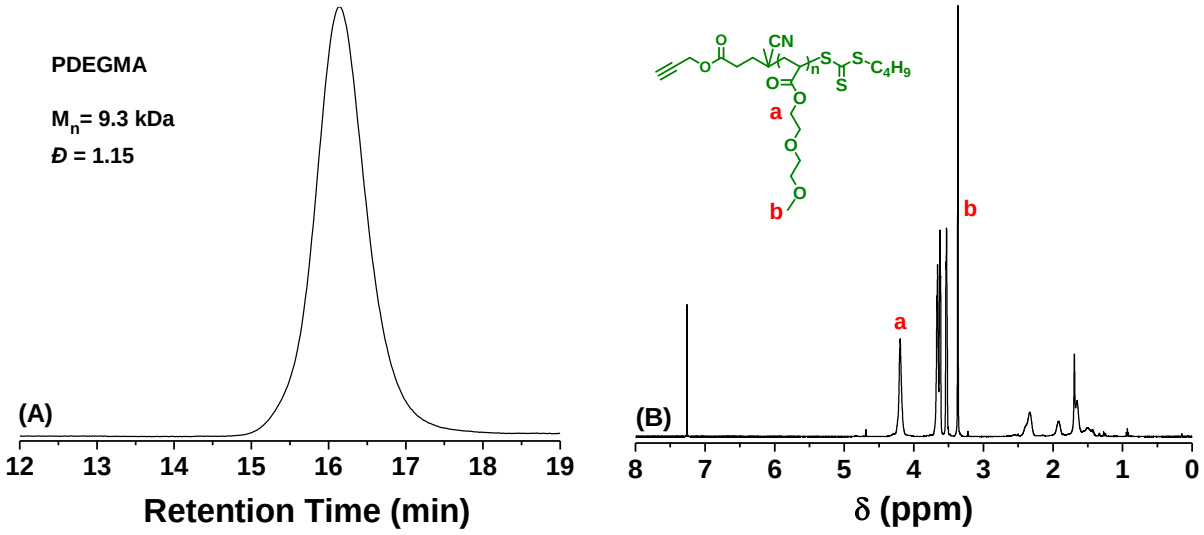

Figure D3. (A) SEC chromatogram of alkyne-end-functionalized PDEGMA with a DP of 55 from SEC analysis using a PL-GPC 20 with mixed-C columns and THF as the eluent and (B) ^{1}H NMR spectrum of PDEGMA in $CDCl_3$.

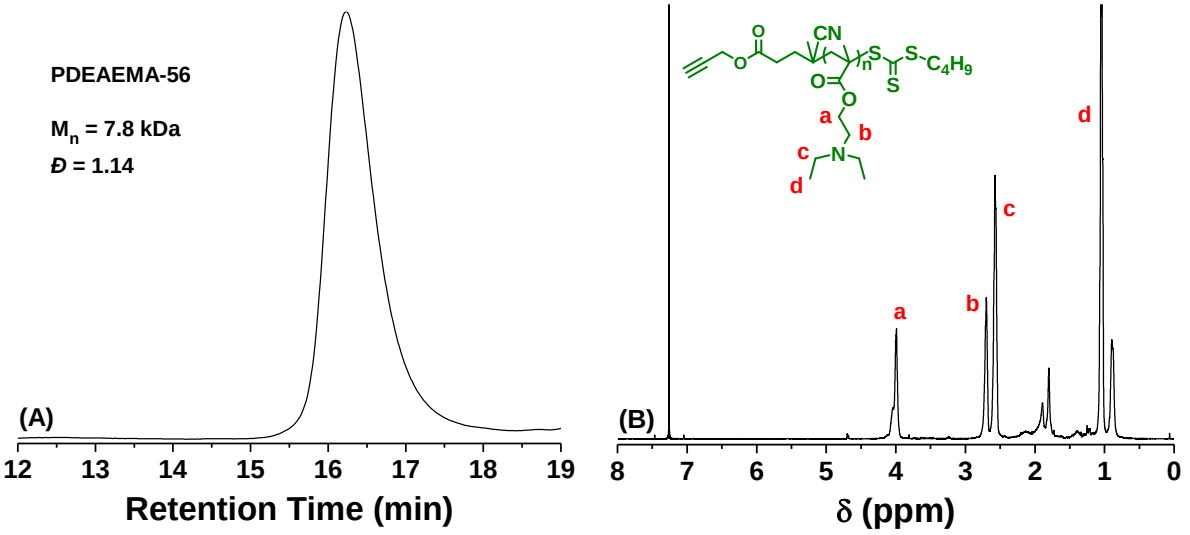

Figure D4. (A) SEC chromatogram of alkyne-end-functionalized PDEAEMA-56 from SEC analysis using a PL-GPC 20 with mixed-C columns and THF as the eluent and (B) ^{1}H NMR spectrum of PDEAEMA-56 in $CDCl_3$.

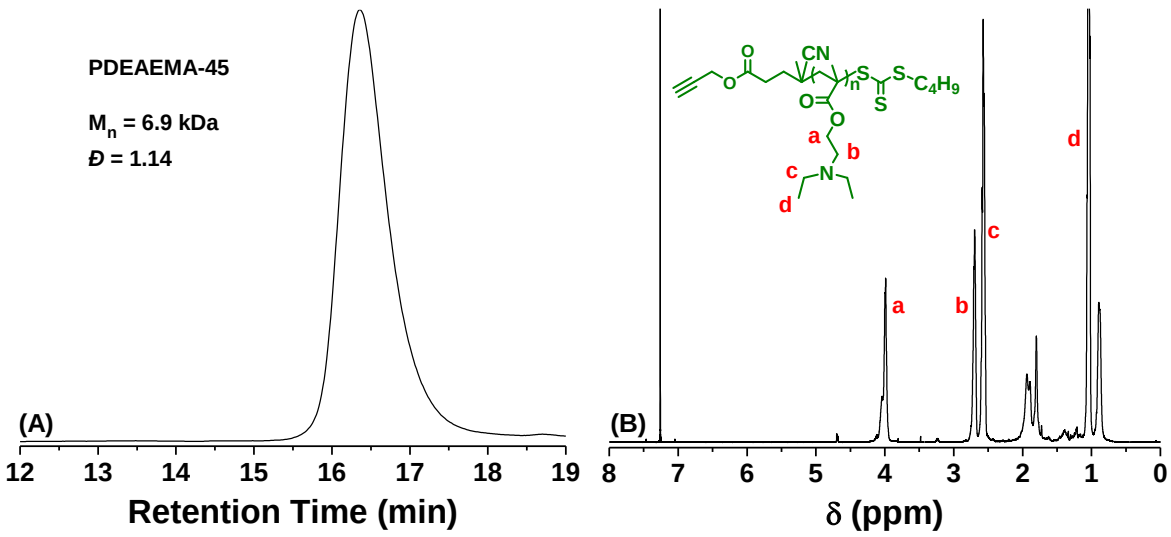

Figure D5. (A) SEC chromatogram of alkyne-end-functionalized PDEAEMA-45 obtained from a PL-GPC 20 with mixed-C columns and THF as the eluent and (B) ^{1}H NMR spectrum of PDEAEMA-45 in $CDCl_3$.

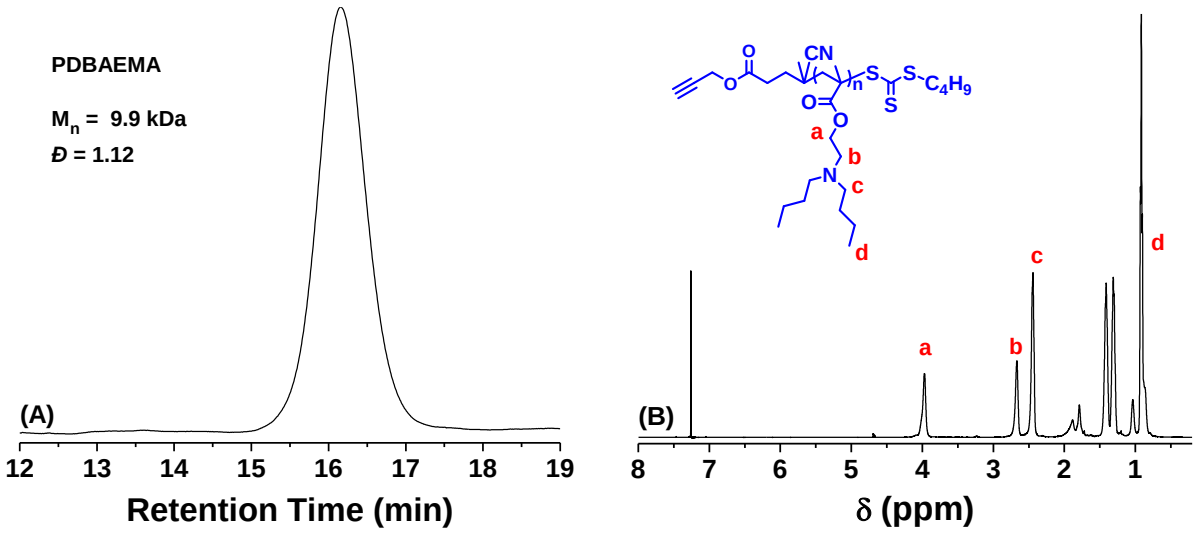

Figure D6. (A) SEC chromatogram of alkyne-end-functionalized PDBAEMA from SEC analysis using a PL-GPC 20 with mixed-C columns and THF as the eluent and (B) ^{1}H NMR spectrum of PDBAEMA in $CDCl_3$.

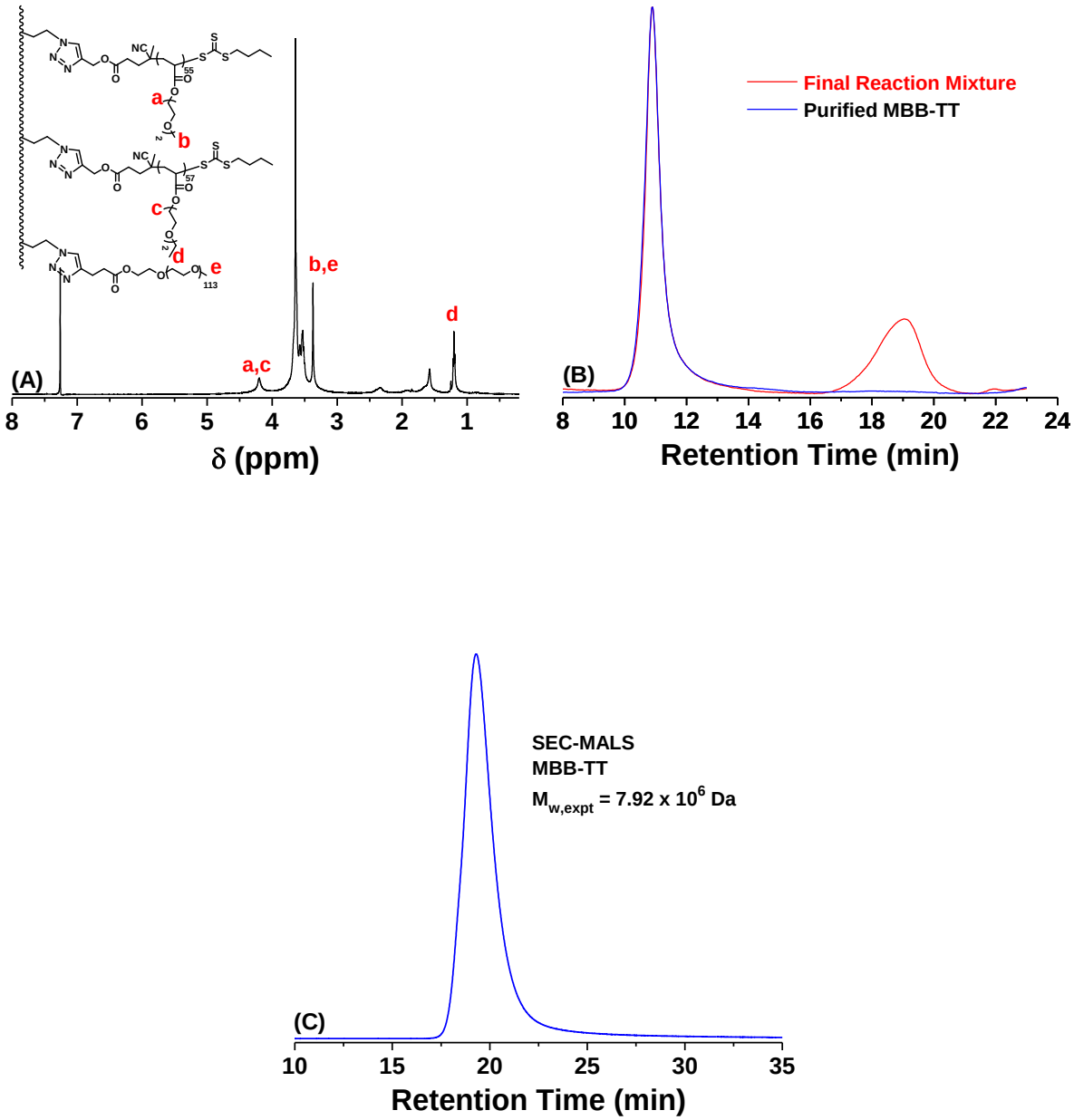

Figure D7. (A) ^{1}H NMR spectrum of MBB-TT in $CDCl_3$. (B) SEC chromatograms of the final reaction mixture for the synthesis of MBB-TT and the purified MBB-TT from SEC analysis using a PL-GPC 50 Plus system equipped with GRAL columns and DMF containing 50 mM LiBr as the eluent. (C) SEC chromatogram of MBB-TT from SEC analysis using a SEC-MALS system comprising PSS GRAM columns and a Varian 390 LC detector system consisting of an RI detector and a two-angle light scattering detector (15° and 90°) at 50 °C. The mobile phase was DMF with 100 mM LiBr.

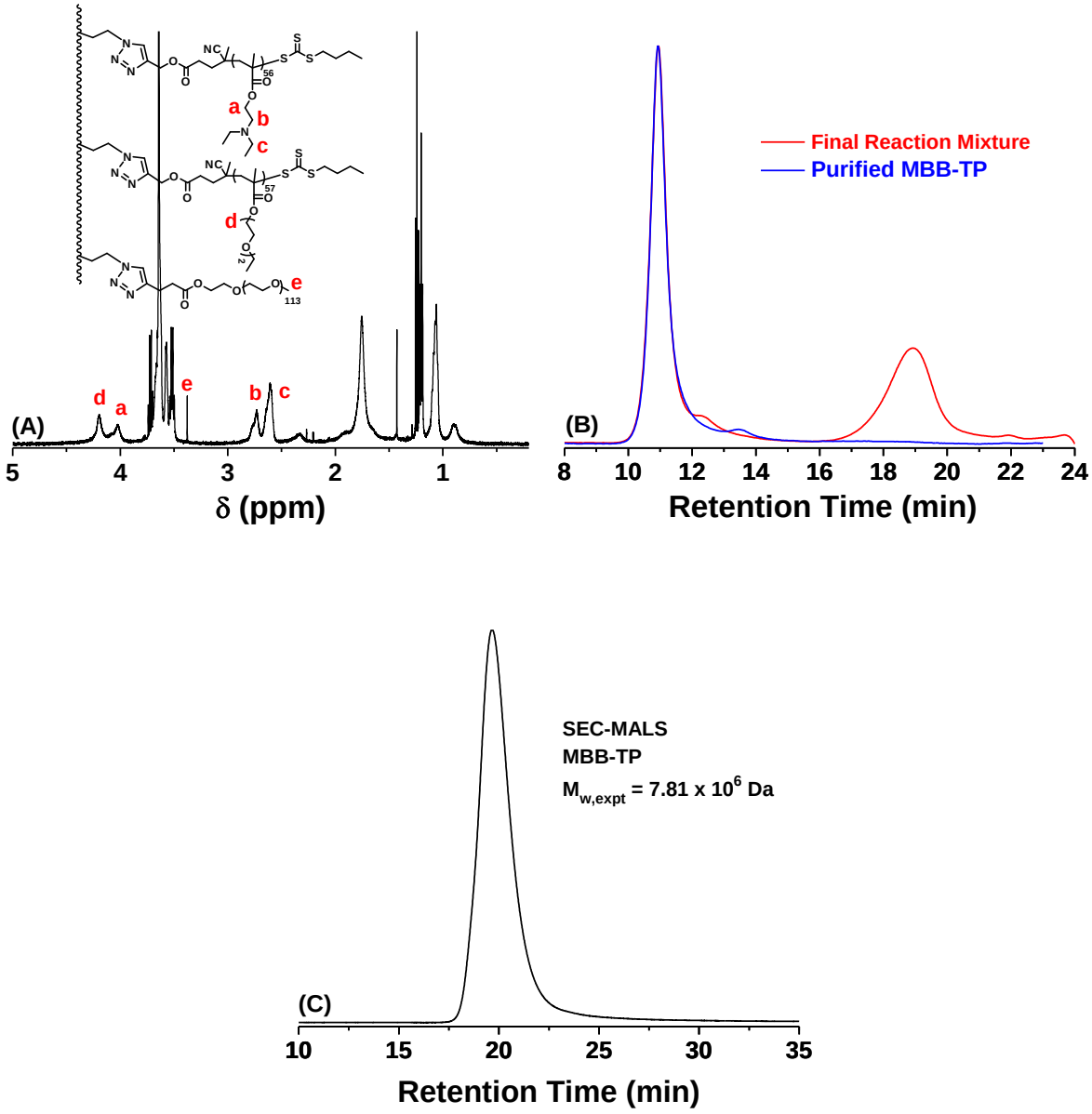

Figure D8. (A) ^{1}H NMR spectrum of purified MBB-TP in $CDCl_3$ and (B) SEC chromatograms of the final reaction mixture and purified MBB-TP from SEC analysis using the PL-GPC 50 Plus system equipped with GRAL columns and DMF containing 50 mM LiBr as the mobile phase. (C) SEC chromatogram of MBB-TP obtained from a SEC-MALS system comprising PSS GRAM columns and a Varian 390 LC detector system consisting of an RI detector and a two-angle light scattering detector (15° and 90°) at 50 °C. The mobile phase was DMF with 100 mM LiBr.

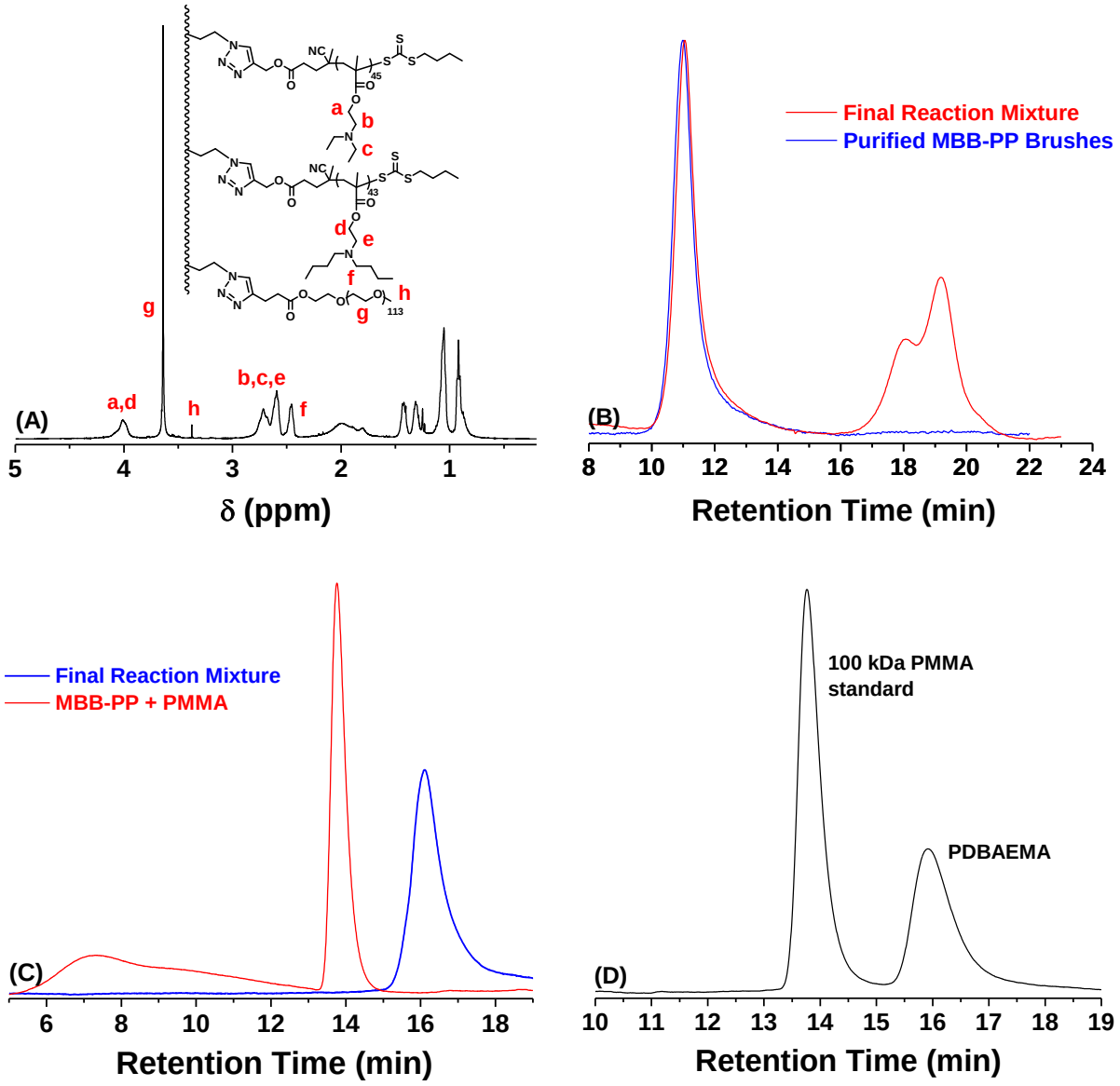

Figure D9. (A) ^{1}H NMR spectrum of purified MBB-PP in $CDCl_3$. (B) SEC chromatograms of the final reaction mixture and the purified MBB-PP from SEC analysis using a PL-GPC-50 equipped with GRAL columns and DMF containing 50 mM LiBr as the eluent. Note that PDBAEMA could not be eluted from this SEC system. The absence of the peaks in the retention time range of 16 – 21 min indicated the complete removal of PDEAEMA-45 and PEO side chain polymers. (C) SEC chromatograms of the final reaction mixture for the synthesis of MBB-PP and a mixture of purified MBB-PP and PMMA from SEC analysis using a PL-GPC 20 system with mixed-C columns and THF as the eluent. MBB-PP was not always eluted out from this PL-GPC 20 system, but the absence of the peak in the retention time range of 15 to 18 min in (C) indicated the removal of PDBAEMA. (D) SEC chromatogram of a mixture of a 100 kDa PMMA standard and PDBAEMA from SEC analysis using the PL-GPC 20 system with mixed-C columns and THF as the eluent.

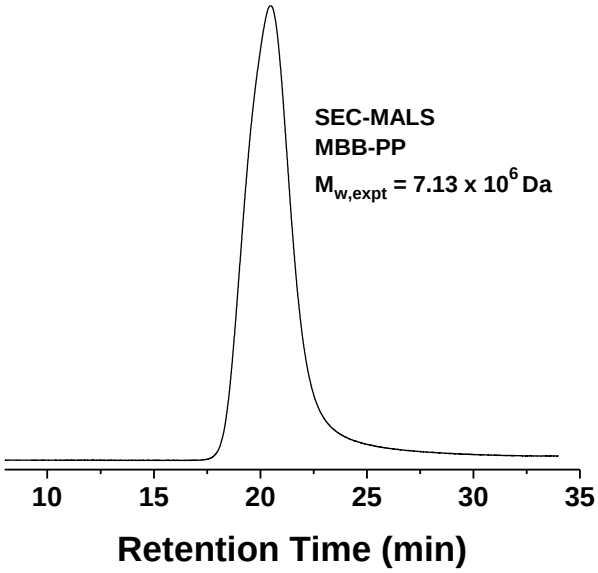

Figure D10. SEC chromatogram of MBB-PP from SEC analysis using a SEC-MALS system comprising PSS GRAM columns and a Varian 390 LC detector system consisting of an RI detector and a two-angle light scattering detector (15° and 90°) at 50 °C. The mobile phase was DMF with 100 mM LiBr. The sample for SEC-MALS analysis was prepared by gradually adding DMF (10 mL) into a solution of MBB-PP in THF (10 mL, conc = 0.10 mg/g) and then evaporating THF under a stream of nitrogen. The final concentration of MBB-PP in DMF was 0.43 mg/g. DLS measurements showed that the apparent hydrodynamic diameter (D_h) was 67.9 nm with a polydispersity index (PDI) of 0.16.

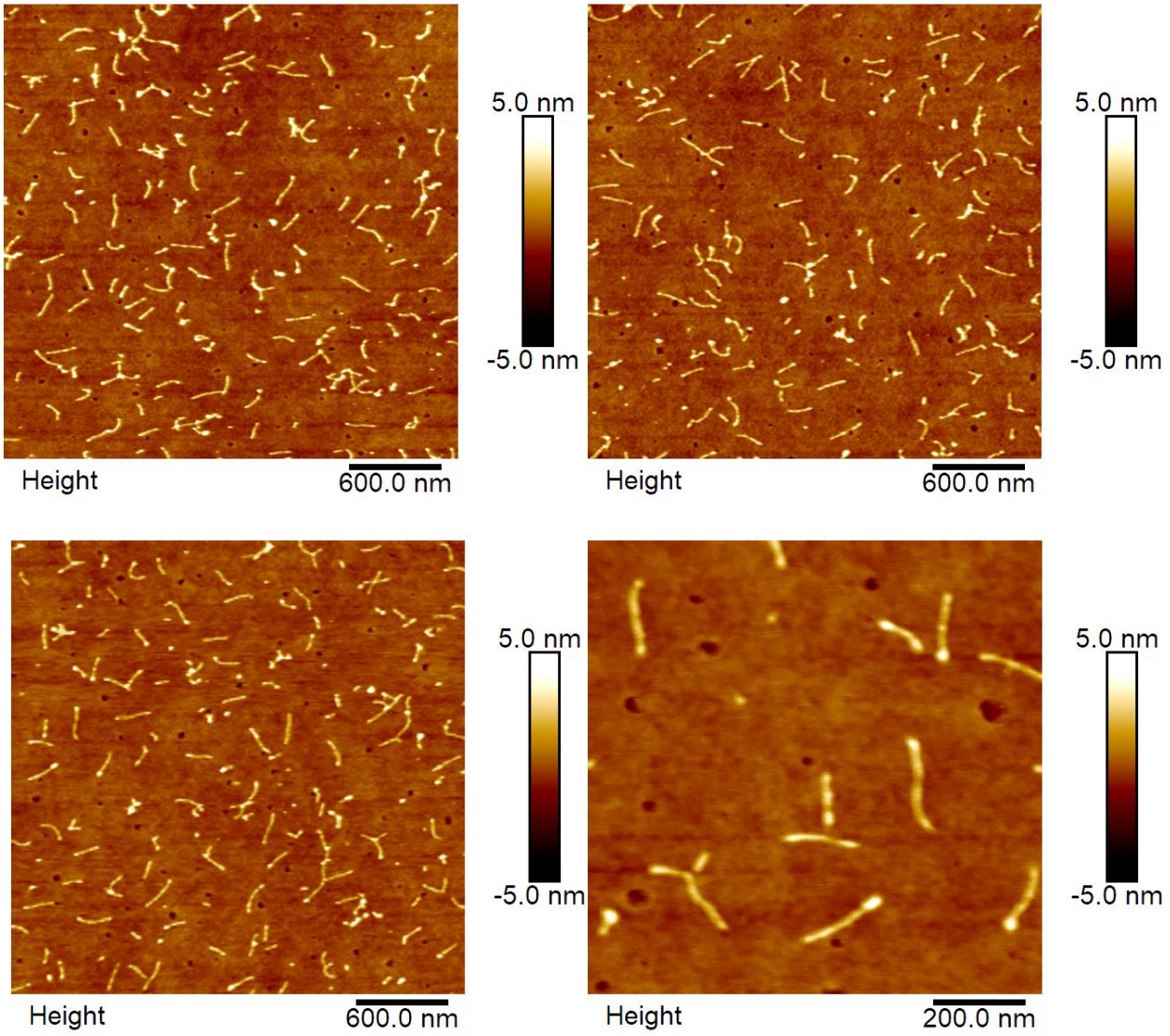

Figure D11. Additional AFM height images of MBB-PP spin cast onto PMMA-coated mica at room temperature (~ 20 °C) from a 0.05 mg/g MBB-PP solution in a 10 mM phosphate buffer with a pH of 4.00. The average length of 131 MBB molecules from the upper left image was 171.1 ± 42.6 nm.

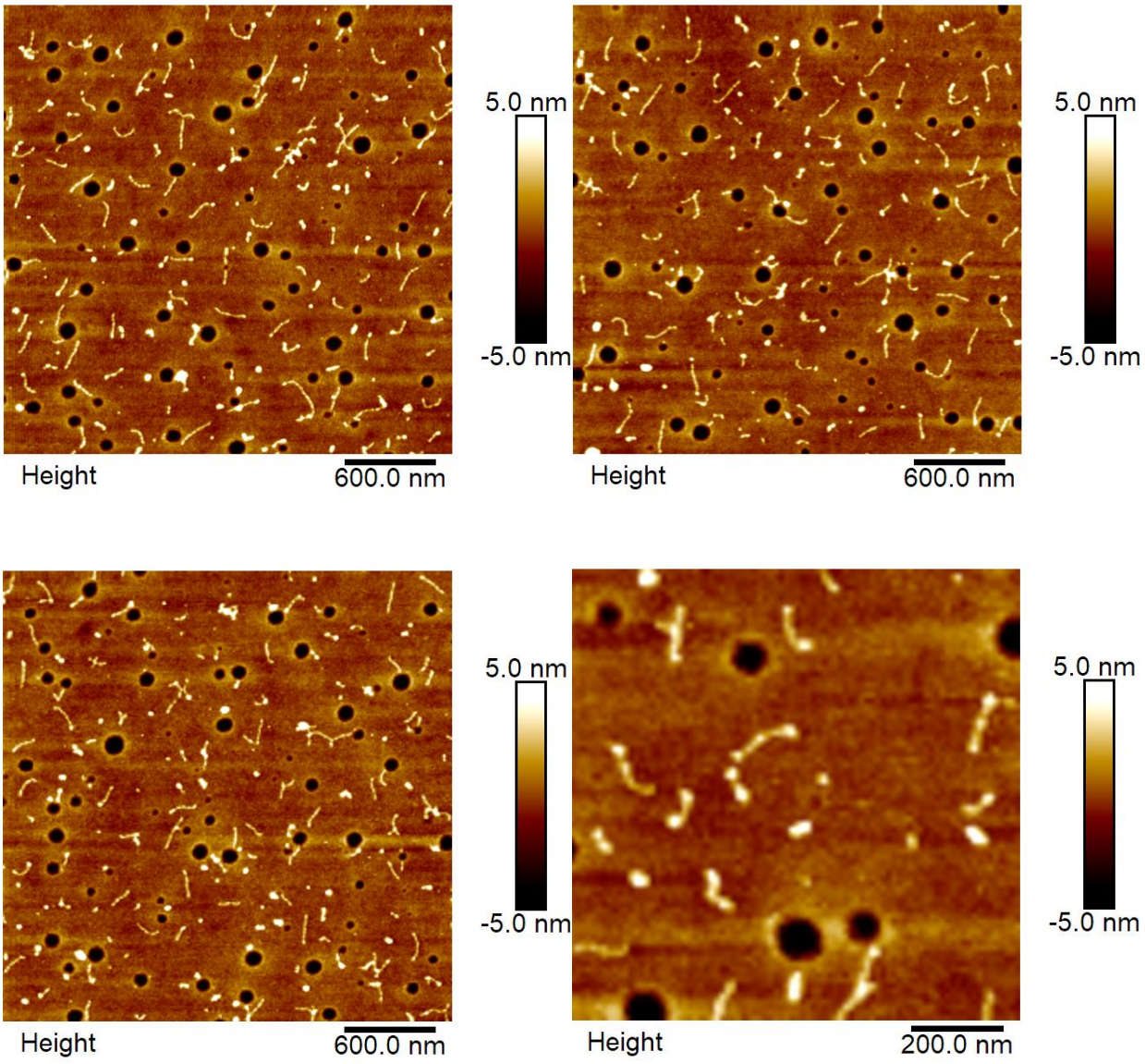

Figure D12. Additional AFM height images of MBB-PP spin cast onto PMMA-coated mica at room temperature (~ 20 °C) from a 0.05 mg/g MBB-PP solution in a 10 mM phosphate buffer with a pH of 6.00. The average length of 144 MBB-PP molecules from the upper left image was 110.9 ± 44.3 nm.

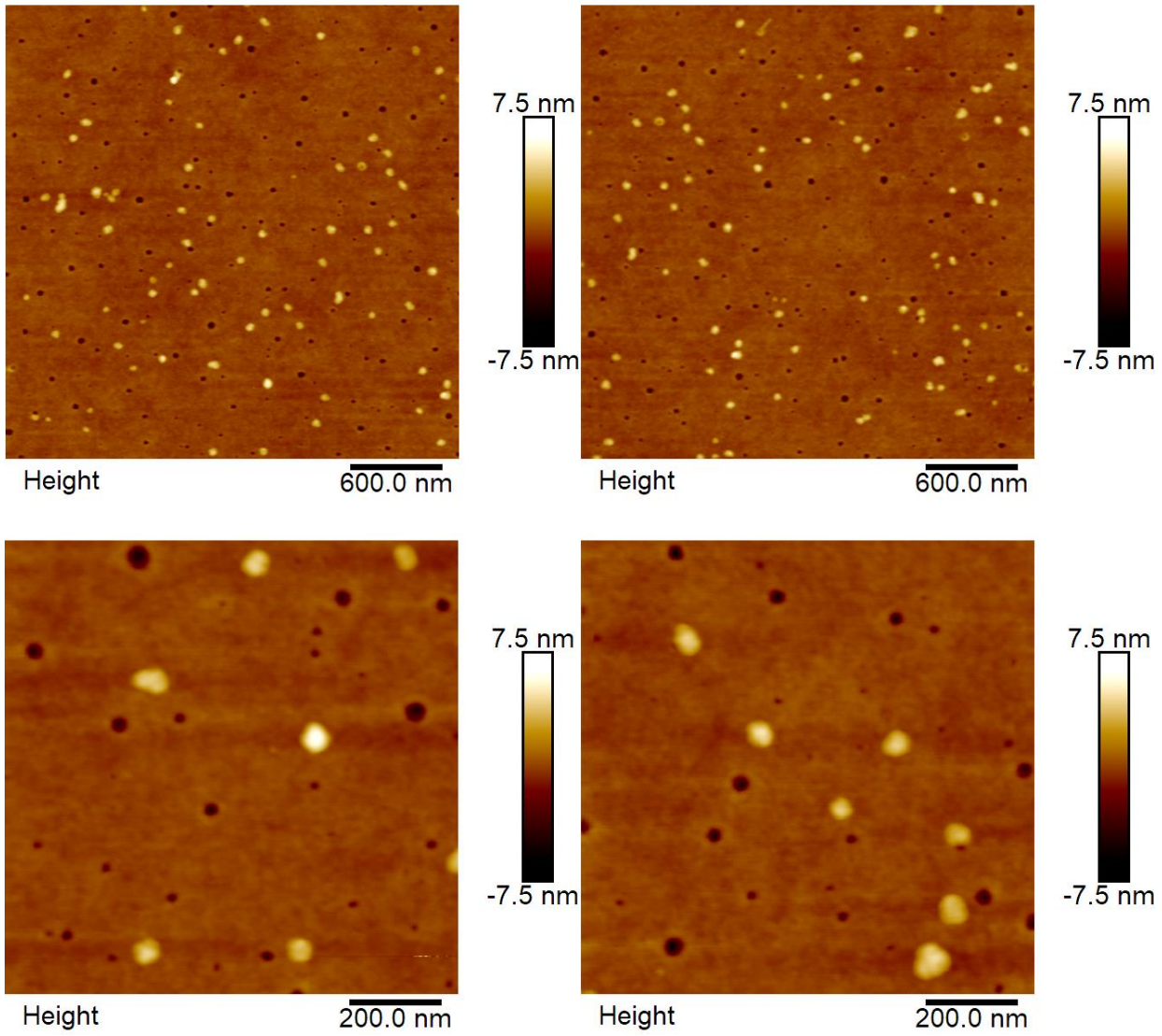

Figure D13. Additional AFM height images of MBB-PP spin cast onto PMMA-coated mica at room temperature (~ 20 °C) from a 0.05 mg/g MBB-PP solution in a 10 mM phosphate buffer with a pH of 9.50. The average diameter of 75 MBB molecules (two measurements for each in perpendicular directions) from the upper left image was 48.9 ± 9.3 nm.

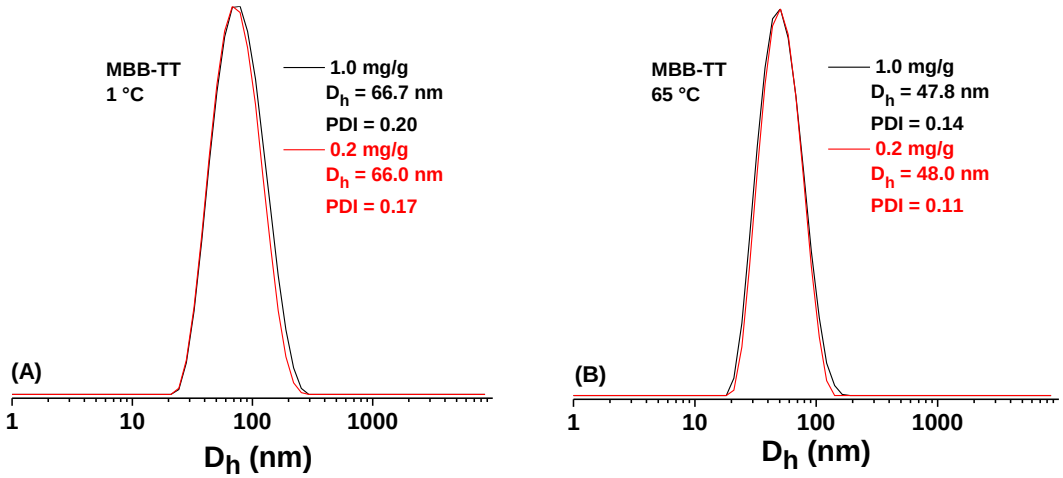

Figure D14. Comparison of hydrodynamic size distributions of MBB-TT in Milli-Q water with concentrations of 1.0 and 0.2 mg/g at 1 °C (A) and 65 °C (B), respectively.

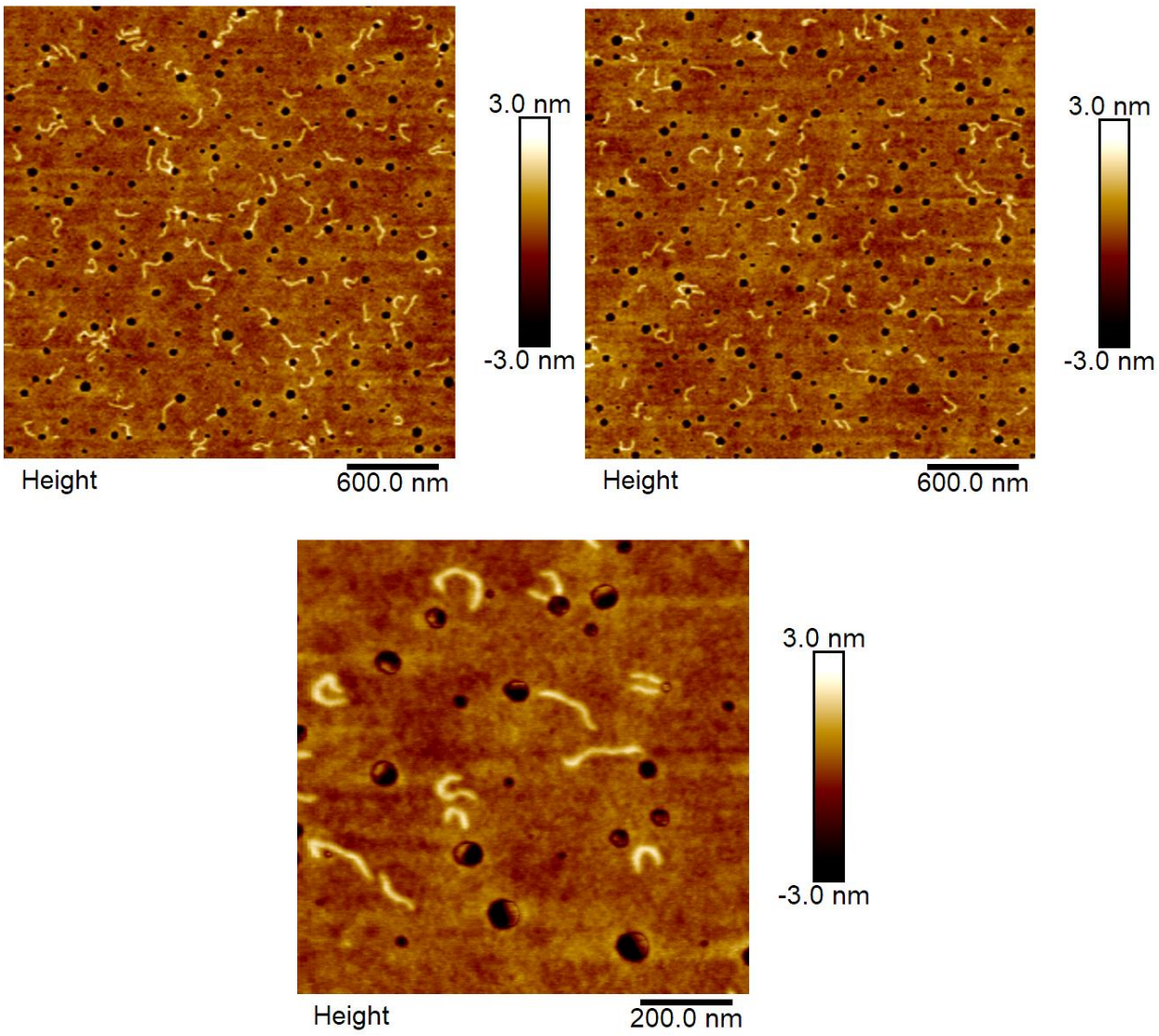

Figure D15. Additional AFM height images of MBB-TT spin cast onto PMMA-coated mica at 0 °C from a 0.05 mg/g MBB-PP solution in Milli-Q water. The average length of 106 MBB molecules from the upper left image was 169.2 ± 37.5 nm.

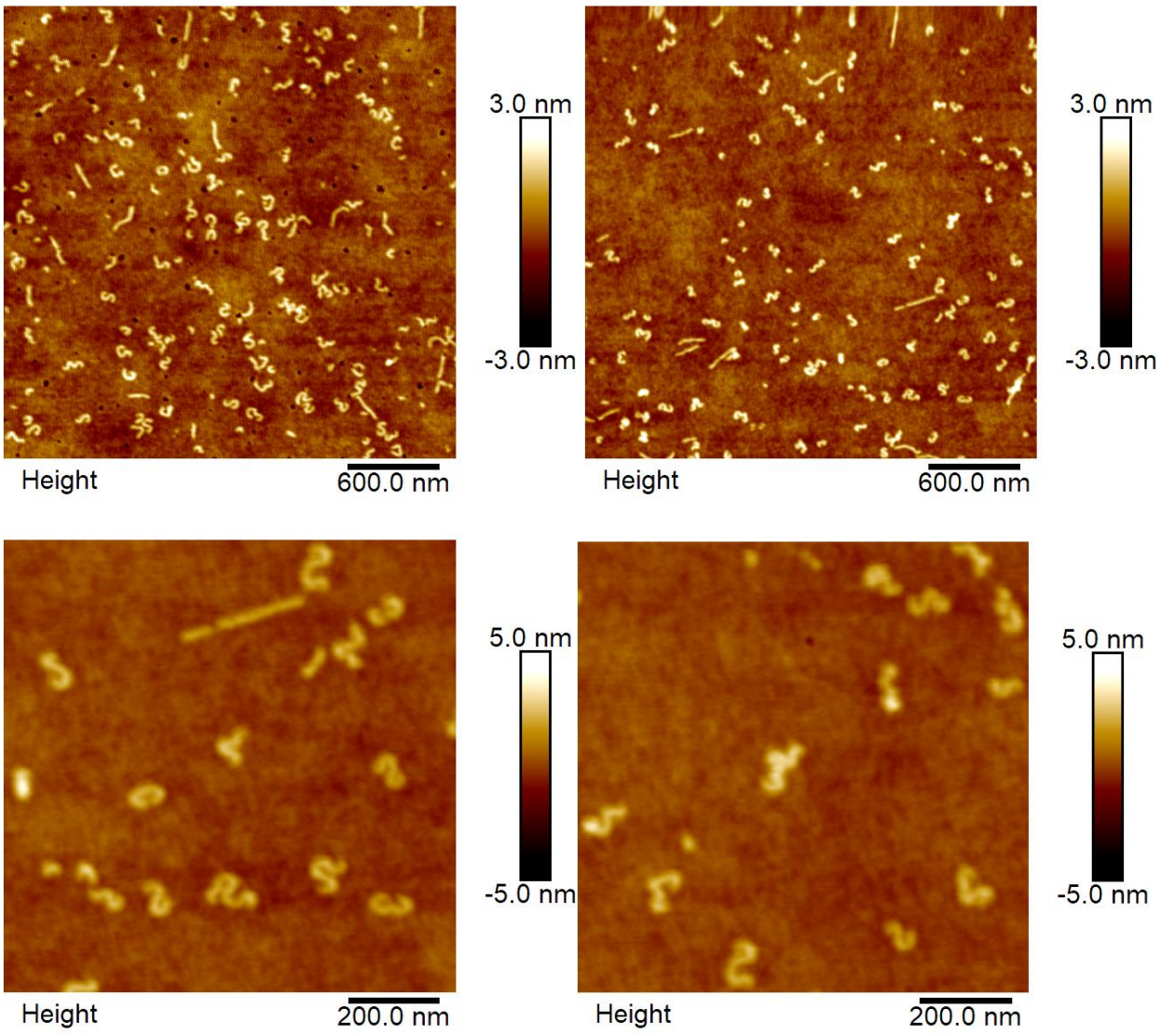

Figure D16. Additional AFM height images of MBB-TT spin cast onto PMMA-coated mica at 30 °C from a 0.05 mg/g MBB-PP solution in Milli-Q water. The average length of 152 MBB molecules from the upper left image: 124.8 ± 42.4 nm.

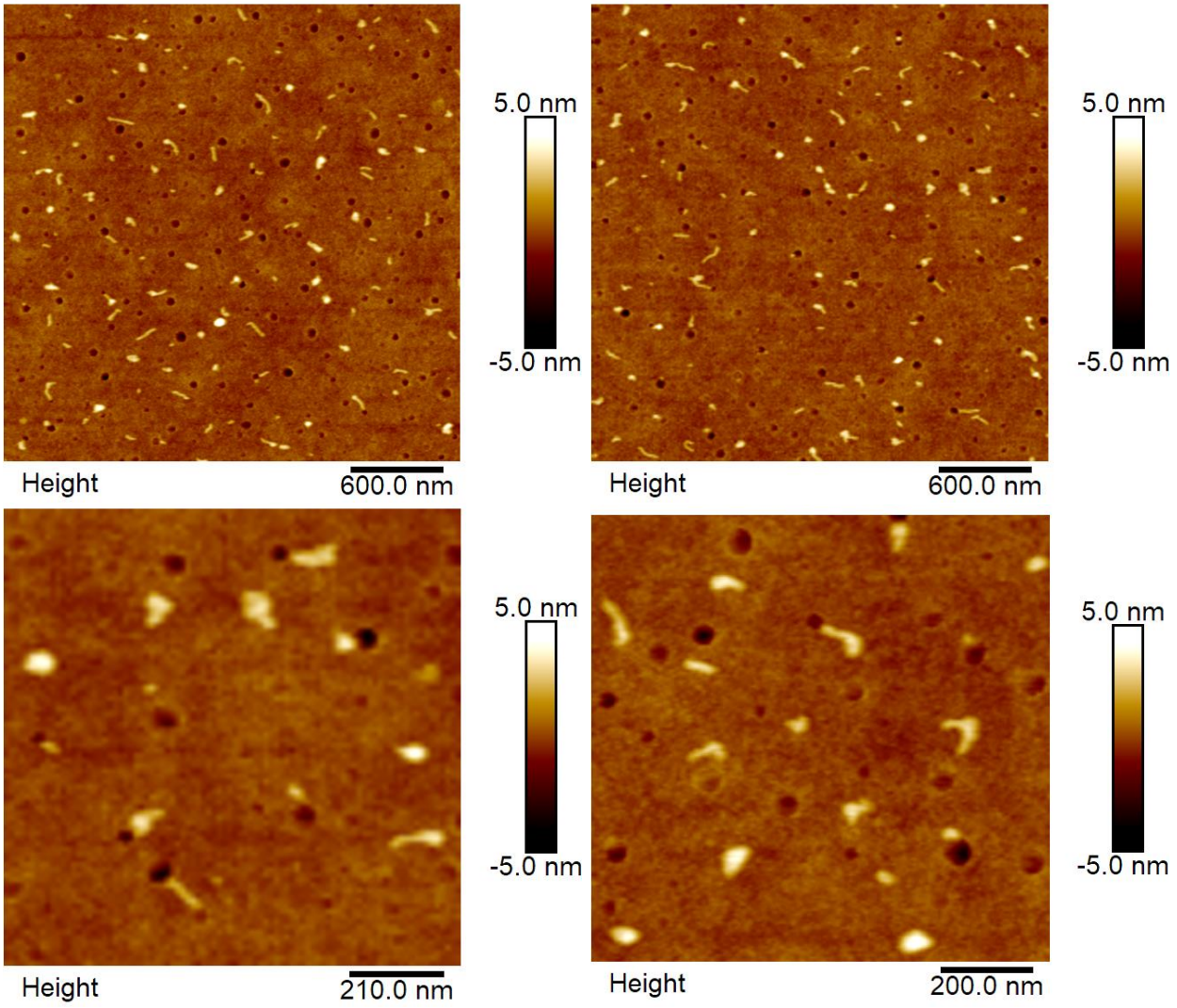

Figure D17. Additional AFM height images of MBB-TT spin cast onto PMMA-coated mica at 65 °C from a 0.05 mg/g MBB-PP solution in Milli-Q water. The average diameter of 66 globular MBB-TT molecules (two measurements for each in perpendicular directions) from the upper left image: 52.1 ± 15.2 nm.

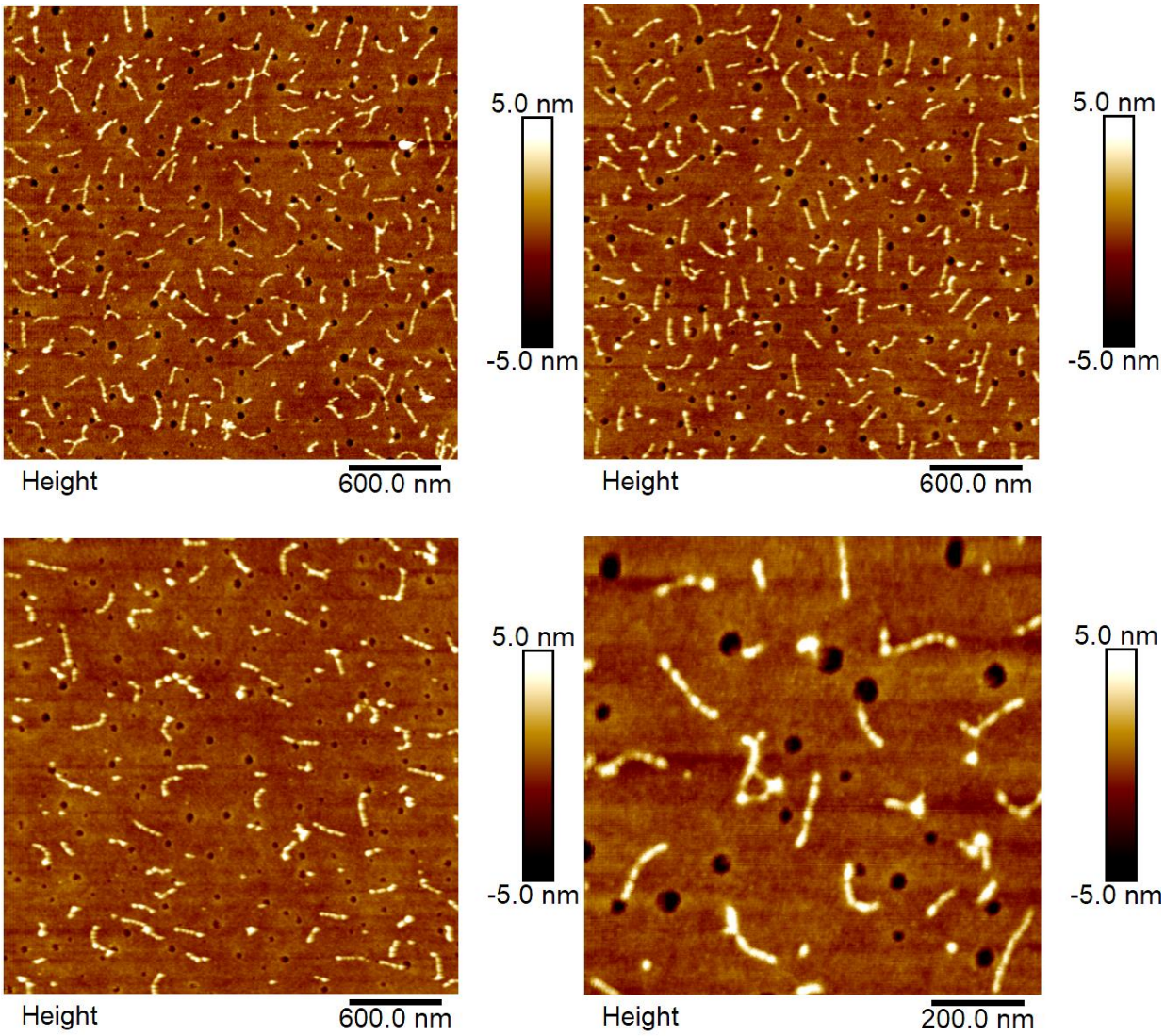

Figure D18. Additional AFM height images of MBB-TP spin cast onto PMMA-coated mica at 0 °C from a 0.05 mg/g MBB-TP solution in a 5 mM phosphate buffer with a pH of 5.00. The average length of 142 MBB molecules from the upper left image was 179.5 ± 41.7 nm.

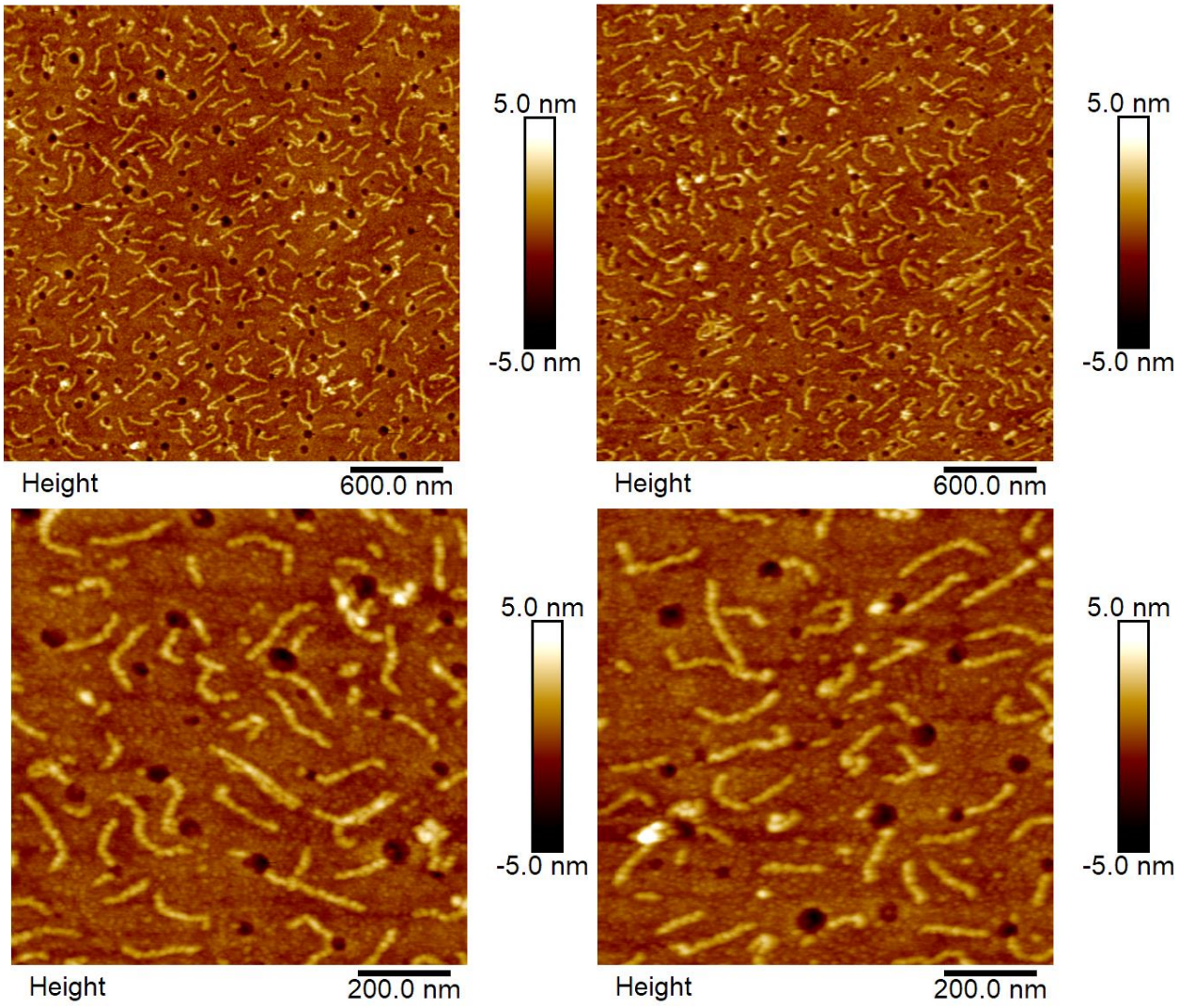

Figure D19. AFM height images of MBB-TP spin cast onto PMMA-coated mica at 0 °C from a 0.05 mg/g MBB-TP solution in a 5 mM phosphate buffer with a pH of 9.50. The average length of 246 MBB-TP molecules from the upper left image: 160.8 ± 40.7 nm.

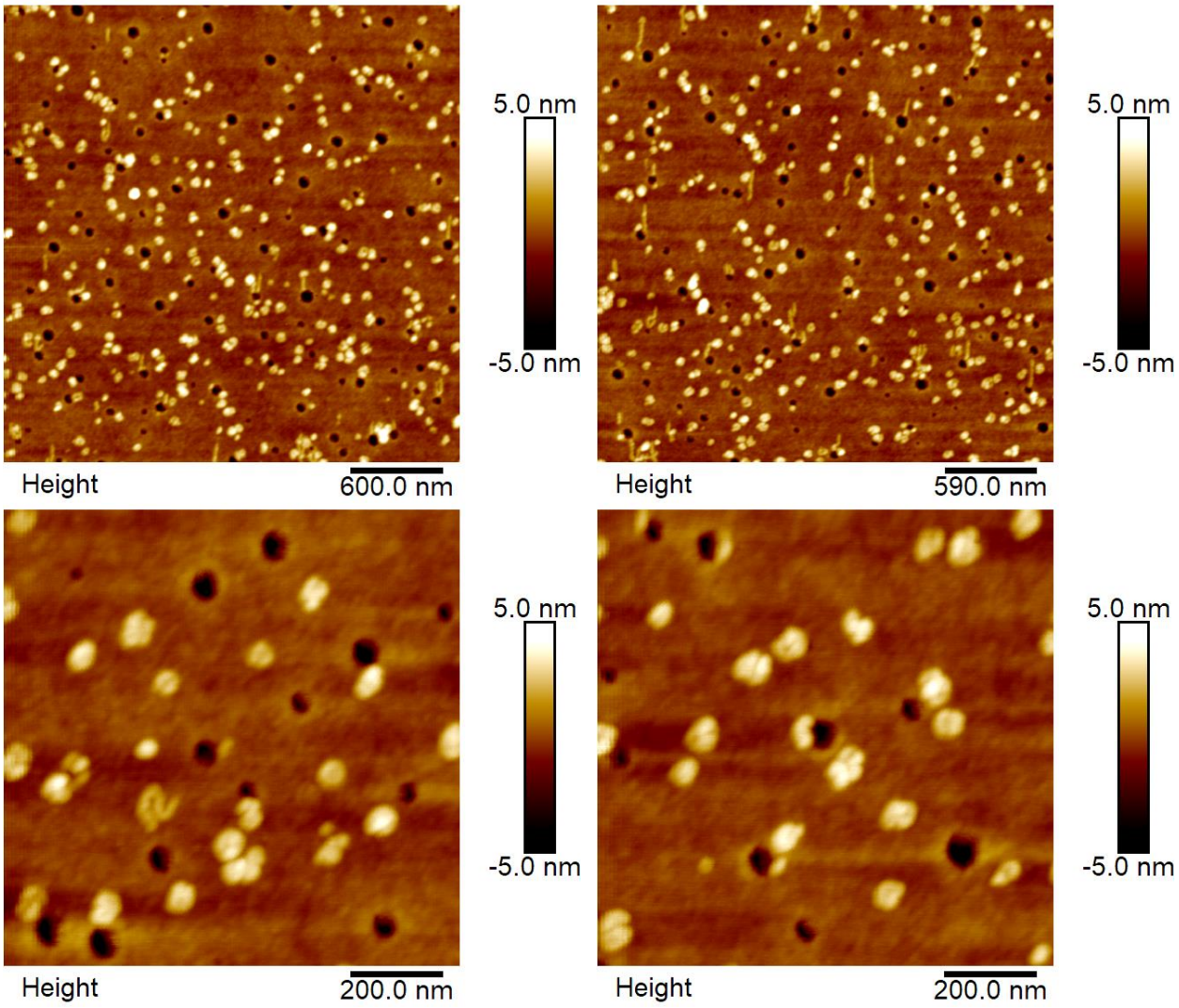

Figure D20. AFM height images of MBB-TP spin cast onto PMMA-coated mica at 20 °C from a 0.05 mg/g MBB-TP solution in a 5 mM phosphate buffer with a pH of 9.50. The solution was prepared by first adjusting the pH from 5.00 to 9.50 and then increasing the temperature from 0 °C to 20 °C. The average length of 100 MBB globular molecules (two measurements for each in perpendicular directions) from the upper left image was 54.5 ± 9.7 nm.

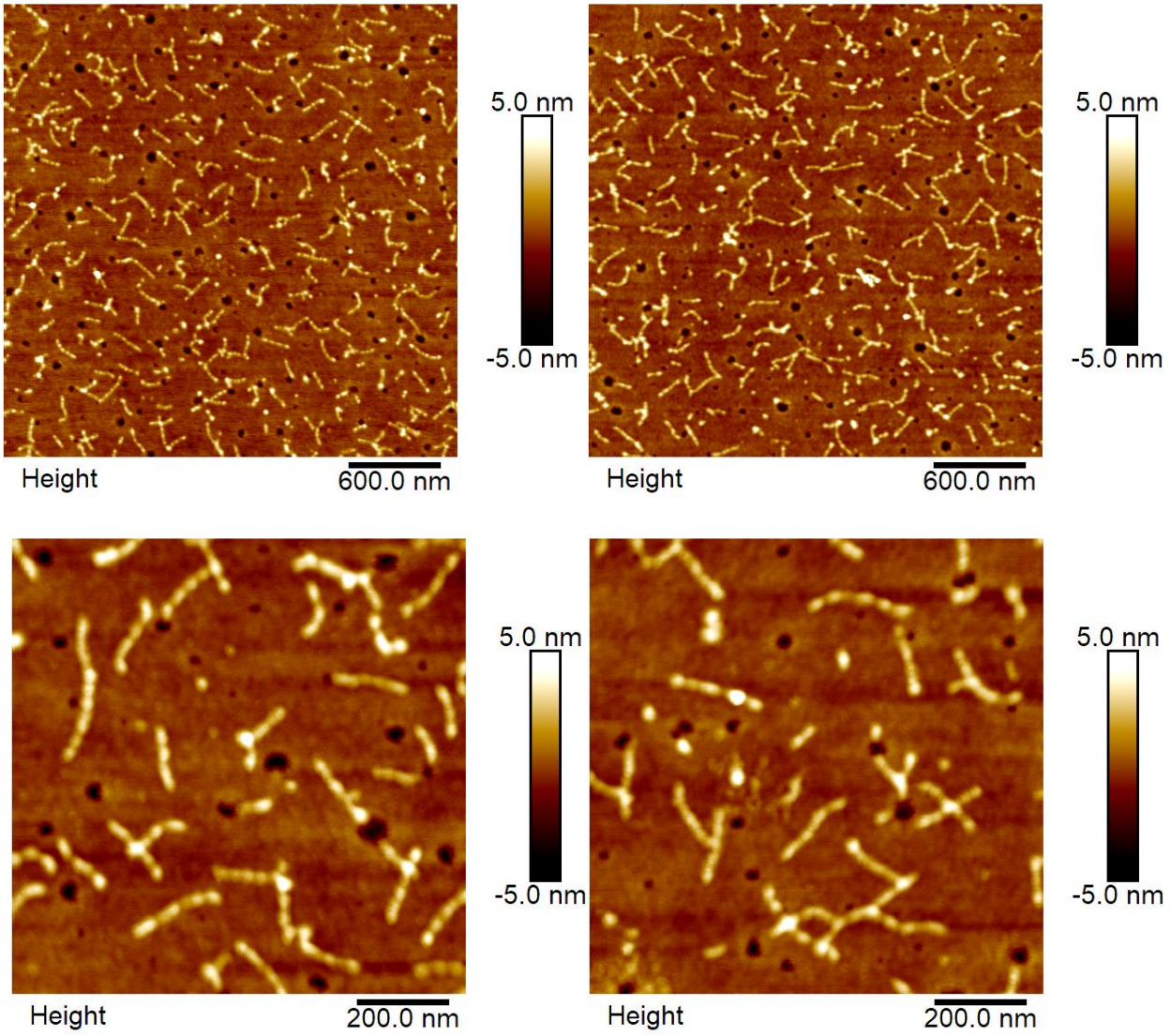

Figure D21. Additional AFM height images of MBB-TP spin cast onto PMMA-coated mica at 20 °C from a 0.05 mg/g MBB-TP solution in a 5 mM phosphate buffer with a pH of 5.00. The average length of 211 MBB-TP molecules from the upper left image was 167.1 ± 36.4 nm.

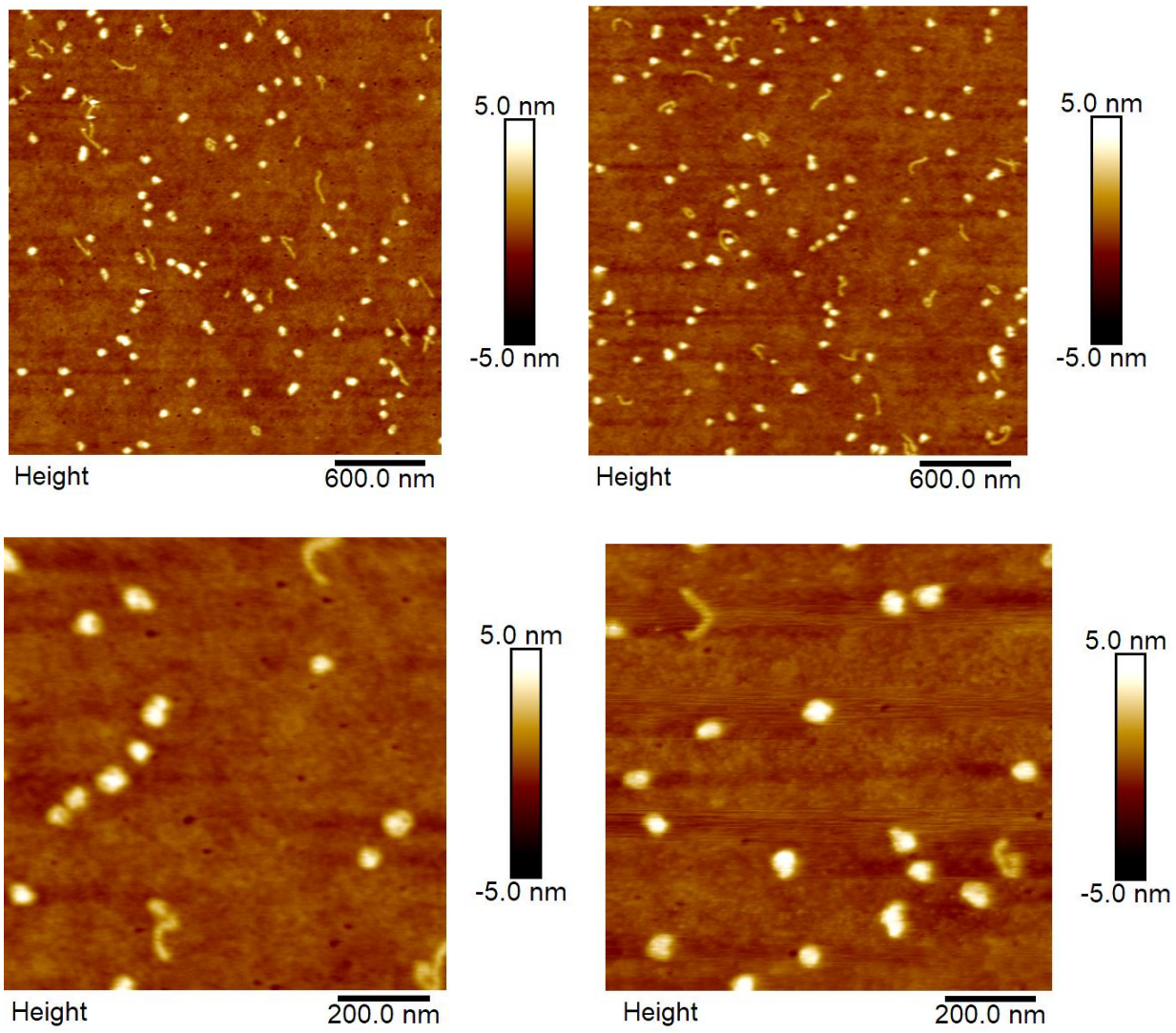

Figure D22. Additional AFM height images of MBB-TP spin cast onto PMMA-coated mica at 20 °C from a 0.05 mg/g MBB-TP solution in a 5 mM phosphate buffer with a pH of 9.50. The solution was prepared by first increasing the temperature from 0 to 20 °C and then the pH from 5.00 to 9.50. The average length of 93 MBB-TP globular molecules (two measurements for each in perpendicular directions) from the upper right image was 51.8 ± 9.9 nm.

Chapter 6. Synthesis of Homografted and Heterografted Molecular Bottlebrushes with Semi-Crystalline Polymer Side Chains

Abstract

Two series of molecular bottlebrushes (MBBs) with semi-crystalline polymer side chains were prepared by a grafting to method using the copper(I)-catalyzed azide-alkyne cycloaddition (CuAAC) reaction for a collaborative effort to study the crystallization behavior of MBBs. The first series was homografted MBBs with poly(ethylene oxide) (PEO) side chains grafted on either a three-arm star or a linear backbone polymer. The grafting density of the brushes was varied from 17.6% to 93.9% by modifying the initial feed ratios of the azide-carrying backbone polymer and the alkyne-end-functionalized PEO. The second series was linear heterografted MBBs containing PEO and poly(ε-caprolactone) (PCL) side chains along with their homografted analogues. Alkyne-end-functionalized PCL side chain polymers were prepared by ring-opening polymerization from a synthesized alkyne-functionalized initiator. The MBBs were then synthesized by grafting alkyne end-functionalized PEO and PCL polymers onto azide-functionalized backbone polymers by the CuAAC click reaction. SEC analysis confirmed the formation of molecular bottlebrushes and the removal of unreacted side chain polymers after purification. The molar side chain compositions of heterografted MBBs were determined by ^{1}H NMR spectroscopy analysis. Our collaborators, Professor Christopher Y. Li's group at Drexel University, use these brush samples to study the effects of grafting density and side chain composition on the crystal habit of MBBs.

Contributions: Dr. Ethan W Kent synthesized the linear backbone polymer PHEMA-N_3 with a DP of 801 and a three-arm star PHEMA-N_3 backbone polymer with a DP of 434 for each arm. Dr. Kent synthesized the SBB samples and MBBs with grafting densities of 19.1%, 46.9%, 72.5%, and 93.9%. I purified all the samples and performed SEC analysis. I synthesized PEO MBBs with grafting densities of 61.1% and 77.9% and all PEO/PCL heterografted MBBs.

6.1. Introduction

Molecular bottlebrush (MBB) polymers have been shown to display many intriguing characteristics, such as large and abrupt conformational transitions from wormlike to globular, negligible backbone chain entanglement, fast self-assembly kinetics, and high and tunable persistence length, which mainly stem from the dense grafting nature in their molecular structures.[1-4] These architecturally complex macromolecules have shown promise in a variety of applications, including photonic crystals, supersoft elastomers, drug delivery, surface modification, lubrication, and emulsion stabilizers.[5-9]

Despite tremendous efforts being invested on the synthesis and characterization of bottlebrush polymers, MBBs with semicrystalline side chains noticeably have received much less attention, and there are only a few reports in the literature on the crystallization behavior of semicrystalline brush polymers. Polymer crystallization occurs through chain folding. While the dense grafting increases the local segment density facilitating nucleation, growth is hindered by the decreased mobility of the side chains due to the end-tethering. In addition, the backbone presents as defects during the crystallization and must be excluded from the lattice. A previous study showed that under dilute solution conditions, MBBs with densely grafted poly(ethylene oxide) (PEO) side chains spontaneously grew into spherical hollow crystals with broken translational symmetry, which were named as MBB crystalsomes.[10] Fluorescence resonance energy transfer experiments revealed that the backbone of PEO MBBs was excluded to the inner surface of the hollow single crystals while the outer surface of the crystals was made up of PEO crystals, resulting in the unbalance of the inner and outer surfaces of the crystals and the bending of crystalline lamellae. The size of hollow spherical crystals depended on crystallization temperature and grafting density of PEO MBBs.

To further study the crystallization behavior of MBBs in a collaborative effort, we synthesized two series of MBBs with semicrystalline side chains: (i) linear and three-arm star PEO MBBs with various grafting densities and (ii) linear heterografted MBB with PEO and poly(ε-caprolactone) (PCL) side chains at various molar ratios. These MBBs were prepared by grafting alkyne-end-functionalized semicrystalline side chain polymers onto azide-bearing polymethacrylate backbone polymers via the copper(I)-catalyzed azide-alkyne cycloaddition (CuAAC) click reaction.[11-13] The brush polymers were thoroughly purified and characterized by size exclusion chromatograph (SEC) and ^{1}H NMR spectroscopy analysis.

6.2. Experimental Section

6.2.1. Materials

4-Pentynoic Acid (98%, TCI), diethylene glycol (99%, Alfa Aesar), *N*-(3-dimethylaminopropyl)-*N*′-ethylcarbodiimide hydrochloride (EDC, Oakwood Chemicals, 99%), and 4-dimethylaminopyridine (DMAP, 99%, TCI) were used as received without any additional purification. CuCl (97%, Alfa Aesar) was purified by stirring in a vial with glacial acetic acid (Certified ACS, Fisher Scientific). The solid was vacuum filtered and washed multiple times with absolute ethanol and inhibitor-free diethyl ether sequentially. The purified CuCl was collected into a vial and dried under a high vacuum to remove residual solvent and stored in a desiccator. *N*,*N*,*N*′,*N*″,*N*″-Pentamethyldiethylenetriamine (PMDETA, 99%, Acros) and ε-caprolactone (99%, Alfa Aesar) were stirred for several hours over calcium hydride and purified by vacuum distillation prior to use. Tin(II) 2-ethylhexanoate (95%, Aldrich) was vacuum distilled and stored under nitrogen before use. Dry THF and toluene were distilled from respective sodium benzophenone

ketyl stills and used immediately. All other chemicals used in this work were purchased from Fisher Scientific or Aldrich and used as received.

Alkyne end-functionalized PEO with a molecular weight of 5000 Da was prepared as reported previously.[12,13] The synthesis procedures of the linear and star azide functionalized backbone polymers in this work are described in detail in previous publications.[14,15] Two linear backbone polymers were used in this work; the first one had a degree of polymerization (DP) of 801, with a degree of azide functionalization of 96.7%; SEC analysis with GRAL columns showed a $M_{n,SEC}$ of 154.1 kDa and Đ of 1.13, relative to polystyrene standards.[14] The second linear backbone polymer had a DP = 734 and an azide functionalization of 97.8%, and SEC analysis with Mixed-B columns yielded a $M_{n,SEC}$ = 243.3 kDa and Đ = 1.15. The three-arm star backbone polymer had a DP of 434 per arm and a degree of azide functionalization of 88.3% with a $M_{n,SEC}$ of 224.5 kDa and Đ = 1.16 from SEC analysis using GRAL columns and polystyrene standards as calibration.[15]

6.2.2. General Characterization

All NMR spectra were recorded on either a Varian VNMRS 500 or a Varian VNMRS 600 NMR spectrometer. SEC analysis of alkyne-end functionalized PEO and PCL were performed under ambient conditions on a PL-GPC 20 system (an integrated GPC/SEC system from Polymer Laboratories, Inc.) equipped with a differential refractive index (RI) detector, a PLgel 5 μm guard column (50 × 7.5 mm, Agilent), and two PLgel 5 μm Mixed-C columns (each 300 × 7.5 mm, linear range of from 200 to 2 000 000 Da, Agilent). The mobile phase was THF with the flow rate set to 1.0 mL/min for analysis. The SEC analysis of the purified and unpurified MBBs was performed at 50 °C on a PL-GPC 50 system (an integrated GPC/SEC system from Polymer Laboratories, Inc.) equipped with an RI detector using *N*,*N*-dimethylformamide (DMF) with 50 mM LiBr as eluent at a flow rate of 1.0 mL/min. Two column configurations were employed for the DMF GPC system

in this work: (i) one PLgel guard column (50 × 7.5 mm, Agilent) and three PLgel 10 μm Mixed-B columns (each 300 × 7.5 mm, with a linear molecular weight range from 500 to 10,000,000 Da, Agilent), and (ii) one PSS GRAL 10 μm guard column (50 × 8 mm, Polymer Standards Service-USA, Inc.) and two PSS GRAL 10 μm linear columns (each 300 × 8 mm, with a linear range of molecular weight from 500 to 1 000 000 Da, PSS-USA, Inc.). Both THF and DMF SEC/GPC systems were calibrated with a set of narrow disperse linear polystyrene standards (Scientific Polymer Products, Inc.). The purified PEO MBBs were freeze-dried from water using a LABCONCO 76705 Series Freeze Dryer, while heterografted PEO/PCL and homografted PCL MBBs were freeze-dried from 1,4-dioxane using a Schlenk line attached to a high vacuum pump.

6.2.3. Synthesis of 2-(2-Hydroxyethoxy)ethyl Pent-4-ynoate (Alkyne-DEG-OH)

4-Pentynoic acid (0.617 g, 6.29 mmol), diethylene glycol (2.605 g, 24.55 mmol), and dichloromethane (10 mL) were combined in a 50 mL two-necked round bottom flask equipped with a magnetic stir bar. The flask was placed in an ice/water bath, and the reaction mixture was placed under nitrogen. After 15 min, EDC (1.759 g, 9.32 mmol) and DMAP (74.3 mg, 0.608 mmol) dissolved in dichloromethane (15 mL) were added dropwise via an addition funnel. The reaction mixture gradually warmed to room temperature and was stirred for a total of 8 h. Thin layer chromatography (TLC) was employed to analyze the crude product using a solvent mixture of ethyl acetate and hexanes (3/1, v/v); the product was identified (R_f ~ 0.45) along with minor impurities near the baseline and at the top of the solvent front. Note that a $KMnO_4$ stain was found to be a good indicator for identifying the spots on the TLC plates. The crude product was purified by column chromatography using the same solvent mixture. The fractions identified to contain the product were concentrated by a rotavapor and dried under high vacuum, yielding a slightly yellow colored oil (0.725 g, 61.9% yield). The purified product was characterized by ^{1}H and ^{13}C NMR

spectroscopy analysis. ^{1}H NMR δ (ppm, $CDCl_3$) = 4.27 (t, -COOC*H*$_2$-, 2H), 3.73 (t, -COOCH$_2$C*H*$_2$-, 2H), 3.70 (t, -(C=O)OCH$_2$H$_2$OCH$_2$C*H*$_2$OH, 2H), 3.59 (t, -COOCH$_2$H$_2$OC*H*$_2$CH$_2$OH, 2H), 2.58 (t, HC≡CCH$_2$C*H*$_2$CO-, 2H), 2.50 (t, HC≡CC*H*$_2$CH$_2$CO-, 2H), (1.97 (s, *H*C≡CCH$_2$-, 1H). ^{13}C NMR δ (ppm, $CDCl_3$) = 171.75 (-CH$_2$*C*OO-), 83.27 (HC≡*C*CH$_2$-), 72.33 (-CH$_2$*C*H$_2$OH), 69.07 (H*C*≡C-), 69.02 (-OCH$_2$*C*H$_2$O-), 63.69 (-COO*C*H$_2$CH$_2$-), 61.70 (-O*C*H$_2$CH$_2$OH), 33.23 (-CH$_2$*C*H$_2$CO-), 14.31 (HC≡C*C*H$_2$CH$_2$-).

6.2.4. Synthesis of Alkyne End-Functionalized PCL

In a glovebox, Alkyne-DEG-OH (68.7 mg, 0.369 mmol), ε-caprolactone (4.217 g, 36.95 mmol), stannous octoate (143.5 mg, 0.354 mmol), and dry toluene (4.258 g) were added into a flame-dried Schlenk flask equipped with a stir bar. The flask was sealed, removed from the glove box, and placed in a 75 °C oil bath to initiate the polymerization. The conversion of ε-caprolactone was monitored using ^{1}H NMR spectroscopy by comparing the integrals of the peaks at 4.23 ppm (-COOC*H*$_2$- of ε-caprolactone) and 4.07 ppm (-COOC*H*$_2$- of PCL). After 4.5 h, the flask was removed from the oil bath and acetic acid (1 mL) was added to quench the polymerization. The polymer was purified by four rounds of precipitation from chloroform into methanol (100 mL) and the polymer was dried under high vacuum yielding a white solid (1.227 g). SEC analysis using the THF GPC with Mixed-C columns yielded a M_n = 7.6 kDa and $Đ$ = 1.10 (relative to polystyrene standards). The DP was 43, calculated from the monomer conversion (43.1%) and the initial monomer-to-initiator ratio. From the end-group analysis using the peaks from the initiator at δ = 4.24 ppm (HC≡CCH$_2$CH$_2$COOC*H*$_2$CH$_2$OCH$_2$C*H*$_2$OOC-, 4H) and from the polymer repeat unit at δ = 4.07 ppm (-COOC*H*$_2$- from PCL, 2H), the DP was found to be 42, essentially the same as that from the monomer conversion.

6.2.5. Synthesis of Homografted MBBs

The following is a representative procedure for the synthesis of linear homografted PEO MBBs. Similar procedures were used to prepare linear and three-arm star PEO MBBs with different grafting densities. The backbone polymer PHEMA-N_3 with a DP of 801 (10.1 mg, 0.0417 mmol monomer units, from a stock solution in THF) was added to a 7.4 mL vial equipped with a stir bar. THF was evaporated using a nitrogen gas stream. In a separate vial, PEO (106.4 mg, 0.0209 mmol) was dissolved in DMF (2 mL) and then added to the vial containing the backbone along with additional *N*,*N*-dimethylformamide (DMF) (3 mL). CuCl (4.2 mg, 0.0424 mmol) was added, and the vial was sealed with a rubber septum. The headspace of the reaction mixture was purged with nitrogen gas for 15 min and then *N*,*N*,*N*′,*N*″,*N*″-pentamethyldiethylenetriamine (PMDETA) (10.0 μL, 0.0480 mmol) was added using a microsyringe. After 24 h, benzyl propargyl ether (25 μL, 0.173 mmol) was injected using a microsyringe to cap unreacted azide groups. The reaction mixture was stirred for an additional 3 h. An aliquot of the reaction mixture was taken and analyzed by SEC analysis to determine the grafting density of the brush polymer. The mixture was the passed through a basic alumina (top)/silica gel (bottom) column to remove the copper catalyst. The excess side chains were removed using several rounds of centrifugal filtration using 50 kDa MWCO filters and a mixture of methanol and water (50/50, v/v) at 5000 rpm (Eppendorf 5804 Centrifuge). The methanol was removed by rotary evaporation, and the MBB solutions were placed in a freezer (-20 °C) and then were freeze-dried using a LABCONCO 76705 Series Freeze Dryer. The procedure for homografted PCL MBBs was very similar except for differences in the purification steps. PCL MBBs were purified by fractionation by dissolving the brushes in THF (~ 2 mL) and slowly adding pentanes (~10 mL) until a precipitate began to form. After five fractionations, there was no side chain polymer as confirmed by the SEC analysis. The PCL MBBs

were then dissolved in 1,4-dioxane, placed in a freezer (-20 °C), and freeze-dried using a Schlenk line. The grafting densities for the homografted PEO MBBs and three-arm star brush polymers (SBBs) were calculated considering the peak area ratios of brushes and unreacted PEO from SEC analysis and the initial feed masses of the backbone and PEO.

6.2.6. Synthesis of Heterografted PEO/PCL MBBs

The following is the procedure for the synthesis of a heterografted PEO/PCL brush polymer with a target molar composition of 0.50 : 0.50 for the two polymers in the side chains. The other samples were prepared similarly, with the difference being the initial molar ratio of PEO to PCL in the feed. The backbone polymer PHEMA-N_3 with a DP of 734 (9.12 mg, 0.0378 mmol of repeat units, added from a stock solution in THF) was added to a 2-dram vial equipped with a stir bar. Alkyne-end-functionalized PEO (96.3 mg, 0.0190 mmol) and PCL (97.5 mg, 0.0192 mmol) were added to the vial along with THF (4 mL total), and the mixture was stirred to form a homogeneous solution. Copper(I) chloride (4.1 mg, 0.0416 mmol) was added, and the vial was sealed with a rubber septum. The reaction mixture was bubbled with N_2 for 15 min at which point PMDETA (9 µL, 0.0431 mmol) was injected by a microsyringe. After 20 h, benzyl propargyl ether (25 µL, 0.173 mmol) was injected by a microsyringe to cap unreacted azide groups. A small portion of the reaction mixture was analyzed by SEC analysis to determine the grafting density of the synthesized MBBs. The MBBs were purified by first passing the reaction mixture through a neutral alumina/silica gel column to remove the copper catalyst. The solvent was removed by rotary evaporation, and the mixture was dissolved in chloroform (3 mL) and transferred to a 4-dram vial. Five fractionations were then performed by adding pentane (10 mL) to the vial to precipitate the MBBs. The supernatant was decanted off and chloroform (3 mL) was added to re-dissolve the brush polymer. SEC analysis was conducted to ensure the complete removal of the two side chain

polymers. The sample was freeze dried by dissolving the MBBs in 1,4-dioxane, placing the solution in a freezer, and then removing the frozen solvent under high vacuum, yielding the product as a white solid. The side chain molar composition was determined by ^{1}H NMR analysis using the integrals of characteristic peaks at 4.07 ppm (-COOC*H*$_2$- of PCL) and 3.37 ppm (-OC*H*$_3$ of PEO). The grafting density of the heterografted MBBs was calculated considering the peak area ratios of MBBs and unreacted side chain polymers from the SEC analysis of the final reaction mixture, the molar composition determined by ^{1}H NMR, and the initial feed masses.

6.3. Results and Discussion

6.3.1. Synthesis of Alkyne End-Functionalized Side Chain Polymers

An alkyne end-functionalized PCL with a DP of 43 was synthesized by ring-opening polymerization from a novel alkyne initiator, Alkyne-DEG-OH, which was prepared by a Steglich esterification of 4-pentynoic acid with diethylene glycol (Scheme 6.1). An excess of diethylene glycol was used in the synthesis of Alkyne-DEG-OH to minimize the formation of the side product with two alkyne groups. The crude product was purified by column chromatography, and the molecular structure was confirmed by ^{1}H and ^{13}C NMR spectroscopy (Figure 6.1A,B). Alkyne DEG-OH was then used as an initiator in the ring opening polymerization of ε-caprolactone using tin(II) 2-ethylhexanoate (Sn(Oct)$_2$) as a catalyst. ^{1}H NMR spectroscopy was used to monitor the progress of the reaction. The DP of the obtained alkyne-end-functionalized PCL was calculated to be 43 from the monomer conversion and the monomer-to-initiator ratio, which was very close to the DP from the end group analysis (DP = 42) using the ^{1}H NMR spectrum of the purified polymer (Figure 6.1C). SEC analysis yielded a $M_{n,SEC}$ of 7.6 kDa and Đ of 1.10 (Figure 6.1D), indicating that the polymerization was well controlled. The alkyne end-functionalized PEO was prepared via

Scheme 6.1. Synthesis of Alkyne-DEG-OH and Alkyne-End-Functionalized PCL

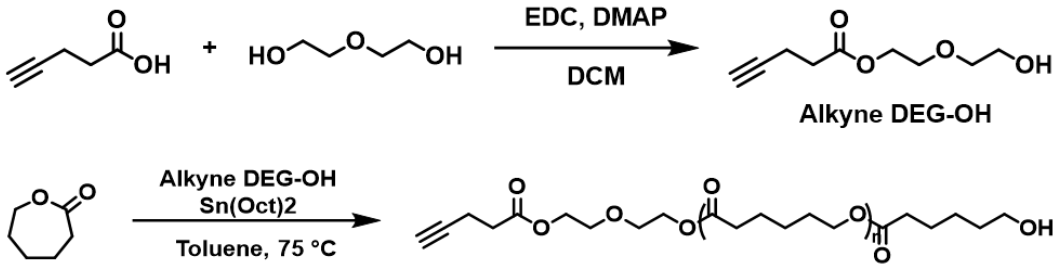

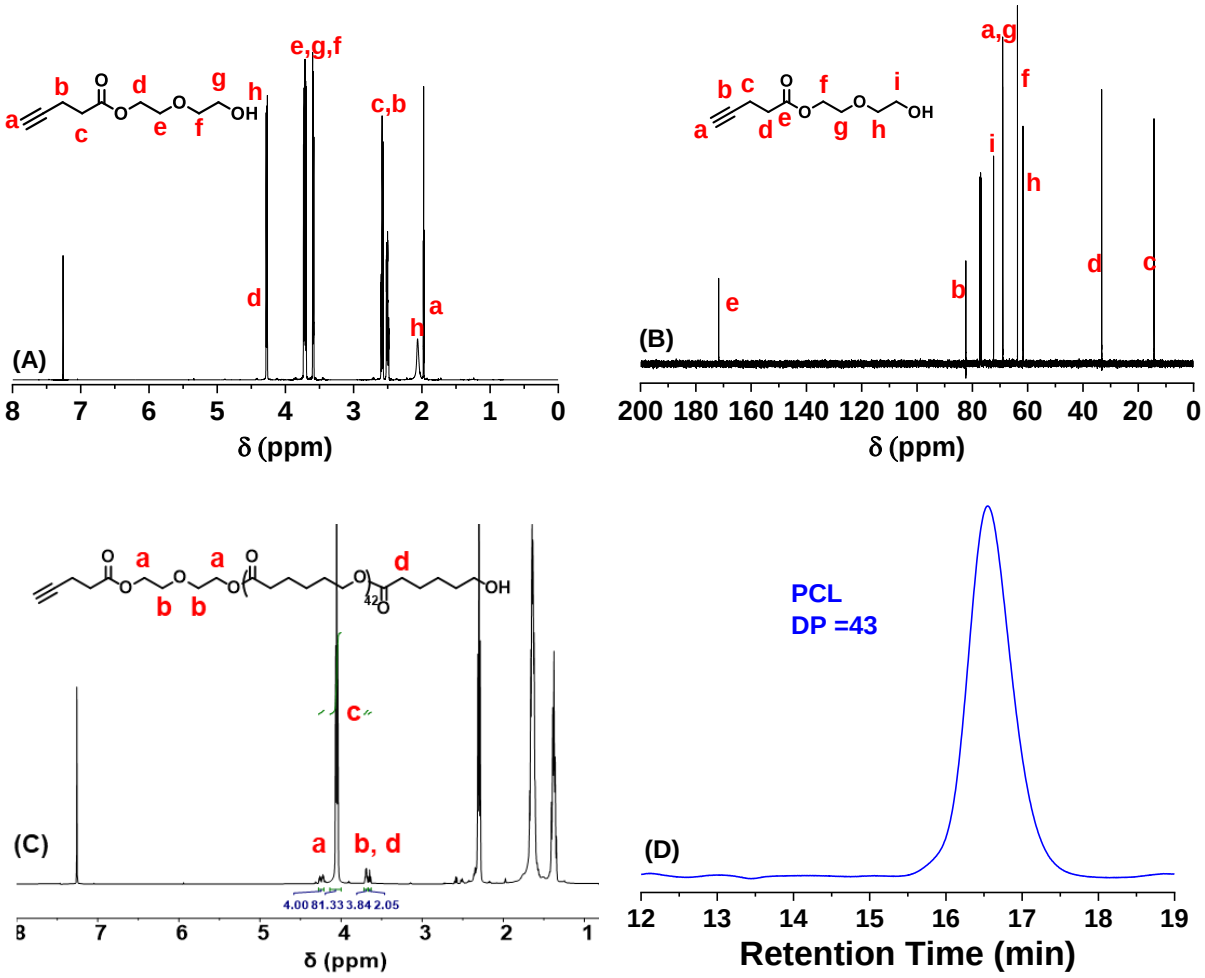

Figure 6.1. (A) ^{1}H and (B) ^{13}C NMR spectra of purified Alkyne DEG-OH in $CDCl_3$. (C) ^{1}H NMR spectrum of PCL in $CDCl_3$. Integrals and peak assignments are shown, which were used to calculate the DP in end-group analysis. (D) SEC analysis of PCL using a GPC system equipped with Mixed-C columns and THF as eluent.

the reaction of 5 kDa PEO monomethyl ether with 4-pentynoic acid as described previously.[12] The calculated molecular weight of the PCL with a DP of 43 was very similar to that of the alkyne-end-functionalized PEO, and so when used for the synthesis of heterografted MBBs, the molar composition of side chains would closely align with the mass ratio of PCL to PEO.

6.3.2. Synthesis of Homografted Linear and Three-Arm Star PEO MBBs with Various Grafting Densities

The characterization data for the backbone and side chain polymers used to synthesize MBBs in this work are summarized in Table 6.1. A total of 11 homografted linear and star PEO MBBs with various grafting densities were synthesized by grafting the alkyne-end-functionalized 5 kDa PEO onto either a linear or a three-arm star azide-functionalized backbone polymer (Scheme 6.2). Two linear backbone polymers, with DPs of 801and 734, were used in this work, from which seven linear PEO brush polymers with grafting densities in the range of 19.1% to 96.1% were prepared. The ^{1}H NMR spectrum and SEC trace of the linear azide-functionalized backbone polymer with a DP of 734 are shown in Figure 6.2. They are denoted as PEO MBB-x, where x represents the grafting density, for example, PEO-MBB-0.19 for the brush polymer with a grafting density of 19.1%. Four three-arm star PEO bottlebrush polymers (SBBs) with grafting densities of 17.6%, 43.5, 66.0%, and 87.8% were made from an azide-functionalized three-arm star backbone polymer with a DP of 434 per arm. SBBs are named similarly to the linear brushes. For both linear and star brushes, the grafting density was varied by changing the initial feed molar ratio of the backbone repeat units and the PEO. The unreacted PEO was removed by centrifugal filtration at a speed of 5000 rpm using a centrifuge, which was verified by SEC analysis. The characterization data for these PEO MBBs are summarized in Table 6.2. Figures 6.3-6.5 show the SEC traces before and after purification as well as ^{1}H NMR spectra of the brushes.

Table 6.1. Characterization Data for Azide-Functionalized Backbone and Alkyne End-Functionalized Side Chain Polymers.

Sample ID	DP	$M_{n,SEC}$ (kDa)	Đ	Azide Functionalization
Linear PHEMA-N_3-1	801[b]	154.1[c]	1.13[c]	96.7%
Star PHEMA-N_3	434[b]	224.5[c]	1.16[c]	88.3%
Linear PHEMA-N_3-2	734[b]	243.3[d]	1.15[d]	97.8%
Alkyne PCL	43[b]	7.6[e]	1.10[e]	n/a
Alkyne PEO	114[f]	7.9[e]	1.04[e]	n/a

[a]Determined by ^{1}H NMR analysis. [b]Determined by ^{1}H NMR analysis from monomer conversion. [c]Number-average molecular weight and Đ determined using a PL-GPC 50 system with GRAL columns relative to polystyrene standards. [d]Number-average molecular weight and Đ determined using a PL-GPC 50 system with Mixed B columns relative to polystyrene standards. [e]Number-average molecular weight and Đ determined using a PL-GPC 20 system with Mixed-C columns relative to polystyrene standards. [f]DP was calculated based on the nominal molecular weight (kDa) divided by the molecular weight of the monomer unit (44).

Scheme 6.2. Synthesis of MBBs with PEO Side Chains with Varying Grafting Density

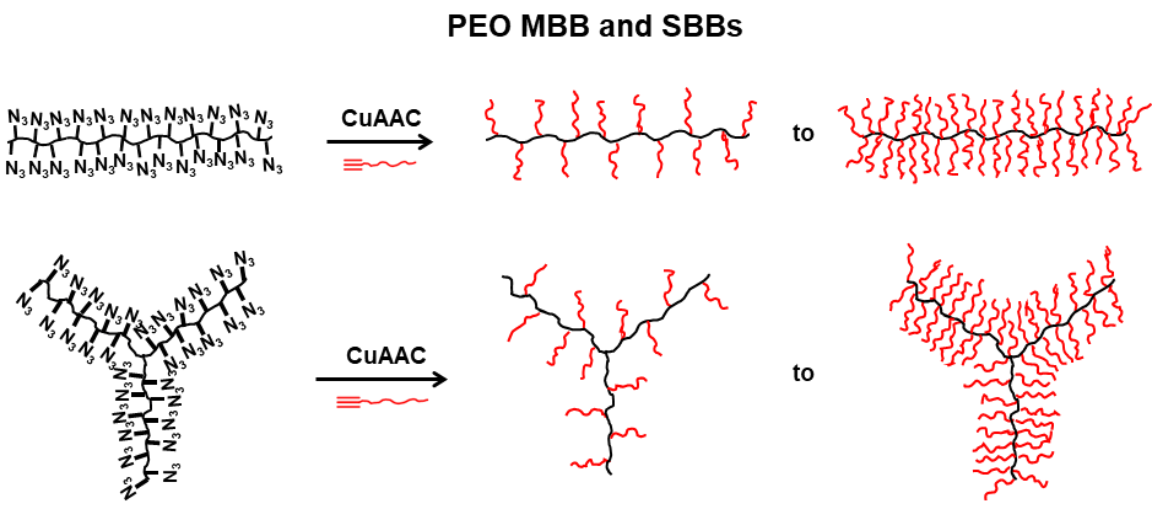

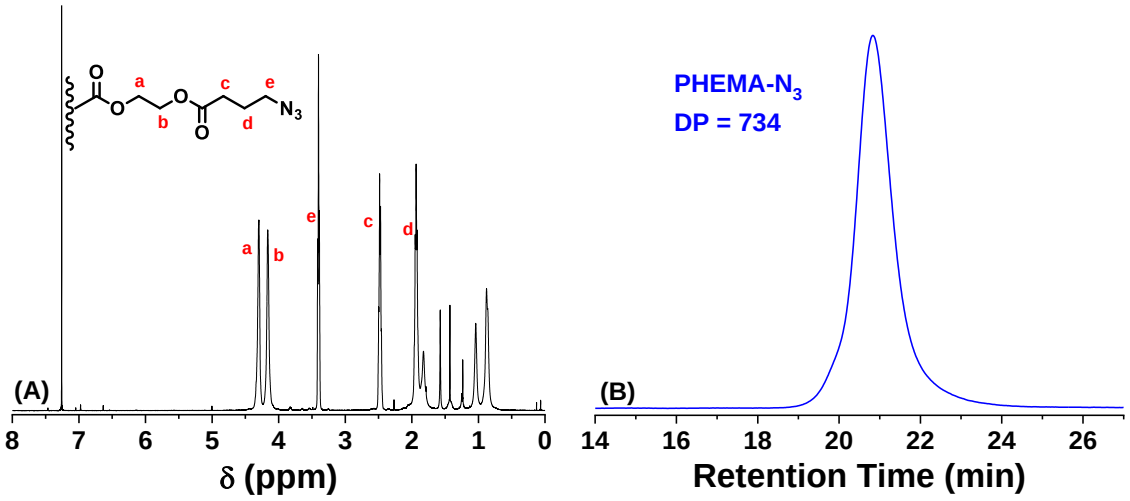

Figure 6.2. (A) ^{1}H NMR spectrum of PHEMA-N_3 in $CDCl_3$. (B) SEC analysis of PHEMA-N_3 using a GPC system equipped with Mixed-B columns and DMF with 50 mM LiBr as eluent.

Table 6.2. Summary of synthetic conditions and characterization data for homografted PEO MBBs

MBB Sample	Feed Molar Ratio of Backbone Monomer Units to PEO	Backbone/ Arm DP [a]	Grafting Density (%)[b]	$M_{n,SEC}$ ($\times 10^6$) Da	Đ
PEO-MBB-0.19	1 : 0.20	801	19.1	0.68[c]	1.15[c]
PEO-MBB-0.47	1 : 0.51	801	46.9	0.91[c]	1.17[c]
PEO-MBB-0.61	1 : 0.63	801	61.1	1.14[d]	1.14[d]
PEO-MBB-0.73	1 : 0.77	801	72.5	1.12[c]	1.14[c]
PEO-MBB-0.78	1 : 0.85	801	77.9	1.19[d]	1.12[d]
PEO-MBB-0.94	1 : 1.43	801	93.9	1.20[c]	1.13[c]
PEO-MBB-0.96	1 : 1.79	734	96.1	1.20[c]	1.16[c]
PEO-SBB-0.18	1 : 0.21	434	17.6	0.79[c]	1.19[c]
PEO-SBB-0.44	1 : 0.51	434	43.5	1.43[c]	1.21[c]
PEO-SBB-0.66	1 : 0.75	434	66.0	1.48[c]	1.18[c]
PEO-SBB-0.88	1 : 1.52	434	87.8	1.76[c]	1.16[c]

[a] Determined by ^{1}H NMR analysis from monomer conversion. [b] Calculated using SEC analysis of the final reaction mixture and feed masses. [c] Number-average molecular weight and Đ determined using a GPC with Mixed-B columns relative to polystyrene standards. [d] Number-average molecular weight and Đ determined using a GPC with GRAL columns relative to polystyrene standards.

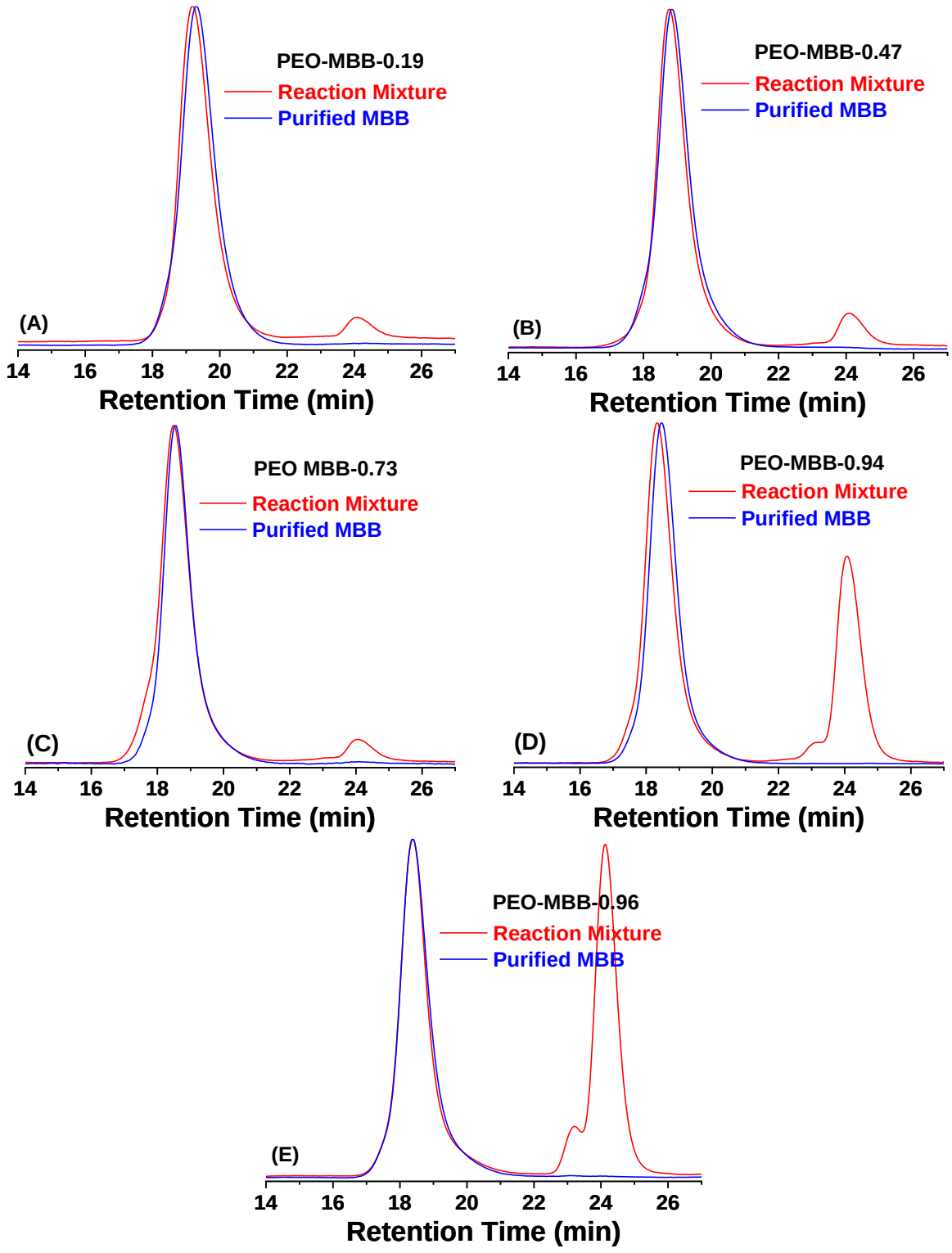

Figure 6.3. SEC analysis of PEO MBBs before and after purification for (A) PEO-MBB-0.19, (B) PEO-MBB-0.47, (C) PEO-MBB-0.73, (D) PEO-MBB-0.94, and (E) PEO-MBB-0.96. SEC was performed with a GPC system equipped with Mixed-B columns and DMF with 50 mM LiBr as eluent.

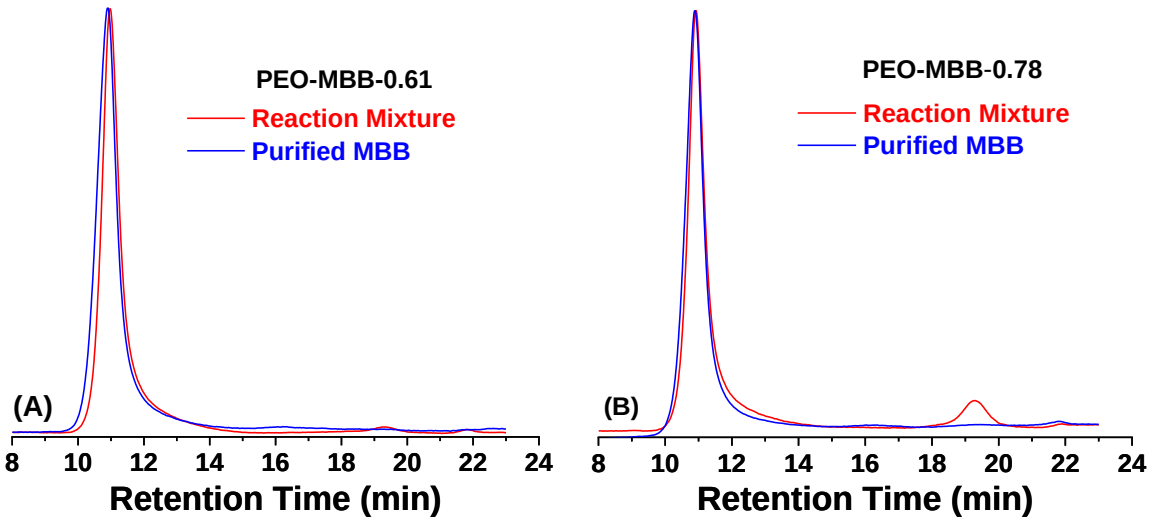

Figure 6.4. SEC analysis of PEO MBBs before and after purification for (A) PEO-MBB-0.61 and (B) PEO-MBB-078. SEC analysis was performed using a GPC system equipped with GRAL columns and DMF with 50 mM LiBr as eluent.

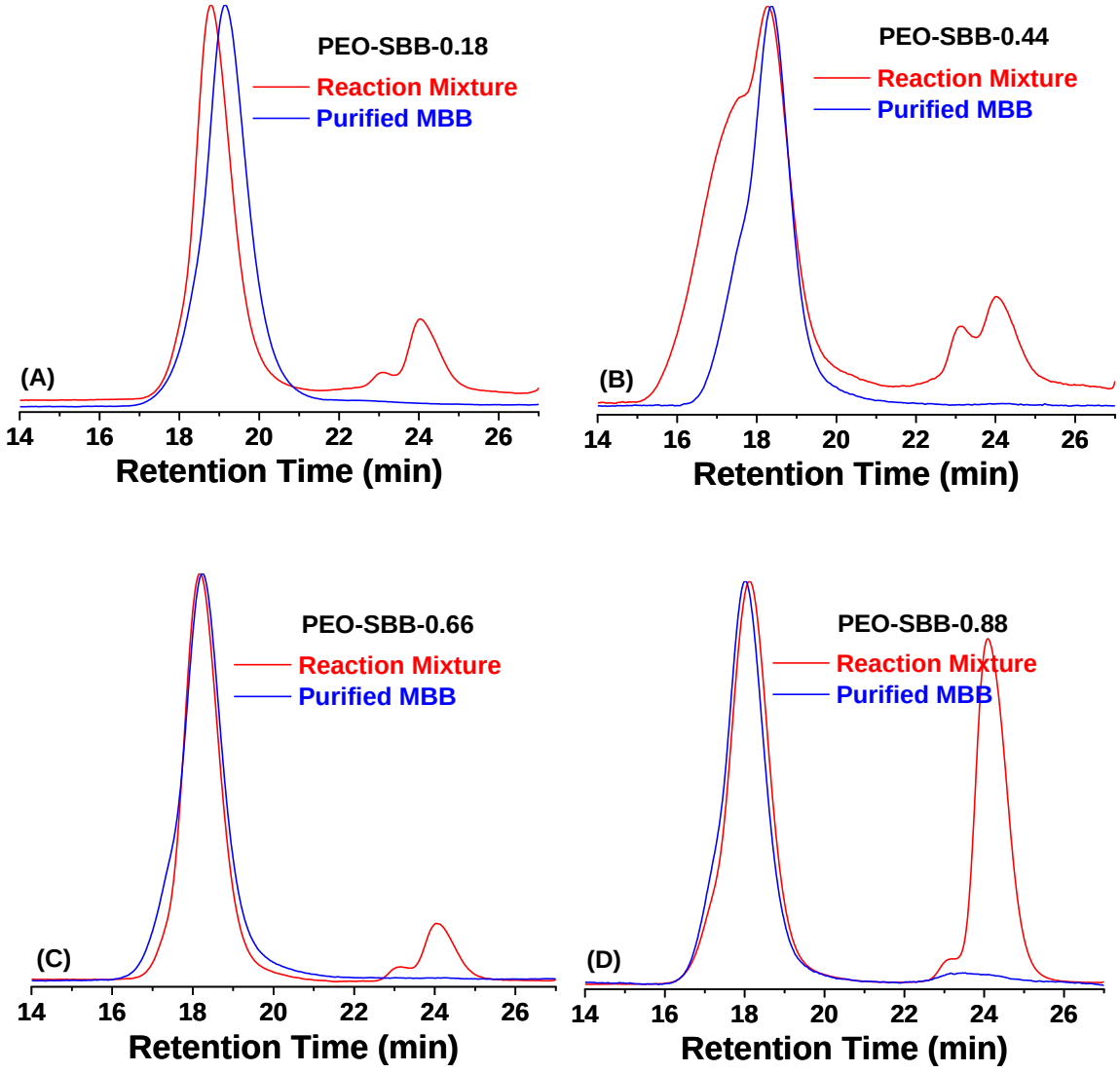

Figure 6.5. SEC analysis of three-arm star PEO brushes (SBBs) before and after purification for (A) PEO-SBB-0.18, (B) PEO-SBB-0.44, (C) PEO-SBB-0.66, and (D) PEO-SBB-0.88. SEC analysis was performed using a GPC system equipped with Mixed-B columns and DMF with 50 mM LiBr as eluent.

A second series of MBBs was prepared for studying the effect of side chain composition on the crystallization behavior of linear heterografted MBBs with two distinct semi-crystalline polymers as side chains (Scheme 6.3). All of these brush polymers were prepared with the linear azide-functionalized backbone polymer with a DP of 734, and the feed ratios were adjusted for achieving the desired molar composition of side chains. SEC analysis of the brush reaction mixture yielded consistent grafting density values close to 80%. The brush polymers were purified by several rounds of fractionation by dissolving them in chloroform and slowly adding pentanes until the brushes precipitated. Typically, five rounds of fractionation afforded pure MBBs. The ^{1}H NMR analysis yielded the molar composition of side chains in each brush polymer that closely matched the initial feed ratio. This correlates well with our prior results where side chain polymers with similar structure typically afford MBBs with compositions closely matching the feed ratio. A total of nine heterografted PEO/PCL brush polymers along with two homografted MBBs were synthesized, and their characterization data are summarized in Table 6.3. The SEC and ^{1}H NMR data for these polymers are shown in Figures 6.6-6.9. The samples are named as MBB-E_xC_y, where E and C represent PEO and PCL, respectively, and x and y are mole fractions.

6.4. Conclusions

In summary, two sets of MBBs were synthesized by grafting alkyne-end-functionalized semicrystalline polymers onto azide-functionalized backbone polymers via the CuAAC click reaction for studying the crystallization of semi-crystalline brushes. These MBBs are: (i) linear and star PEO MBBs with various grafting densities and (ii) linear heterografted MBBs with PEO and PCL side chains along with two homografted brush polymers. SEC analysis showed that the unreacted side chain polymers were completely removed after the purification, and the side chain compositions of heterografted PEO/PCL MBBs closed matched the molar ratios in the feeds.

Scheme 6.3. Synthesis of MBBs with Semi-Crystalline Polymer Side Chains

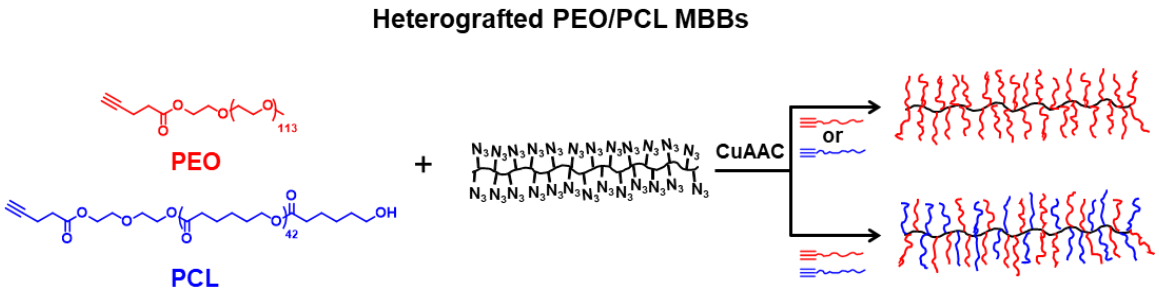

Table 6.3. Summary of MBBs with PEO and/or PCL side chains

Sample ID	Feed Ratio (PEO : PCL)	Molar Ratio of PEO to PCL Side Chains [a]	Grafting Density[b]	$M_{n,SEC}$ ($\times 10^6$ Da) [c]	Đ [c]
MBB-$E_{1.00}C_{0.00}$	1.00 : 0.00	1.00 : 0.00	78.6%	1.19	1.16
MBB-$E_{0.91}C_{0.09}$	0.90 : 0.10	0.91: 0.09	77.6%	1.15	1.15
MBB-$E_{0.81}C_{0.19}$	0.80 : 0.20	0.81: 0.19	78.0 %	1.27	1.15
MBB-$E_{0.71}C_{0.29}$	0.70 : 0.30	0.71 : 0.29	76.8%	1.18	1.15
MBB-$E_{0.61}C_{0.39}$	0.60 : 0.40	0.61 : 0.39	77.5%	1.22	1.14
MBB-$E_{0.49}C_{0.51}$	0.50 : 0.50	0.49 : 0.51	79.5%	1.16	1.16
MBB-$E_{0.40}C_{0.60}$	0.40 : 0.60	0.40 : 0.60	80.0%	1.16	1.16
MBB-$E_{0.30}C_{0.70}$	0.30 : 0.70	0.30 : 0.70	81.5%	1.11	1.14
MBB-$E_{0.21}C_{0.79}$	0.20 : 0.80	0.21 : 0.79	79.7%	0.99	1.14
MBB-$E_{0.10}C_{0.90}$	0.10 : 0.90	0.10 : 0.90	79.4%	1.02	1.16
MBB-$E_{0.00}C_{1.00}$	0.00 : 1.00	0.00 : 1.00	80.6%	1.03	1.14

[a] Determined by ^{1}H NMR analysis of the purified MBBs.
[b] Grafting density was calculated assuming 100% azide functionalization using a combination of SEC analysis of the reaction mixture, feed masses, and molar composition of side chains.
[c] Number-average molecular weights were determined using GPC analysis with Mixed B columns relative to linear polystyrene standards.

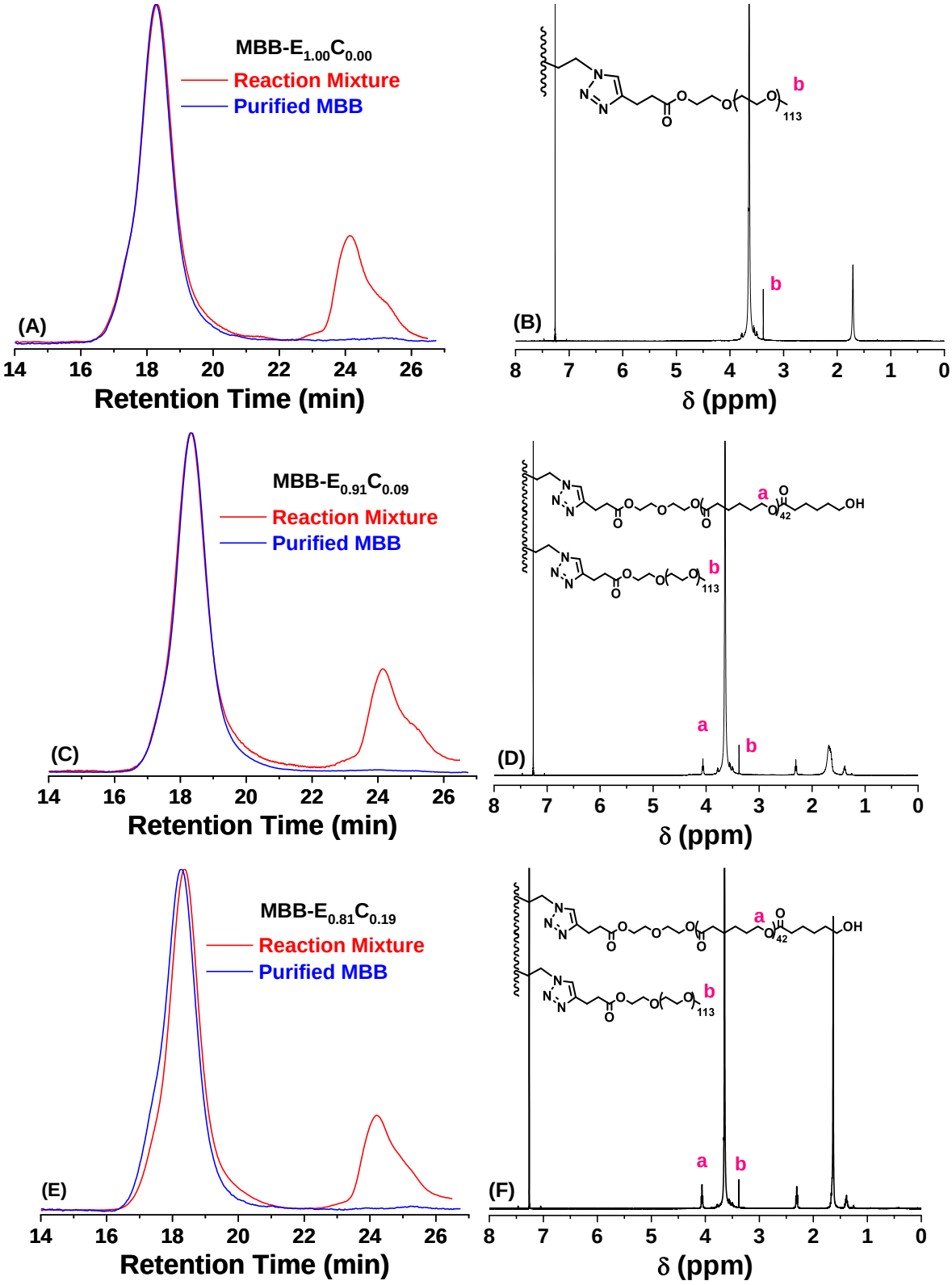

Figure 6.6. SEC (A,C,E) of crude and purified MBBs and ^{1}H NMR spectra of purified brushes in $CDCl_3$ (B,D,F) for MBB-$E_{1.00}C_{0.00}$ (A,B), MBB-$E_{0.91}C_{0.09}$ (C,D), and MBB-$E_{0.81}C_{0.19}$ (E,F).

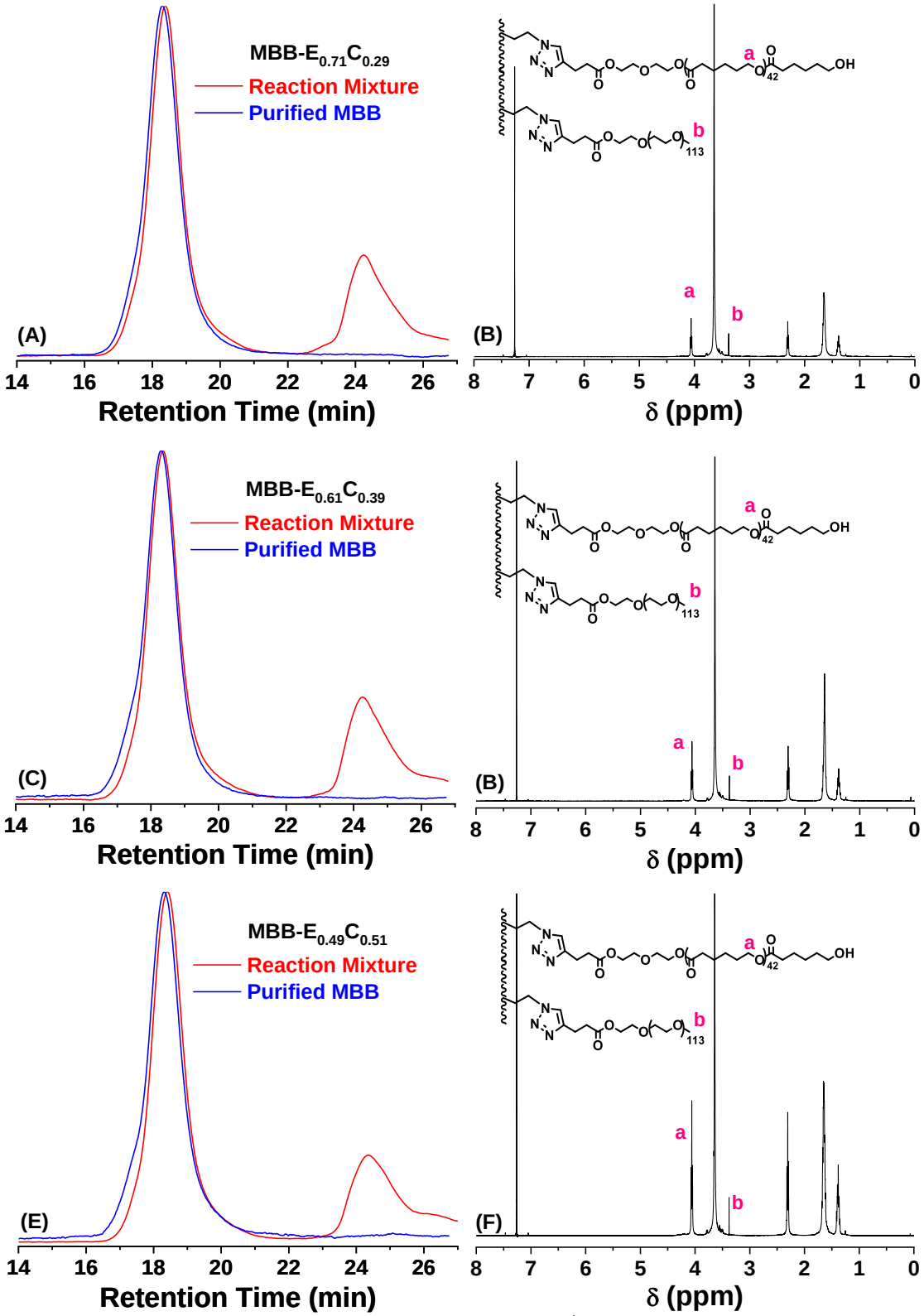

Figure 6.7. SEC (A,C,E) of crude and purified MBBs and ^{1}H NMR spectra of purified brushes in $CDCl_3$ (B,D,F) for MBB-$E_{0.71}C_{0.29}$ (A,B), MBB-$E_{0.61}C_{0.39}$ (C,D), and MBB-$E_{0.49}C_{0.51}$ (E,F).

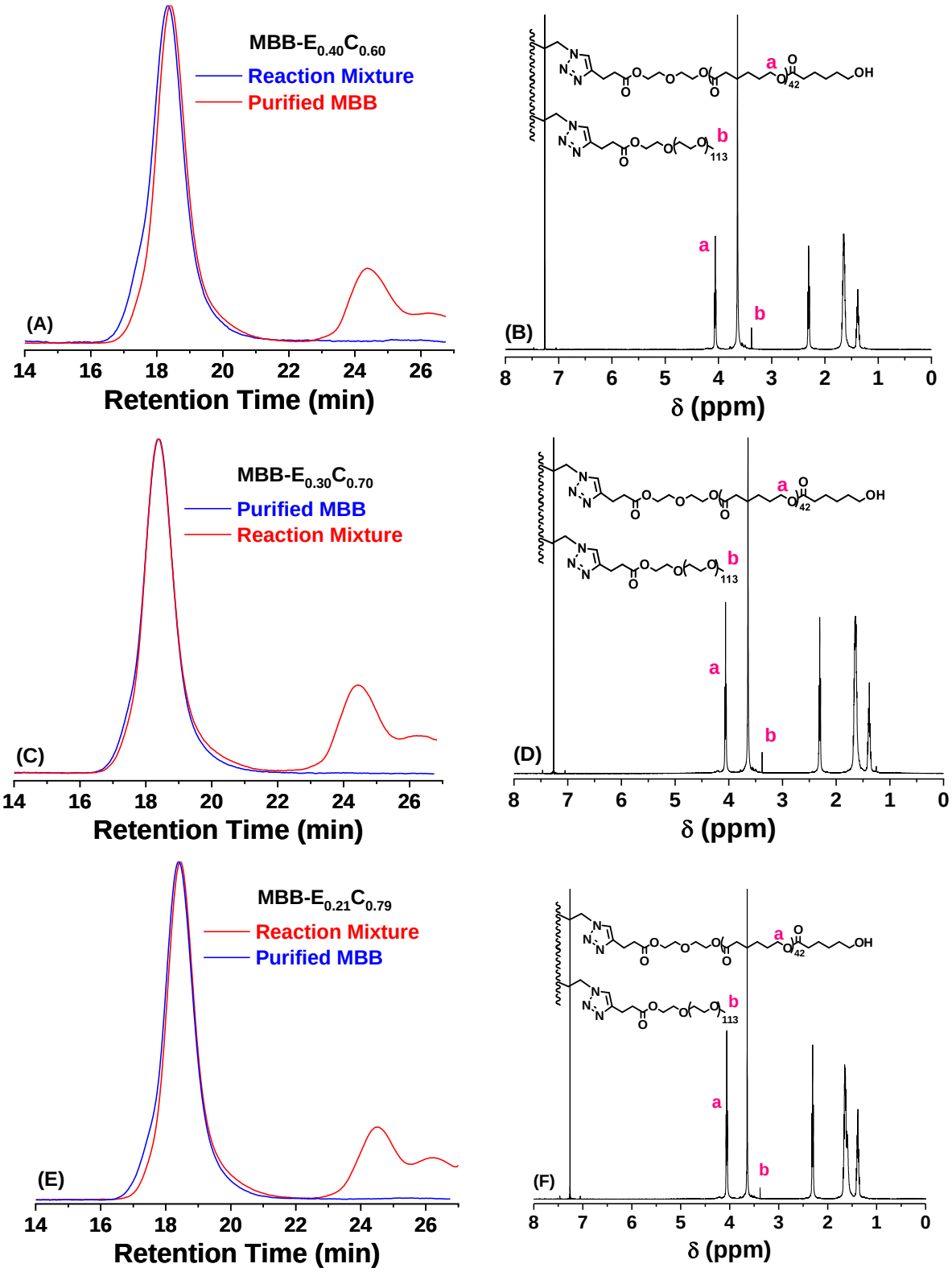

Figure 6.8. SEC (A,C,E) of crude and purified MBBs and ^{1}H NMR spectra of purified brushes in $CDCl_3$ (B,D,F) for MBB-$E_{0.40}C_{0.60}$ (A,B), MBB-$E_{0.30}C_{0.70}$ (C,D), and MBB-$E_{0.21}C_{0.79}$ (E,F).

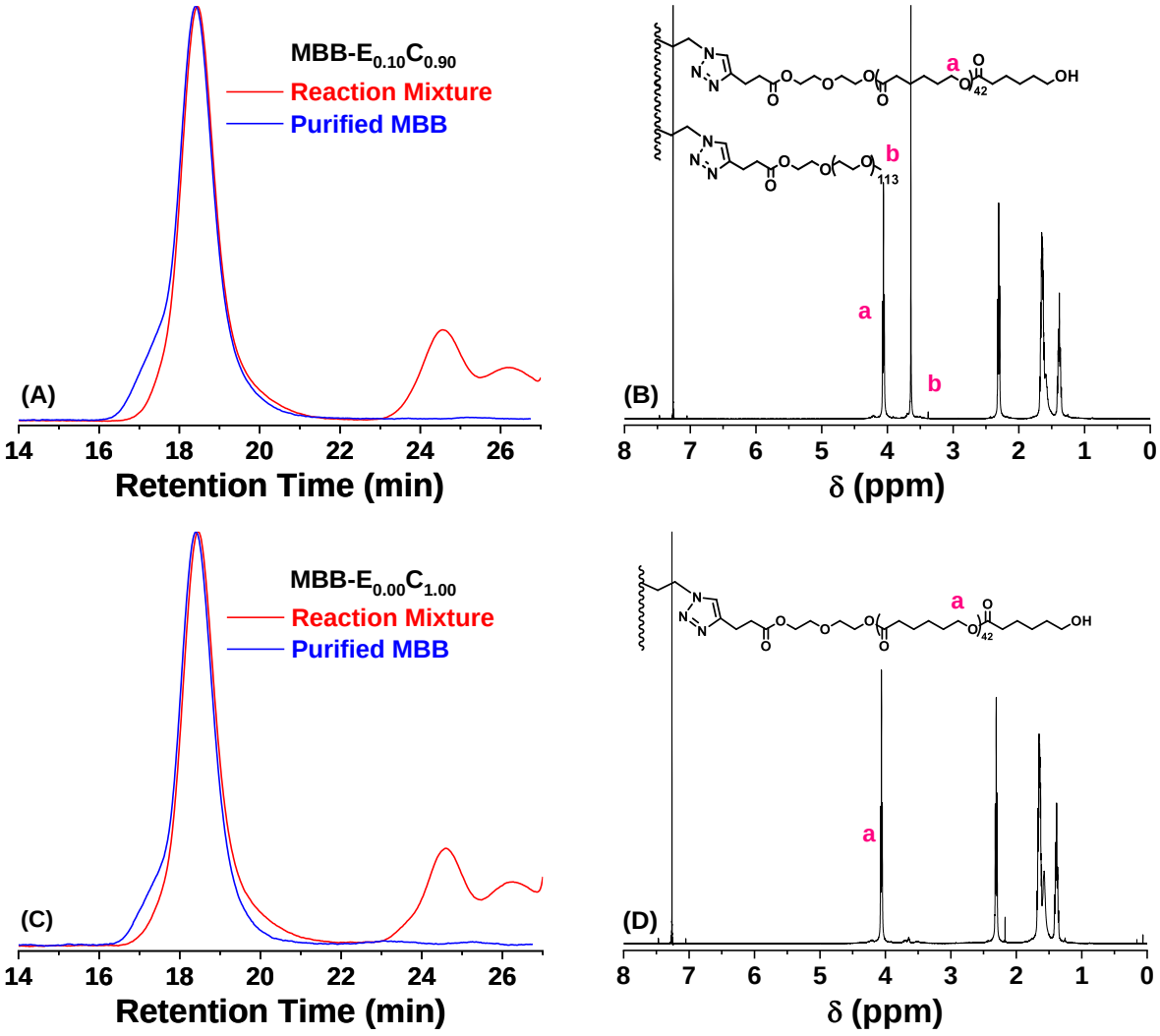

Figure 6.9. SEC (A,C) of crude and purified MBBs and ^{1}H NMR spectra of purified brushes in $CDCl_3$ (B,D) for MBB-$E_{0.10}C_{0.90}$ (A,B), and MBB-$E_{0.00}C_{1.00}$ (C,D).

References

1. Zhao, B. Shape-Changing Bottlebrush Polymers. *J. Phys. Chem. B* **2021**, *125*, 6373-6389.
2. Sheiko, S. S.; Sumerlin, B. S.; Matyjaszewski, K. Cylindrical Molecular Brushes: Synthesis, Characterization, and Properties. *Prog. Polym. Sci.* **2008**, *33*, 759-785.
3. Lee, H.-I.; Pietrasik, J.; Sheiko, S. S.; Matyjaszewski, K. Stimuli-Responsive Molecular Brushes. *Prog. Polym. Sci.* **2010**, *35*, 24-44.
4. Xie, G.; Martinez, M. R.; Olszewski, M.; Sheiko, S. S.; Matyjaszewski, K. Molecular Bottlebrushes as Novel Materials. *Biomacromolecules* **2019**, *20*, 27-54.
5. Liberman-Martin, A. L.; Chu, C. K.; Grubbs, R. H. Application of Bottlebrush Block Copolymers as Photonic Crystals. *Macromol. Rapid Commun.* **2017**, *38*, 1700058.
6. Daniel , W. F.; Burdynska, J.; Vatankhah-Varnoosfaderani, M.; Matyjaszewski, K.; Paturej, J.; Rubinstein, M.; Dobrynin, A. V.; Sheiko, S. S. Solvent-Free, Supersoft and Superelastic Bottlebrush Melts and Networks. *Nat. Mater*. **2016**, 15, 183-189.
7. Sheiko, S. S.; Dobrynin, A. V. Architectural Code for Rubber Elasticity: From Supersoft to Superfirm Materials. *Macromolecules* **2019**, *52*, 7531-7546.
8. Liao, L.; Liu, J.; Dreaden, E. C.; Morton, S. W.; Shopsowitz, K. E.; Hammond, P. T.; Johnson, J. A. A Convergent Synthetic Platform for Single-Nanoparticle Combination Cancer Therapy: Ratiometric Loading and Controlled Release of Cisplatin, Doxorubicin, and Camptothecin. *J. Am. Chem. Soc.* **2014**, *136*, 5896–5899.
9. Banquy, X.; Burdyńska, J.; Lee, D. W.; Matyjaszewski, K.; Israelachvili, J. Bioinspired Bottle-Brush Polymer Exhibits Low Friction and Amontons-Like Behavior. *J. Am. Chem. Soc.* **2014**, *136*, 6199 -6202.

10. Qi, H.; Liu, X. T.; Henn, D. M.; Mei, S.; Staub, M. C.; Zhao, B.; Li, C. Y. Breaking Translational Symmetry via Polymer Chain Overcrowding in Molecular Bottlebrush Crystallization. *Nature Communications* **2020**, *11*, 2152.

11. Yan, Y.; Shi, Y.; Zhu, W.; Chen, Y. Highly Efficient Synthesis of Cylindrical Polymer Brushes with Various Side Chains via Click Grafting-Onto Approach. *Polymer* **2013**, *54*, 5634−5642.

12. Henn, D. M.; Fu, W. X.; Mei, S.; Li, C. Y.; Zhao, B. Temperature-Induced Shape Changing of Thermosensitive Binary Heterografted Linear Molecular Brushes between Extended Worm-Like and Stable Globular Conformations. *Macromolecules* **2017**, *50*, 1645-1656.

13. Kelly, M. T.; Kent, E. W.; Zhao, B. Stepwise Conformational Changes of Linear Ternary Molecular Bottlebrushes with Dually Responsive Side Chains. *Macromolecules* **2022**, *55(5)*, 1629-1641.

14. Kent, E. W.; Lewoczko, E. M.; Zhao, B. Effect of Buffer Anions on Pearl-Necklace Morphology of Tertiary Amine-Containing Binary Heterografted Linear Molecular Bottlebrushes in Acidic Aqueous Buffers. *Langmuir* **2020**, *36*, 13320-13330.

15. Kent, E. W.; Zhao, B. Stimuli-Induced Star-Globule Shape Transitions of Dually Responsive Binary Heterografted Three-Arm Star Molecular Brushes in Aqueous Solution. *Macromolecules* **2019**, *52(17)*, 6714-6724.

Chapter 7. Conclusions and Future Work

The work in this dissertation focuses on the synthesis and behavior of stimuli-responsive multicomponent heterografted linear molecular bottlebrushes (MBBs),[1-11] particularly amphiphilic pH-responsive tertiary amine-containing heterografted bicomponent MBBs. In Chapter 2, a series of linear amphiphilic MBBs with a combination of pH-responsive and hydrophobic polymer side chains were synthesized and shown to be effective as emulsion stabilizers, while also being responsive to pH variations. Chapter 3 is a follow-up study on the mechanism of the interfacial activity of the amphiphilic brush polymers at water-toluene interfaces using pendant drop tensiometry. In Chapter 4, we moved to the two-dimensional air-water interface and explored the effects that pH changes and lateral compression have on molecular conformation of MBBs. In Chapter 5, we shifted into solution and studied the shape changing behavior of three ternary linear molecular bottlebrushes with two distinct pH- and/or temperature-responsive polymer side chains along with a stabilizing PEO graft. Chapter 6 covers the use of the grafting-to approach to prepare two series of molecular brushes with semi-crystalline polymer studies: homografted with various grafting densities and heterografted with tunable side chain compositions.

Chapter 2 presents a systematic study on a series of linear amphiphilic heterografted MBBs with a combination of hydrophobic poly(*n*-butyl acrylate) (P*n*BA) and pH-responsive poly(2-(*N*,*N*-diethylamino)ethyl methacrylate) (PDEAEMA) side chains as pH-responsive emulsifiers. We synthesized a total of six MBB samples, four heterografted with different molar compositions of side chains and two homografted MBBs. We found that within a certain composition range the brush polymers were able to act as efficient emulsifiers stabilizing water-in-toluene emulsions, even at concentrations as low as 0.005 wt%. These emulsions were stable for at least six weeks. In addition, we found that we could reversibly break and reform the emulsions by adjusting the pH of the aqueous phase between 4.0 and 10.0, and this could be performed at least 10 cycles. Atomic

force microscopy (AFM) studies showed that there was no noticeable change in the morphology of the brush molecules, demonstrating their robust nature. In the study of the emulsion droplet morphology under an optical microscope, we noticed that the emulsion droplets at pH 4.0 crumpled to form winkled polymer films upon the evaporation of solvent, which gave some indication of the strong interfacial activity of the MBBs. This study demonstrates the first example of amphiphilic pH-responsive heterografted MBBs as stimuli-responsive brush emulsifiers.

Chapter 3 is a natural extension of the previous chapter, where we explore the interfacial activity of the amphiphilic MBBs using pendant drop tensiometry. By analyzing a toluene droplet containing a brush polymer in an aqueous phase, we examined the influence of side chain composition on the interfacial tension of MBBs under acidic and basic conditions. We found that heterografted brushes showed an increase in reduction of interfacial tension with increasing mole fraction of PDEAEMA side chains ($\chi_{PDEAEMA}$) under acidic conditions, while similar interfacial tension reductions were observed for heterografted MBBs with $\chi_{PDEAEMA}$ under basic conditions. However, the stability of emulsions did not correlate well with the interfacial tension reduction. Additionally, we observed the wrinkling of the interface when the toluene droplet was withdrawn from the acidic aqueous phase, which is indicative of jamming of MBBs at the interface. This is strong evidence that heterografted MBBs with appropriate side chain compositions at pH = 4.0 were strongly adsorbed at the water-toluene interface and could not be desorbed by compression.

In Chapter 4, we studied the behavior of these MBBs at the air/water interface using a Langmuir-Blodgett trough. Compression isotherms were obtained to relate molecular area to surface pressure, and we transferred the monolayers of these MBBs to glass disks for study of the morphology of brush molecules at different pH values and under different degrees of compression by atomic force microscopy (AFM). We found that under acidic conditions the brush molecules

tended to collapse into globular shapes when the P*n*BA molar content in the side chains was ≥ 51%, whereas MBBs with larger PDEAEMA contents did not undergo large conformational changes.

Chapter 5 dives into the solution behavior of three ternary heterografted linear MBBs with a combination of permanently hydrophilic and two distinct types of stimuli-responsive polymer side chains.[11] We observed an interesting stepwise decrease in hydrodynamic size (D_h) from dynamic light scattering (DLS) measurements by introducing pH and/or temperature changes sequentially. ^{1}H NMR spectroscopy studies provided clear evidence that these changes in D_h correlated well with the corresponding changes in solubility of the responsive side chain polymers, at different pH values or at temperatures above the LCST. A comprehensive AFM study showed clear conformational changes for all three ternary MBB samples from an extended wormlike state to partially collapsed, and finally to a compact globular shape. We also demonstrated a stepwise release of a fluorescent probe, Nile Red, from a ternary brush polymer, which shows a potential application for stimuli-responsive MBBs in drug delivery.

Lastly, we present in Chapter 6 the synthesis of two series of MBBs with semicrystalline polymer side chains for a collaborative study using a "grafting to" method via the copper(I)-catalyzed azide-alkyne cycloaddition reaction. The first set was composed of linear and star brushes in which the grafting density of PEO side chains was altered. By adjusting the amount of alkyne-end-functionalized PEO in the initial reaction mixture with respect to the backbone polymer, we were able to tailor the grafting density from ~ 20% to as high as 96% for linear MBBs. The second series was composed of heterografted brush polymers with PEO and PCL side chains and their analogous homografted versions. This chapter demonstrates the utility of the click "grafting to" approach for preparing molecular bottlebrushes with tailored side chain compositions

while keeping parameters such as backbone and side chain lengths consistent among different samples.[2-11] Our collaborators are studying the crystallization behavior of these samples.

The work in this dissertation provides insight into the behavior of stimuli-responsive molecular bottlebrushes, particularly at liquid/liquid and liquid/air interfaces, and their potential applications.[1,12-14] In Chapter 2, we demonstrated the utility of MBBs as pH-responsive emulsion stabilizers. Future studies could explore other stimuli to induce breaking of emulsions stabilized by responsive amphiphilic MBBs. In addition, by adjusting the side chain composition, it may be possible to prepare oil-in-water emulsions, which would likely be more sensitive to pH changes. Similarly, at the air-water interface, it may be possible to achieve changes in molecular conformation without lateral compression, by incorporating a more hydrophobic side chain polymer or a different stimuli-responsive polymer.

References

1. Zhao, B. Shape-Changing Bottlebrush Polymers. *J. Phys. Chem. B* **2021**, *125(24)*, 6373-6389.
2. Henn, D. M.; Fu, W. X.; Mei, S.; Li, C. Y.; Zhao, B. Temperature-Induced Shape Changing of Thermosensitive Binary Heterografted Linear Molecular Brushes between Extended Worm-Like and Stable Globular Conformations. *Macromolecules* **2017**, *50*, 1645-1656.
3. Henn, D. M.; Lau, C. M.; Li, C. Y.; Zhao, B. Light-Triggered Unfolding of Single Linear Molecular Bottlebrushes from Compact Globular to Wormlike Nano-Objects in Water. *Polym. Chem.* **2017**, *8*, 2702-2712.
4. Henn, D. M.;† Holmes, J. A.;† Kent, E. W.; Zhao, B. Worm-to-Sphere Shape Transition of Thermoresponsive Linear Molecular Bottlebrushes in Moderately Concentrated Aqueous Solution. *J. Phys. Chem. B* **2018**, *122*, 7015-7025. † Contributed equally
5. Kent, E. W.; Henn, D. M.; Zhao, B. Shape-Changing Linear Molecular Bottlebrushes with Dually pH- and Thermo-Responsive Diblock Copolymer Side Chains. *Polym. Chem.* **2018**, *9*, 5133-5144.
6. Kent, E. W.; Zhao, B. Stimuli-Induced Star-Globule Shape Transitions of Dually Responsive Binary Heterografted Three-Arm Star Molecular Brushes in Aqueous Solution. *Macromolecules* **2019**, *52(17)*, 6714-6724.
7. Kent, E. W.; Lewoczko, E. M.; Zhao, B. Effect of Buffer Anions on Pearl-Necklace Morphology of Tertiary Amine-Containing Binary Heterografted Linear Molecular Bottlebrushes in Acidic Aqueous Buffers. *Langmuir* **2020**, *36*, 13320-13330.

8. Qi, H.;† Liu, X. T.;† Henn, D. M.;† Mei, S.; Staub, M. C.; Zhao, B.;* Li, C. Y.* Breaking Translational Symmetry via Polymer Chain Overcrowding in Molecular Bottlebrush Crystallization. *Nature Communications* **2020**, *11*, 2152.

9. Kent, E. W.; Lewoczko, E. M.; Zhao, B. pH- and Chaotropic Anion-Induced Conformational Changes of Tertiary Amine-Containing Binary Heterografted Star Molecular Bottlebrushes in Aqueous Solution. *Polymer Chemistry* **2021**, *12*, 265-276.

10. Lewoczko, E. M.; Kelly, M. T.; Kent, E. W.; Zhao, B. Effects of Temperature on Chaotropic Anion-Induced Shape Transitions of Star Molecular Bottlebrushes with Heterografted Poly(ethylene oxide) and Poly(*N*,*N*-dialkylaminoethyl methacrylate) Side Chains in Acidic Water. *Soft Matter* **2021**, *17*, 6566-6579.

11. Kelly, M. T.; Kent, E. W.; Zhao, B. Stepwise Conformational Transitions of Stimuli-Responsive Linear Ternary Heterografted Bottlebrush Polymers in Aqueous Solution. *Macromolecules* **2022**, *55(5)*, 1629-1641.

12. Lee, H.-i.; Pietrasik, J.; Sheiko, S. S.; Matyjaszewski, K., Stimuli-responsive molecular brushes. *Progress in Polymer Science* **2010,** *35* (1), 24-44.

13. Xie, G.; Martinez, M. R.; Olszewski, M.; Sheiko, S. S.; Matyjaszewski, K., Molecular Bottlebrushes as Novel Materials. *Biomacromolecules* **2019,** *20* (1), 27-54.

14. Hu, M.; Russell, T. P., Polymers with advanced architectures as emulsifiers for multi-functional emulsions. *Materials Chemistry Frontiers* **2021,** *5* (3), 1205-1220.

Vita

Michael Thomas Kelly was born in Fort Bragg, North Carolina in 1994. He completed his BS in Chemistry from the Armstrong campus of Georgia Southern University in May 2018. During the last two years of his undergraduate education, he interned with the Kraton Corporation at their R&D facility in Savannah, GA. In August of 2018, he enrolled as a graduate student at the University of Tennessee, Knoxville and shortly thereafter joined Dr. Bin Zhao's research group. His research efforts were primarily focused on the synthesis of stimuli-responsive molecular bottlebrush polymers and the study of their behavior at interfaces and in solution.